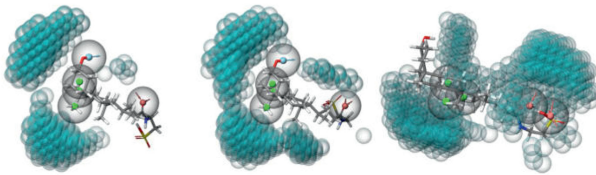


**MICHAEL KIRSTGEN**

---

Identifizierung und Testung niedermolekularer  
HBV/HDV Entry-Inhibitoren



Inaugural-Dissertation zur Erlangung des Grades eines  
**Dr. med. vet.**  
beim Fachbereich Veterinärmedizin der Justus-Liebig-Universität Gießen

**Das Werk ist in allen seinen Teilen urheberrechtlich geschützt.**

**Die rechtliche Verantwortung für den gesamten Inhalt dieses Buches liegt ausschließlich bei dem Autoren dieses Werkes.**

Jede Verwertung ist ohne schriftliche Zustimmung der Autoren oder des Verlages unzulässig. Das gilt insbesondere für Vervielfältigungen, Übersetzungen, Mikroverfilmungen und die Einspeicherung in und Verarbeitung durch elektronische Systeme.

1. Auflage 2022

All rights reserved. No part of this publication may be reproduced, stored in a retrieval system, or transmitted, in any form or by any means, electronic, mechanical, photocopying, recording, or otherwise, without the prior written permission of the Authors or the Publisher.

1<sup>st</sup> Edition 2022

© 2022 by VVB LAUFERSWEILER VERLAG, Giessen  
Printed in Germany



*édition scientifique*  
**VVB LAUFERSWEILER VERLAG**

STAUFENBERGRING 15, 35396 GIESSEN, GERMANY  
Tel: 0641-5599888 Fax: 0641-5599890  
email: [redaktion@doktorverlag.de](mailto:redaktion@doktorverlag.de)

[www.doktorverlag.de](http://www.doktorverlag.de)

Aus dem Institut für Pharmakologie und Toxikologie  
des Fachbereichs Veterinärmedizin  
der Justus-Liebig-Universität Gießen

Betreuer: Prof. Dr. Joachim Geyer

# **Identifizierung und Testung niedermolekularer HBV/HDV Entry-Inhibitoren**

## **Inauguraldissertation**

zur Erlangung des Grades eines Dr. med. vet.

am Fachbereich Veterinärmedizin

der Justus-Liebig-Universität Gießen

eingereicht von

**Michael Kirstgen**

Tierarzt aus Tondorf in der Eifel

Gießen 2021

**Mit Genehmigung des Fachbereichs Veterinärmedizin  
der Justus-Liebig-Universität Gießen  
Dekan: Prof. Dr. Dr. Stefan Arnhold**

**1. Gutachter: Prof. Dr. Joachim Geyer**  
**2. Gutachter: Prof. Dr. Dr. Benjamin Lamp**

**Tag der Disputation: 27.04.2022**

**Prüfungskommission: Prof. Dr. Joachim Geyer**  
**Prof. Dr. Dr. Benjamin Lamp**  
**Prof. Dr. Sybille Mazurek**

## Erklärung zur selbstständigen Anfertigung

Ich erkläre hiermit die vorgelegte Dissertation mit dem Titel

### **„Identifizierung und Testung niedermolekularer HBV/HDV Entry-Inhibitoren“**

selbständig und ohne unerlaubte fremde Hilfe und nur mit den Hilfen angefertigt zu haben, die ich in der Dissertation angegeben habe. Alle Textstellen, die wörtlich oder sinngemäß aus veröffentlichten oder nicht veröffentlichten Schriften entnommen sind, und alle Angaben, die auf mündlichen Auskünften beruhen, sind als solche kenntlich gemacht. Bei den von mir durchgeführten und in der Dissertation erwähnten Untersuchungen habe ich die Grundsätze guter wissenschaftlicher Praxis, wie sie in der "Satzung der Justus-Liebig-Universität Gießen zur Sicherung guter wissenschaftlicher Praxis" niedergelegt sind, eingehalten. Diese Arbeit hat in gleicher oder ähnlicher Form noch keiner anderen Prüfungsbehörde vorgelegen.

A handwritten signature in blue ink, reading "M. Kirstgen", written over a horizontal dotted line.

Michael Kirstgen

# Inhalt

<b>I Abkürzungen</b> .....	6
<b>II Kurzeinleitung in das Thema der Arbeit</b> .....	8
<b>1 Literaturübersicht</b> .....	10
1.1 Das Hepatitis B Virus.....	10
1.2 Das Hepatitis D Virus .....	12
1.3 Das Na <sup>+</sup> /Taurocholate Cotransporting Polypeptide (NTCP) .....	13
1.4 Viruseintritt in die Leberzelle .....	16
1.5 Therapieansätze .....	17
1.5.1 Interferon $\alpha$ .....	17
1.5.2 Nukleos(t)id Analoga .....	17
1.5.3 Entry-Inhibitoren .....	20
1.5.4 Weitere therapeutische Strategien .....	21
1.5.5 Laufende klinische Studien zur HBV Therapie .....	24
1.5.6 Laufende klinische Studien zur HDV Therapie .....	27
1.6 Bioinformatische Applikationen .....	28
1.6.1 Pharmakophor Modelle .....	28
1.6.2 Modelle zur quantitativen Analyse der Struktur-Wirkungs-Beziehungen (QSAR)..	30
1.6.3 Virtuelles Screening .....	33
<b>2 Publikationen</b> .....	36
2.1 Publikation I .....	36
2.2 Publikation II.....	38
2.3 Publikation III .....	40
2.4 Publikation IV .....	42
<b>3 Diskussion</b> .....	44
<b>4 Ausblick</b> .....	59
<b>5 Zusammenfassung (Deutsch)</b> .....	62

<b>6 Summary (English)</b> .....	64
<b>7 Literaturverzeichnis</b> .....	66
<b>8 Danksagungen</b> .....	76
<b>9 Anhang</b> .....	78

# I Abkürzungen

Abkürzung	Bedeutung
[ <sup>3</sup> H]	Tritium; Isotop des Wasserstoffs, dessen Kern aus einem Proton und zwei Neutronen besteht
[ <sup>3</sup> H]preS1	Tritium markiertes präS1 Peptid
[ <sup>3</sup> H]TC	Tritium markierte Taurocholsäure
μM	Mikromolar
mM	Millimolar
APOBEC3	<i>Apolipoprotein B mRNA editing enzyme catalytic polypeptide 3</i> (Engl.), Apolipoprotein B mRNA editierendes Enzym katalytisches Polypeptid 3 (Dt.)
ASBT, SLC10A2	<i>Apical Sodium-dependent Bile Acid Transporter</i> (Engl.), Apikaler Natriumabhängiger Gallensäure Transporter (Dt.)
BARIs	<i>Bile Acid Reabsorption Inhibitors</i> (Engl.), Gallensäure Reabsorptions Hemmer (Dt.)
cccDNA	<i>Circular covalently closed DNA</i> (Engl.), zirkuläre, kovalent geschlossene DNA (Dt.)
CpAMs	<i>Core protein allosteric modulators</i> (Engl.), Kernprotein allosterische Modulatoren (Dt.)
CRISPR/Cas	<i>Clustered Regularly Interspaced Short Palindromic Repeats/CRISPR associated Protein</i> (Engl.), CRISPR ≙ gruppierte kurze palindromische Wiederholungen mit regelmäßigen Abständen (Dt.), Cas ≙ CRISPR assoziiertes Protein
CYP7A1	Cytochrom P450 7A1 oder Cholesterin-7-alpha-Hydroxylase
DHEAS	Dehydroepiandrosteronsulfat
DNA	<i>Deoxyribonucleic acid</i> (Engl.), Desoxyribonukleinsäure (Dt.)
EC <sub>50</sub>	Mittlere effektive Konzentration = Konzentration bei der ein halbmaximaler Effekt erreicht wird
EMA	<i>European Medicines Agency</i> (Engl.), Europäische Arzneimittel Agentur (Dt.)
FGF15/19	<i>Fibroblast growth factor 15/19</i> (Engl.), Fibroblasten Wachstumsfaktor 15/19 (Dt.)
FXR	<i>Farnesoid X Receptor</i> (Engl.), Farnesoid X Rezeptor (Dt.)
GLP-1	<i>Glucagone-like peptide 1</i> (Engl.), Glukagon-ähnliches Peptid 1 (Dt.)
GPBAR1 oder TGR5	<i>G protein-coupled bile acid receptor 1</i> (Engl.), G-Protein-gekoppelter Gallensäure Rezeptor 1 (Dt.)
HBc	<i>HBV core-antigen</i> (Engl.), HBV Kern-Antigen (Dt.)
HBe	HBV e-Antigen
HBs	<i>Hepatitis B surface proteins</i> (Engl.), Hepatitis B Hüllproteine (Dt.)
HBV	Humanes Hepatitis B Virus
HBx	HBV x-Antigen
HCC	<i>Hepatocellular carcinoma</i> (Engl.), Hepatozelluläres Karzinom (Dt.)
HDV	Humanes Hepatitis Delta Virus
HTS	<i>High-throughput-screening</i> (Engl.), Hoch-Durchsatz-Screening (Dt.)
IC <sub>50</sub>	Mittlere inhibitorische Konzentration = Konzentration bei der eine halbmaximale Hemmung erreicht wird
IFN-α	Interferon α
kb	<i>Kilobases</i> (Engl.), Kilobasen (Dt.)



K <sub>i</sub>	Inhibitionskonstante = Inhibitorkonzentration, bei der die Hälfte der Zielproteine inhibiert sind
LHBs	<i>Large hepatitis B surface protein</i> (Engl.), großes hepatitis B Hüllprotein (Dt.)
LHDAg	<i>Large hepatitis delta antigen</i> (Engl.), großes hepatitis delta Antigen (Dt.)
LRH-1	<i>Liver receptor homolog-1</i> (Engl.), Leber Rezeptor Homolog-1 (Dt.)
MHBs	<i>Middle hepatitis B surface protein</i> (Engl.), mittleres hepatitis B Hüllprotein (Dt.)
ns	Nicht signifikant
NTCP, <i>SLC10A1</i>	Na <sup>+</sup> /Taurocholate Cotransporting Polypeptide
PAMPs	<i>Pathogen-Associated Molecular Patterns</i> (Engl.), Pathogen-assoziierte molekulare Muster (Dt.)
pKa	Säurekonstante, im deutschen Gebrauch auch als pKs abgekürzt
PLS	<i>Partial least squares</i> (Engl.), partielle kleinste Quadrate (Dt.)
PRRs	<i>Pattern-Recognition Receptors</i> (Engl.), Mustererkennungs-Rezeptoren (Dt.)
QSAR	<i>Quantitative Structure-Activity Relationship</i> (Engl.), Quantitative Struktur-Wirkungs Beziehung (Dt.)
RIG-I	<i>Retinoic acid inducible gene 1</i> (Engl.), Retinsäure-induzierbares Gen I (Dt.)
RNA	<i>Ribonucleic acid</i> (Engl.), Ribonukleinsäure (Dt.)
SD	<i>Standard Deviation</i> (Engl.), Standardabweichung (Dt.)
SHBs	<i>Small hepatitis B surface protein</i> (Engl.), kleines hepatitis B Hüllprotein (Dt.)
sHDAg	<i>Small hepatitis delta antigen</i> (Engl.), kleines hepatitis delta Antigen (Dt.)
SHP	<i>Small heterodimer partner</i> (Engl.), kleiner Heterodimer Partner (Dt.)
siRNAs	<i>Small interfering RNAs</i> (Engl.), kleine interferierende RNAs (Dt.)
SLC10	<i>Solute Carrier Family 10</i> (Engl.)
Smc5/6	<i>Structural maintenance of chromosomes' complex 5/6</i> (Engl.), Strukturhaltung des Chromosomenkomplexes 5/6 (Dt.)
SOAT, <i>SLC10A6</i>	<i>Sodium-dependent Organic Anion Transporter</i> (Engl.), Natriumabhängiger Transporter organischer Anionen (Dt.)
T3	Trijodthyronin
TLR	<i>Toll-Like Receptor</i> (Engl.), "Toll-artiger Rezeptor" (Dt.)
uPA/SCID Mäuse	Mäuse, die genetisch einen schweren kombinierten Immundefekt aufweisen (Engl. <i>severe combined immunodeficiency</i> = <i>SCID</i> ) und zusätzlich transgen ein Protein namens Urokinase Plasminogen Aktivator (uPA) überexprimieren, welches Tumorprogression begünstigt
VS	<i>Virtual screening</i> (Engl.), virtuelles Screening (Dt.)

## II Kurzeinleitung in das Thema der Arbeit

Infektionen mit dem Hepatitis B (HBV) und D Virus (HDV) sind die Hauptursache für Lebertumoren als Folge chronischer Hepatitiden. Die ausgeprägte weltweite Prävalenz von HBV/HDV Infektionen ist nicht von der Hand zu weisen. Auch die Verfügbarkeit von Impfungen gegen HBV verhindert nicht, dass jährlich mehr als 800.000 Menschen, vor allem in armen Regionen der Welt, an den Folgen dieser Erkrankung sterben. Mit antiviraler Therapie lässt sich die chronische Hepatitis zwar meist unter Kontrolle bringen, sie führt allerdings in den seltensten Fällen zur Heilung. Es liegt also nahe, sich Gedanken um andere therapeutische Herangehensweisen zu machen.

Ein vielversprechendes therapeutisch nutzbares Zielmolekül ist das „Na<sup>+</sup>/Taurocholate Cotransporting Polypeptide“ (NTCP, Gensymbol: *SLC10A1*), welches im Jahr 2012 als spezifischer zellulärer Rezeptor für HBV und HDV identifiziert wurde. Physiologischerweise handelt es sich bei NTCP um einen natriumgekoppelten Transporter für Gallensäuren, welcher spezifisch in Hepatozyten exprimiert wird und dort Gallensäuren aus dem Blut wieder der Leber zuführt. Somit ist NTCP ein wichtiger Bestandteil des enterohepatischen Kreislaufs der Gallensäuren.

Der exakte Mechanismus des HBV/HDV Eintritts über NTCP in die Leber, auch als „entry“ bezeichnet, ist noch nicht geklärt. Allerdings weiß man, dass ein bestimmter Bereich eines HBV/HDV Hüllproteins, die sogenannte präS1 Region, mit NTCP interagiert und für eine hochaffine Bindung zwischen Virus und Transportprotein sorgt. Man vermutet, dass das Virus daraufhin endozytotisch aufgenommen wird.

Einige Arbeitsgruppen beschäftigen sich mit der Suche nach entsprechenden „Entry-Inhibitoren“, welche die Bindung von HBV und HDV an den NTCP-Rezeptor verhindern sollen. Dadurch sollen die Leberzellen vor einer Infektion geschützt werden. Mit manchen Substanzen, wie z.B. Cyclosporin A, konnte man bereits effektiv NTCP blockieren und somit die Virusbindung reduzieren. Außerdem ist im Juli 2020 durch die europäische Arzneimittel-Agentur ein Präparat namens Hepcludex® als erster Entry-Inhibitor zur Therapie einer HDV Infektion zugelassen worden. Dieser stellt ein synthetisches präS1 Peptid dar, welches an NTCP bindet und dieses somit für die Bindung von HBV und HDV unzugänglich macht.

Ein nicht zu vernachlässigendes Problem ergibt sich jedoch daraus, dass durch dieses Peptid auch die Funktion des NTCP vermittelten Gallensäuretransportes gehemmt wird und somit der enterohepatische Kreislauf der Gallensäuren beeinträchtigt ist. Dies führt zu einem Anstieg der

Gallensäurekonzentrationen in der Blutzirkulation mit bisher unzureichend untersuchten Auswirkungen.

Daher sollte das Ziel dieser Promotionsarbeit sein, herauszufinden, ob die Virus-Rezeptor- und die Gallensäure-Transportfunktion von NTCP durch Inhibitoren getrennt voneinander adressiert werden können. Außerdem wurden die erhobenen Daten bioinformatisch aufgearbeitet und zur Generierung von Pharmakophor-Modellen und Modellen zur quantitativen Analyse der Struktur-Wirkungs-Beziehung verwendet, mit deren Hilfe neue Entry-Inhibitoren identifiziert werden konnten.

# 1 Literaturübersicht

## 1.1 Das Hepatitis B Virus

Erste Beschreibungen gehen auf das Jahr 1965 zurück, als Baruch Samuel Blumberg im Blut eines australischen Ureinwohners ein Isoantigen nachwies, welches daraufhin als „Australia Antigen“ bezeichnet wurde (Blumberg et al., 1967; Lok, 2016). 1970 wurden von Dane und seinen Kollegen die ersten HBV Virionen elektronenmikroskopisch gesichtet, weshalb diese Virionen auch Dane Partikel genannt werden (Dane et al., 1970; Karayiannis, 2017). Inzwischen sind zehn Genotypen des HBV bekannt, welche von Genotyp A-J reichen (Littlejohn et al., 2016).

HBV gehört zum Genus *Orthohepadnavirus* der Familie *Hepadnaviridae*. Es handelt sich um ein behülltes DNA Virus mit partiell doppelsträngiger DNA, welche 3,2 kilobasen (kb) umfasst und an den überlappenden Enden durch Basenpaarungen verbunden, einen Komplex mit der viralen Polymerase eingeht. Die kovalente Verknüpfung der doppelsträngigen DNA zur „circular covalently closed DNA“ (cccDNA) findet allerdings erst im Zellkern der Wirtszelle statt (Glebe and Bremer, 2013).

Diese cccDNA dient als Vorlage zur Bildung von messenger RNAs, aus denen die viralen Proteine hervorgehen (Seeger and Mason, 2015). Dazu zählen: Die virale Polymerase, das „HBx“ Protein, das „HBe“ Protein und das „Core“ Kapsidprotein (HBc). Des Weiteren sind drei Hüllproteine (hepatitis B surface proteins (HBs)) für das Virus bekannt, namentlich das kleine (SHBs), mittlere (MHBs) und große (LHBs) Hüllprotein (Glebe and Bremer, 2013). Diese Hüllproteine entstammen alle dem gleichen Leserahmen, welcher jedoch für jedes der drei Proteine anders abgelesen wird. Als Resultat weisen sie C-terminal identische Aminosäuresequenzen auf, wobei sie sich N-terminal unterscheiden (Glebe and Urban, 2007). Der starke Tropismus zu Hepatozyten wird auf die myristoylierte präS1-Domäne des großen Hüllproteins zurückgeführt, die den ersten 47 N-terminalen Aminosäuren dieses Proteins zugeordnet ist. Nachweislich bindet diese präS1-Domäne hochaffin an NTCP, welches in der basolateralen Membran von Hepatozyten exprimiert wird. Man vermutet eine durch diesen Kontakt induzierte Internalisierung des Virus-Rezeptor Komplexes, der dem Virus letztendlich den Zugang in die Wirtszelle ermöglicht (Fukano et al., 2019).

Zur Reproduktion seines Genoms verwendet HBV prägenomische RNA. Diese RNA bildet im Zytoplasma zusammen mit Kapsidproteinen, zellulären Proteinen und der viralen Polymerase unreife Kapside. Die „Reifung“ des Genoms geschieht durch reverse Transkription der

prägenomischen RNA zur viralen DNA durch die virale Polymerase. Die nun Reifen Kapside wandern entweder in den Zellkern der Wirtszelle und bilden dort erneut cccDNA und erhöhen damit deren Konzentration oder sie werden im Zytoplasma mit einer Lipidmembran und Hüllproteinen ummantelt und als vollständige Virionen aus der Wirtszelle abgegeben (Glebe and Bremer, 2013).

Diese Virionen haben einen Durchmesser von ca. 52 nm und bergen ein icosahedrales Nukleokapsid mit einem Durchmesser von ca. 36 nm, das aus 240 Kapsidproteinen gebildet wird. Das „HBx“ Protein konnte bisher nicht in Virionen nachgewiesen werden und wird als Nichtstrukturprotein klassifiziert. Seine Funktion ist die Regulation der Transkription des viralen Genoms in der Wirtszelle (Glebe and Bremer, 2013).

Bemerkenswert im Zusammenhang mit HBV Infektionen ist, dass nicht nur vollständige Virionen die Wirtszelle verlassen, sondern auch sogenannte subvirale Partikel gebildet und in großen Mengen aus der Zelle ausgeschieden werden. Diese Partikel stellen in eine Lipidmembran eingebettete Hüllproteine dar und können verschieden groß ausgebildet sein. Sie enthalten weder virales Genom noch Kapside. Man vermutet, dass diese subviralen Partikel, bei der Infektion des Wirtes, einen positiven Einfluss auf die Replikation des Virus haben, da durch sie das Immunsystem des Wirtes belastet und sozusagen „abgelenkt“ wird (Glebe and Urban, 2007). Man könnte auch von einem Verdünnungseffekt sprechen, der die Wahrscheinlichkeit reduziert, dass Immunzellen auf echte Virionen treffen. Diese subviralen Partikel waren es, die im Jahre 1967 von Blumberg als „Australia Antigen“ betitelt wurden (Blumberg et al., 1967).

Die Übertragung des Virus kann auf verschiedene Wege geschehen, z.B. durch Kontakt mit Blut einer infizierten Person. Aber auch durch andere Körperflüssigkeiten, wie Sperma und Vaginalsekret, kann das Virus übertragen werden. Zuletzt spielt die perinatale Übertragung von einer infizierten Mutter auf ihren Säugling eine wichtige Rolle (Trépo et al., 2014).

Insgesamt stellt HBV ein sehr relevantes humanpathogenes Virus dar, welches eine globale Prävalenz aufweist. Chronische Hepatitiden nach HBV Infektionen sind die Hauptursache für das Auftreten hepatozellulärer Karzinome (HCC) sowie Leberzirrhose. Selbst die Verfügbarkeit von Impfungen verhindert nicht, dass jährlich mehr als 800.000 Menschen an den Folgen einer chronischen Leberentzündung im Zusammenhang mit HBV Infektionen sterben (World Health Organisation, 2017).

## 1.2 Das Hepatitis D Virus

HDV ist das Prototypvirus des Genus *Deltavirus*. Die 1,7 kb umfassende RNA von HDV codiert für zwei Proteine, das „large hepatitis delta antigen“ (IHDAg) und das „small hepatitis delta antigen“ (sHDAg). Für die Replikation des genetischen Materials bedient sich das HDV der RNA Polymerase der Wirtszelle (Sureau and Negro, 2016). Das sHDAg stellt dabei einen regulatorischen Cofaktor dar. Das IHDAg stabilisiert das virale RNA Genom und beeinflusst die Umhüllung desselben.

Allerdings birgt das Genom dieses Virus selbst keine Informationen für Hüllproteine. Daher agiert HDV als sogenanntes Satellitenvirus und bedient sich der Hüllproteine, die aus dem HBV-Genom stammen (Glebe et al., 2005; Gripon et al., 2005). Dies ist der Grund, warum HDV nur in Gegenwart einer aktiven HBV-Infektion einen ständigen Replikationszyklus durchlaufen kann. Darüber hinaus beruht der gleiche Mechanismus der Interaktion der Viren mit ihrem Eintrittsrezeptor NTCP auf der identischen Virushülle, die jeweils mit der präS1-Domäne des großen Hüllproteins die hochaffine Bindung an NTCP vermittelt (Hughes et al., 2011).

Die RNA des HDV selbst stellt allerdings nicht ausschließlich die Vorlage zur Proteinbiosynthese dar, sie enthält insbesondere auch sogenannte „self-cleaving Sequences“. Durch diese Sequenzen ist es möglich „Ribozyme“ auszubilden, die in diesem Fall als HDV Ribozyme bezeichnet werden (Alfaiate et al., 2015). Damit sind enzymartige Komplexe gemeint, die aus Nukleinsäuren bestehen und in der Lage sind, den RNA Strang, auf dem sie sich selbst aufhalten, zu schneiden (engl. „self-cleaving“).

Etwa 5 % aller chronisch infizierten HBV-Träger sind zusätzlich auch mit HDV infiziert (World Health Organisation, 2017). Diese Coinfektion verursacht ein schnelleres Fortschreiten der Krankheit, eine erhöhte Sterblichkeitsrate und eine erhöhte Inzidenz von HCC und Leberzirrhose (Sureau and Negro, 2016).

### 1.3 Das Na<sup>+</sup>/Taurocholate Cotransporting Polypeptide (NTCP)

Als Mitglied der „Solute Carrier Family 10“ (SLC10) stellt das „Na<sup>+</sup>/Taurocholate Cotransporting Polypeptide“ (NTCP, *SLC10A1*) einen spezifisch in der basolateralen Membran von Hepatozyten exprimierten Gallensäuretransporter dar (Geyer et al., 2006; Ananthanarayanan et al., 1994; Stieger et al., 1994). Zusammen mit einem weiteren Mitglied dieser Familie, dem „Apical Sodium-dependent Bile Acid Transporter“ (ASBT, *SLC10A2*) ist NTCP wesentlich an der Aufrechterhaltung des enterohepatischen Kreislaufs der Gallensäuren beteiligt (Anwer and Stieger, 2014). Dabei werden Gallensäuren im Dünndarm durch ASBT rückresorbiert und gelangen über das Pfortaderblut zurück zur Leber, wo sie durch NTCP wieder in die Hepatozyten aufgenommen werden. Die Transportvorgänge beider genannten Proteine werden durch den physiologischen Natriumgradienten energetisiert. Es handelt sich folglich um sekundär aktive Transportvorgänge, abhängig von der Aktivität der Natrium-Kalium-ATPase. Der Natriumgradient ist von extrazellulär nach intrazellulär gerichtet, womit sich ein Cotransport von Gallensäuren und Natriumionen ergibt. Die Stöchiometrie liegt dabei bei zwei Natriumionen, um ein Gallensäuremolekül transportieren zu können (Weinman, 1997).

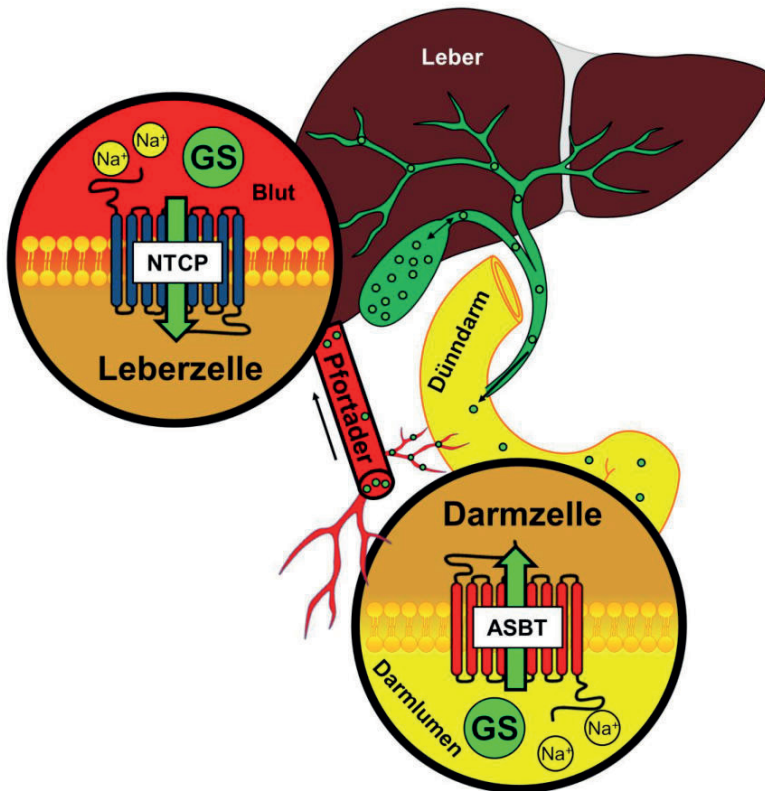


**Abbildung 2 – Der enterohepatische Kreislauf der Gallensäuren**

Diese Abbildung verdeutlicht die Rolle der beiden SLC10 Transporter NTCP und ASBT an der Zirkulation der Gallensäuren (GS) zwischen Leber und Darm. Zunächst werden Gallensäuren in der Leber synthetisiert und mit der Gallenflüssigkeit in der Gallenblase zwischengespeichert. Wenn durch Nahrungsaufnahme Bedarf an Gallensäuren im Darm besteht, wird die Gallenflüssigkeit in den Dünndarm abgegeben, wo die Gallensäuren Fette emulgieren. Im distalen Bereich des Dünndarms werden Gallensäuren zusammen mit Natriumionen (Na<sup>+</sup>) über ASBT reabsorbiert und gelangen über das Pfortaderblut zurück zur Leber. Dort werden diese ebenfalls gemeinsam mit Natriumionen über NTCP in die Leberzellen aufgenommen und anschließend erneut der Gallenflüssigkeit zugeführt. Damit ist der Kreislauf geschlossen. Da Gallensäuren nicht vollständig aus dem Darm zurückgewonnen werden können, muss stetig ein geringer Anteil in der Leber neu synthetisiert werden. Der Recyclingprozess der Gallensäuren ist energetisch sinnvoll, da die Neusynthese nur unter hohem energetischen Aufwand stattfindet.

Da NTCP und ASBT als erste Vertreter der SLC10 Familie identifiziert wurden, bezeichnet man diese Familie auch als „Sodium Bile Acid Cotransporter Family“ (Geyer et al., 2006). Derzeit zählt man noch vier weitere Proteine zur SLC10 Familie. Es handelt sich um P3 (*SLC10A3*), P4 (*SLC10A4*), P5 (*SLC10A5*), den „Sodium-dependent Organic Anion Transporter“ (SOAT, *SLC10A6*) und RCAS/SLC10A7 (Geyer et al., 2006; Godoy et al., 2007;



Fernandes et al., 2007; Geyer et al., 2007; Karakus et al., 2020). Diese Zuordnungen wurden aufgrund von Sequenzhomologien getroffen. Für die Mitglieder P3, P4, P5 und P7 konnte bislang keine signifikante Transportaktivität für Gallensäuren nachgewiesen werden. Eine Sonderstellung wird in diesem Fall SOAT zuteil. Vergleichende Studien der Transportproteine NTCP, ASBT und SOAT zeigten, dass die Taurin konjugierte Gallensäure Taurolithocholsäure bislang als einzige Gallensäure auch von SOAT als Substrat erkannt und transportiert wird (Grosser et al., 2021). Ansonsten stellt SOAT einen selektiven Transporter sulfatierter Steroide dar (Geyer et al., 2007). Für RCAS/SLC10A7 wird eine regulatorische Wirkung auf intrazelluläre Calciumsignalwege angenommen (Karakus et al., 2020). Allerdings wird RCAS/SLC10A7 bis zu seiner eindeutigen Charakterisierung zusammen mit den bisher ebenfalls nicht vollständig charakterisierten Proteinen P3, P4 und P5 als sogenannter „Orphan Carrier“ bezeichnet.

Die physiologische Hauptfunktion von NTCP besteht, wie bereits beschrieben, in dem Transport von Gallensäuren in Leberzellen. Als Substrate werden dabei sowohl unkonjugierte als auch Glycin oder Taurin konjugierte Gallensäuren erkannt (Hagenbuch et al., 1991; Grosser et al., 2021). Da Gallensäuren einen pKs von 5 bis 2 aufweisen, liegen sie bei einem physiologischen pH von 7,4 zu einem großen Anteil ionisiert vor (Hofmann and Hagey, 2008). Die resultierende negative Ladung stellt dabei einen wichtigen Aspekt bei der Substraterkennung dar, wie es unter anderem auch in Publikation I dieser Dissertationsschrift diskutiert wird (Kouzuki et al., 2000; Kirstgen et al., 2020).

Das Substratspektrum von NTCP beschränkt sich allerdings nicht ausschließlich auf Gallensäuren. So werden beispielsweise auch Steroidsulfate (Schroeder et al., 1998; Grosser et al., 2021), Schilddrüsenhormone (Friesema et al., 1999) und verschiedene 3-Hydroxy-3-Methylglutaryl-Coenzym A-(HMG-CoA)-Reduktasehemmer wie z.B. Rosuvastatin (Ho et al., 2006) transportiert. Generell scheint NTCP eine Rolle bei der sogenannten „hepatobiliären Clearance“ von Arzneistoffen zu spielen (Kim et al., 1999; Kouzuki et al., 1998; Kouzuki et al., 2000; Mita et al., 2006).

NTCP hat indirekt regulatorische Einflüsse auf Stoffwechselforgänge des Körpers. So fungieren primäre Gallensäuren als Liganden für den „Farnesoid X Receptor“ (FXR), der über die Herunterregulation der Cholesterin-7-alpha-Hydroxylase oder auch „Cytochrom P450 7A1“ (CYP7A1) die Neusynthese von Gallensäuren limitiert. In der Leber ist an dieser Rückkopplungsregulation der „small heterodimer partner“ (SHP) und das „liver receptor homolog-1“ (LRH-1) beteiligt. Im Darm gibt es eine Rückkopplungsschleife, die die

Expression des „fibroblast growth factor 15/19“ (FGF15/19) in Enterozyten und seine Bindung an den hepatischen FGF-Rezeptorkomplex beinhaltet (Wahlström et al., 2016).

Der G-Protein-gekoppelte Gallensäure Rezeptor 1 (GPBAR1 oder TGR5) ist ein weiterer Interaktionspartner der Gallensäuren mit regulatorischer Wirkung auf die Energie- und Glukosehomöostase. TGR5 wird durch die sekundären Gallensäuren Lithocholsäure und Deoxylithocholsäure aktiviert und veranlasst die Freisetzung von Trijodthyronin (T3) und die Sekretion des „glucagone-like peptide 1“ (GLP-1), das die Insulinsekretion stimuliert (Wahlström et al., 2016).

Es lässt sich also festhalten, dass NTCP durch seine Rolle bei der Aufrechterhaltung der enterohepatischen Zirkulation von Gallensäuren indirekt auch eine wichtige Funktion bei der Regulation von gallensäureabhängigen Stoffwechselfvorgängen des Körpers zukommt.

## **1.4 Viruseintritt in die Leberzelle**

Bis heute sind die Mechanismen, welche dem Eintritt (engl. „entry“) von HBV und HDV in Leberzellen zugrunde liegen, nicht vollständig geklärt. Allerdings hat die Entdeckung von NTCP als spezifischen hepatozellulären Rezeptor für beide Viren im Jahr 2012 stark zum Verständnis dieses Mechanismus beigetragen (Yan et al., 2012). Die aktuell gängige Meinung beschreibt eine zunächst unspezifische Interaktion der Viren mit Heparansulfat Proteoglykanen, welche die Oberfläche von vielen Zelltypen, unter anderem auch von Hepatozyten, säumen (Lamas Longarela et al., 2013). Darauf folgend findet eine hochaffine Bindung der Virionen an NTCP statt, welche laut Theorie schließlich in der Endozytose des Virus-Rezeptorkomplexes mündet (Fukano et al., 2019). Virusseitig ist die myristoylierte präS1-Domäne des großen viralen Hüllproteins (LHBs) an der Bindung mit dem Rezeptor beteiligt, wie bereits in Kapitel 1.1 erläutert. Auf der Seite von NTCP als Virusrezeptor konnte man mehrere Bereiche identifizieren, welche für die Virusbindung essentiell sind, insbesondere die Aminosäuren 157-165 des NTCP (Yan et al., 2012). Interessanterweise ergibt sich bei Mutation des Glycin an Position 158 zu Arginin ein Verlust der Bindungsfähigkeit der präS1-Domäne an NTCP bei erhaltener Gallensäuretransportaktivität (Müller et al., 2018). Diese Beobachtungen waren unter anderem ausschlaggebend dafür, dass im Rahmen dieser Dissertation die Möglichkeit der selektiven Hemmung der Virusrezeptorfunktion von NTCP mit chemischen Substanzen angenommen wurde, mit geringem Einfluss auf dessen Gallensäuretransportfunktion.

Des Weiteren konnten die Aminosäuren 84-87 als essentiell für eine erfolgreiche Infektion identifiziert werden, bei erhaltener Fähigkeit der Virusbindung (Ni et al., 2014; Yan et al., 2014).

Obwohl der genaue Ablauf des Viruseintritts in Leberzellen noch nicht vollständig geklärt ist, haben die bisher erläuterten Erkenntnisse über die Interaktion von Virus und zellulärem Rezeptor eine vielversprechende Therapiemöglichkeit eröffnet, bei der ein Kontakt von Virus und Rezeptor verhindert werden soll. Somit war der Weg zur Identifizierung von HBV und HDV Entry-Inhibitoren geebnet.

## **1.5 Therapieansätze**

Trotz der Verfügbarkeit einer Impfung gegen das HBV, die effektiv sowohl vor einer HBV als auch HDV Infektion schützt, zeigen die weltweite Prävalenz sowie die jährlichen Todeszahlen, dass dringend auch Therapieansätze gegen bestehende Infektionen benötigt werden (Robert Koch Institut, 2021). Die aktuell meist angewandten Therapien umfassen die Behandlung mit Interferon  $\alpha$  (IFN- $\alpha$ ) Derivaten und Nukleos(t)id Analoga (Martinez et al., 2020).

### **1.5.1 Interferon $\alpha$**

Derzeit existieren zwei pegylierte (PEG) Derivate des IFN- $\alpha$ , die für therapeutische Zwecke eingesetzt werden. Diese sind das PEG-IFN- $\alpha$ 2a, welches unter dem Handelsnamen Pegasys<sup>®</sup> von der Firma Roche vertrieben wird sowie PEG-IFN- $\alpha$ 2b, welches unter dem Namen Pegintron<sup>®</sup> von der Firma Merck produziert wird. Die verbesserte Pharmakokinetik mit verlängerter Halbwertszeit ermöglicht die wöchentliche subkutane Administration dieser Medikamente (Woo et al., 2017). Diese Interferone weisen sowohl direkt antivirale als auch immunmodulatorische Effekte auf (Prifti et al., 2021). Studien zeigen, dass ca. 30% der behandelten Patienten nach einem Jahr HBe Serokonversion aufweisen und in bis zu 7% der Fälle anhaltend reduzierte HBs Level beobachtet werden (Trépo et al., 2014; Janssen et al., 2005). Allerdings sind diese Zahlen nicht zufriedenstellend. Außerdem bringt die beschriebene Therapie einige Probleme mit sich. Eine dauerhafte Behandlung mit INF- $\alpha$  kann zu zahlreichen Nebenwirkungen führen. Diese äußern sich in grippeähnlichen Symptomen sowie Knochenmarksuppression, Müdigkeit bis hin zu Depressionen (Trépo et al., 2014; Prifti et al., 2021; Zoulim et al., 2016).

### **1.5.2 Nukleos(t)id Analoga**

Nukleos(t)id Analoga hemmen die Replikation der viralen DNA, indem sie als Substrate der Reversen Transkriptase einen frühzeitigen Abbruch der Transkription verursachen. Sie können

oral eingenommen werden und unterdrücken Virämien in bis zu 93% der Fälle, bei einjähriger Behandlung (Prifti et al., 2021). Allerdings treten beim Absetzen der Therapie nahezu immer Rückfälle auf, weshalb diese Medikamente ein Leben lang eingenommen werden müssen (Pierra Rouviere et al., 2020).

**Tabelle 1 – Nukleos(t)id Analoga**

<b>Zulassung</b>	<b>Wirkstoff</b>	<b>Handelsname</b>	<b>Bemerkungen</b>
1998	Lamivudin	Epivir <sup>®</sup> , Zeffix <sup>®</sup> , Heptodin <sup>®</sup> , Hepitec <sup>®</sup>	Resistenzbildung durch Mutationen der viralen Reversen Transkriptase
2002	Adefovir Dipivoxil	Hepsera <sup>®</sup> , Preveon <sup>®</sup>	Mittel der Wahl bei bestehender Resistenz; Überwachung der Nierenfunktion erforderlich
2005	Entecavir	Baraclude <sup>®</sup>	Medikament zur Erstbehandlung
2006	Telbivudin	Tyzeka <sup>®</sup> , Sebivo <sup>®</sup>	Den Wirkstoffen Lamivudin und Adefovir Dipivoxil überlegen; Nierenschonend; Nebenwirkungen wie Muskeltoxizität und periphere Neuropathie möglich
[2006]	Clevudin	Levovir <sup>®</sup> , Revovir <sup>®</sup>	Revidierung der Zulassung wegen skelettaler Myopathie
2008	Tenofovir Disoproxil Fumarat	Viread <sup>®</sup>	Fälle von Nephrotoxizität; selten Resistenzentwicklung
2016	Tenofovir Alafenamid Fumarat	Vemlidy <sup>®</sup>	Geringere Nephrotoxizität als Tenofovir Disoproxil Fumarat
2017	Besifovir Dipivoxil Maleat	Besivo <sup>®</sup>	Verbesserte toxikologische Eigenschaften
Derzeit in Entwicklung	Tenofovir Exalidex	-	Soll verbessertes Sicherheitsprofil aufweisen

Das erste Nukleos(t)id Analogon wurde 1998 in den USA zur Behandlung von HBV zugelassen (Pierra Rouviere et al., 2020). Es handelt sich um den Wirkstoff Lamivudin, welcher unter den Handelsnamen Epivir<sup>®</sup>, Zeffix<sup>®</sup>, Heptodin<sup>®</sup> und Hepitec<sup>®</sup> vertrieben wird. Limitierend für den Einsatz von Lamivudin ist die sich entwickelnde Resistenz durch Mutationen im YMDD (Tyrosin-Methionin-Asparaginsäure-Asparaginsäure) Motiv des Aktiven Zentrums der viralen reversen Transkriptase. Diese Resistenz tritt meist innerhalb von ein bis fünf Jahren nach Therapiebeginn auf (Kwon et al., 2013).

2002 wurde Adefovir Dipivoxil zugelassen, bekannt als Hepsera<sup>®</sup> oder Preveon<sup>®</sup>. Es wird als Mittel der Wahl bei bestehender Resistenz gegen Lamivudin eingesetzt. Allerdings sollte bei der Behandlung die Nierenfunktion überwacht werden (Hepatitis B Foundation, 2021).

Im Jahr 2005 wurde der Wirkstoff Entecavir zur Behandlung von HBV zugelassen, welcher heute noch ein gängiges Mittel für die Erstbehandlung darstellt (Pierra Rouviere et al., 2020). Er wird unter dem Handelsnamen Baraclude<sup>®</sup> vertrieben.

2006 wurde Telbivudin zugelassen und wird heute unter den Namen Tyzeka<sup>®</sup> und Sebivo<sup>®</sup> vermarktet (Hepatitis B Foundation, 2021). Studien zeigen, dass eine Therapie mit Telbivudin den beiden Wirkstoffen Lamivudin und Adefovir Dipivoxil überlegen ist (Liaw et al., 2009; Hou et al., 2008; Lai et al., 2007). Positiv zu vermerken ist die Tatsache, dass Telbivudin nierenschonend ist (Abd El Aziz et al., 2020). Allerdings können Nebenwirkungen wie Muskeltoxizität und periphere Neuropathie auftreten (Wong et al., 2018; Wu et al., 2016).

Auch Clevudin wurde 2006 in Südkorea und den Philippinen zugelassen und unter den Handelsnamen Levovir<sup>®</sup> und Revovir<sup>®</sup> vermarktet. Allerdings sorgten Fälle von skelettaler Myopathie, hervorgerufen durch induzierte mitochondriale Dysfunktion, für eine rasche Revidierung der Zulassung (Pierra Rouviere et al., 2020).

2008 wurde Tenofovir Disoproxil Fumarat unter dem Namen Viread<sup>®</sup> zugelassen. Allerdings ist auch hier die Nephrotoxizität ein limitierender Faktor, obwohl dieser Wirkstoff durch eine nur selten auftretende Resistenzenentwicklung von Interesse ist (Liu et al., 2017).

Das Derivat Tenofovir Alafenamid Fumarat, bekannt als Vemlidy<sup>®</sup>, wurde 2016 zugelassen und wird als Alternative zu Tenofovir Disoproxil Fumarat eingesetzt, mit geringerer renaler Toxizität (Prifti et al., 2021).

2017 wurde der Wirkstoff Besifovir Dipivoxil Maleat zugelassen, welcher stark verbesserte toxikologische Eigenschaften aufweist und als Besivo<sup>®</sup> gehandelt wird (Pierra Rouviere et al., 2020).

Ein weiterer Wirkstoff namens Tenofovir Exalidex, der ebenfalls die Sicherheit der Therapie verbessern soll, ist derzeit noch in der frühen klinischen Entwicklung (Lopatin, 2019).

Insgesamt treten bei der Behandlung mit Nukleos(t)id Analoga geringere Nebenwirkungen auf als bei der Therapie mit INF- $\alpha$ . Allerdings führen beide Therapieansätze nur in seltenen Fällen zu einer sogenannten funktionellen Heilung der Virusinfektion. Unter funktioneller Heilung versteht man die anhaltende Reduktion viraler Antigene und des viralen Genoms auf ein nicht

nachweisbares Niveau im Serum des Patienten nach Abschluss der Behandlung (Lok et al., 2017).

### **1.5.3 Entry-Inhibitoren**

Mit der Entdeckung von NTCP als spezifischen Rezeptor für den Eintritt (engl. „entry“) von HBV und HDV in Hepatozyten im Jahr 2012 ergab sich ein neuer Ansatz für potenzielle Therapien (Yan et al., 2012). Die spezifische Suche nach Substanzen, die eine Bindung von Virus an NTCP verhindern sollen, begann in diesem Moment. Solche Substanzen werden als „Entry-Inhibitoren“ bezeichnet.

Einen Durchbruch erzielte man im Juli 2020 als die europäische Arzneimittel-Agentur ein Präparat namens Hepcludex<sup>®</sup> als ersten Entry-Inhibitor zur Behandlung der HDV Infektion zugelassen hat (Zulassungsnummer EU/1/20/1446/001). Zuvor konnten sowohl in der Zellkultur als auch in humanisierten uPA/SCID Mäusen effektiv HBV Infektionsraten reduziert werden (Schulze et al., 2010; Volz et al., 2013). Es handelt sich bei Hepcludex<sup>®</sup> um ein synthetisches präS1 Peptid, welches am NTCP die Bindungsstellen für HBV und HDV blockiert. Weitere Untersuchungen am Menschen ergaben, dass dieses Peptid nach Applikation von 10 mg zu einem erhöhten Pegel an Gallensäuren im peripheren Blut führt (Blank et al., 2018). Somit beeinflusst dieser Entry-Inhibitor zusätzlich die Gallensäuretransportfunktion von NTCP. Allerdings beträgt die empfohlene tägliche Standarddosis dieses Medikamentes 2 mg, womit die getestete Dosis aus der genannten Veröffentlichung einer fünffachen Überdosierung entspricht (siehe Produktinformation Hepcludex<sup>®</sup>).

Grundsätzlich beweisen die Daten zu Hepcludex<sup>®</sup>, dass ein Therapieansatz mit Entry-Inhibitoren erfolgsversprechend scheint. Basierend auf dem genannten Prinzip sind bereits einige Studien abgelaufen, die auf die Identifizierung weiterer potenter Entry-Inhibitoren abzielten. Zu diesen Studien zählen ebenfalls jene, die in dieser Dissertationsschrift behandelt werden.

Folgende Substanzen sind in der Literatur als Entry-Inhibitoren genannt: Ezetimib (Lucifora et al., 2013), (-)-epigallocatechin-3-gallat (Huang et al., 2014), Proanthocyanidin (Tsukuda et al., 2017), Oolonghomobisflavan C (Fukano et al., 2019), Temsirolimus (Saso et al., 2018), Cyclosporin A und weitere Derivate (Liu et al., 2020; Shimura et al., 2017; Watashi et al., 2014; Nkongolo et al., 2014), Rosiglitazon (Donkers et al., 2017), Ciglitazon (Fukano et al., 2018), Irbesartan (Wang et al., 2015), Zafirlukast (Donkers et al., 2017), TRIAC (ein Thyroidhormon

Analog) (Donkers et al., 2017), Vanitarazin A (Kaneko et al., 2015), Ritonavir (Blanchet et al., 2014), Ro41-5253 (Tsukuda et al., 2015), Sulfasalazin und Chicago Sky Blue 6B (Donkers et al., 2017).

Vergleichbar mit den bisher genannten Substanzen, zielen aktuelle Studien darauf ab, monoklonale Antikörper ebenfalls als effektive HBV Entry-Inhibitoren einzusetzen (Wi et al., 2017; Hong et al., 2004; Zhang et al., 2016; Li et al., 2017). Klinische Studien der Phase I zeigten ein gutes Sicherheitsprofil sowie Wirksamkeit gegen HBV Infektionen bei kombinierter Gabe zweier monoklonaler Antikörper namens HBV-Ab17 und HBV-Ab19 (Galun et al., 2002).

#### **1.5.4 Weitere therapeutische Strategien**

##### *Angriff an der viralen cccDNA*

Die sogenannte „funktionelle Heilung“ der chronischen HBV Infektion ist definiert durch eine dauerhafte Inaktivierung der viralen cccDNA (Prifti et al., 2021; Zhao and Guo, 2020; Lopatin, 2019).

Studien zeigten, dass das „apolipoprotein B mRNA editing enzyme catalytic polypeptide 3“ (APOBEC3) in der Lage ist, cccDNA zu degradieren (Sawyer et al., 2004). Dieser Effekt lässt das genannte Protein für potentielle HBV Therapien interessant erscheinen. Weitere Studien zeigten, dass INF- $\alpha$  die Expression von APOBEC3 induziert (Bockmann et al., 2019). Allerdings kommen an dieser Stelle erneut die kritischen Punkte einer dauerhaften INF- $\alpha$  Therapie aus Kapitel 1.5.1 zu tragen.

Eine weitere Möglichkeit zur cccDNA Degradierung stellt ein Endonucleasesystem zur Genom-Editierung namens CRISPR/Cas9 (engl. „*Clustered Regularly Interspaced Short Palindromic Repeats/CRISPR associated Protein*“) dar. Dabei ist die CRISPR/Cas9 Endonuclease in einem Komplex mit einer „Leit-RNA“ (engl. „guide RNA“) gebunden, die zu spezifischen Regionen der viralen cccDNA passt. Der Komplex verursacht an den durch die RNA zugeordneten Bereichen der viralen cccDNA Strangbrüche (Prifti et al., 2021). Für die vollständige Inaktivierung der cccDNA bedarf es allerdings mehrerer verschiedener Leit-RNAs, die unterschiedliche Bereiche adressieren (Seeger and Sohn, 2016; Kostyushev et al., 2019). Weitere potentielle Nucleasesysteme sind durch die Zink-Finger- und die „*Transcription activator-like effector-*“ Nucleasen gegeben (Fanning et al., 2019; Mohd-Ismail et al., 2019). Die Genom-Editierung stellt heutzutage jedoch noch keine gängige Therapiemethode in der Medizin dar und bedarf noch weitreichender Forschung.

Zuletzt kann auch indirekt Einfluss auf die Formierung der cccDNA genommen werden, indem das HBx Protein gehemmt wird. Da das HBx Protein die Degradierung des sogenannten „*structural maintenance of chromosomes' complex 5/6*“ (Smc5/6) induziert, kann dieser Komplex nicht mehr die cccDNA Transkription unterdrücken (Seeger, 2018). Umgekehrt sorgt die Hemmung des HBx Proteins also dafür, dass eine Transkription der viralen cccDNA nicht mehr stattfinden kann, aufgrund der Aktivität von Smc5/6 (Seeger, 2018).

### *Immuntherapie*

Das menschliche Immunsystem ist nicht machtlos gegen eine HBV Infektion (Bertoletti and Gehring, 2006). So existieren Strukturen des angeborenen Immunsystems, die zu den sogenannten „*Pattern-Recognition Receptors*“ (PRRs) gehören. Es handelt sich dabei um Proteine, die an der Erkennung „*Pathogen-Associated Molecular Patterns*“ (PAMPs) beteiligt sind, welche bestimmte Strukturen von Krankheitserregern darstellen (Akira et al., 2006). Beispiele für PRRs stellen der „*toll-like receptor*“ (TLR) und „*retinoic acid inducible gene I*“ (RIG-I) dar (Prifti et al., 2021). Es finden derzeit diverse klinische Studien statt, welche Agonisten von TLR7, TLR8 und TLR9 auf ihre immunstimulatorische Wirkung untersuchen (Lucifora et al., 2018; Ma et al., 2018; Gehring and Protzer, 2019; Meng et al., 2019). Diese Stimulation des Immunsystems soll bei einer antiviralen Kombinationstherapie signifikant zur „funktionellen Heilung“ beitragen (Prifti et al., 2021).

### *Post-transkriptionale Kontrolle der viralen mRNA*

Die post-transkriptionale Kontrolle einer HBV Infektion soll auf mRNA Ebene geschehen. Dabei sollen Inhibitoren hoch spezifisch an der viralen mRNA binden und somit die Expression viraler Proteine durch Unterdrückung der Translation verhindern (Fanning et al., 2019). Dazu können sogenannte „siRNAs“ (engl. „*small interfering RNAs*“) verwendet werden, welche zwischen 20 und 30 Nukleotide umfassen und mit der viralen mRNA interagieren (Grimm et al., 2011). Nachteile ergeben sich aus der Notwendigkeit subcutaner oder sogar intravenöser Applikation dieser Stoffe und potentieller „off-target“ Bindung, d.h. die Bindung an andere Strukturen als ausschließlich der viralen mRNA, sowie der gegebenenfalls auftretenden Hepatotoxizität (Lok et al., 2017). Trotzdem befindet sich beispielsweise die Substanz JNJ-3989 als gemeinsames Projekt der Unternehmen Arrowhead Pharmaceuticals und Janssen Pharmaceutica in klinischen Studien der Phase II und zeigt bisher gute Wirksamkeit gegen HBV, sowie Sicherheit und keine schwerwiegenden Arzneimittelinteraktionen (Lopatin, 2019; Soriano et al., 2020).



Alternativ können auch sogenannte „antisense“ Oligonukleotide eine Degradierung der viralen mRNA verursachen. Sie stellen einsträngige, kurze DNA oder RNA Fragmente dar, die ihrem Namen entsprechend „entgegen dem ursprünglichen Sinn“, d.h. entgegengesetzt zur ursprünglichen Basensequenz der viralen mRNA, aufgebaut sind und somit komplementär an diese binden (Prifti et al., 2021). Die finale Degradierung der Komplexe geschieht schließlich durch die Ribonuklease H der Wirtszelle (Billioud et al., 2016).

#### *Inhibitoren der viralen Ribonuklease H*

Auch HBV verwendet eine Ribonuklease H bei seinem Replikationsvorgang. Während der Synthese der viralen negativ Strang DNA durch die virale Reverse Transkriptase (vgl. Kapitel 1.1) degradiert die virale Ribonuklease H die prägenomische RNA des HBV, um die Bildung von DNA:RNA Hybriden zu verhindern (Edwards et al., 2019; Tavis and Lomonosova, 2015). Die Inhibition der viralen Ribonuklease H führt also zu diesen Hybridformen, welche in nicht infektiösen Virionen resultieren (Gerelsaikhhan et al., 1996). Dieser Therapieansatz bietet ebenfalls vielversprechende synergistische Effekte für potentielle Kombinationstherapien gegen HBV (Prifti et al., 2021).

#### *Inhibitoren bzw. Modulatoren der Nukleokapsid Bildung*

Man unterscheidet zwei Klassen von Inhibitoren bzw. Modulatoren der Nukleokapsid Bildung. Zur Klasse I der sogenannten „core protein allosteric modulators“ (CpAMs) zählt man Heteroaryldihydropyrimidine, welche die Bildung deformierter Nukleokapside verursachen (Morikawa et al., 2016). Klasse II besteht aus Phenylpropenamiden und Sulfamoylbenzamid, die die Bildung morphologisch normaler Nukleokapside bewirken, denen jedoch das Virale Genom fehlt (Prifti et al., 2021; Yang et al., 2019). Als Beispiel eines Vertreters der Klasse II lässt sich die Substanz NVR3-778 nennen, welche als Sulfamoylbenzamid-Derivat in den USA entwickelt wurde und derzeit in klinischen Studien der Phase Ia (NCT02112799) getestet wird (Soriano et al., 2020). Es kann oral eingenommen werden und zeigt synergistische Effekte in Kombination mit PEG-INF- $\alpha$  (Prifti et al., 2021).

## 1.5.5 Laufende klinische Studien zur HBV-Therapie

Tabelle 2: Studienlagen 2021 zur HBV-Therapie.

Studien-Nr.	Wirkstoff/e	Titel	Ziel	Phase
NCT05017116	RBD1016	A Single and Repeated Dose Escalation of RBD1016 in Subjects With Chronic Hepatitis B Virus (HBV) Infection.	Analyse von Wirkung und Sicherheit/Verträglichkeit; Pharmakokinetik	1
NCT04069858	Entecavir (Baracle®)	Maintaining Antiviral Efficacy After Switching to Generic Entecavir 1 mg for Chronic Hepatitis B.	Analyse von Wirkung	4
NCT04507269	VIR-2218	Study of VIR-2218 in Patients With Chronic Hepatitis B in Mainland China.	Analyse von Wirkung und Sicherheit/Verträglichkeit; Pharmakokinetik	2
NCT03471624	Tenofovir Alafenamide	Treatment Outcomes in Chronic Hepatitis B Patients on Sequential Therapy With Tenofovir Alafenamide (TAF).	Analyse von Wirkung und Sicherheit/Verträglichkeit	4
NCT03772249	DCR-HBVS	Study of Safety and Tolerability of DCR-HBVS.	Analyse von Sicherheit/Verträglichkeit	1
NCT03801798	GC1102	A Study of GC1102(Recombinant Hepatitis B Immunoglobulin) in Chronic Hepatitis B Patients.	Analyse von Wirkung	2
NCT04465890	ASC22	A Phase II Study of Subcutaneously Injected PD-L1 Antibody ASC22 in Chronic Hepatitis B Patients.	Analyse von Wirkung	2
NCT04032860	Tenofovir Disoproxil; Entecavir	RCT of Different Effects of Nucleot(s)ide Analogues on the Prognosis of HBV-HCC Patients After Curative Resection.	Analyse der Sterblichkeit	4
NCT04182321	Metformin & Entecavir	Adding Metformin to the Standard Treatment for Patients With HBeAg-Negative Chronic Hepatitis B.	Analyse von Wirkung und Sicherheit/Verträglichkeit	-
NCT03905655	Nitazoxanide	Study of Nitazoxanide Compared to Placebo in Subjects With HBeAg-Negative Chronic Hepatitis B.	Analyse von Wirkung	2
NCT02849132	Entecavir	Effect of Entecavir Treatment on Regression and Disease Outcome in HBV-induced Liver Fibrosis and Cirrhosis Patients.	Analyse von Wirkung und Sicherheit/Verträglichkeit	4
NCT01519960	PEG-IFN- $\alpha$ 2a	A Study of Pegasys (Peginterferon Alfa-2a) Versus Untreated Control in Children With HBeAg Positive Chronic Hepatitis B.	Analyse von Wirkung	3
NCT03084250	PEG-IFN- $\alpha$ 2a	The Investigation of Peginterferon Alfa-2a on Optimal in Chronic Hepatitis B Patients Who Have a High Risk of HCC.	Analyse von Wirkung	4

Studien-Nr.	Wirkstoff/e	Titel	Ziel	Phase
NCT01369212	PEG-IFN- $\alpha$ 2a	Combination Therapy of Pegylated Interferon Alfa-2a and Tenofovir Versus Tenofovir Monotherapy in Chronic Hepatitis B.	Analyse der Wirkung	3
NCT01651403	Tenofovir Disoproxil Fumarate	Study to Evaluate the Antiviral Efficacy, Safety and Tolerability of Tenofovir Disoproxil Fumarate Versus Placebo in Pediatric Participants With Chronic Hepatitis B Infection.	Analyse der Wirkung	3
NCT02600117	Tenofovir disoproxil fumarate	Use of TDF in Patients With Inactive Chronic Hepatitis B Infection.	Analyse der Wirkung	3
NCT01937806	Besifovir	Phase 3 and Extensional Study of Besifovir.	Analyse der Wirkung	3
NCT04365933	EYP001a	A Study of the Oral Farnesoid X Receptor Modulator EYP001a to Assess Its Safety and Anti-viral Effect in Chronic Hepatitis B Patients in Combination With Pegylated Interferon alpha2a Alone and With Entecavir.	Analyse von Wirkung und Sicherheit/Verträglichkeit; Pharmakokinetik	2
NCT03123653	PEG-IFN- $\alpha$ 2b	To Study the Efficacy of PEG-IFN Alpha in HBeAg Negative Chronic Hepatitis B Patients After Stopping Nucleotide Analogue Therapy.	Analyse der Wirkung	-
NCT03489239	Tenofovir Alafenamide	Entecavir to TAF Switch.	Analyse von Wirkung und Sicherheit/Verträglichkeit	3
NCT03585322	APG-1387	APG-1387 Study of Safety, Tolerability ,PK/PD in Patients With Chronic Hepatitis B.	Analyse von Wirkung und Sicherheit/Verträglichkeit; Pharmakokinetik	1
NCT04449029	GSK3228836	A Study of GSK3228836 in Participants With Chronic Hepatitis B (CHB).	Analyse von Wirkung und Sicherheit/Verträglichkeit; Pharmakokinetik	2
NCT04846491	PEG-IFN- $\alpha$ 2b	A Study of Peginterferon Alfa-2b Combined With TDF in Patients With Chronic Hepatitis B.	Analyse der Wirkung	3
NCT02836249	Tenofovir Alafenamide	Tenofovir Alafenamide Versus Tenofovir Disoproxil Fumarate for Treatment of Hepatitis B e Antigen-Positive Hepatitis B (China).	Analyse von Wirkung und Sicherheit/Verträglichkeit	3
NCT02836236	Tenofovir Alafenamide	Tenofovir Alafenamide Versus Tenofovir Disoproxil Fumarate for Treatment of Hepatitis B e Antigen-Negative Hepatitis B (China).	Analyse von Wirkung und Sicherheit/Verträglichkeit	3

Studien-Nr.	Wirkstoff/e	Titel	Ziel	Phase
NCT01940471	Tenofovir Alafenamide	Tenofovir Alafenamide Versus Tenofovir Disoproxil Fumarate for Treatment of Hepatitis B e Antigen-Positive Hepatitis B.	Analyse von Wirkung und Sicherheit/Verträglichkeit	3
NCT02937779	Tenofovir disoproxil fumarate	Tenofovir As Prevention Of Hepatitis b Mother-to-child Transmission.	Analyse von Wirkung und Sicherheit/Verträglichkeit	4
NCT01940341	Tenofovir Alafenamide	Tenofovir Alafenamide Versus Tenofovir Disoproxil Fumarate for Treatment of Hepatitis B e Antigen-Negative Hepatitis B.	Analyse von Wirkung und Sicherheit/Verträglichkeit	3
NCT04465916	EYP001a	Study of EYP001a to Assess Its Safety and Anti-viral Effect in CHB Patients in Combination With NA (ETV or TD).	Analyse von Wirkung und Sicherheit/Verträglichkeit; Pharmakokinetik	2
NCT03620474	PRI-724	Safety and Effectiveness of PRI-724 for Hepatitis C or B Virus Derived Liver Cirrhosis.	Analyse von Wirkung und Sicherheit/Verträglichkeit; Pharmakokinetik	2
NCT03982186	JNJ-73763989; JNJ-56136379	A Study of Different Combination Regimens Including JNJ-73763989 and/or JNJ-56136379 for the Treatment of Chronic Hepatitis B Virus Infection.	Analyse von Wirkung und Sicherheit/Verträglichkeit; Pharmakokinetik	2
NCT04189276	T101	Safety and Efficacy of Therapeutic Hepatitis B Adenovirus Injection (T101) Combined With Nucleoside (Acid) Analogues in Chronic Hepatitis B Patients.	Analyse von Wirkung und Sicherheit/Verträglichkeit	2
NCT04129554	JNJ-73763989; JNJ-56136379; Nukleos(t)id Analoga	A Study of JNJ 73763989+JNJ 56136379+Nucleos(t)Ide Analog (NA) Regimen Compared to NA Alone in e Antigen Negative Virologically Suppressed Participants With Chronic Hepatitis B Virus Infection.	Analyse von Wirkung und Sicherheit/Verträglichkeit; Pharmakokinetik	2

Quelle: <https://clinicaltrials.gov/>

## 1.5.6 Laufende klinische Studien zur HDV-Therapie

Tabelle 3: Studienlage 2021 zur HDV-Therapie.

Studien-Nr.	Wirkstoff/e	Titel	Ziel	Phase
NCT01316185	EBP921	Proof-of-concept Study Evaluating the Safety and Efficacy of EBP921 in Delta Hepatitis (HDV).	Analyse der Wirkung	1
NCT04166266	Bulevirtide	Observatory of Efficacy and Safety of Bulevirtide in Patients With Chronic HBV/HDV Co-infection.	Analyse von Wirkung und Sicherheit/Verträglichkeit	-
NCT03719313	Lonafarnib; Ritonavir	Study of the Efficacy and Safety of Lonafarnib / Ritonavir With and Without Pegylated Interferon -Alfa-2a.	Analyse von Wirkung und Sicherheit/Verträglichkeit	3
NCT02968641	Lonafarnib	A Study of Lonafarnib With or Without Ritonavir in Patients With HDV.	Analyse von Wirkung und Sicherheit/Verträglichkeit	2
NCT04535544	JNJ-73763989; Nucleos(t)id Analoga	A Study of JNJ-73763989 + Nucleos(t)ide Analog in Participants Co-Infected With Hepatitis B and Hepatitis D Virus.	Analyse von Wirkung und Sicherheit/Verträglichkeit	2
NCT04847440	ATI-2173; Tenofovir Disoproxil Fumarate	A Study of Safety and Efficacy of ATI-2173 in Combination With Tenofovir Disoproxil Fumarate in Subjects With Chronic Hepatitis B Virus Infection and in Subjects With Hepatitis D Virus Coinfection.	Analyse von Wirkung und Sicherheit/Verträglichkeit; Pharmakokinetik	2
NCT03099278	Ezetimib	Ezetimibe for Patients With Chronic Hepatitis D.	Analyse der Wirkung	2
NCT04638439	Ropeginterferon Alfa-2b (P1101); Nivolumab	The Safety and Efficacy of Sequential Treatment of Ropeginterferon Alfa-2b (P1101) and Anti-PD1 in Interferon-Naïve Adults With Chronic Hepatitis B or D Infection.	Analyse von Wirkung und Sicherheit/Verträglichkeit	1

Quelle: <https://clinicaltrials.gov/>

Die in Tabellen 2 und 3 gelisteten klinischen Studien zielen auf neue potentielle Therapiemöglichkeiten gegen bestehende HBV und HDV Infektionen ab und sind Teil des klinischen Zulassungsprozesses. Teilweise geht es auch darum, bestehende Behandlungsschemata zu optimieren. Die große Zahl der Studien zu HBV im Vergleich zu den nur acht Studien zu HDV lässt sich damit erklären, dass eine erfolgreiche Bekämpfung des HBV auch Konsequenzen auf HDV hat. Wie in Kapitel 1.2 bereits erläutert, kann HDV ohne eine bestehende HBV Infektion keinen vollständigen Replikationszyklus durchlaufen. Mit der

Ausrottung von HBV könnte man also wahrscheinlich sprichwörtlich zwei Fliegen mit einer Klappe schlagen.

Zusammenfassend beweist die Datenlage zu den klinischen Studien allerdings erneut die Notwendigkeit neuer Therapiemöglichkeiten von HBV und HDV Infektionen. Daher wird große Hoffnung insbesondere in die Entwicklung von Entry-Inhibitoren gesetzt.

## **1.6 Bioinformatische Applikationen**

Für die computergestützte Identifizierung reaktiver Substanzen für eine definierte Fragestellung an einer bekannten Zielstruktur kann auf verschiedene bioinformatische Applikationen zurückgegriffen werden. Folgend werden gängige Methoden vorgestellt und erläutert.

### **1.6.1 Pharmakophor Modelle**

Als Pharmakophor bezeichnet man ein Modell, das eine Ansammlung chemischer Gruppen in einer definierten dreidimensionalen Anordnung darstellt, die Einfluss auf die Aktivität an einer biologischen Zielstruktur haben (Schaller et al., 2020). Die darin abgebildeten funktionellen Charakteristika stellen Wasserstoffbrücken-Akzeptoren, Wasserstoffbrücken-Donatoren, hydrophobe Gruppen, sowie positiv und negativ ionisierbare Gruppen dar, die jeweils als Sphären mit definiertem Durchmesser dargestellt werden (Schaller et al., 2020; Santana et al., 2021). Im Falle der Wasserstoffbrückenwechselwirkungen sind diese Sphären zusätzlich mit Vektoren versehen, welche die Richtung der Wechselwirkung von potentiellm Ligand und Zielstruktur angeben. Ergänzend zu den Bereichen, die sich positiv auf eine Interaktion von Ligand und Zielstruktur auswirken, können zusätzlich Bereiche in der dreidimensionalen Darstellung des Modells errechnet werden, die nicht von einem Liganden tangiert werden sollten, da dies potentiell zu einem Verlust der Aktivität des Liganden an der Zielstruktur führt (Dixon et al., 2006). Diese Bereiche werden „*excluding values*“ (engl. für ausschließende Werte) genannt.

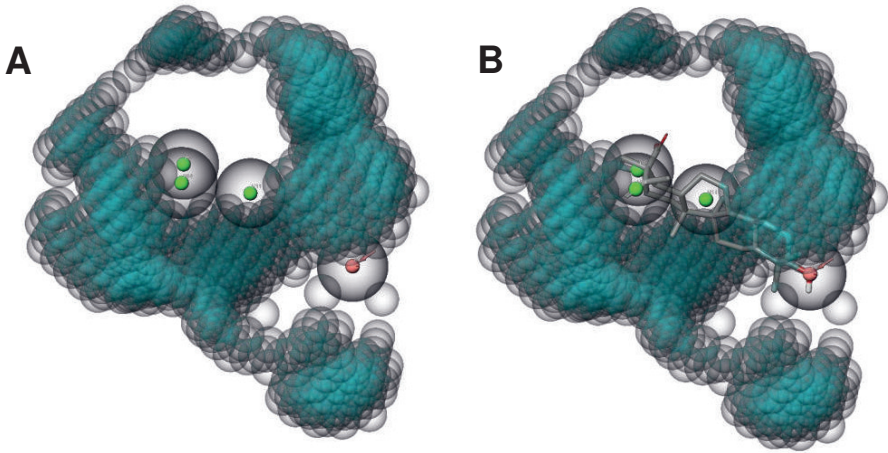


**Abbildung 3 – Grafische Darstellung eines Pharmakophor Modells**

Diese Abbildung zeigt die grafische Darstellung eines leeren Pharmakophor Modells (A) und desselben Modells mit einem passenden Liganden am Beispiel von Betulinsäure (B). Dieses Modell stammt aus Publikation III dieser Dissertationsschrift und beschreibt die Grundvoraussetzungen für eine Hemmung der präS1 Peptid Bindung durch Liganden am NTCP. Es besteht aus drei Sphären mit grünem Zentrum, welche hydrophobe Bereiche beschreiben und einer Sphäre mit rotem Zentrum und Vektorpfeilen, die die räumliche Orientierung einer Wasserstoffbrückenakzeptor Wechselwirkung beschreiben. Die kleineren blauen Sphären beschreiben „*excluding values*“. Ein optimaler Inhibitor der Bindung des präS1 Peptides an NTCP sollte alle vier dargestellten funktionellen Charakteristika des Modells abdecken, ohne dabei die „*excluding values*“ zu tangieren. Dies ist am Beispiel der Betulinsäure gezeigt (B).

Bei der Generierung eines Pharmakophor Modells unterscheidet man im Allgemeinen zwei Varianten. Bei Vorhandensein einer Kristallstruktur des zu untersuchenden Zielproteins mit gebundenem aktiven Liganden, kann auf den sogenannten Struktur basierten Ansatz zurückgegriffen werden (Jiang et al., 2020). Dabei richtet sich die Anordnung und Art der funktionellen Charakteristika des Modells nach dem gebundenen aktiven Liganden und dessen Interaktion mit dem Zielprotein.

In der vorliegenden Dissertationsarbeit konnte nicht auf eine valide Struktur des NTCP zurückgegriffen werden, weshalb hier die zweite Variante zur Erzeugung eines Pharmakophor Modells Anwendung gefunden hat. Man spricht vom Liganden basierten Ansatz, weil alle Informationen zur Generierung des Modells rein aus Daten zu Liganden stammen, deren Interaktion mit der Zielstruktur experimentell nachgewiesen wurde (Pal et al., 2019). Dies setzt ausgiebige experimentelle Vorarbeit voraus, bei der zunächst Daten zu den Aktivitäten strukturell diverser chemischer Verbindungen an der Zielstruktur zusammengetragen werden müssen (z.B.  $IC_{50}$ ,  $EC_{50}$ ,  $K_i$ , etc.). Bei der Aufarbeitung der experimentellen Daten wird bei

Pharmakophor Modellierung kategorisch vorgegangen. Dies bedeutet, dass die experimentell untersuchten Liganden für das jeweilige Zielprotein entweder der Kategorie „aktiv“ oder „inaktiv“ zugeordnet werden. Liganden, die weder eindeutig als aktiv, noch inaktiv kategorisiert werden können, werden für die folgende bioinformatische Aufarbeitung ausgeschlossen, um das Modell nicht zu verzerren. Mit der verwendeten Software wird daraufhin ein sogenanntes „*flexible ligand alignment*“ der kategorisierten Liganden durchgeführt. Die dreidimensionalen Strukturdaten der Liganden werden dabei von der Software verarbeitet und eine Überlagerung aller eingespeister Liganden möglichst deckungsgleich durchgeführt. Je nach Vorhandensein von flexiblen Strukturen, werden einzelne Liganden dabei so „zurecht gebogen“, dass sie zu den nicht flexiblen Liganden passen. Daher auch der Name dieses wichtigen Schrittes. Wenn die Überlagerung stattgefunden hat, wird eine frei wählbare Anzahl chemischer Gruppen definiert, welche alle Liganden in dieser Überlagerung gemeinsam haben. Diesen Gruppen werden dann die oben genannten funktionellen Charakteristika zugeordnet. So werden die Art und Position der einzelnen Pharmakophor Punkte festgelegt (Dixon et al., 2006). Man spricht hier vom sogenannten „*common feature pharmacophore*“ (engl. für Pharmakophor gemeinsamer Merkmale).

Die oben genannten „*excluding values*“ werden anhand der Strukturdaten der Liganden definiert, die als inaktiv kategorisiert sind. Diese Liganden können gegebenenfalls auch alle Pharmakophor Punkte abdecken, allerdings können zusätzlich vorhandene Seitengruppen, welche außerhalb der Pharmakophor Punkte liegen, negativen Einfluss auf die Interaktion mit dem Zielprotein haben. Ob dies durch sterische Hinderung, das Vorhandensein störender Ladungen oder sonstiger physikochemischer Eigenschaften hervorgerufen wird, ist von dem jeweiligen Liganden abhängig.

Pharmakophor Modelle werden immer intensiver für virtuelle Screening Vorhaben, Leitstrukturoptimierung und sogenanntem „*de novo drug design*“ eingesetzt (da Costa et al., 2019; El Kerdawy et al., 2019; Jade et al., 2020). Sie geben dabei die Richtschnur dafür, welche Grundeigenschaften eine Substanz aufweisen muss, um an der Zielstruktur einen gewünschten Effekt zu erzielen.

### **1.6.2 Modelle zur quantitativen Analyse der Struktur-Wirkungs-Beziehungen (QSAR)**

Im Gegensatz zum reinen Pharmakophor Modell, das qualitative Analysen der Wirkung von Liganden in Bezug auf eine Zielstruktur erlaubt (aktiv vs. inaktiv), können mit sogenannten „*Quantitative Structure-Activity Relationship*“ (QSAR) Modellen quantitative Analysen durchgeführt werden (Dixon et al., 2016). Diese Methode dient dazu, für bisher nicht



experimentell getestete Substanzen, Aussagen über deren Wirkung an einer definierten Zielstruktur zu treffen. Es werden also Vorhersagen getroffen, bei denen einer beliebigen chemischen Verbindung, auf Grundlage des QSAR Modells, ein fixer Zahlenwert für eine bestimmte Art der Aktivität (z.B.  $IC_{50}$ ,  $EC_{50}$ ,  $K_i$ , etc.) an der Zielstruktur zugewiesen wird.

Vom Grundprinzip ist zur Erzeugung eines QSAR Modells die gleiche Vorarbeit nötig, wie bereits in Kapitel 1.6.1 zur Erzeugung eines Pharmakophor Modells beschrieben. Allerdings wird in diesem Fall die bioinformatische Aufarbeitung nicht kategorisch, sondern kontinuierlich vorgenommen. Es findet also keine Unterteilung in aktive oder inaktive Untergruppen statt, sondern jedem getesteten Liganden wird dessen spezifische Aktivität an der Zielstruktur, beispielsweise in Form eines ermittelten  $IC_{50}$  Wertes, zugeordnet. Wie bei der Erzeugung des Pharmakophor Modells folgt auch hier die flexible Überlagerung aller eingespeister Liganden.

Ab diesem Punkt können verschiedene Arten von QSAR Modellen generiert werden. Zum einen kann zunächst ein Pharmakophor Modell erzeugt werden. Dieses Modell unterscheidet sich allerdings zu dem beschriebenen Modell aus Kapitel 1.6.1 darin, dass die gemessene Aktivität eines Liganden mit dessen „Passgenauigkeit“ in das Pharmakophor Modell korreliert wird (Dixon et al., 2016; Dixon et al., 2006). Dies bedeutet, dass ein Ligand, der optimal die Pharmakophor Punkte besetzt, eine hohe Aktivität, z.B. in Form eines niedrigen  $IC_{50}$  Wertes, aufweist. Wohingegen ein Ligand, der die Pharmakophor Punkte suboptimal besetzt, als Konsequenz eine niedrige Aktivität an der Zielstruktur zeigt, z.B. in Form eines hohen  $IC_{50}$  Wertes. Dabei können die einzelnen Pharmakophor Punkte unterschiedlich gewichtet sein. Als Beispiel kann es vorkommen, dass z.B. der Pharmakophor Punkt eines Wasserstoffbrückenakzeptors auf jeden Fall optimal besetzt sein muss, damit ein Ligand Aktivität an der Zielstruktur zeigt, wohingegen eine suboptimale Besetzung beispielsweise eines hydrophoben Bereiches des Modells lediglich eine gewisse Reduktion der Aktivität verursacht. Diese Variante der QSAR Analyse kann man als relativ grob beschreiben, da nur die Bereiche von Liganden in die Vorhersageberechnung der Aktivität mit einbezogen werden, die auch mit den Pharmakophor Punkten interagieren. Man nennt diese Variante die Pharmakophor basierte Methode (Dixon et al., 2006). Sie findet vor allem dann Anwendung, wenn die zur Generierung des Modells herangezogenen Liganden strukturell sehr unähnlich sind (Dixon et al., 2006).

Eine andere Möglichkeit zur Erstellung eines QSAR Modells stellt die Atom basierte Methode dar. Dabei wird jedes einzelne Atom eines Liganden berücksichtigt und mit in die Korrelation

der Struktur-Wirkungs-Beziehung eingebunden (Dixon et al., 2006). Dabei wird ausgehend von den flexibel überlagerten Liganden zur Generierung des Modells die räumliche Anordnung jedes einzelnen Atoms mit der Wirkung des entsprechenden Liganden korreliert. Als Regressionsmethode wird dabei die Regression der partiellen kleinsten Quadrate verwendet (engl. „*partial least squares*“, PLS). Das Modell selbst kann grafisch dargestellt werden und repräsentiert die relativen räumlichen Anteile von Bereichen mit Wasserstoffbrücken-Donatoren, sowie hydrophober/unpolarer, negativ ionischer, positiv ionischer und elektronenziehender Bereiche am Gesamtmodell, das aus den überlagerten Liganden hervorgeht (Dixon et al., 2016). Außerdem ist das Modell nach den Vorzeichen der Koeffizienten gefärbt: blau für positive Koeffizienten und rot für negative Koeffizienten. Positive Koeffizienten bedeuten eine Zunahme der Aktivität, negative Koeffizienten eine Abnahme.

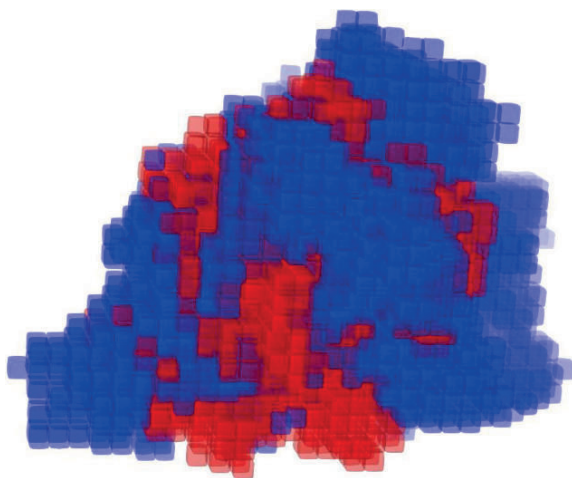


**Abbildung 4 – Grafische Darstellung eines Atom basierten QSAR Modells**

Diese Abbildung zeigt die grafische Darstellung eines Atom basierten QSAR Modells. Es stammt aus Publikation III dieser Dissertationsschrift und beschreibt die Struktur-Wirkungs-Beziehung für die Hemmung der präS1 Peptid Bindung durch Liganden am NTCP. Das Modell ist nach den Vorzeichen der Koeffizienten gefärbt: blau für positive Koeffizienten und rot für negative Koeffizienten. Positive Koeffizienten bedeuten eine Zunahme der hemmenden Aktivität, negative Koeffizienten eine Abnahme. Die Darstellung ist als dreidimensionales Gebilde zu betrachten, bestehend aus Würfeln mit einer Kantenlänge von jeweils einem Ångström ( $1\text{Å} = 10^{-10}\text{ m}$ ). Die verwendete Software (MAESTRO Molecular Modeling Interface, SCHRÖDINGER, Inc.) hinterlegt für jeden dargestellten Würfel die Anteile von Bereichen mit Wasserstoffbrücken-Donatoren, sowie hydrophober/unpolarer, negativ ionischer, positiv ionischer und elektronenziehender Bereiche. Ob sich das Vorhandensein des jeweiligen Anteils positiv oder negativ auf die Aktivität auswirkt, ist farblich dargelegt, wie vorhin beschrieben.

Für die Bewertung des Modells hat sich eine Methode etabliert, bei der nicht alle Liganden, zu denen Aktivitätsdaten ermittelt wurden, zur Erzeugung des Modells herangezogen werden. In

der Regel werden 20-30% der Liganden zunächst ausgeklammert und dienen als sogenanntes Test Set. Aus den anderen 70-80% der Liganden, auch als Training Set bezeichnet, wird das QSAR Modell generiert und dessen Vorhersagekraft dann anhand des Test Sets erstmalig überprüft (Dixon et al., 2006). Die Aufteilung in Training Set und Test Set geschieht nicht nach einem erkennbaren Schema, sondern willkürlich. Daher wird dieser Split des Datensatzes viele Male durchgeführt und resultiert jedes Mal in einem anderen QSAR Modell. Wie stark sich die jeweiligen Modelle voneinander unterscheiden, hängt von den zugrundeliegenden Daten ab. Es kann eine Größe errechnet werden, welche die „Stabilität“ des Modells beschreibt. Diese Größe ist jedoch kein Gütekriterium, sondern gibt lediglich an, ob bei erneutem Split des Datensatzes in Training und Test Set ein signifikant anderes QSAR Modell zu erwarten ist. Letztlich ist das Ziel dieser Methode, ein Modell zu entwickeln, das einen möglichst großen Anteil korrekter Aktivitätsvorhersagen für nicht in das Modell mit einbezogene Liganden trifft (Dixon et al., 2016). Der Anteil korrekter Vorhersagen dieser Methode liegt laut Literatur zwischen 1% und 40% (Neves et al., 2018). Basierend auf den beschriebenen Zusammenhängen wurden inzwischen einige Algorithmen entwickelt, welche eine automatisierte Wiederholung der Generierung von QSAR Modellen ermöglicht. Ein maschineller Lernprozess (engl. „*machine learning*“) soll dabei in dem optimalen Modell für den als Input verwendeten Datensatz resultieren. Ein Beispiel dafür stellt das System *AutoQSAR* des Herstellers SCHRÖDINGER, Inc. dar, welches über das MAESTRO Molecular Modeling Interface ausgeführt werden kann (Dixon et al., 2016). Weitere Vertreter stellen *QSAR Workbench* (Cox et al., 2013) und *AstraZeneca's AutoQSAR* (Wood et al., 2011) dar.

Auch QSAR Studien werden für virtuelle Screening Vorhaben, Leitstrukturoptimierung und de novo drug design eingesetzt und stellen eine Ergänzende Methode zur reinen Pharmakophor Modellierung dar (Santana et al., 2021).

### 1.6.3 Virtuelles Screening

Das Verfahren der Computer gestützten Durchmusterung großer digitaler Datenbanken nennt man „virtuelles Screening“ (VS). Dieses innovative Verfahren leistet mit der heutzutage verfügbaren Technik einen wichtigen Beitrag zur Identifizierung neuer Substanzen mit spezifischer Bioaktivität an definierten Zielmolekülen, welche auch als „Targets“ (engl. für Ziele) bezeichnet werden. Dabei unterscheidet man zwischen Liganden basiertem und Struktur basiertem VS (Santana et al., 2021). Bei Liganden basiertem VS basieren die genutzten Computermodelle allein auf den Daten der Substanzen, die bereits experimentell am Target getestet wurden. Diese Daten stellen topologische, physikochemische und strukturelle

Eigenschaften der Liganden dar (Garcia-Hernandez et al., 2019). Bei Struktur basiertem VS hingegen basieren die verwendeten Modelle auf Daten zur dreidimensionalen Struktur des Targets, welche im Idealfall eine Kristallstruktur des Zielmoleküls mit einem gebundenen aktiven Liganden darstellen (da Costa et al., 2019; Santana et al., 2021). Dies ermöglicht auch die Durchführung von sogenannten „docking“ Studien, bei denen Substanzen virtuell auf ihre Interaktion mit spezifischen Bereichen des Targets untersucht werden (Wang et al., 2020). Da für den humanen NTCP derzeit keine Kristallstruktur existiert, ist bei dieser Dissertationsarbeit auf das Liganden basierte VS zurückgegriffen worden, wie in Publikation III erläutert.

Eine alternative Methode, welche bis heute vor allem im industriellen Format Anwendung findet, ist das sogenannte „*High-Throughput-Screening*“ (HTS). Bei dieser Technik werden unter Zuhilfenahme von automatisierten, experimentellen Methoden schnell große Datenmengen zu diversen chemischen Verbindungen zusammengetragen (Mueller et al., 2012). Die Trefferrate dieser Methode, sprich der Anteil der tatsächlich aktiven Substanzen an der Summe aller getesteten Verbindungen, liegt beim HTS bei 0,01% bis 0,1% (Thorne et al., 2010; Butkiewicz et al., 2013). Das sorgt, zusammen mit den Anforderungen an die laboratorische Infrastruktur für HTS Vorhaben, für immense Kosten bei der Identifizierung neuer Leitmoleküle (Butkiewicz et al., 2013).

Im Gegensatz dazu liegt die Trefferrate bei Ansätzen basierend auf virtuellem Screening bei 1% bis 40%, je nach Güte der Verwendeten Computermodelle (Neves et al., 2018). Dabei werden nur jene Substanzen experimentell untersucht, welche laut Modell eine hohe Aktivität am Target haben (Kar and Roy, 2013). Dadurch werden sowohl finanzieller als auch zeitlicher Aufwand für die Identifizierung neuer Leitmoleküle stark reduziert (Macalino et al., 2015).

Auch die Daten aus den zu durchmusternden Substanzdatenbanken werden zunächst für das virtuelle Screening optimiert. So spielt die sogenannte „*drug-likeness*“ eine wichtige Rolle, welche physikochemische Eigenschaften von Substanzen beschreibt, die diese potentiell für den medikamentellen Einsatz tauglich machen (Mignani et al., 2018; Jia et al., 2020). Die wohl bekanntesten „Regeln“, die diese Tauglichkeit beschreiben, sind die sogenannten „*rule of five*“, welche 1997 von dem Chemiker Christopher Lipinski aufgestellt wurden (Lipinski et al., 2001). Diese Faustregeln beschreiben Grundvoraussetzungen, die eine Substanz erfüllen muss, um eine gute Absorption und Permeation nach oraler Einnahme aufzuweisen. Eine gute Bioverfügbarkeit setzt laut dieser Regeln folgende Punkte voraus: 1. Die Substanz darf nicht mehr als fünf Donatoren von Wasserstoffbrückenbindungen (z. B. OH- oder NH-Gruppen) aufweisen, 2. Die Substanz darf ein Molekulargewicht von 500 Dalton nicht überschreiten, 3.

Die Substanz darf einen Oktanol-Wasser-Verteilungskoeffizienten von maximal 5 aufweisen und 4. Die Substanz darf nicht mehr als zehn Akzeptoren von Wasserstoffbrückenbindungen (z. B. Sauerstoff- oder Stickstoffatome) aufweisen (Lipinski et al., 2001). Es wird von Fünferregel gesprochen, da alle genannten Zahlenwerte der einzelnen Regeln gleich oder ein geradzahliges Vielfaches von fünf sind. Einige Datenbanken chemischer Verbindungen bieten von vornherein schon eine Filterfunktion an, mit der beispielsweise nur Substanzen aus der Datenbank heruntergeladen werden, die den „*rule of five*“ entsprechen. So ist es auch im Rahmen dieser Dissertationsarbeit mit der ZINC Datenbank (<https://zinc.docking.org/>) umgesetzt worden, was in einer Summe von ca. 11 Millionen „*drug-like*“ Substanzen mündete. Weitere verfügbare Datenbanken sind DrugCentral (<https://drugcentral.org/>), ChEMBL (<https://www.ebi.ac.uk/chembl/>), PubChem (<https://pubchem.ncbi.nlm.nih.gov/>), ChemSpider (<http://www.chemspider.com/>) und viele mehr.

Die Strukturdaten der Stoffdatenbank müssen schließlich noch bereinigt und auf die experimentellen Gegebenheiten angepasst werden (Dixon et al., 2006; Chen and Foloppe, 2010). Dies bedeutet, dass doppelt aufgelistete Substanzen aus dem Datensatz entfernt werden, potentielle Ionisierungszustände bei dem experimentellen Ziel pH (hier 7,4) bestimmt werden und eine definierte Anzahl potentieller Konformationen jeder Substanz errechnet werden.

Ist dies alles geschehen, kann unter Zuhilfenahme der in den Kapiteln 1.6.1 und 1.6.2 beschriebenen Modelle das virtuelle Screening durchgeführt werden. Dabei kann man sich die Modelle als Art Schablonen vorstellen, in die von dem genutzten Computerprogramm jede zuvor errechnete Konformation der Substanzen der zu durchmusternden Datenbank hineingelegt und auf Passgenauigkeit überprüft wird. Als Ergebnis erhält man im Falle des Screenings mit einem Pharmakophor Modell eine sortierte Auflistung aller Substanzen der untersuchten Datenbank, bei der für jede Substanz eine Wertung (engl. „*score*“) für die Passgenauigkeit in das Pharmakophor Modell hinterlegt ist. Im Falle des Screenings mit einem QSAR Modell, erhält man eine Auflistung aller Substanzen mit einer vorhergesagten Aktivität an der Zielstruktur, z.B. in Form eines IC<sub>50</sub> Wertes.

## 2 Publikationen

Dieser kumulativen Arbeit liegen folgende Veröffentlichungen zu Grunde:

### 2.1 Publikation I

#### „Selective hepatitis B and D virus entry inhibitors from the group of pentacyclic lupane-type betulin-derived triterpenoids

Michael Kirstgen, Kira Alessandra Alicia Theresa Lowjaga, Simon Franz Müller, Nora Goldmann, Felix Lehmann, Sami Alakurtti, Jari Yli-Kauhaluoma, Dieter Glebe & Joachim Geyer

*Sci. Rep.* **10**, 21772, doi:10.1038/s41598-020-78618-2 (2020).

Abstract:

Current treatment options against hepatitis B and D virus (HBV/HDV) infections have only limited curative effects. Identification of Na<sup>+</sup>/taurocholate co-transporting polypeptide (NTCP) as the high-affinity hepatic receptor for both viruses in 2012 enables target-based development of HBV/HDV cell-entry inhibitors. Many studies already identified appropriate NTCP inhibitors. However, most of them interfere with NTCP's physiological function as a hepatic bile acid transporter. To overcome this drawback, the present study aimed to find compounds that specifically block HBV/HDV binding to NTCP without affecting its transporter function. A novel assay was conceptualized to screen for both in parallel; virus binding to NTCP (measured via binding of a preS1-derived peptide of the large HBV/HDV envelope protein) and bile acid transport via NTCP. Hits were subsequently validated by in vitro HDV infection studies using NTCP-HepG2 cells. Derivatives of the birch-derived pentacyclic lupane-type triterpenoid betulin revealed clear NTCP inhibitory potency and selectivity for the virus receptor function of NTCP. Best performing compounds in both aspects were 2, 6, 19, and 25. In conclusion, betulin derivatives show clear structure–activity relationships for potent and selective inhibition of the HBV/HDV virus receptor function of NTCP without tackling its physiological bile acid transport function and therefore are promising drug candidates.

#### 2.1.1 Darstellung des Eigenanteils an Publikation I

Bei der Publikation „Selective hepatitis B and D virus entry inhibitors from the group of pentacyclic lupane-type betulin-derived triterpenoids (*Sci. Rep.* **10**, 21772,

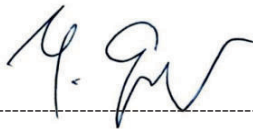
doi:10.1038/s41598-020-78618-2 (2020)) war der Autor dieser Dissertation der Erstautor und führte nach Einführung in die experimentellen Methoden durch Dr. Gary Grosser und Dr. Simon Franz Müller wesentliche Experimente für die Publikation weitestgehend selbstständig durch. Auch wurden die Methoden durch den Autor zunächst optimiert oder teils neu etabliert. Alle Infektionsexperimente wurden von der Co-Autorin Kira Lowjaga durchgeführt. Der Eigenanteil des Autors entspricht dieser Darstellung aus der Veröffentlichung:

**Authors' contributions:**

M.K., S.F.M., K.A.A.T.L. and J.G. conceived the experiments, M.K., S.F.M. and K.A.A.T.L. performed the experiments, M.K., S.F.M., K.A.A.T.L. and J.G. analyzed and interpreted the results, N.G., F.L. and D.G. provided materials and laboratories for infection studies, S.A. and J.Y.K. provided derivatives of betulin, M.K., S.F.M., K.A.A.T.L. and J.G. wrote the manuscript. All authors reviewed the manuscript.

**2.1.2 Bescheinigung der Richtigkeit der Angaben in 2.1.1 durch den Seniorautor**

Da die „authors‘ contributions“ bereits bei Publikation der Arbeit von allen Autoren bestätigt wurden, wird hier auf eine Unterschrift aller Co-Autoren verzichtet. Stellvertretend bescheinigt hier der Seniorautor Prof. Dr. Joachim Geyer Herrn Michael Kirstgen den unter 2.1.1 aufgeführten Eigenanteil an der Publikation.

A handwritten signature in black ink, appearing to read 'J. Geyer', is written above a horizontal dashed line.

**Prof. Dr. Joachim Geyer**

Institute of Pharmacology and Toxicology  
Biomedical Research Center Seltersberg  
Justus Liebig University Giessen, Germany

## 2.2 Publikation II

### „Hepatitis D Virus Entry Inhibitors Based on Repurposing Intestinal Bile Acid Reabsorption Inhibitors

Michael Kirstgen, Kira Alessandra Alicia Theresa Lowjaga, Simon Franz Müller, Nora Goldmann, Felix Lehmann, Dieter Glebe, Karl-Heinz Baringhaus, Joachim Geyer

*Viruses*, **13**, 666, doi:10.3390/v13040666 (2021).

Abstract:

Identification of Na<sup>+</sup>/taurocholate co-transporting polypeptide (NTCP) as high-affinity hepatic entry receptor for the Hepatitis B and D viruses (HBV/HDV) opened the field for target-based development of cell-entry inhibitors. However, most of the HBV/HDV entry inhibitors identified so far also interfere with the physiological bile acid transporter function of NTCP. The present study aimed to identify more virus-selective inhibitors of NTCP by screening of 87 propanolamine derivatives from the former development of intestinal bile acid reabsorption inhibitors (BARIs), which interact with the NTCP-homologous intestinal apical sodium-dependent bile acid transporter (ASBT). In NTCP-HEK293 cells, the ability of these compounds to block the HBV/HDV-derived preS1-peptide binding to NTCP (virus receptor function) as well as the taurocholic acid transport via NTCP (bile acid transporter function) were analyzed in parallel. Hits were subsequently validated by performing in vitro HDV infection experiments in NTCP-HepG2 cells. The most potent compounds S985852, A000295231, and S973509 showed in vitro anti-HDV activities with IC<sub>50</sub> values of 15, 40, and 70 µM, respectively, while the taurocholic acid uptake inhibition occurred at much higher IC<sub>50</sub> values of 24, 780, and 490 µM, respectively. In conclusion, repurposing of compounds from the BARI class as novel HBV/HDV entry inhibitors seems possible and even enables certain virus selectivity based on structure-activity relationships.

#### 2.2.1 Darstellung des Eigenanteils an Publikation II

Bei der Publikation „Hepatitis D Virus Entry Inhibitors Based on Repurposing Intestinal Bile Acid Reabsorption Inhibitors (*Viruses*, **13**, 666, doi:10.3390/v13040666 (2021)) war der Autor dieser Dissertation der Erstautor und führte wesentliche Experimente für die Publikation weitestgehend selbstständig durch. Alle Infektionsexperimente wurden von der Co-Autorin



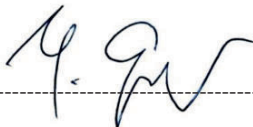
Kira Lowjaga durchgeführt. Der Eigenanteil des Autors entspricht dieser Darstellung aus der Veröffentlichung:

**Authors' contributions:**

M.K., S.F.M., K.A.A.T.L. and J.G. conceived the experiments, M.K., S.F.M. and K.A.A.T.L. performed the experiments, M.K., S.F.M., K.A.A.T.L. and J.G. analyzed and interpreted the results, N.G., F.L. and D.G. provided materials and laboratories for infection studies, K.H.B. provided the test compounds, M.K. and J.G. wrote the manuscript. All authors have read and agreed to the published version of the manuscript.

**2.2.2 Bescheinigung der Richtigkeit der Angaben in 2.2.1 durch den Seniorautor**

Da die „authors' contributions“ bereits bei Publikation der Arbeit von allen Autoren bestätigt wurden, wird hier auf eine Unterschrift aller Co-Autoren verzichtet. Stellvertretend bescheinigt hier der Seniorautor Prof. Dr. Joachim Geyer Herrn Michael Kirstgen den unter 2.2.1 aufgeführten Eigenanteil an der Publikation.



**Prof. Dr. Joachim Geyer**

Institute of Pharmacology and Toxicology  
Biomedical Research Center Seltersberg  
Justus Liebig University Giessen, Germany

### 2.3 Publikation III

#### „Identification of Novel HBV/HDV Entry Inhibitors by Pharmacophore- and QSAR-Guided Virtual Screening

Michael Kirstgen, Simon Franz Müller, Kira Alessandra Alicia Theresa Lowjaga, Nora Goldmann, Felix Lehmann, Sami Alakurtti, Jari Yli-Kauhaluoma, Karl-Heinz Baringhaus, Reimar Krieg, Dieter Glebe, Joachim Geyer

*Viruses*, **13**, 1489, doi:10.3390/v13081489 (2021).

#### Abstract:

The hepatic bile acid transporter Na<sup>+</sup>/taurocholate co-transporting polypeptide (NTCP) was identified in 2012 as the high-affinity hepatic receptor for the hepatitis B and D viruses (HBV/HDV). Since then, this carrier has emerged as promising drug target for HBV/HDV virus entry inhibitors, but the synthetic peptide Hepcludex<sup>®</sup> of high molecular weight is the only approved HDV entry inhibitor so far. The present study aimed to identify small molecules as novel NTCP inhibitors with anti-viral activity. A ligand-based bioinformatical approach was used to generate and validate appropriate pharmacophore and QSAR (quantitative structure-activity relationship) models. Half-maximal inhibitory concentrations (IC<sub>50</sub>) for binding inhibition of the HBV/HDV-derived preS1 peptide (as surrogate parameter for virus binding to NTCP) were determined in NTCP-expressing HEK293 cells for 150 compounds of different chemical classes. IC<sub>50</sub> values ranged from 2 μM up to >1000 μM. The generated pharmacophore and QSAR models were used for virtual screening of drug-like chemicals from the ZINC database (~11 million compounds). The 20 best-performing compounds then were experimentally tested for preS1-peptide binding inhibition in NTCP-HEK293 cells. Among them, four compounds were quite active and revealed experimental IC<sub>50</sub> values for preS1-peptide binding inhibition of 9, 19, 20, and 35 μM, which were comparable to the QSAR-based predictions. All these compounds also significantly inhibited *in vitro* HDV infection of NTCP-HepG2 cells, without showing any cytotoxicity. The best-performing compound in all assays was ZINC000253533654. In conclusion, the present study demonstrates that virtual compound screening based on NTCP-specific pharmacophore and QSAR models can predict novel active hit compounds for the development of HBV/HDV entry inhibitors.

### 2.3.1 Darstellung des Eigenanteils an Publikation III

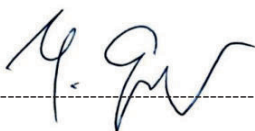
Bei der Publikation „Identification of Novel HBV/HDV Entry Inhibitors by Pharmacophore- and QSAR-Guided Virtual Screening (*Viruses*, **13**, 1489, doi:10.3390/v13081489 (2021)) war der Autor dieser Dissertation der Erstautor und führte wesentliche Experimente für die Publikation weitestgehend selbstständig durch. Auch wurden die Methoden durch den Autor teils neu etabliert. Alle Infektionsexperimente wurden von der Co-Autorin Kira Lowjaga durchgeführt. Der Eigenanteil des Autors entspricht dieser Darstellung aus der Veröffentlichung:

#### **Authors' contributions:**

M.K., S.F.M., K.A.A.T.L., and J.G. conceived the experiments, M.K., S.F.M., and K.A.A.T.L. performed the experiments, M.K., S.F.M., K.A.A.T.L., and J.G. analyzed and interpreted the results, N.G., F.L., and D.G. provided materials and laboratories for infection studies, S.A., J.Y.K., K.H.B., R.K. provided test compounds, M.K. and J.G. wrote the manuscript. All authors reviewed the manuscript.

### 2.3.2 Bescheinigung der Richtigkeit der Angaben in 2.3.1 durch den Seniorautor

Da die „authors' contributions“ bereits bei Publikation der Arbeit von allen Autoren bestätigt wurden, wird hier auf eine Unterschrift aller Co-Autoren verzichtet. Stellvertretend bescheinigt hier der Seniorautor Prof. Dr. Joachim Geyer Herrn Michael Kirstgen den unter 2.3.1 aufgeführten Eigenanteil an der Publikation.

A handwritten signature in black ink, appearing to read 'J. Geyer', is written over a horizontal dashed line.

**Prof. Dr. Joachim Geyer**

Institute of Pharmacology and Toxicology

Biomedical Research Center Seltersberg

Justus Liebig University Giessen, Germany

## 2.4 Publikation IV

### „Substrate Specificities and Inhibition Pattern of the Solute Carrier Family 10 Members NTCP, ASBT and SOAT

Gary Grosser, Simon Franz Müller, Michael Kirstgen, Barbara Döring, Joachim Geyer

*Front. Mol. Biosci.* **8**, 689757, doi:10.3389/fmolb.2021.689757 (2021).

Abstract:

Three carriers of the solute carrier family SLC10 have been functionally characterized so far. Na<sup>+</sup>/taurocholate cotransporting polypeptide NTCP is a hepatic bile acid transporter and the cellular entry receptor for the hepatitis B and D viruses. Its intestinal counterpart, apical sodium-dependent bile acid transporter ASBT, is responsible for the reabsorption of bile acids from the intestinal lumen. In addition, sodium-dependent organic anion transporter SOAT specifically transports sulfated steroid hormones, but not bile acids. All three carriers show high sequence homology, but significant differences in substrate recognition that makes a systematic structure-activity comparison attractive in order to define the protein domains involved in substrate binding and transport. By using stably transfected NTCP-, ASBT-, and SOAT-HEK293 cells, systematic comparative transport and inhibition experiments were performed with more than 20 bile acid and steroid substrates as well as different inhibitors. Tauroolithocholic acid (TLC) was identified as the first common substrate of NTCP, ASBT and SOAT with  $K_m$  values of 18.4, 5.9, and 19.3  $\mu\text{M}$ , respectively. In contrast, lithocholic acid was the only bile acid that was not transported by any of these carriers. Troglitazone, BSP and erythrosine B were identified as pan-SLC10 inhibitors, whereas cyclosporine A, irbesartan, ginkgolic acid 17:1, and betulinic acid only inhibited NTCP and SOAT, but not ASBT. The HBV/HDV-derived myr-preS1 peptide showed equipotent inhibition of the NTCP-mediated substrate transport of taurocholic acid (TC), dehydroepiandrosterone sulfate (DHEAS), and TLC with  $IC_{50}$  values of 182 nM, 167 nM, and 316 nM, respectively. In contrast, TLC was more potent to inhibit myr-preS1 peptide binding to NTCP with  $IC_{50}$  of 4.3  $\mu\text{M}$  compared to TC ( $IC_{50} = 70.4 \mu\text{M}$ ) and DHEAS ( $IC_{50} = 52.0 \mu\text{M}$ ). Based on the data of the present study, we propose several overlapping, but differently active binding sites for substrates and inhibitors in the carriers NTCP, ASBT, SOAT.

#### **2.4.1 Darstellung des Eigenanteils an Publikation IV**

Bei der Publikation „Substrate Specificities and Inhibition Pattern of the Solute Carrier Family 10 Members NTCP, ASBT and SOAT (*Front. Mol. Biosci.* **8**, 689757, doi:10.3389/fmolb.2021.689757 (2021)) war der Autor dieser Dissertation als Co-Autor beteiligt. Der Eigenanteil des Autors entspricht dieser Darstellung aus der Veröffentlichung:

##### **Authors' contributions:**

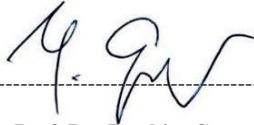
G.G., S.M., M.K., and J.G. conceived the experiments; G.G., S.M., M.K., and B.D. performed the experiments; G.G., S.M., M.K., and J.G. analyzed and interpreted the results; G.G., S.M., M.K., and J.G. wrote the manuscript. All authors reviewed the manuscript. All authors contributed to the article and approved the submitted version.

##### **Zur Erläuterung:**

Durch den Autor wurden Versuche geplant, durchgeführt, statistisch ausgewertet, grafisch dargestellt sowie methodisch beschrieben, welche das Hemmmuster ausgewählter nicht-Substrat Inhibitoren aus der Substanzklasse der Betulin-Derivate an den drei nahe verwandten Transportproteinen NTCP, ASBT und SOAT analysierten. Daraus sind Tabelle 4 und Abbildung 4 der Publikation hervorgegangen. Des Weiteren wurden die in Abbildung 7 dargestellten Substrat-Pharmakophor Modelle der drei genannten Transportproteine vom Autor generiert und grafisch aufgearbeitet. Am Schaubild in Abbildung 8 war der Autor maßgeblich beteiligt in Zusammenarbeit mit dem Hauptautor Simon Müller.

#### **2.4.2 Bescheinigung der Richtigkeit der Angaben in 2.4.1 durch den Seniorautor**

Da die „authors' contributions“ bereits bei Publikation der Arbeit von allen Autoren bestätigt wurden, wird hier auf eine Unterschrift aller Co-Autoren verzichtet. Stellvertretend bescheinigt hier der Seniorautor Prof. Dr. Joachim Geyer Herrn Michael Kirstgen den unter 2.4.1 aufgeführten Eigenanteil an der Publikation.



**Prof. Dr. Joachim Geyer**

Institute of Pharmacology and Toxicology

Biomedical Research Center Seltersberg

Justus Liebig University Giessen, Germany

### 3 Diskussion

Die Anwendung der in dieser Dissertationsschrift erläuterten computergestützten Verfahren dient der zielgerichteten Suche nach neuen Leitstrukturen chemischer Moleküle, welche Aktivität an einer definierten Zielstruktur (Target) aufweisen sollen. In diesem Beispiel wurde nach Substanzen gesucht, welche von ihren Grundeigenschaften her als oral anwendbare Medikamente geeignet erscheinen und an einem klar definierten Target, repräsentiert durch den leberspezifischen Gallensäuretransporter und Virusrezeptor NTCP, eine Hemmung der Bindung von HBV und HDV verursachen sollen. Der Bedarf innovativer Behandlungsmethoden der folgenschweren chronischen Infektion mit diesen beiden Viren wurde im Einleitungsteil dieser Arbeit bereits dargelegt.

Das vorwiegend industriell als gängige Methode angewandte Hoch-Durchsatz-Screening (HTS) kam für die Identifizierung neuer aktiver Substanzen nicht in Frage, da für dieses höchst aufwändige Verfahren weder finanzielle Mittel noch technische Voraussetzungen in ausreichendem Maße gegeben waren. Eine zielgerichtete Vorfilterung potentiell aktiver Verbindungen war nötig, um eine akzeptable Trefferquote erzielen zu können, die wiederum für mehr Effizienz und Kostenersparnis sorgt.

Das Mittel der Wahl stellte in diesem Fall die bioinformatische Methode des Virtuellen Screenings (VS) dar, welche als Liganden basierter Ansatz durchgeführt wurde. Dies ist, wie in Kapitel 1.6 bereits erwähnt, dem Umstand geschuldet, dass zum jetzigen Zeitpunkt keine 3D-Struktur des Targets NTCP existiert, die einen Struktur basierten Ansatz möglich machen würde. Einen vermeintlichen Nachteil sollte man jedoch nicht darin sehen. Zunächst scheint es logisch, dass Studien unter Zuhilfenahme der genau definierten Zielstruktur, eine bessere Vorhersagekraft haben sollten. Dem ist allerdings nicht so. Es sollte bedacht werden, dass z.B. eine Kristallstruktur zunächst eine starre Momentaufnahme darstellt. Das biologische System einer Zellmembran mit eingebetteten Proteinstrukturen ist hingegen ganz und gar nicht starr. Es stellt ein sehr dynamisches und vor allem flexibles Arrangement dar. Auch die Membranproteine selbst stellen flexible Gebilde dar, die auf äußere Reize reagieren können. So wurde beispielsweise ein Phänomen namens „*induced fit*“ beschrieben, bei dem die Annäherung eines Liganden an ein Zielprotein durch Wechselwirkungen zunächst eine Konformationsänderung des Proteins verursacht, bevor die tatsächliche Bindung des Liganden erfolgen kann (Galburt and Tomko, 2017). Der Ligand induziert also die Ausbildung seiner eigenen Bindungstasche am Zielprotein. Hinzu kommt, dass unzureichende Auflösung (Beeley and Sage, 2003) oder kristallisationsbedingte Artefakte des Liganden-Protein-Komplexes

(Klebe, 2006) zu ungenauen Kristallstruktur Modellen führen können. Da sich diese relativ geringgradigen Ungenauigkeiten bereits negativ auf die Qualität des VS auswirken können, sollte auf einen Struktur basierten Ansatz unter Verwendung eines Homologiemodells von vornherein verzichtet werden.

Der Liganden basierte Ansatz birgt allerdings auch einige Fallstricke, die es zu beachten gilt. So ist Grundvoraussetzung, dass alle für diesen Ansatz verwendeten experimentellen Daten auch aus demselben experimentellen Hintergrund stammen (Dixon et al., 2006). Das bedeutet, dass Daten aus demselben Labor stammen müssen und auf dieselbe Art und Weise für das selbe Target gemessen worden sein müssen. Dies ist darin zu begründen, dass alle Messergebnisse denselben Messfehler aufweisen sollten, damit das aus den Daten resultierende Modell nicht verzerrt wird. Es ist auch möglich auf Aktivitätsdaten aus der Literatur zurückzugreifen, sofern diese ebenfalls denselben Messfehler aufweisen. Folglich dürfen keine Daten aus verschiedenen Publikationen gemischt werden, wenn diese nicht in demselben Labor unter denselben experimentellen Bedingungen erzeugt wurden.

Die experimentellen Daten zu den Aktivitäten der getesteten Liganden an der Zielstruktur können weitere Probleme für die generierten Modelle darstellen. Im Bezug auf Pharmakophor Modelle, die beispielsweise auf  $IC_{50}$  Werten beruhen, müssen diese kontinuierlichen numerischen Daten zunächst kategorisiert werden (vgl. Kapitel 1.6.1). Dabei ist es willkürlich, wo die Grenze zwischen aktiven und inaktiven Liganden gezogen wird. Eine genaue Grenze ist meist nicht klar definierbar. So wurden die Daten aus Publikation III dieser Arbeit als Beispiel so kategorisiert, dass  $IC_{50}$  Werte kleiner als  $10 \mu\text{M}$  als aktiv definiert wurden und  $IC_{50}$  Werte über  $20 \mu\text{M}$  als inaktiv. Die Grauzone zwischen  $10 \mu\text{M}$  und  $20 \mu\text{M}$  wurde dabei aus der Berechnung des Pharmakophor Modells ausgeschlossen. Eine gewisse Lücke zwischen aktiven und inaktiven Liganden ist wichtig, da vor allem die Berechnung der „*excluding values*“ (vgl. Kapitel 1.6.1) von den Eigenschaften der inaktiven Liganden abhängen (Dixon et al., 2006). Bei zweifelhaften Liganden würde die Güte des Modells leiden, da „*excluding values*“ definiert würden, welche nicht zwangsläufig ausgeschlossen werden sollten.

Bei der Generierung eines QSAR Modells sind numerische Daten, wie z.B.  $IC_{50}$  Werte, zwingend erforderlich. Dies geht bereits aus dem Wort „quantitative“ hervor, das in der Beschreibung dieser Art des Computermodells enthalten ist. Dabei hängt die Qualität des Modells unter anderem davon ab, wie breit die eingespeisten  $IC_{50}$  Werte gefächert sind. Ein Modell, das auf Daten beruht, die nur einen kleinen Aktivitätsbereich abdecken, kann bei der Vorhersage der Aktivität von ungetesteten Substanzen auch nur auf diesen Bereich

zurückgreifen. Als Faustregel kann man festhalten, dass drei bis vier Zehner Potenzen an Aktivitätsdaten abgedeckt sein sollten, damit dem Modell genügend Referenzen für seine Vorhersagen zugrunde liegen (Grosser et al., 2016).

Nicht nur die Daten zu den Aktivitäten der getesteten Liganden spielen eine grundlegende Rolle, sondern auch die Strukturdaten derselben. Zum einen sollten die einfließenden Liganden eine gewisse Diversität aufweisen, damit ein möglichst großer Raum abgedeckt werden kann. Andererseits ist es von Vorteil, wenn Daten von strukturell nahe Verwandten Derivaten einfließen, da damit Einflüsse einzelner chemischer Modifikationen auf die Aktivität zum Tragen kommen. Wenn jedoch zu viele Liganden mit ähnlicher Struktur in die Modellierung einfließen, führt das vor allem bei der Pharmakophor Modellierung dazu, dass beim anschließenden virtuellen Screening, die Diversität der Treffersubstanzen stark reduziert wird (Schaller et al., 2020; Santana et al., 2021). Außerdem können so „*common feature*“ Pharmakophor Modelle (vgl. Kapitel 1.6.1) entstehen, die lediglich die Grundstrukturen der Liganden beschreiben, ohne dabei die für die Aktivität an der Zielstruktur wichtigen Seitengruppen mit einzubeziehen. Als Beispiel kann man sich einen Datensatz vorstellen, der aus einer Reihe von Liganden besteht, die allesamt modifizierte Steroide darstellen. Bei der Generierung der Pharmakophor Hypothese, für die vier bis fünf Charakteristika voreingestellt sind, kann es passieren, dass diese vier bis fünf Charakteristika ausschließlich das Grundgerüst der Steroide beschreiben. Ein virtuelles Screening mit diesem Modell wäre nicht zielführend, da damit ausschließlich Formen von Steroiden herausgefiltert würden. Um dieses Phänomen zu umgehen, kann versucht werden, für die Generierung der Pharmakophor Hypothese mehr als fünf funktionelle Charakteristika zu erlauben. Allerdings sollte vor diesem Hintergrund nicht grundsätzlich die Anzahl der erlaubten Charakteristika manuell erhöht werden, da dies zu einer Überinterpretation des Einflusses einzelner Charakteristika führen kann, was wiederum das Modell verzerren würde (Dixon et al., 2006).

Wie in Kapitel 1.6.3 bereits erwähnt, spielt die Strukturbereinigung der bioinformatisch verwerteten Liganden eine wichtige Rolle für das virtuelle Screening. Diese Strukturbereinigung ist jedoch nicht nur für die Präparation der zu durchmusternden Datenbanken von Nöten, sondern muss auch auf die Strukturen der Liganden angewendet werden, welche zur Generierung der Pharmakophor und QSAR Modelle dienen. Wenn diese Bereinigung nicht ordnungsgemäß durchgeführt wird, werden die experimentell bestimmten Aktivitätsdaten Strukturen zugeordnet, welche so im Experiment nicht vorliegen. Folglich würden falsche Struktur-Wirkungs-Beziehungen angenommen (Dixon et al., 2006).



Alle genannten bioinformatischen Methoden stellen hohe Anforderungen an die Rechenleistung der verwendeten Hardware. Als Beispiel kann die Berechnung verschiedener Konformationen der Moleküle einer Datenbank herangezogen werden. Bei Verwendung eines 1,7 GHz Pentium 4 Prozessors könnten pro Sekunde 50 Konformationen für ein bis zwei Moleküle berechnet werden (Dixon et al., 2006). Bei einer Datenbank mit 10 Millionen Molekülen entspräche dies einer Rechenzeit zwischen drei und sechs Stunden ausschließlich für die Berechnung von Konformationen. Um mit Pharmakophor oder QSAR Modellen ein komplettes Screening einer Datenbank durchzuführen, kommt man so auf Rechenzeiten von mehreren Tagen bis hin zu Wochen.

Als Methode für die Regressionsanalyse bei der Generierung eines QSAR Modells hat sich die Regression der partiellen kleinsten Quadrate bewährt. Die Wahl dieser Methode ergibt sich aus dem Umstand, dass mehr Prädiktoren (z.B. verschiedene physikochemische Eigenschaften) als Beobachtungen (z.B. Aktivität in Form eines IC<sub>50</sub> Wertes) vorhanden sind. Bei der Regression der partiellen kleinsten Quadrate wird, anders als bei der multiplen Regression, nicht davon ausgegangen, dass die Prädiktoren fest sind. Das bedeutet, dass die Prädiktoren Messfehler enthalten können, wodurch diese Regressionsmethode robuster gegenüber Messunsicherheiten ist (Minitab LLC, 2021).

Einen alternativen Ansatz zu dem virtuellen Screening mittels Pharmakophor oder QSAR Modellen stellt das sogenannte „*shape similarity*“ (zu deutsch: Ähnlichkeit der Form) Screening dar (Santana et al., 2021). Dabei dient ein aktiver Ligand als Muster. Datenbanken werden nach Substanzen durchsucht, die zu diesem Muster eine gewisse Ähnlichkeit aufweisen. Der bioinformatische Vorgang selbst kann dabei „*alignment-free*“ (Seddon et al., 2019), sprich ohne eine berechnete Überlagerung der Liganden aus der Datenbank mit dem Musterliganden, erfolgen oder aber „*alignment-based*“ (Kumar and Zhang, 2018) stattfinden. Allerdings werden mit dieser Methode, wie der Name bereits verrät, nur solche Liganden gefunden, welche dem reaktiven Musterliganden strukturell sehr ähnlich sind. Ein Vorteil des Screenings mit Pharmakophor oder QSAR Modellen besteht darin, auch strukturell unterschiedliche Liganden herauszufiltern, was gegebenenfalls zu neuen Leitstrukturen führen kann.

### **Gemeinsame Diskussion der Veröffentlichungen**

Die Identifizierung des leberspezifischen Gallensäuretransporters NTCP im Jahr 2012 (Yan et al., 2012) als hochaffinen Rezeptor für HBV und HDV, war die Grundlage für die Entwicklung einer neuen Klasse von Medikamenten, die als „Entry-Inhibitoren“ bezeichnet werden und

darauf abzielen, die Virusbindung an NTCP zu verhindern. Einige Substanzen wurden bereits als HBV/HDV Entry-Inhibitoren identifiziert (vgl. Kapitel 1.5.3), allerdings wurde erst ein einziges Medikament im Juli 2020 durch die europäische Arzneimittel-Agentur als solches zugelassen. Es handelt sich um den Arzneistoff Hepcludex<sup>®</sup>, einem synthetischen Peptid, das auf der präS1 Domäne des viralen LHBs basiert (Zulassungsnummer EU/1/20/1446/001). Dieses Peptid kann nicht oral eingenommen werden, sondern setzt subcutane Applikation voraus. Hinzu kommen komplexe Anforderungen an Herstellung, Lagerung und Vertrieb dieses Arzneistoffs. Da besonders ärmere Gebiete des globalen Südens mit chronischen HBV und HDV Infektion zu kämpfen haben, bedarf es einfacher Therapiemethoden, wie einer Arzneimittelapplikation in Tablettenform. Eine dauerhafte Kühlung selbst von Lyophilisat des Peptids könnte in den meisten Fällen nicht bis zur Anwendung sichergestellt werden.

Einige identifizierte Entry-Inhibitoren, wie beispielsweise Cyclosporin A, waren vorher bereits für ihre hemmenden Eigenschaften der Gallensäuretransportfunktion von NTCP bekannt (Döring et al., 2012). Die Interferenz von Gallensäuretransportfunktion und Virusrezeptorfunktion indizieren, dass Domänen des NTCP, die für die Substraterkennung und den Substrattransport von Bedeutung sind, mit Domänen der Virusbindung überlappen müssen. Absolut identisch können sie allerdings nicht sein, da in unserem Labor bereits in früheren Studien gezeigt werden konnte, dass bei einer Mutation von Glycin zu Arginin an Position 158 des NTCP, die Fähigkeit der Virusbindung verloren geht, bei erhaltener Transportfunktion für Gallensäuren (Müller et al., 2018). Vergleichbar damit konnte von Shimura et al. nachgewiesen werden, dass das Cyclosporin-Derivat SCY995 stärkere Hemmung auf *in vitro* HBV Infektionen zeigt als auf die *in vitro* Gallensäuretransportfunktion von NTCP (Shimura et al., 2017). Dies sind Hinweise darauf, dass es möglich sein sollte, diese beiden Funktionen von NTCP separat voneinander mit Inhibitoren zu adressieren.

Um diesen Aspekt genauer beleuchten zu können, wurden die Studien dieser Arbeit so ausgelegt, dass zu jeder getesteten Substanz von vornherein sowohl die Hemmeigenschaften auf die Bindung des viralen präS1 Peptides an NTCP als auch auf die Transportfunktion von Taurocholsäure durch NTCP analysiert wurden. Für die quantitativen Analysen wurde auf ein mit Tritium (<sup>3</sup>H) markiertes präS1 Peptid (<sup>3</sup>H]preS1) vom HBV Genotyp D3 zurückgegriffen und auf Tritium markierte Taurocholsäure (<sup>3</sup>H]TC). Die Bindung des präS1 Peptides stellte dabei zunächst repräsentativ die Virusbindung an NTCP dar. Substanzen mit interessanter Hemmkinetik wurden schließlich in einem *in vitro* Infektionsmodell weiter untersucht.

In der ersten Studie wurde auf diese Weise eine neue chemische Klasse von vielversprechenden HBV/HDV Entry-Inhibitoren identifiziert, die durch Derivate des natürlichen pentacyclischen Lupan-Typ-Triterpenoids Betulin repräsentiert werden. Betulin kann aus verschiedenen Pflanzenarten einer Vielzahl von Familien wie *Betulaceae*, *Platanaceae*, *Dilleniaceae*, *Rhamnaceae*, *Rosaceae* und *Fagaceae* isoliert werden (Cichewicz and Kouzi, 2004; Ghaffari Moghaddam et al., 2012). Charakteristisch für das Lupangerüst von Betulin sind die fünfgliedrige Ringstruktur und eine Isopropylidengruppe (Zhang et al., 2015). Nahezu alle analysierten Betulin-Derivate zeigten hemmende Wirkung auf die Transport- und Virusrezeptorfunktion von NTCP. Bemerkenswert ist dabei, dass manche Derivate, wie z.B. Betulinsäure, beide Funktionen mit dem nahezu identischen  $IC_{50}$  (hier 1-2  $\mu M$ ) hemmen und andere Derivate, wie z.B. 20,29-Dihydrobetulin, zwar einen niedrigen  $IC_{50}$  für die Hemmung der präS1 Peptid Bindung aufweisen (hier 4  $\mu M$ ), den Gallensäuretransport allerdings vielfach schlechter hemmen (hier  $IC_{50}$  von 260  $\mu M$ ). Manche Substanzen stechen damit heraus, dass sie selbst bei höchsten Konzentrationen von 1 mM überhaupt keine Hemmung des Gallensäuretransportes bewirken. Zu diesen Substanzen zählen 3,28-Di-O-acetylbetulin, 3,28-Di-O-acetyl-29-hydroxybetulin, 3,28-Di-O-acetyl-18,19-dehydro-20,29-dihydrobetulin und 3-Oxoallobetulin, wobei zumindest 3,28-Di-O-acetyl-29-hydroxybetulin noch eine relativ potente Hemmung der präS1 Peptid Bindung verursacht ( $IC_{50} = 8 \mu M$ ).

Es konnten Struktur-Wirkungs-Beziehungen festgestellt werden, sowohl für die Potenz der präS1 Peptid Hemmung als auch für die selektive Hemmung der Virusrezeptorfunktion von NTCP. Dabei reichen kleinste chemische Modifikationen aus, um das Verhalten des Hemmstoffes grundlegend zu beeinflussen.

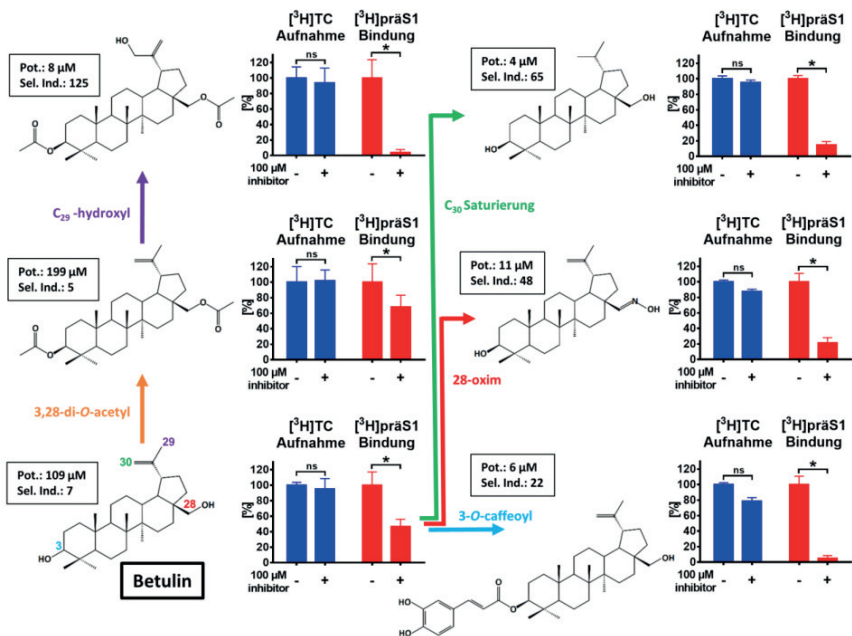


Abbildung 5 – Struktur-Wirkungs-Analyse ausgewählter Betulinderivate

Diese Abbildung zeigt den Einfluss bestimmter chemischer Modifikationen am Betulin Grundgerüst auf die Potenz (Pot.;  $\text{IC}_{50}$  der präS1 Peptid Bindungshemmung) und den Selektivitätsindex (Sel. Ind.; Quotient vom  $\text{IC}_{50}$  der Gallensäuretransporthemmung/  $\text{IC}_{50}$  der präS1 Peptid Bindungshemmung) der getesteten Derivate. Der jeweils resultierende hemmende Einfluss an NTCP ist durch Säulendiagramme dargestellt. Die  $[^3\text{H}]\text{TJC}$  Aufnahme (blau) bzw. die  $[^3\text{H}]\text{präS1}$  Bindung (rot) in Anwesenheit bzw. Abwesenheit einer fixen Konzentration (100  $\mu\text{M}$ ) des jeweiligen Betulin-Derivates wurden ermittelt. Die Diagramme zeigen Mittelwerte  $\pm$  Standardabweichung (SD) von vier Messpunkten. \*Signifikant unterschiedlich mit  $p < 0,01$  (TWO-WAY-ANOVA mit Sidak's multiplem Vergleichstest); ns, nicht signifikant. Abbildung modifiziert nach Kirstgen et al. 2021.

Auf Grundlage der Beobachtung, dass alle potent, aber unselektiv hemmenden Betulin-Derivate mindestens eine saure Gruppe tragen und pKa-Werte von 4-5 aufweisen, wurden weitere Inhibitionsstudien bei einem angepassten pH von 5,5 statt 7,4 durchgeführt. Bei dem physiologischen Standard-pH von 7,4 liegen diese Verbindungen überwiegend deprotoniert und somit negativ geladen vor. Bei angepasstem pH von 5,5 ist die relative Ladung dieser Verbindungen reduziert. Es zeigt sich, dass der veränderte pH keinen Einfluss auf die Hemmung der Bindung des präS1 Peptides an NTCP durch die getesteten Substanzen hat. Die hemmende Wirkung auf den Gallensäuretransport hingegen wurde stark reduziert. Für die Erörterung dieses Phänomens ist es sinnvoll zu betrachten, dass auch konjugierte Gallensäuren ( $\text{pKa} = 1-4$ ) bei physiologischem pH überwiegend deprotoniert als Anionen vorliegen (Greupink et al., 2012; Kouzuki et al., 2000). Wir vermuten daher, dass Betulin-Derivate,

welche Säuregruppen tragen, nicht nur Inhibitoren am NTCP darstellen, sondern aufgrund ihrer Ähnlichkeit zu Gallensäuren auch als Substrate erkannt werden könnten. Zukünftige Studien sollen dies genauer beleuchten. Es lässt sich festhalten, dass eine negative Ladung nicht zwingend erforderlich ist, damit ein Inhibitor die Virusrezeptor Funktion von NTCP hemmt. Allerdings scheint die Bindungstasche für Taurocholsäure derart gestaltet zu sein, dass hier eine negative Ladung für die Interaktion notwendig ist.

Besonders Betulinsäure wurde bereits ausgiebig toxikologisch untersucht und als sicher eingestuft (Cichewicz and Kouzi, 2004; Kessler et al., 2007; Zuco et al., 2002; Pisha et al., 1995). Grund für diese intensiven Untersuchungen sind die Vielzahl pharmakologischer Wirkungen, die bereits für diese Substanzgruppe festgestellt wurden. So wurden bereits tumorsupprimierende, antivirale, antimikrobielle, antiinflammatorische und antifibrotische Effekte nachgewiesen (Zhan et al., 2018; Chen et al., 2018; Adeleke and Adaramoye, 2017; Laavola et al., 2016; Wan et al., 2012). Betulin selbst ist sogar bereits für die medizinische Anwendung beim Menschen zugelassen und ist derzeit als betulinhaltiges Gel (Oleogel-S10, Episalvan) erhältlich. Es wurde 2016 von der Europäischen Arzneimittel Agentur (EMA) für die Behandlung von oberflächlichen Hautwunden bei Erwachsenen zugelassen. Es besteht aus 10% Birkenrindenextrakt und 90% Sonnenblumenöl. Die Menge an Betulin liegt bei 72-88 mg pro 100 mg Extrakt. Darüber hinaus befindet sich Episalvan derzeit in einer Phase-III-Wirksamkeits- und Sicherheitsstudie (NCT03068780) bei Patienten mit vererbter *Epidermolysis bullosa*, einer Erkrankung, bei der ein Gendefekt für eine sehr fragile Haut sorgt, die bei geringsten mechanischen Belastungen bereits offene Wunden davon trägt (Bardhan et al., 2020). Das gute Sicherheitsprofil macht Betulin zu einer interessanten Leitstruktur bei der Suche nach HBV/HDV Entry-Inhibitoren. In anknüpfenden Studien gilt es, durch chemische Modifikation, die Selektivität von beispielsweise Betulinsäure zur Hemmung der Virusrezeptorfunktion von NTCP zu verbessern oder die Potenz von bereits selektiven Substanzen wie Lupenon zu erhöhen. Mit jeder Modifikation muss allerdings auch das toxikologische Profil erneut überprüft werden.

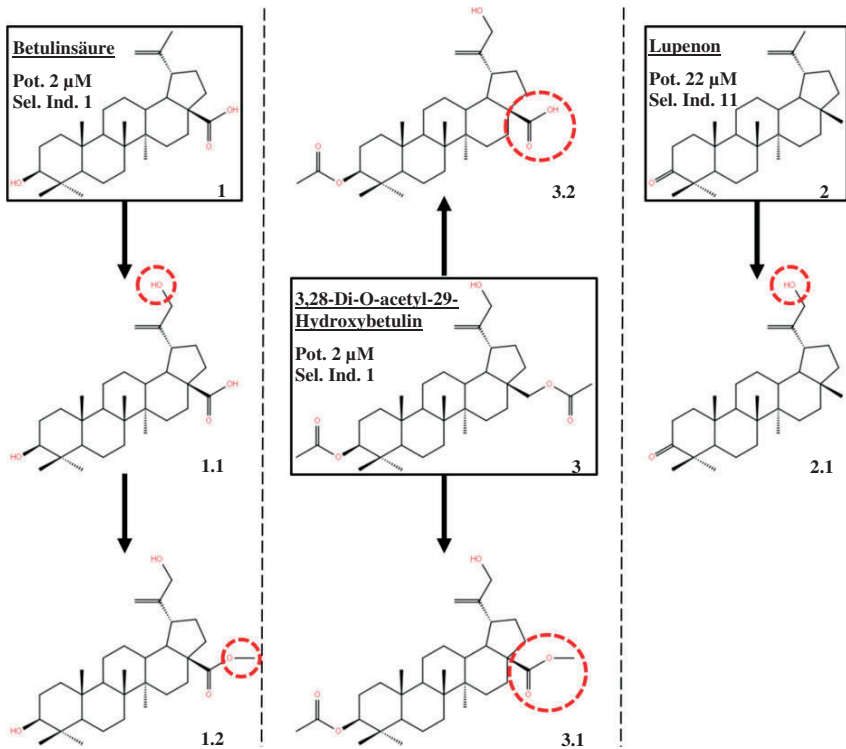


**Abbildung 6 – Mögliche Derivatisierungen zur Steigerung der Wirksamkeit und Selektivität**

Diese Abbildung zeigt potentielle Derivatisierungsoptionen der Substanzen Betulinsäure (1), Lupenon (2) und 3,28-Di-O-acetyl-29-Hydroxybetulin (3), die auf den Erkenntnissen aus **Publikation I** dieser Dissertationsschrift beruhen. Grundlage der Art sowie Position der chemischen Modifikationen für die Substanzen 1.1 und 2.1 ist die Substanz 3,28-Di-O-acetyl-29-Hydroxybetulin, welche in den Studien den besten Selektivitätsindex (Sel. Ind.) von 125 aufwies, bei einer Potenz (Pot.) von 8  $\mu\text{M}$ . Ziel ist es, den Selektivitätsindex der Betulinsäure (Pot. 2  $\mu\text{M}$ ; Sel. Ind. 1) zu erhöhen oder die Potenz der bereits selektiven Substanz Lupenon (Pot. 22  $\mu\text{M}$ ; Sel. Ind. 11) zu verbessern. Die Methylierung der Carboxylreste der Strukturen 1.2 sowie 3.1 beruht auf der Erkenntnis aus **Publikation I**, dass eine deprotonierte Säure einen stärkeren hemmenden Effekt auf die Gallensäuretransportfunktion von NTCP hat als eine protonierte Säure, während die präS1 Peptid Bindung davon unbeeinträchtigt bleibt. Durch die Methylgruppe wird eine Deprotonierung der Säure bei physiologischem pH verhindert, wodurch im Idealfall eine selektive Hemmung der Virusrezeptorfunktion von NTCP verursacht werden soll. Mit dem Austausch eines Acetyl-Restes durch eine Carboxylgruppe an Position 28, wie es in der Struktur 3.2 markiert ist, könnte die Potenz des 3,28-Di-O-acetyl-29-Hydroxybetulin eventuell noch weiter gesteigert werden und sich der Potenz der Betulinsäure annähern.

Betulinsäure spielt noch eine weitere interessante Rolle, da in Studien aus dem Jahr 2009 von Yao et al. gezeigt werden konnte, dass diese Substanz eine HBV hemmende Wirkung verursacht, hervorgerufen durch die Hemmung der Superoxid Dismutase 2 und folgender Übergenerierung reaktiver Sauerstoffspezies (Sauerstoffradikale) (Yao et al., 2009). So könnte Betulinsäure durch zwei unabhängige Wirkmechanismen ein potentes Therapeutikum der HBV Infektion darstellen. Auch andere Betulin-Derivate sollten daher auf ihre Fähigkeit zur Hemmung der Superoxid Dismutase 2 untersucht werden.

Insgesamt konnte in der ersten Studie gezeigt werden, dass das entwickelte experimentelle Setup, unter Zuhilfenahme eines Tritium-markierten präS1 Peptides, valide Vorhersagen der Infektionshemmung durch chemische Substanzen zulässt. Zwar unterscheiden sich die ermittelten IC<sub>50</sub> Werte aus den präS1 Bindungsexperimenten um ein bis zwei Zehnerpotenzen von den IC<sub>50</sub> Werten aus den Infektionsversuchen, allerdings wird dies multifaktorielle Ursachen haben. Es handelt sich um verschiedene Zellsysteme zwischen den Experimenten mit verschiedenen Inkubationszeiten und unterschiedlicher Komposition der verwendeten Nährmedien. Vor allem das Vorhandensein von Albumin im Medium der Infektionsexperimente könnte starken Einfluss auf die tatsächlich in Lösung befindliche Konzentration der Inhibitoren haben. In Studien von Oh et al. aus 2018 wurde gezeigt, dass Albumin signifikant die inhibitorische Potenz von Betulinsäure reduzieren kann, als Folge auftretender Proteinbindung (Oh et al., 2018). Trotzdem konnten durch die beschriebene Methode qualitative Aussagen getroffen werden, welche Testsubstanzen als potentielle Entry-Inhibitoren in Frage kommen. Damit war die Grundvoraussetzung zur Erhebung von Aktivitätsdaten in größerem Umfang gegeben, um die Grundlage für eine bioinformatische Aufarbeitung in Form von Pharmakophor und QSAR Modellierungen zu schaffen, wie sie im Diskussionsteil zu Publikation III näher erläutert werden.

Nachdem ausführliche Daten zu den Betulin-Derivaten erhoben wurden, konnte das gerade beschriebene experimentelle Verfahren auch für die Analyse einer weiteren Stoffgruppe verwendet werden. Dabei handelt es sich um 87 verschiedene Propanolamin-Derivate, deren Strukturen ursprünglich zur Entwicklung von cholesterinsenkenden Substanzen zur oralen Applikation dienen. Diese sogenannten „BARIs“ (von engl. „*bile acid reabsorption inhibitors*“) interagieren mit dem spezifisch im Dünndarm exprimierten Gallensäuretransporter ASBT, welcher, wie in Kapitel 1.3 erläutert, zur selben Transporterfamilie gehört, wie NTCP. Elobixibat, Odevixibat, Limerixibat, Volixibat und Maralixibat stellen solche BARIs dar. Sie verhindern durch die Blockierung von ASBT die Rückresorption von Gallensäuren aus dem Darm, reduzieren somit den Rückfluss von Gallensäuren zur Leber und erhöhen letztlich die

Neusynthese von Gallensäuren aus Cholesterin in der Leber. Die Konsequenz ist ein Blutcholesterin senkender Effekt (Kramer and Glombik, 2006).

Aufgrund der nahen Verwandtschaft von NTCP und ASBT nahmen wir an, dass Inhibitoren von ASBT gegebenenfalls auch hemmende Effekte am NTCP bewirken könnten. Tatsächlich konnten wir drei Propranolamin-Derivate identifizieren, die letztendlich *in vitro* hemmende Wirkung auf die HDV Infektionsrate haben. Diese Derivate haben folgende Bezeichnungen: S985852, S973509 und A000295231.

Bemerkenswert ist, dass die Substanzen S973509 und A000295231 sogar eine gewisse Selektivität für die Hemmung der Virusrezeptorfunktion von NTCP aufweisen. Auch bei diesem Set an Substanzen hat sich der etablierte Versuchsablauf als sinnvoll erwiesen, um potentielle Entry-Inhibitoren zu identifizieren. Hervorzuheben ist dabei besonders die Substanz S985852, welche sowohl im präS1 Bindungsversuch als auch im HDV Infektionsversuch einen nahezu identischen IC<sub>50</sub> Wert von ca. 15 µM hervorbrachte. Im Vergleich zu den Betulin-Derivaten scheint die Aktivität dieser Stoffgruppe weniger stark von den unterschiedlichen experimentellen Rahmenbedingungen der präS1 Bindungsversuche und HDV Infektionsversuche beeinflusst zu werden.

Die Verwendung von Verbindungen, die mit ASBT interagieren, könnte Vorteile für die Entwicklung von Entry-Inhibitoren am NTCP bieten. Würde ein Hemmstoff von ASBT als Substrat erkannt werden, würde dies dessen intestinale Absorption erhöhen und zu hohen Inhibitorkonzentrationen im Portalblut führen. Folglich wären die Wirkstoffkonzentrationen am Ort der NTCP Expression, sprich an der basolateralen Membran der Hepatozyten, relativ hoch. Wenn ein Wirkstoff Substrat beider genannter Carrier wäre, könnte dies sogar theoretisch einen enterohepatischen Kreislauf ermöglichen, ähnlich dem physiologischen Kreislauf der Gallensäuren zwischen Leber und Darm (vgl. Kapitel 1.3). Dieser Effekt hätte starken Einfluss auf die nötige Dosierung dieses Wirkstoffs. Allerdings muss berücksichtigt werden, dass eine potentielle Hemmung der Gallensäuretransportfunktion von ASBT durch einen solchen Wirkstoff zu den typischen Nebenwirkungen von BARIs führen könnte, nämlich Diarrhö, Fettstuhl und Bauchschmerzen (Kramer and Glombik, 2006).

Um die strukturelle Diversität der für die bioinformatische Aufarbeitung herangezogenen Testsubstanzen noch auszuweiten, wurden nach demselben Verfahren weitere Substanzgruppen untersucht. Zum einen wurden Daten zu 18 Arylmethylamino Steroiden erhoben, welche in früheren Studien antiparasitäre Wirkung gegen *Plasmodium falciparum* und *Schistosoma mansoni* zeigten (Krieg et al., 2017). Des Weiteren wurde der Datensatz mit Substanzen



ergänzt, die in der Literatur als interagierende Liganden mit NTCP beschrieben wurden (Fukano et al., 2018; McRae et al., 2006; Dong et al., 2013; Liu et al., 2020; Shen et al., 2016; Dong et al., 2015; Saso et al., 2018; Soichiro Hata et al., 2003; Mita et al., 2006; Nkongolo et al., 2014; Shimura et al., 2017; Watashi et al., 2014).

Das Resultat ist ein großer Datensatz mit Aktivitätsdaten zu über 150 Substanzen, die zur Generierung von Pharmakophor und QSAR Modellen herangezogen werden können. Obwohl alle Substanzen in demselben experimentellen Aufbau untersucht wurden, liegen dennoch einige Limitationen vor, die nicht außer Acht gelassen werden sollten. Da Studien aus unserem Labor zeigen konnten, dass NTCP wahrscheinlich unterschiedliche Bindungsdomänen für verschiedene Substrate und Inhibitoren besitzt (Grosser et al., 2021), können wir nicht sicher davon ausgehen, dass alle getesteten Substanzen mit hemmender Aktivität der präS1 Peptid Bindung auch tatsächlich an die gleiche Domäne von NTCP binden. Außerdem kann zunächst auch nicht eindeutig zwischen allosterischen und kompetitiven Hemmprozessen differenziert werden. Eine optimale Modellierung würde nur mit Substanzen durchgeführt werden, von denen bekannt ist, dass sie alle an die gleiche Domäne der Zielstruktur binden. Da dies allerdings im Rahmen des Versuchsaufbaus nicht genau bestimmt werden kann, muss diese Unsicherheit bei der Modellierung in Kauf genommen werden.

Der experimentelle Ablauf der Studien wurde jedoch so konzipiert, dass speziell nach der Wirkung von Entry-Inhibitoren gesucht wurde. So kann bei einer Hemmung der [<sup>3</sup>H]preS1 Peptid Bindung davon ausgegangen werden, dass eine vergleichbare Wirkung auch im Infektionsversuch auftreten sollte. Außerdem wurden die Inhibitoren bei den Infektionsversuchen nur während der Inkubationszeit mit Virus auf den Zellen belassen (6 Stunden). Da man allerdings nicht ausschließen kann, dass manche Substanzen während der Inkubationszeit auch in die Zellen transportiert werden, können zusätzliche intrazelluläre Effekte nach dem Entry Schritt nicht komplett ausgeschlossen werden.

Trotz dieser Unsicherheiten konnten mit dem entwickelten Screening Verfahren gute Ergebnisse erzielt werden. Bei dem zweistufigen Virtuellen Screening Ansatz wurden zunächst ca. 11 Millionen Substanzen der ZINC Datenbank mit einem Pharmakophor Modell durchmustert. Die resultierenden 177.000 Treffer wurden anschließend mit einem QSAR Modell analysiert und die 20 kommerziell verfügbaren Substanzen mit der stärksten vorhergesagten Aktivität wurden daraufhin näher untersucht. Es stellte sich heraus, dass 4 der 20 getesteten Substanzen tatsächlich die gewünschte hemmende Aktivität am NTCP aufweisen und auch im HDV Infektionsversuch eine konzentrationsabhängige Reduktion der

Infektionsraten verursachen. Damit liegt eine Vorhersagekraft von ca. 20% für unser Screening Verfahren vor, was einem guten Durchschnitt der zu erwarteten Vorhersagekraft solcher Modelle entspricht. Laut Literatur reicht die Prädiktivität solcher Screening Methoden von 1% bis 40% (Neves et al., 2018). Diese Ergebnisse indizieren, dass der Anteil der Substanzen, die die Grundvoraussetzungen für das Liganden basierte virtuelle Screening nicht optimal erfüllen, in unserem Datensatz gering genug sein sollte, um eine zuverlässige Vorhersage zu erhalten. Im Vergleich zum klassischen Hoch-Durchsatz-Screening mit einer Trefferquote von 0,01% bis 0,1% (Thorne et al., 2010; Butkiewicz et al., 2013) stellt unser aufgestelltes Screening System also eine vielversprechende Methode zur Identifizierung neuer HBV und HDV Entry-Inhibitoren dar.

Die Daten der Publikationen I bis III beleuchten gemeinsam einen wichtigen Punkt bei der Entwicklung von Arzneistoffen. Diesen Punkt kann man als „Wirkungs-Selektivität“ oder „Spezifität“ eines Wirkstoffes an der Zielstruktur bezeichnen. Gemeint ist im konkreten Fall dieser Forschungsarbeit, dass ein potentieller Entry-Inhibitor idealerweise spezifisch nur die Virusrezeptorfunktion von NTCP blockieren soll, ohne dessen Gallensäuretransportfunktion zu beeinträchtigen. Dies wurde in den bisherigen Kapiteln unter Einführung des Faktors „Selektivitätsindex“ bereits ausgiebig erörtert.

In einer vierten Publikation, die ebenfalls Teil der vorliegenden Arbeit darstellt, wurden zwei weitere wichtige Punkte analysiert, welche bei der Wirkstoffentwicklung Beachtung finden müssen.

Der erste dieser Punkte lässt sich durch den Begriff „Target-Spezifität“ beschreiben. Damit ist gemeint, dass ein potentieller Wirkstoff, um möglichst nebenwirkungsarm zu sein, idealerweise spezifisch nur an einer einzigen Zielstruktur (Target) wirken sollte, ohne sogenannte „Off-Target Effekte“ durch Interaktion mit anderen Strukturen zu verursachen. In diesem konkreten Fall handelt es sich bei der Zielstruktur um NTCP. Im Rahmen der Studien in Publikation IV wurden daher systematisch die drei nahe verwandten Transportproteine NTCP, ASBT und SOAT untersucht, wobei deren Gemeinsamkeiten und Unterschiede im Hinblick auf Substrat- und Inhibitoren-Spektrum ausgearbeitet wurden. Mit dem Inhibitor Betulinsäure lässt sich hier ein wunderbares Beispiel für Target-Spezifität darstellen. Vergleicht man die Hemmung des Transportes von Taurocholsäure über die Transporter NTCP und ASBT, stellt man fest, dass Betulinsäure den Transport am NTCP mit einem  $IC_{50}$  von 800 nM hemmt, wobei der  $IC_{50}$  am ASBT bei über 1 mM liegt. Das gleiche Substrat wird an den beiden verwandten Transportproteinen durch den gleichen Inhibitor also mit sehr unterschiedlicher Potenz

gehemmt. Ein Gegenbeispiel stellt Betulin als Inhibitor dar. Vergleicht man die Hemmkurven von NTCP, ASBT und SOAT für das Substrat Tauroolithocholsäure, stellt man fest, dass Betulin alle drei Transportproteine mit ähnlicher Hemmkinetik beeinflusst. Damit scheint Betulin in Bezug auf das Substrat Tauroolithocholsäure keine Target-Spezifität aufzuweisen.

Ein weiterer Faktor stellt einen Unterpunkt zu den gerade erläuterten Beobachtungen dar. Da sich die untersuchten Transporter NTCP, ASBT und SOAT in ihrem Substratspektrum unterscheiden, gilt es nicht nur die Target-Spezifität eines Inhibitors zu charakterisieren, sondern auch die Hemmeigenschaften auf jedes einzelne Substrat des entsprechenden Targets. NTCP transportiert alle drei getesteten Substrate der Studie (Taurocholsäure, Tauroolithocholsäure und Dehydroepiandrosteronsulfat). Von ASBT hingegen wird das Dehydroepiandrosteronsulfat nicht als Substrat erkannt. Im Falle von SOAT wird Taurocholsäure nicht transportiert. In Bezug auf das hier erläuterte wissenschaftliche Projekt kommt die Frage auf, ob ein potentieller Wirkstoff, der als viraler Entry-Inhibitor fungieren soll, Einfluss auf den Transport eines beliebigen Substrates des Zielproteins sowie dessen nächst verwandter Transportproteine haben könnte. Hier kann der Begriff der „Substrat-Spezifität“ eingeführt werden. In Publikation IV wurde Tabelle 5 erstellt, die ein Screening auf Substrat-Spezifität ausgewählter Hemmstoffe veranschaulicht. Am Beispiel von Cyclosporin A erkennt man, dass dieser Hemmstoff an NTCP mit hoher Spezifität den Dehydroepiandrosteronsulfat Transport hemmt und im Vergleich einen moderaten Einfluss auf die Transportrate von Taurocholsäure hat sowie nur geringen Einfluss auf den Transport von Tauroolithocholsäure. Im Fall von ASBT hemmt Cyclosporin A mit der getesteten Konzentration keines der Substrate, wobei die Hemmung der Transportaktivität von SOAT für beide Substrate nur gering ist. Eine Substrat-Spezifität konnte für diesen Hemmstoff also für das Substrat Dehydroepiandrosteronsulfat am NTCP gezeigt werden. Ein Beispiel für einen sogenannten „Pan-Inhibitor“ stellt Troglitazon dar. Diese Substanz zeigt weder Target-Spezifität noch Substrat-Spezifität. Sie hemmt alle drei Transportproteine mit sehr hoher Potenz bei allen untersuchten Substraten.

Als Fazit lässt sich festhalten, dass für die erfolgreiche Entwicklung eines HBV/HDV Entry-Inhibitors nicht allein das Zielprotein NTCP betrachtet werden sollte. Zwar ist die Wirkungs-Selektivität eines potentiellen Inhibitors für die Blockierung der Virusrezeptorfunktion dieses Targets von essentieller Bedeutung, allerdings spielen die beschriebene Target-Spezifität sowie Substrat-Spezifität von Inhibitoren eine nicht zu vernachlässigende Rolle. Dies mit einzubeziehen, stellt ein größeres Unterfangen dar, da besonders NTCP, wie in Kapitel 1.3 erläutert, ein recht großes Substratspektrum aufweist. Daher ist auf Grundlage dieser

Forschungsarbeit angedacht, das beschriebene experimentelle Verfahren zur Generierung von  $IC_{50}$  Daten am NTCP auch auf die Transportproteine ASBT und SOAT auszuweiten und alle bekannten Substrate dieser Transporter in Hemmstudien mit einzubeziehen.

## 4 Ausblick

Die stets fortschreitende Technisierung und Digitalisierung ermöglicht immer stärkere Einbindung von computergestützten Methoden in wissenschaftlichen Studien. Das in dieser Arbeit beschriebene virtuelle Screening ist ein Paradebeispiel dafür. Bis heute ist das klassische Hoch-Durchsatz-Screening immer noch eine gängige Methode, um neue Leitstrukturen für potentielle Arzneistoffe zu identifizieren. Selbst wenn die zu testenden Substanzen nach einem gewissen Prinzip ausgewählt werden, zum Beispiel mit dem Fokus auf einer bestimmten Substanzklasse, wie den Triterpenoiden, gleicht diese Methode doch einer Suche nach der oder den Nadeln im Heuhaufen. Außerdem ist für diesen Ansatz, wie bereits erläutert, ein hoher technischer und finanzieller Aufwand nötig, da jede in Frage kommende Substanz tatsächlich physisch vorliegen und experimentell getestet werden muss. Durch stetige Erzeugung neuer Derivate bestimmter Substanzen oder der Identifizierung neuer natürlich vorkommender Stoffe, sammeln sich immer größere Datenbanken an, die auch als „Substanzbibliotheken“ bezeichnet werden. Heutzutage stehen besonders Naturstoffe aus dem marinen Bereich im Fokus, da dort überwiegend die chemische Kommunikation von Bedeutung ist und eine hohe Diversität chemischer Verbindungen hervorgebracht hat (Bugni et al., 2008). Diese gigantische Auswahl an Substanzen für eine spezielle Fragestellung experimentell durchzutesten stellt eine unerfüllbare Aufgabe dar, wie sie Sisyphos aus der griechischen Mythologie aufgetragen wurde. Somit hilft die computergestützte virtuelle Filterung von Substanzbibliotheken dabei, zwar alle verfügbaren Substanzen einer Bibliothek mit einzubeziehen, allerdings nur solche tatsächlich experimentell zu validieren, die laut bioinformatischer Berechnungen auch potentielle Wirkungen an der Zielstruktur haben. Ein offensichtliches Manko besteht darin, dass durch die verwendeten Computermodelle für das virtuelle Screening gegebenenfalls Substanzen ausgeschlossen werden könnten, die doch eine Wirkung an der Zielstruktur hätten zeigen können. Anders herum betrachtet ist das Hoch-Durchsatz-Screening allerdings auch nicht unfehlbar, da in der Regel aufgrund der Menge an zu testenden Stoffen, zunächst keine Wiederholungsversuche mit einer Einzelsubstanz stattfinden. Wenn zufällige Einflüsse im Testsystem des Hoch-Durchsatz-Verfahrens das Ergebnis verfälschen, kann es auch hier passieren, dass Substanzen als unreaktiv herausfallen, die eigentlich Reaktivität zeigen würden. Vermutlich werden sowohl das virtuelle Screening als auch das Hoch-Durchsatz-Screening zukünftig weiter optimiert, um die immer größer werdende Anzahl verfügbarer Substanzen für bestimmte Fragestellungen zu analysieren. Beim Hoch-Durchsatz-Screening wird dies durch immer stärker automatisiert ablaufende Versuchsabläufe geschehen, durch welche experimentelle Schwankungen durch menschlichen Einfluss immer stärker reduziert werden.

Im Falle des virtuellen Screenings bieten sich vielseitige Möglichkeiten der Optimierung. Im Zeitalter der künstlichen Intelligenz wird auch hier versucht, personenbedingte Ungenauigkeiten und Fehler zu umgehen. Wie bereits in Kapitel 1.6.2 erwähnt, gibt es bereits jetzt die Möglichkeit, auch die Generierung von Computermodellen automatisiert und durch maschinelle Lernmethoden (engl. „*machine learning*“) durchführen zu lassen. Des Weiteren ist ein Modell genau genommen nie vollkommen. D.h., dass jedes Modell mit neuen Daten ergänzt und neu berechnet werden kann. Man kann von einem perpetuierenden Modell sprechen, das laut Theorie stetig mit neuen Daten angepasst und im optimalen Fall dadurch immer prädiktiver für die gegebene Fragestellung wird.

Die in dieser Arbeit aufgeführten Studien bieten noch weitere Möglichkeiten des wissenschaftlichen Wertgewinns. So können alle in einem identischen Versuchsaufbau generierten Aktivitätsdaten aus dieser Arbeit als wissenschaftlich wertvoller Datensatz angesehen werden. Nicht nur für eigene Studien aus diesem Labor, sondern auch für andere Arbeitsgruppen eröffnen sich durch die Veröffentlichung dieser Daten Möglichkeiten, eigene bioinformatische Aufarbeitungen durchzuführen. So können mit unterschiedlicher Software aus dem gleichen Datensatz diverse Modelle entstehen, die untereinander in ihren Eigenschaften verglichen werden können. Auch die Etablierung neuer Algorithmen wird ermöglicht mit der Möglichkeit des Vergleiches mit bereits ausgiebig getesteten Verfahren.

Die generierten Modelle dieser Arbeit können zusätzlich dazu genutzt werden, zielgerichtetes molekulares Wirkstoff Design (engl. „*molecular drug design*“) durchzuführen (Verma et al., 2010). Dabei können die Computermodelle Aufschluss darüber geben, welche Form der Derivatisierung bestimmter Leitstrukturen sinnvoll sein könnten, die gewünschte Aktivität an der Zielstruktur zu verbessern. Dies ermöglicht Chemikern zielgerichtete Modifikation der Leitstruktur und verhindert die willkürliche Erzeugung einer Vielzahl von Derivaten, die im Endeffekt zeit- und kostenintensiv wäre.

QSAR und Pharmakophor Modelle können nicht nur für die Vorhersage von Aktivitäten in Form von IC<sub>50</sub>, EC<sub>50</sub> etc. herangezogen werden, sondern dienen auch der ersten Einschätzung toxikologischer Einflüsse von Substanzen. Dabei entsprechen die für das Modell hinterlegten „Aktivitätsdaten“ der Substanzen einem Index für die Toxizität des jeweiligen Stoffes in dem getesteten System.

Trotz aller virtueller Vorhersagen und *in vitro* Aktivitätsdaten der genannten Substanzen, besteht ein nächster Schritt unserer Arbeitsgruppe bei der Identifizierung von HBV/HDV Entry-Inhibitoren darin, die Wirksamkeit und die Pharmakokinetik ausgewählter Substanzen

im Lebewesen zu untersuchen. Dafür kommen die in Kapitel 1.5.3 erwähnten humanisierten uPA/SCID Mäuse in Frage, die bereits bei Studien zum derzeit als einziger Entry-Inhibitor zugelassenen Arzneimittel Hepcludex verwendet wurden (Schulze et al., 2010; Volz et al., 2013).

Doch egal wie weitreichend Studien zu Entry-Inhibitoren auch sein mögen und wie vielversprechend einzelne Substanzen auch scheinen, sind sich die Forschenden Experten auf dem Gebiet der HBV und HDV Infektionen einig, dass es wahrscheinlich nie DAS eine Medikament als Monotherapie geben wird. Das wahrscheinlichere Szenario wäre eine Kombinationstherapie, bei der sich gegenseitig begünstigende Effekte einzelner Therapeutika optimal ausgenutzt werden, um Viruseintritt, -replikation und -freisetzung von HBV und HDV auf verschiedenen Ebenen attackieren zu können (Prifti et al., 2021; Reville et al., 2019; Alter et al., 2018).

## 5 Zusammenfassung (Deutsch)

Infektionen mit dem Hepatitis B (HBV) und D Virus (HDV) sind die Hauptursache für Lebertumoren als Folge chronischer Hepatitiden. Trotz Verfügbarkeit der Impfung gegen HBV, welche auch erfolgreich vor HDV Infektionen schützt, sterben jährlich mehr als 800.000 Menschen, vor allem in armen Regionen der Welt, an dieser folgenschweren Erkrankung. Antivirale Therapien mit Interferonen und/oder Nukleos(t)id Analoga ermöglichen es, die chronische Hepatitis in den meisten Fällen unter Kontrolle zu halten. Diese Therapien müssen allerdings meist ein Leben lang erfolgen, bei teilweise gravierenden Nebenwirkungen und bergen nur geringe Aussicht auf vollständige Heilung.

Mit dem Jahr 2012 eröffnete sich allerdings ein ganz neues Feld für Therapiemöglichkeiten, da zu diesem Zeitpunkt das „Na<sup>+</sup>/Taurocholate Cotransporting Polypeptide“ (NTCP, Gensymbol: *SLC10A1*) als spezifischer hepatozellulärer Rezeptor für HBV und HDV identifiziert wurde. NTCP war bis dahin nur als natriumgekoppelter Transporter für Gallensäuren bekannt, welcher in der basolateralen Membran von Leberzellen exprimiert wird und dort Gallensäuren aus dem Blut zurück in Leberzellen transportiert. Somit ist NTCP ein wichtiger Bestandteil des enterohepatischen Kreislaufs der Gallensäuren.

Mit seiner zweiten Funktion als Rezeptor für HBV und HDV stellt NTCP ein interessantes therapeutisch nutzbares Zielmolekül dar. Mit einer medikamentellen Blockierung von NTCP wird versucht, den Eintritt (engl. „entry“) der beiden genannten Viren zu verhindern. Es dauerte bis zum Jahr 2020, bis der erste sogenannte „Entry-Inhibitor“ für die Therapie von HDV Infektionen zugelassen wurde. Es handelt sich um ein synthetisches Peptid mit dem Markennamen Hepcludex<sup>®</sup>, das seinen Ursprung in den Virushüllen von HBV und HDV selbst hat und nach subkutaner Applikation an NTCP bindet. NTCP wird dadurch für eine Virusbindung unzugänglich gemacht. Da besonders in armen Regionen der Welt Bedarf an Therapeutika besteht, ist ein Entry-Inhibitor auf Grundlage eines injizierbaren Peptides jedoch für diesen Bedarf nicht die beste Wahl, da Anforderung an Lagerung und Transport schwerer zu gewährleisten sind als bei einem Medikament in Tablettenform. Hinzu kommt, dass durch dieses Peptid auch die Gallensäuretransportfunktion von NTCP gehemmt wird und so in die Gallensäurehomöostase eingegriffen wird.

In der vorliegenden Arbeit konnten Struktur-Wirkungs-Beziehungen aufgezeigt werden, die veranschaulichen, dass eine selektive Hemmung der Virusrezeptorfunktion bei erhaltener Gallensäuretransportaktivität an NTCP grundsätzlich möglich ist. Aus der Gruppe der Betulin-Derivate zeigte 3,28-Di-O-acetyl-29-Hydroxybetulin das beste Profil mit einem IC<sub>50</sub> der präS1



Peptid Bindung von 8  $\mu\text{M}$  und einem Selektivitätsindex von 125. Unter den Propanolamin-Derivaten weist Substanz A000295231 das beste Profil auf mit einem  $\text{IC}_{50}$  von 16  $\mu\text{M}$  und Selektivitätsindex von 65.

Außerdem konnte durch ein einheitliches experimentelles Verfahren ein großer Datensatz generiert werden, der die weitere bioinformatische Aufarbeitung unter Verwendung von Pharmakophor und QSAR Modellen ermöglicht. Es konnte ein virtuelles Screeningverfahren durchgeführt werden, mit dem die Identifizierung neuartiger, potentiell oral anwendbarer Entry-Inhibitoren ermöglicht wird. Unter diesen Substanzen zeigte die Verbindung ZINC000253533654 mit einem  $\text{IC}_{50}$  von 9  $\mu\text{M}$  die beste Aktivität, welche auch durch *in vitro* Infektionsexperimente bestätigt werden konnte. Allerdings liegt der Selektivitätsindex dieser Verbindung bei 1. Trotzdem sind die gewonnenen Daten und Erkenntnisse geeignet, molekulares Medikamentendesign durchzuführen und im Idealfall einen Wirkstoff zu entwickeln, der selektiv die Virusbindung an NTCP hemmt ohne Einfluss auf den Gallensäurekreislauf zu nehmen, bei einfacher oraler Verabreichung.

Das Resultat der vorliegenden wissenschaftlichen Arbeit ist eine Plattform, die sowohl experimentell als auch bioinformatisch derart ausgestaltet ist, dass umfangreiche Grundlagenstudien auf dem Weg zu einem Entry-Inhibitor durchgeführt und analysiert werden können. Die in Kapitel 3 erläuterten Begriffe der Wirkungs-Selektivität, Target-Spezifität und Substrat-Spezifität werden dabei mit einbezogen und sind wegweisend bei der Entwicklung neuer HBV/HDV Entry-Inhibitoren aus der Gruppe der small molecules.

## 6 Summary (English)

Infections with hepatitis B (HBV) and D virus (HDV) are the main cause of liver carcinoma as a result of chronic hepatitis. Despite the availability of vaccination against HBV, which also successfully protects against HDV infections, more than 800,000 people annually die from this serious disease, mainly in poor regions of the world. Antiviral therapies using interferons and/or nucleos(t)id analoga are usually sufficient to keep chronic hepatitis under control. However, these therapeutics usually have to be given lifelong causing some serious side effects. Furthermore, the chance of curation is very low.

In 2012, however, a new field of therapeutic opportunities opened up, as the "Na<sup>+</sup>/taurocholate cotransporting polypeptide" (NTCP, gene symbol: *SLC10A1*) was identified as the specific hepatocellular receptor for HBV and HDV. Previously, NTCP was known to be a sodium-coupled transporter of bile acids expressed at the basolateral membrane of hepatocytes. There it delivers bile acids from the portal blood back to the liver. Thus, NTCP represents an important component of the enterohepatic circulation of bile acids.

Due to its second function as receptor for HBV and HDV, NTCP represents an interesting drug target. Blocking of NTCP with small molecules is an attempt to prevent the entry of the two mentioned viruses. In 2020, a first so-called entry inhibitor was approved for therapy of HDV infections. It represents a synthetic peptide with the brand name Hepcludex<sup>®</sup>, which originates from the viral envelopes of HBV and HDV and binds to NTCP after subcutaneous application. This makes NTCP inaccessible for virus binding. However, due to the particular need for therapeutics in poor regions of the world, an entry inhibitor based on an injectable peptide drug is not optimal, since storage and transport requirements are difficult to guarantee. In addition, many substances, including the above-mentioned peptide, also inhibit the bile acid transport function of NTCP, thus interfering with bile acid homeostasis.

The present study demonstrates that structure-activity relationships can be defined for selective inhibition of the viral receptor function of NTCP without tackling its bile acid transport function. Among the group of betulin derivatives, 3,28-di-O-acetyl-29-hydroxybetulin showed the best profile with an IC<sub>50</sub> of preS1 peptide binding inhibition of 8 μM and selectivity index of 125. Among the propanolamine derivatives, compound A000295231 showed the best performance with IC<sub>50</sub> of 16 μM and selectivity index of 65, respectively.

In addition, the uniform experimental procedure of the present study generated a large dataset enabling further bioinformatics processing by using pharmacophore and QSAR models. A virtual screening could already be performed that identified novel, potential oral HBV/HDV

entry inhibitors. Among them, compound ZINC000253533654 showed the best activity against preS1 peptide binding with an  $IC_{50}$  of 9  $\mu$ M, which was also confirmed by *in vitro* infection experiments. Unfortunately, the selectivity index of this compound was low at 1. Nevertheless, the data and findings obtained are suitable to perform molecular drug design and to develop a drug that selectively blocks virus binding to NTCP without affecting bile acid circulation, with simple oral administration of the drug.

The overall outcome of the present study is an experimental and virtual screening platform suitable for identification of potent and virus-selective HBV/HDV entry inhibitors. The concepts of selectivity, target specificity and substrate specificity explained in chapter 3 are basic components of this platform and pioneer in the further development of HBV/HDV entry inhibitors from the group of small molecules.

## 7 Literaturverzeichnis

- ABD EL AZIZ, M. A., SACCO, R. & FACCIORUSSO, A. 2020. Nucleos(t)ide analogues and Hepatitis B virus-related hepatocellular carcinoma: A literature review. *Antivir Chem Chemother*, 28, 2040206620921331.
- ADELEKE, G. E. & ADARAMOYE, O. A. 2017. Betulinic acid protects against N-nitrosodimethylamine-induced redox imbalance in testes of rats. *Redox Rep.*, 22, 556-562.
- AKIRA, S., UEMATSU, S. & TAKEUCHI, O. 2006. Pathogen recognition and innate immunity. *Cell*, 124, 783-801.
- ALFAIATE, D., DENY, P. & DURANTEL, D. 2015. Hepatitis delta virus: From biological and medical aspects to current and investigational therapeutic options. *Antiviral Res*, 122, 112-29.
- ALTER, H., BLOCK, T., BROWN, N., BROWNSTEIN, A., BROSGART, C., CHANG, K. M., CHEN, P. J., CHISARI, F. V., COHEN, C., EL-SERAG, H., FELD, J., GISH, R., GLENN, J., GRETEN, T., GUO, H., GUO, J. T., HOSHIDA, Y., HU, J., KOWDLEY, K. V., LI, W., LIANG, J., LOCARNINI, S., LOK, A. S., MASON, W., MCMAHON, B., MEHTA, A., PERRILLO, R., REVILL, P., RICE, C. M., RINAUDO, J., SCHINAZI, R., SEEGER, C., SHETTY, K., TAVIS, J. & ZOULIM, F. 2018. A research agenda for curing chronic hepatitis B virus infection. *Hepatology*, 67, 1127-1131.
- ANANTHANARAYANAN, M., NG, O. C., BOYER, J. L. & SUCHY, F. J. 1994. Characterization of cloned rat liver Na(+)-bile acid cotransporter using peptide and fusion protein antibodies. *Am J Physiol*, 267, G637-43.
- ANWER, M. S. & STIEGER, B. 2014. Sodium-dependent bile salt transporters of the SLC10A transporter family: more than solute transporters. *Pflugers Arch*, 466, 77-89.
- BARDHAN, A., BRUCKNER-TUDERMAN, L., CHAPPLE, I. L. C., FINE, J. D., HARPER, N., HAS, C., MAGIN, T. M., MARINKOVICH, M. P., MARSHALL, J. F., MCGRATH, J. A., MELLERIO, J. E., POLSON, R. & HEAGERTY, A. H. 2020. Epidermolysis bullosa. *Nat Rev Dis Primers*, 6, 78.
- BEELEY, N. R. A. & SAGE, C. 2003. GPCRs: an update on structural approaches to drug discovery. *Targets*, 2, 19-25.
- BERTOLETTI, A. & GEHRING, A. J. 2006. The immune response during hepatitis B virus infection. *J Gen Virol*, 87, 1439-1449.
- BILLIoud, G., KRUSE, R. L., CARRILLO, M., WHITTEN-BAUER, C., GAO, D., KIM, A., CHEN, L., MCCALEB, M. L., CROSBY, J. R., HAMATAKE, R., HONG, Z., GARAIGORTA, U., SWAYZE, E., BISSIG, K. D. & WIELAND, S. 2016. In vivo reduction of hepatitis B virus antigenemia and viremia by antisense oligonucleotides. *J Hepatol*, 64, 781-9.
- BLANCHET, M., SUREAU, C. & LABONTE, P. 2014. Use of FDA approved therapeutics with hNTCP metabolic inhibitory properties to impair the HDV lifecycle. *Antiviral Res.*, 106, 111-5.
- BLANK, A., EIDAM, A., HAAG, M., HOHMANN, N., BURHENNE, J., SCHWAB, M., VAN DE GRAAF, S., MEYER, M. R., MAURER, H. H., MEIER, K., WEISS, J., BRUCKNER, T., ALEXANDROV, A., URBAN, S., MIKUS, G. & HAEFELI, W. E. 2018. The NTCP-inhibitor Myrcludex B: Effects on Bile Acid Disposition and Tenofovir Pharmacokinetics. *Clin. Pharmacol. Ther.*, 103, 341-348.
- BLUMBERG, B. S., GERSTLEY, B. J., HUNGERFORD, D. A., LONDON, W. T. & SUTNICK, A. I. 1967. A serum antigen (Australia antigen) in Down's syndrome, leukemia, and hepatitis. *Ann Intern Med*, 66, 924-31.
- BOCKMANN, J. H., STADLER, D., XIA, Y., KO, C., WETTENGEL, J. M., SCHULZE ZUR WIESCH, J., DANDRI, M. & PROTZER, U. 2019. Comparative Analysis of the Antiviral Effects Mediated by Type I and III Interferons in Hepatitis B Virus-Infected Hepatocytes. *J Infect Dis*, 220, 567-577.
- BUGNI, T. S., RICHARDS, B., BHOITE, L., CIMBORA, D., HARPER, M. K. & IRELAND, C. M. 2008. Marine natural product libraries for high-throughput screening and rapid drug discovery. *J Nat Prod*, 71, 1095-8.

- BUTKIEWICZ, M., LOWE, E. W., JR., MUELLER, R., MENDENHALL, J. L., TEIXEIRA, P. L., WEAVER, C. D. & MEILER, J. 2013. Benchmarking ligand-based virtual High-Throughput Screening with the PubChem database. *Molecules*, 18, 735-56.
- CHEN, I. J. & FOLOPPE, N. 2010. Drug-like bioactive structures and conformational coverage with the LigPrep/ConfGen suite: comparison to programs MOE and catalyst. *J Chem Inf Model*, 50, 822-39.
- CHEN, Y., SIT, S. Y., CHEN, J., SWIDORSKI, J. J., LIU, Z., SIN, N., VENABLES, B. L., PARKER, D. D., NOWICKA-SANS, B., LIN, Z., LI, Z., TERRY, B. J., PROTACK, T., RAHEMATPURA, S., HANUMEGOWDA, U., JENKINS, S., KRYSTAL, M., DICKER, I. D., MEANWELL, N. A. & REGUEIRO-REN, A. 2018. The design, synthesis and structure-activity relationships associated with C28 amine-based betulinic acid derivatives as inhibitors of HIV-1 maturation. *Bioorg. Med. Chem. Lett.*, 28, 1550-1557.
- CICHEWICZ, R. H. & KOUZI, S. A. 2004. Chemistry, biological activity, and chemotherapeutic potential of betulinic acid for the prevention and treatment of cancer and HIV infection. *Med. Res. Rev.*, 24, 90-114.
- COX, R., GREEN, D. V., LUSCOMBE, C. N., MALCOLM, N. & PICKETT, S. D. 2013. QSAR workbench: automating QSAR modeling to drive compound design. *J Comput Aided Mol Des*, 27, 321-36.
- DA COSTA, K. S., GALUCIO, J. M., DA COSTA, C. H. S., SANTANA, A. R., DOS SANTOS CARVALHO, V., DO NASCIMENTO, L. D., LIMA, E. L. A. H., NEVES CRUZ, J., ALVES, C. N. & LAMEIRA, J. 2019. Exploring the Potentiality of Natural Products from Essential Oils as Inhibitors of Odorant-Binding Proteins: A Structure- and Ligand-Based Virtual Screening Approach To Find Novel Mosquito Repellents. *ACS Omega*, 4, 22475-22486.
- DANE, D. S., CAMERON, C. H. & BRIGGS, M. 1970. Virus-like particles in serum of patients with Australia-antigen-associated hepatitis. *Lancet*, 1, 695-8.
- DIXON, S. L., DUAN, J., SMITH, E., VON BARGEN, C. D., SHERMAN, W. & REPASKY, M. P. 2016. AutoQSAR: an automated machine learning tool for best-practice QSAR modeling. *Future Med. Chem.*, 8, 1825-1839.
- DIXON, S. L., SMONDYREV, A. M., KNOLL, E. H., RAO, S. N., SHAW, D. E. & FRIESNER, R. A. 2006. PHASE: a new engine for pharmacophore perception, 3D QSAR model development, and 3D database screening: 1. Methodology and preliminary results. *J Comput Aided Mol Des*, 20, 647-71.
- DONG, Z., EKINS, S. & POLLI, J. E. 2013. Structure-activity relationship for FDA approved drugs as inhibitors of the human sodium taurocholate cotransporting polypeptide (NTCP). *Mol Pharm*, 10, 1008-19.
- DONG, Z., EKINS, S. & POLLI, J. E. 2015. A substrate pharmacophore for the human sodium taurocholate co-transporting polypeptide. *Int J Pharm*, 478, 88-95.
- DONKERS, J. M., ZEHNDER, B., VAN WESTEN, G. J. P., KWAKKENBOS, M. J., AP, I. J., OUDE ELFERINK, R. P. J., BEUERS, U., URBAN, S. & VAN DE GRAAF, S. F. J. 2017. Reduced hepatitis B and D viral entry using clinically applied drugs as novel inhibitors of the bile acid transporter NTCP. *Sci. Rep.*, 7, 15307.
- DÖRING, B., LÜTTEKE, T., GEYER, J. & PETZINGER, E. 2012. The SLC10 carrier family: transport functions and molecular structure. *Curr. Top. Membr.*, 70, 105-68.
- EDWARDS, T. C., PONZAR, N. L. & TAVIS, J. E. 2019. Shedding light on RNaseH: a promising target for hepatitis B virus (HBV). *Expert Opin Ther Targets*, 23, 559-563.
- EL KERDAWY, A. M., OSMAN, A. A. & ZAATER, M. A. 2019. Receptor-based pharmacophore modeling, virtual screening, and molecular docking studies for the discovery of novel GSK-3beta inhibitors. *J Mol Model*, 25, 171.
- FANNING, G. C., ZOULIM, F., HOU, J. & BERTOLETTI, A. 2019. Therapeutic strategies for hepatitis B virus infection: towards a cure. *Nat Rev Drug Discov*, 18, 827-844.
- FERNANDES, C. F., GODOY, J. R., DÖRING, B., CAVALCANTI, M. C., BERGMANN, M., PETZINGER, E. & GEYER, J. 2007. The novel putative bile acid transporter SLC10A5 is highly expressed in liver and kidney. *Biochem Biophys Res Commun*, 361, 26-32.

- FRIESEMA, E. C., DOCTER, R., MOERINGS, E. P., STIEGER, B., HAGENBUCH, B., MEIER, P. J., KRENNING, E. P., HENNEMANN, G. & VISSER, T. J. 1999. Identification of thyroid hormone transporters. *Biochem Biophys Res Commun*, 254, 497-501.
- FUKANO, K., TSUKUDA, S., OSHIMA, M., SUZUKI, R., AIZAKI, H., OHKI, M., PARK, S. Y., MURAMATSU, M., WAKITA, T., SUREAU, C., OGASAWARA, Y. & WATASHI, K. 2018. Troglitazone Impedes the Oligomerization of Sodium Taurocholate Cotransporting Polypeptide and Entry of Hepatitis B Virus Into Hepatocytes. *Front. Microbiol.*, 9, 3257.
- FUKANO, K., TSUKUDA, S., WATASHI, K. & WAKITA, T. 2019. Concept of Viral Inhibitors via NTCP. *Semin. Liver Dis.*, 39, 78-85.
- GALBURT, E. A. & TOMKO, E. J. 2017. Conformational selection and induced fit as a useful framework for molecular motor mechanisms. *Biophys Chem*, 223, 11-16.
- GALUN, E., EREN, R., SAFADI, R., ASHOUR, Y., TERRAULT, N., KEEFFE, E. B., MATOT, E., MIZRACHI, S., TERKIELTAUB, D., ZOHAR, M., LUBIN, I., GOPHER, J., SHOUVAL, D. & DAGAN, S. 2002. Clinical evaluation (phase I) of a combination of two human monoclonal antibodies to HBV: safety and antiviral properties. *Hepatology*, 35, 673-9.
- GARCIA-HERNANDEZ, C., FERNANDEZ, A. & SERRATOSA, F. 2019. Ligand-Based Virtual Screening Using Graph Edit Distance as Molecular Similarity Measure. *J Chem Inf Model*, 59, 1410-1421.
- GEHRING, A. J. & PROTZER, U. 2019. Targeting Innate and Adaptive Immune Responses to Cure Chronic HBV Infection. *Gastroenterology*, 156, 325-337.
- GERELSAIKHAN, T., TAVIS, J. E. & BRUSS, V. 1996. Hepatitis B virus nucleocapsid envelopment does not occur without genomic DNA synthesis. *J Virol*, 70, 4269-74.
- GEYER, J., DÖRING, B., MEERKAMP, K., UGELE, B., BAKHIYA, N., FERNANDES, C. F., GODOY, J. R., GLATT, H. & PETZINGER, E. 2007. Cloning and functional characterization of human sodium-dependent organic anion transporter (SLC10A6). *J. Biol. Chem.*, 282, 19728-41.
- GEYER, J., WILKE, T. & PETZINGER, E. 2006. The solute carrier family SLC10: more than a family of bile acid transporters regarding function and phylogenetic relationships. *Arch. Pharmacol.*, 372, 413-31.
- GHAFFARI MOGHADDAM, M., BIN H. AHMAD, F. & SAMZADEH-KERMANI, A. 2012. Biological Activity of Betulinic Acid: A Review. *Pharmacol. Pharm.*, 03, 119-123.
- GLEBE, D. & BREMER, C. M. 2013. The molecular virology of hepatitis B virus. *Semin. Liver. Dis.*, 33, 103-12.
- GLEBE, D. & URBAN, S. 2007. Viral and cellular determinants involved in hepadnaviral entry. *World J Gastroenterol*, 13, 22-38.
- GLEBE, D., URBAN, S., KNOOP, E. V., CAG, N., KRASS, P., GRUN, S., BULAVAITE, A., SASNAUSKAS, K. & GERLICH, W. H. 2005. Mapping of the hepatitis B virus attachment site by use of infection-inhibiting preS1 lipopeptides and tupaia hepatocytes. *Gastroenterology*, 129, 234-45.
- GODOY, J. R., FERNANDES, C., DÖRING, B., BEUERLEIN, K., PETZINGER, E. & GEYER, J. 2007. Molecular and phylogenetic characterization of a novel putative membrane transporter (SLC10A7), conserved in vertebrates and bacteria. *Eur J Cell Biol*, 86, 445-60.
- GREUPINK, R., NABUURS, S. B., ZARZYCKA, B., VERWEIJ, V., MONSHOUWER, M., HUISMAN, M. T. & RUSSEL, F. G. 2012. In silico identification of potential cholestasis-inducing agents via modeling of Na(+)-dependent taurocholate cotransporting polypeptide substrate specificity. *Toxicol Sci*, 129, 35-48.
- GRIMM, D., THIMME, R. & BLUM, H. E. 2011. HBV life cycle and novel drug targets. *Hepatol Int*, 5, 644-53.
- GRIPON, P., CANNIE, I. & URBAN, S. 2005. Efficient inhibition of hepatitis B virus infection by acylated peptides derived from the large viral surface protein. *J. Virol.*, 79, 1613-22.
- GROSSER, G., BARINGHAUS, K. H., DÖRING, B., KRAMER, W., PETZINGER, E. & GEYER, J. 2016. Identification of novel inhibitors of the steroid sulfate carrier 'sodium-dependent organic anion transporter' SOAT (SLC10A6) by pharmacophore modelling. *Mol Cell Endocrinol*, 428, 133-41.

- GROSSER, G., MÜLLER, S. F., KIRSTGEN, M., DÖRING, B. & GEYER, J. 2021. Substrate Specificities and Inhibition Pattern of the Solute Carrier Family 10 Members NTCP, ASBT and SOAT. *Frontiers in Molecular Biosciences*, 8.
- HAGENBUCH, B., STIEGER, B., FOGUET, M., LUBBERT, H. & MEIER, P. J. 1991. Functional expression cloning and characterization of the hepatocyte Na<sup>+</sup>/bile acid cotransport system. *Proc Natl Acad Sci U S A*, 88, 10629-33.
- HEPATITIS B FOUNDATION. 2021. *Approved Drugs for Adults* [Online]. Available: <https://www.hepb.org/treatment-and-management/treatment/approved-drugs-for-adults/> [Accessed May 20<sup>th</sup>, 2021].
- HO, R. H., TIRONA, R. G., LEAKE, B. F., GLAESER, H., LEE, W., LEMKE, C. J., WANG, Y. & KIM, R. B. 2006. Drug and bile acid transporters in rosuvastatin hepatic uptake: function, expression, and pharmacogenetics. *Gastroenterology*, 130, 1793-806.
- HOFMANN, A. F. & HAGEY, L. R. 2008. Bile acids: chemistry, pathochemistry, biology, pathobiology, and therapeutics. *Cell Mol Life Sci*, 65, 2461-83.
- HONG, H. J., RYU, C. J., HUR, H., KIM, S., OH, H. K., OH, M. S. & PARK, S. Y. 2004. In vivo neutralization of hepatitis B virus infection by an anti-preS1 humanized antibody in chimpanzees. *Virology*, 318, 134-41.
- HOU, J., YIN, Y. K., XU, D., TAN, D., NIU, J., ZHOU, X., WANG, Y., ZHU, L., HE, Y., REN, H., WAN, M., CHEN, C., WU, S., CHEN, Y., XU, J., WANG, Q., WEI, L., CHAO, G., CONSTANCE, B. F., HARB, G., BROWN, N. A. & JIA, J. 2008. Telbivudine versus lamivudine in Chinese patients with chronic hepatitis B: Results at 1 year of a randomized, double-blind trial. *Hepatology*, 47, 447-54.
- HUANG, H. C., TAO, M. H., HUNG, T. M., CHEN, J. C., LIN, Z. J. & HUANG, C. 2014. (-)-Epigallocatechin-3-gallate inhibits entry of hepatitis B virus into hepatocytes. *Antiviral Res.*, 111, 100-11.
- HUGHES, S. A., WEDEMEYER, H. & HARRISON, P. M. 2011. Hepatitis delta virus. *Lancet*, 378, 73-85.
- JADE, D. D., PANDEY, R., KUMAR, R. & GUPTA, D. 2020. Ligand-based pharmacophore modeling of TNF-alpha to design novel inhibitors using virtual screening and molecular dynamics. *J Biomol Struct Dyn*, 1-17.
- JANSSEN, H. L., VAN ZONNEVELD, M., SENTURK, H., ZEUZEM, S., AKARCA, U. S., CAKALOGLU, Y., SIMON, C., SO, T. M., GERKEN, G., DE MAN, R. A., NIESTERS, H. G., ZONDERVAN, P., HANSEN, B., SCHALM, S. W., GROUP, H. B. V. S. & ROTTERDAM FOUNDATION FOR LIVER, R. 2005. Pegylated interferon alfa-2b alone or in combination with lamivudine for HBeAg-positive chronic hepatitis B: a randomised trial. *Lancet*, 365, 123-9.
- JIA, C. Y., LI, J. Y., HAO, G. F. & YANG, G. F. 2020. A drug-likeness toolbox facilitates ADMET study in drug discovery. *Drug Discov Today*, 25, 248-258.
- JIANG, S., FEHER, M., WILLIAMS, C., COLE, B. & SHAW, D. E. 2020. AutoPH4: An Automated Method for Generating Pharmacophore Models from Protein Binding Pockets. *J Chem Inf Model*, 60, 4326-4338.
- KANEKO, M., WATASHI, K., KAMISUKI, S., MATSUNAGA, H., IWAMOTO, M., KAWAI, F., OHASHI, H., TSUKUDA, S., SHIMURA, S., SUZUKI, R., AIZAKI, H., SUGIYAMA, M., PARK, S. Y., ITO, T., OHTANI, N., SUGAWARA, F., TANAKA, Y., MIZOKAMI, M., SUREAU, C. & WAKITA, T. 2015. A Novel Tricyclic Polyketide, Vanitaracin A, Specifically Inhibits the Entry of Hepatitis B and D Viruses by Targeting Sodium Taurocholate Cotransporting Polypeptide. *J. Virol.*, 89, 11945-53.
- KAR, S. & ROY, K. 2013. How far can virtual screening take us in drug discovery? *Expert Opin Drug Discov*, 8, 245-61.
- KARAKUS, E., WANNOWIUS, M., MÜLLER, S. F., LEITING, S., LEIDOLF, R., NOPPES, S., OSWALD, S., DIENER, M. & GEYER, J. 2020. The orphan solute carrier SLC10A7 is a novel negative regulator of intracellular calcium signaling. *Sci. Rep.*, 10, 7248.
- KARAYIANNIS, P. 2017. Hepatitis B virus: virology, molecular biology, life cycle and intrahepatic spread. *Hepatol Int*, 11, 500-508.

- KESSLER, J. H., MULLAUER, F. B., DE ROO, G. M. & MEDEMA, J. P. 2007. Broad in vitro efficacy of plant-derived betulinic acid against cell lines derived from the most prevalent human cancer types. *Cancer Lett.*, 251, 132-45.
- KIM, R. B., LEAKE, B., CVETKOVIC, M., RODEN, M. M., NADEAU, J., WALUBO, A. & WILKINSON, G. R. 1999. Modulation by drugs of human hepatic sodium-dependent bile acid transporter (sodium taurocholate cotransporting polypeptide) activity. *J Pharmacol Exp Ther*, 291, 1204-9.
- KIRSTGEN, M., LOWJAGA, K., MÜLLER, S. F., GOLDMANN, N., LEHMANN, F., ALAKURTTI, S., YLI-KAUHALUOMA, J., GLEBE, D. & GEYER, J. 2020. Selective hepatitis B and D virus entry inhibitors from the group of pentacyclic lupane-type betulin-derived triterpenoids. *Sci. Rep.*, 10, 21772.
- KLEBE, G. 2006. Virtual ligand screening: strategies, perspectives and limitations. *Drug Discov Today*, 11, 580-94.
- KOSTYUSHEV, D., BREZGIN, S., KOSTYUSHEVA, A., ZARIFYAN, D., GOPTAR, I. & CHULANOV, V. 2019. Orthologous CRISPR/Cas9 systems for specific and efficient degradation of covalently closed circular DNA of hepatitis B virus. *Cell Mol Life Sci*, 76, 1779-1794.
- KOUZUKI, H., SUZUKI, H., ITO, K., OHASHI, R. & SUGIYAMA, Y. 1998. Contribution of sodium taurocholate co-transporting polypeptide to the uptake of its possible substrates into rat hepatocytes. *J Pharmacol Exp Ther*, 286, 1043-50.
- KOUZUKI, H., SUZUKI, H., STIEGER, B., MEIER, P. J. & SUGIYAMA, Y. 2000. Characterization of the transport properties of organic anion transporting polypeptide 1 (oatp1) and Na(+)/taurocholate cotransporting polypeptide (Ntcp): comparative studies on the inhibitory effect of their possible substrates in hepatocytes and cDNA-transfected COS-7 cells. *J Pharmacol Exp Ther*, 292, 505-11.
- KRAMER, W. & GLOMBIK, H. 2006. Bile acid reabsorption inhibitors (BARI): novel hypolipidemic drugs. *Curr. Med. Chem.*, 13, 997-1016.
- KRIEG, R., JORTZIK, E., GOETZ, A. A., BLANDIN, S., WITTLIN, S., ELHABIRI, M., RAHBARI, M., NURYEVA, S., VOIGT, K., DAHSE, H. M., BRAKHAGE, A., BECKMANN, S., QUACK, T., GREVELDING, C. G., PINKERTON, A. B., SCHONECKER, B., BURROWS, J., DAVIOUD-CHARVET, E., RAHLFS, S. & BECKER, K. 2017. Arylmethylamino steroids as antiparasitic agents. *Nat Commun*, 8, 14478.
- KUMAR, A. & ZHANG, K. Y. J. 2018. Advances in the Development of Shape Similarity Methods and Their Application in Drug Discovery. *Front Chem*, 6, 315.
- KWON, J. H., JANG, J. W., CHOI, J. Y., PARK, C. H., YOO, S. H., BAE, S. H. & YOON, S. K. 2013. Should lamivudine monotherapy be stopped or continued in patients infected with hepatitis B with favorable responses after more than 5 years of treatment? *J Med Virol*, 85, 34-42.
- LAAVOLA, M., HAAVIKKO, R., HAMALAINEN, M., LEPPANEN, T., NIEMINEN, R., ALAKURTTI, S., MOREIRA, V. M., YLI-KAUHALUOMA, J. & MOILANEN, E. 2016. Betulin Derivatives Effectively Suppress Inflammation in Vitro and in Vivo. *J. Nat. Prod.*, 79, 274-80.
- LAI, C. L., GANE, E., LIAW, Y. F., HSU, C. W., THONGSAWAT, S., WANG, Y., CHEN, Y., HEATHCOTE, E. J., RASENACK, J., BZOWEJ, N., NAOUMOV, N. V., DI BISCEGLIE, A. M., ZEUZEM, S., MOON, Y. M., GOODMAN, Z., CHAO, G., CONSTANCE, B. F., BROWN, N. A. & GLOBE STUDY, G. 2007. Telbivudine versus lamivudine in patients with chronic hepatitis B. *N Engl J Med*, 357, 2576-88.
- LAMAS LONGARELA, O., SCHMIDT, T. T., SCHONEWEIS, K., ROMEO, R., WEDEMAYER, H., URBAN, S. & SCHULZE, A. 2013. Proteoglycans act as cellular hepatitis delta virus attachment receptors. *PLoS One*, 8, e58340.
- LI, D., HE, W., LIU, X., ZHENG, S., QI, Y., LI, H., MAO, F., LIU, J., SUN, Y., PAN, L., DU, K., YE, K., LI, W. & SU, J. 2017. A potent human neutralizing antibody Fc-dependently reduces established HBV infections. *Elife*, 6.
- LIAW, Y. F., GANE, E., LEUNG, N., ZEUZEM, S., WANG, Y., LAI, C. L., HEATHCOTE, E. J., MANN, M., BZOWEJ, N., NIU, J., HAN, S. H., HWANG, S. G., CAKALOGLU, Y., TONG, M. J., PAPATHEODORIDIS, G., CHEN, Y., BROWN, N. A., ALBANIS, E.,



- GALIL, K., NAOUMOV, N. V. & GROUP, G. S. 2009. 2-Year GLOBE trial results: telbivudine is superior to lamivudine in patients with chronic hepatitis B. *Gastroenterology*, 136, 486-95.
- LIPINSKI, C. A., LOMBARDO, F., DOMINY, B. W. & FEENEY, P. J. 2001. Experimental and computational approaches to estimate solubility and permeability in drug discovery and development settings. *Adv Drug Deliv Rev*, 46, 3-26.
- LITTLEJOHN, M., LOCARNINI, S. & YUEN, L. 2016. Origins and Evolution of Hepatitis B Virus and Hepatitis D Virus. *Cold Spring Harb Perspect Med*, 6, a021360.
- LIU, Y., CORSA, A. C., BUTI, M., CATHCART, A. L., FLAHERTY, J. F., MILLER, M. D., KITRINOS, K. M., MARCELLIN, P. & GANE, E. J. 2017. No detectable resistance to tenofovir disoproxil fumarate in HBeAg+ and HBeAg- patients with chronic hepatitis B after 8 years of treatment. *J Viral Hepat*, 24, 68-74.
- LIU, Y., RUAN, H., LI, Y., SUN, G., LIU, X., HE, W., MAO, F., HE, M., YAN, L., ZHONG, G., YAN, H., LI, W. & ZHANG, Z. 2020. Potent and Specific Inhibition of NTCP-Mediated HBV/HDV Infection and Substrate Transporting by a Novel, Oral-Available Cyclosporine A Analogue. *J. Med. Chem.*
- LOK, A. S. 2016. Hepatitis B: 50 years after the discovery of Australia antigen. *J Viral Hepat*, 23, 5-14.
- LOK, A. S., ZOULIM, F., DUSHEIKO, G. & GHANY, M. G. 2017. Hepatitis B cure: From discovery to regulatory approval. *J Hepatol*, 67, 847-861.
- LOPATIN, U. 2019. Drugs in the Pipeline for HBV. *Clin Liver Dis*, 23, 535-555.
- LUCIFORA, J., BONNIN, M., AILLOT, L., FUSIL, F., MAADADI, S., DIMIER, L., MICHELET, M., FLORIOT, O., OLLIVIER, A., RIVOIRE, M., AIT-GOUGHOUTE, M., DAFFIS, S., FLETCHER, S. P., SALVETTI, A., COSSET, F. L., ZOULIM, F. & DURANTE, D. 2018. Direct antiviral properties of TLR ligands against HBV replication in immune-competent hepatocytes. *Sci Rep*, 8, 5390.
- LUCIFORA, J., ESSER, K. & PROTZER, U. 2013. Ezetimibe blocks hepatitis B virus infection after virus uptake into hepatocytes. *Antiviral Res*, 97, 195-7.
- MA, Z., CAO, Q., XIONG, Y., ZHANG, E. & LU, M. 2018. Interaction between Hepatitis B Virus and Toll-Like Receptors: Current Status and Potential Therapeutic Use for Chronic Hepatitis B. *Vaccines (Basel)*, 6.
- MACALINO, S. J., GOSU, V., HONG, S. & CHOI, S. 2015. Role of computer-aided drug design in modern drug discovery. *Arch Pharm Res*, 38, 1686-701.
- MARTINEZ, M. G., VILLERET, F., TESTONI, B. & ZOULIM, F. 2020. Can we cure hepatitis B virus with novel direct-acting antivirals? *Liver Int.*, 40 Suppl 1, 27-34.
- MCRAE, M. P., LOWE, C. M., TIAN, X., BOURDET, D. L., HO, R. H., LEAKE, B. F., KIM, R. B., BROUWER, K. L. & KASHUBA, A. D. 2006. Ritonavir, saquinavir, and efavirenz, but not nevirapine, inhibit bile acid transport in human and rat hepatocytes. *J Pharmacol Exp Ther*, 318, 1068-75.
- MENG, Z., CHEN, Y. & LU, M. 2019. Advances in Targeting the Innate and Adaptive Immune Systems to Cure Chronic Hepatitis B Virus Infection. *Front Immunol*, 10, 3127.
- MIGNANI, S., RODRIGUES, J., TOMAS, H., JALAL, R., SINGH, P. P., MAJORAL, J. P. & VISHWAKARMA, R. A. 2018. Present drug-likeness filters in medicinal chemistry during the hit and lead optimization process: how far can they be simplified? *Drug Discov Today*, 23, 605-615.
- MINITAB LLC. 2021. *Regression der partiellen kleinsten Quadrate* [Online]. Available: <https://support.minitab.com/de-de/minitab/18/help-and-how-to/modeling-statistics/regression/supporting-topics/partial-least-squares-regression/what-is-partial-least-squares-regression/> [Accessed June 30<sup>th</sup>, 2021].
- MITA, S., SUZUKI, H., AKITA, H., HAYASHI, H., ONUKI, R., HOFMANN, A. F. & SUGIYAMA, Y. 2006. Inhibition of bile acid transport across Na+/taurocholate cotransporting polypeptide (SLC10A1) and bile salt export pump (ABCB 11)-coexpressing LLC-PK1 cells by cholestasis-inducing drugs. *Drug Metab Dispos*, 34, 1575-81.
- MOHD-ISMAIL, N. K., LIM, Z., GUNARATNE, J. & TAN, Y. J. 2019. Mapping the Interactions of HBV cccDNA with Host Factors. *Int J Mol Sci*, 20.

- MORIKAWA, K., SUDA, G. & SAKAMOTO, N. 2016. Viral life cycle of hepatitis B virus: Host factors and druggable targets. *Hepatol Res*, 46, 871-7.
- MUELLER, R., DAWSON, E. S., MEILER, J., RODRIGUEZ, A. L., CHAUDER, B. A., BATES, B. S., FELTS, A. S., LAMB, J. P., MENON, U. N., JADHAV, S. B., KANE, A. S., JONES, C. K., GREGORY, K. J., NISWENDER, C. M., CONN, P. J., OLSEN, C. M., WINDER, D. G., EMMITTE, K. A. & LINDSLEY, C. W. 2012. Discovery of 2-(2-benzoxazolyl amino)-4-aryl-5-cyanopyrimidine as negative allosteric modulators (NAMs) of metabotropic glutamate receptor 5 (mGlu(5)): from an artificial neural network virtual screen to an in vivo tool compound. *ChemMedChem*, 7, 406-14.
- MÜLLER, S. F., KÖNIG, A., DÖRING, B., GLEBE, D. & GEYER, J. 2018. Characterisation of the hepatitis B virus cross-species transmission pattern via Na<sup>+</sup>/taurocholate co-transporting polypeptides from 11 New World and Old World primate species. *PLoS One*, 13, e0199200.
- NEVES, B. J., BRAGA, R. C., MELO-FILHO, C. C., MOREIRA-FILHO, J. T., MURATOV, E. N. & ANDRADE, C. H. 2018. QSAR-Based Virtual Screening: Advances and Applications in Drug Discovery. *Front Pharmacol*, 9, 1275.
- NI, Y., LEMPP, F. A., MEHRLE, S., NKONGOLO, S., KAUFMAN, C., FALTH, M., STINDT, J., KONIGER, C., NASSAL, M., KUBITZ, R., SULTMANN, H. & URBAN, S. 2014. Hepatitis B and D viruses exploit sodium taurocholate co-transporting polypeptide for species-specific entry into hepatocytes. *Gastroenterology*, 146, 1070-83.
- NKONGOLO, S., NI, Y., LEMPP, F. A., KAUFMAN, C., LINDNER, T., ESSER-NOBIS, K., LOHMANN, V., MIER, W., MEHRLE, S. & URBAN, S. 2014. Cyclosporin A inhibits hepatitis B and hepatitis D virus entry by cyclophilin-independent interference with the NTCP receptor. *J. Hepatol.*, 60, 723-31.
- OH, Y., JEONG, Y. S., KIM, M. S., MIN, J. S., RYOO, G., PARK, J. E., JUN, Y., SONG, Y. K., CHUN, S. E., HAN, S., BAE, S. K., CHUNG, S. J. & LEE, W. 2018. Inhibition of Organic Anion Transporting Polypeptide 1B1 and 1B3 by Betulinic Acid: Effects of Preincubation and Albumin in the Media. *J. Pharm. Sci.*, 107, 1713-1723.
- PAL, S., KUMAR, V., KUNDU, B., BHATTACHARYA, D., PREETHY, N., REDDY, M. P. & TALUKDAR, A. 2019. Ligand-based Pharmacophore Modeling, Virtual Screening and Molecular Docking Studies for Discovery of Potential Topoisomerase I Inhibitors. *Comput Struct Biotechnol J*, 17, 291-310.
- PIERRA ROUVIERE, C., DOUSSON, C. B. & TAVIS, J. E. 2020. HBV replication inhibitors. *Antiviral Res*, 179, 104815.
- PISHA, E., CHAI, H., LEE, I. S., CHAGWEDERA, T. E., FARNSWORTH, N. R., CORDELL, G. A., BEECHER, C. W., FONG, H. H., KINGHORN, A. D., BROWN, D. M. & ET AL. 1995. Discovery of betulinic acid as a selective inhibitor of human melanoma that functions by induction of apoptosis. *Nat. Med.*, 1, 1046-51.
- PRIFTI, G.-M., MOIANOS, D., GIANNAKOPOULOU, E., PARDALI, V., TAVIS, J. E. & ZOIDIS, G. 2021. Recent Advances in Hepatitis B Treatment. *Pharmaceuticals*, 14.
- REVILL, P. A., CHISARI, F. V., BLOCK, J. M., DANDRI, M., GEHRING, A. J., GUO, H., HU, J., KRAMVIS, A., LAMPERTICO, P., JANSSEN, H. L. A., LEVRERO, M., LI, W., LIANG, T. J., LIM, S. G., LU, F., PENICAUD, M. C., TAVIS, J. E., THIMME, R., MEMBERS OF THE, I. C. E. H. B. V. W. G., CHAIRS, I.-H. S. G., ADVISORS, I.-H. S. & ZOULIM, F. 2019. A global scientific strategy to cure hepatitis B. *Lancet Gastroenterol Hepatol*, 4, 545-558.
- ROBERT KOCH INSTITUT. 2021. *RKI-Ratgeber Hepatitis B und D* [Online]. Available: [https://www.rki.de/DE/Content/Infekt/EpidBull/Merkblaetter/Ratgeber\\_HepatitisB.html?jsessioid=81E8BCC5AD1DC27202CFEBD4EC88A148.internet121](https://www.rki.de/DE/Content/Infekt/EpidBull/Merkblaetter/Ratgeber_HepatitisB.html?jsessioid=81E8BCC5AD1DC27202CFEBD4EC88A148.internet121) [Accessed July 9<sup>th</sup>, 2021].
- SANTANA, K., DO NASCIMENTO, L. D., LIMA, E. L. A., DAMASCENO, V., NAHUM, C., BRAGA, R. C. & LAMEIRA, J. 2021. Applications of Virtual Screening in Bioprospecting: Facts, Shifts, and Perspectives to Explore the Chemo-Structural Diversity of Natural Products. *Front Chem*, 9, 662688.
- SASO, W., TSUKUDA, S., OHASHI, H., FUKANO, K., MORISHITA, R., MATSUNAGA, S., OHKI, M., RYO, A., PARK, S. Y., SUZUKI, R., AIZAKI, H., MURAMATSU, M., SUREAU, C., WAKITA, T., MATANO, T. & WATASHI, K. 2018. A new strategy to

- identify hepatitis B virus entry inhibitors by AlphaScreen technology targeting the envelope-receptor interaction. *Biochem. Biophys. Res. Commun.*
- SAWYER, S. L., EMERMAN, M. & MALIK, H. S. 2004. Ancient adaptive evolution of the primate antiviral DNA-editing enzyme APOBEC3G. *PLoS Biol*, 2, E275.
- SCHALLER, D., ŠRIBAR, D., NOONAN, T., DENG, L., NGUYEN, T. N., PACH, S., MACHALZ, D., BERMUDEZ, M. & WOLBER, G. 2020. Next generation 3D pharmacophore modeling. *WIREs Computational Molecular Science*, 10.
- SCHROEDER, A., ECKHARDT, U., STIEGER, B., TYNES, R., SCHTEINGART, C. D., HOFMANN, A. F., MEIER, P. J. & HAGENBUCH, B. 1998. Substrate specificity of the rat liver Na(+)-bile salt cotransporter in *Xenopus laevis* oocytes and in CHO cells. *Am J Physiol*, 274, G370-5.
- SCHULZE, A., SCHIECK, A., NI, Y., MIER, W. & URBAN, S. 2010. Fine mapping of pre-S sequence requirements for hepatitis B virus large envelope protein-mediated receptor interaction. *J Virol*, 84, 1989-2000.
- SEDDON, M. P., COSGROVE, D. A., PACKER, M. J. & GILLET, V. J. 2019. Alignment-Free Molecular Shape Comparison Using Spectral Geometry: The Framework. *J Chem Inf Model*, 59, 98-116.
- SEEGER, C. 2018. Control of viral transcripts as a concept for future HBV therapies. *Curr Opin Virol*, 30, 18-23.
- SEEGER, C. & MASON, W. S. 2015. Molecular biology of hepatitis B virus infection. *Virology*, 479-480, 672-86.
- SEEGER, C. & SOHN, J. A. 2016. Complete Spectrum of CRISPR/Cas9-induced Mutations on HBV cccDNA. *Mol Ther*, 24, 1258-66.
- SHEN, Z.-W., LUO, M.-Y., HU, H.-H., ZHOU, H., JIANG, H.-D., YU, L.-S. & ZENG, S. 2016. Screening and verifying potential NTCP inhibitors from herbal medicinal ingredients using the LLC-PK1 cell model stably expressing human NTCP. *Chinese Journal of Natural Medicines*, 14, 549-560.
- SHIMURA, S., WATASHI, K., FUKANO, K., PEEL, M., SLUDER, A., KAWAI, F., IWAMOTO, M., TSUKUDA, S., TAKEUCHI, J. S., MIYAKE, T., SUGIYAMA, M., OGASAWARA, Y., PARK, S. Y., TANAKA, Y., KUSUHARA, H., MIZOKAMI, M., SUREAU, C. & WAKITA, T. 2017. Cyclosporin derivatives inhibit hepatitis B virus entry without interfering with NTCP transporter activity. *J Hepatol*, 66, 685-692.
- SOICHIRO HATA, PIJUN WANG, NICOLE EFTYCHIOU, MEENAKSHISUNDARAM ANANTHANARAYANAN, ASHOK BATTI, GERALD SALEN, K. SANDY PANG & WOLKOFF, A. W. 2003. Substrate specificities of rat oatp1 and ntcp: implications for hepatic organic anion uptake. *Am J Physiol Gastrointest Liver Physiol*, 285, 829-839.
- SORIANO, V., BARREIRO, P., CACHAY, E., KOTTILIL, S., FERNANDEZ-MONTERO, J. V. & DE MENDOZA, C. 2020. Advances in hepatitis B therapeutics. *Ther Adv Infect Dis*, 7, 2049936120965027.
- STIEGER, B., HAGENBUCH, B., LANDMANN, L., HOCHLI, M., SCHROEDER, A. & MEIER, P. J. 1994. In situ localization of the hepatocytic Na+/Taurocholate cotransporting polypeptide in rat liver. *Gastroenterology*, 107, 1781-7.
- SUREAU, C. & NEGRO, F. 2016. The hepatitis delta virus: Replication and pathogenesis. *J Hepatol*, 64, S102-S116.
- TAVIS, J. E. & LOMONOSOVA, E. 2015. The hepatitis B virus ribonuclease H as a drug target. *Antiviral Res*, 118, 132-8.
- THORNE, N., AULD, D. S. & INGLESE, J. 2010. Apparent activity in high-throughput screening: origins of compound-dependent assay interference. *Curr. Opin. Chem. Biol.*, 14, 315-24.
- TRÉPO, C., CHAN, H. L. & LOK, A. 2014. Hepatitis B virus infection. *Lancet*, 384, 2053-63.
- TSUKUDA, S., WATASHI, K., HOJIMA, T., ISOGAWA, M., IWAMOTO, M., OMAGARI, K., SUZUKI, R., AIZAKI, H., KOJIMA, S., SUGIYAMA, M., SAITO, A., TANAKA, Y., MIZOKAMI, M., SUREAU, C. & WAKITA, T. 2017. A new class of hepatitis B and D virus entry inhibitors, proanthocyanidin and its analogs, that directly act on the viral large surface proteins. *Hepatology*, 65, 1104-1116.
- TSUKUDA, S., WATASHI, K., IWAMOTO, M., SUZUKI, R., AIZAKI, H., OKADA, M., SUGIYAMA, M., KOJIMA, S., TANAKA, Y., MIZOKAMI, M., LI, J., TONG, S. &

- WAKITA, T. 2015. Dysregulation of retinoic acid receptor diminishes hepatocyte permissiveness to hepatitis B virus infection through modulation of sodium taurocholate cotransporting polypeptide (NTCP) expression. *J. Biol. Chem.*, 290, 5673-84.
- VERMA, J., KHEDKAR, V. M. & COUTINHO, E. C. 2010. 3D-QSAR in drug design—a review. *Curr Top Med Chem*, 10, 95-115.
- VOLZ, T., ALLWEISS, L., BEN, M. M., WARLICH, M., LOHSE, A. W., POLLOK, J. M., ALEXANDROV, A., URBAN, S., PETERSEN, J., LUTGEHETMANN, M. & DANDRI, M. 2013. The entry inhibitor Myrcludex-B efficiently blocks intrahepatic virus spreading in humanized mice previously infected with hepatitis B virus. *J Hepatol*, 58, 861-7.
- WAHLSTRÖM, A., SAYIN, S. I., MARSCHALL, H. U. & BÄCKHED, F. 2016. Intestinal Crosstalk between Bile Acids and Microbiota and Its Impact on Host Metabolism. *Cell Metab*, 24, 41-50.
- WAN, Y., WU, Y. L., LIAN, L. H., XIE, W. X., LI, X., OUYANG, B. Q., BAI, T., LI, Q., YANG, N. & NAN, J. X. 2012. The anti-fibrotic effect of betulinic acid is mediated through the inhibition of NF-kappaB nuclear protein translocation. *Chem. Biol. Interact.*, 195, 215-23.
- WANG, X. J., HU, W., ZHANG, T. Y., MAO, Y. Y., LIU, N. N. & WANG, S. Q. 2015. Irbesartan, an FDA approved drug for hypertension and diabetic nephropathy, is a potent inhibitor for hepatitis B virus entry by disturbing Na(+)-dependent taurocholate cotransporting polypeptide activity. *Antiviral Res.*, 120, 140-6.
- WANG, Z., SUN, H., SHEN, C., HU, X., GAO, J., LI, D., CAO, D. & HOU, T. 2020. Combined strategies in structure-based virtual screening. *Phys Chem Chem Phys*, 22, 3149-3159.
- WATASHI, K., SLUDER, A., DAITO, T., MATSUNAGA, S., RYO, A., NAGAMORI, S., IWAMOTO, M., NAKAJIMA, S., TSUKUDA, S., BORROTO-ESODA, K., SUGIYAMA, M., TANAKA, Y., KANAI, Y., KUSUHARA, H., MIZOKAMI, M. & WAKITA, T. 2014. Cyclosporin A and its analogs inhibit hepatitis B virus entry into cultured hepatocytes through targeting a membrane transporter, sodium taurocholate cotransporting polypeptide (NTCP). *Hepatology*, 59, 1726-37.
- WEINMAN, S. A. 1997. Electrogenicity of Na(+)-coupled bile acid transporters. *Yale J Biol Med*, 70, 331-40.
- WI, J., JEONG, M. S. & HONG, H. J. 2017. Construction and Characterization of an Anti-Hepatitis B Virus preS1 Humanized Antibody that Binds to the Essential Receptor Binding Site. *J Microbiol Biotechnol*, 27, 1336-1344.
- WONG, G. L., SETO, W. K., WONG, V. W., YUEN, M. F. & CHAN, H. L. 2018. Review article: long-term safety of oral anti-viral treatment for chronic hepatitis B. *Aliment Pharmacol Ther*, 47, 730-737.
- WOO, A. S. J., KWOK, R. & AHMED, T. 2017. Alpha-interferon treatment in hepatitis B. *Ann Transl Med*, 5, 159.
- WOOD, D. J., BUTTAR, D., CUMMING, J. G., DAVIS, A. M., NORINDER, U. & RODGERS, S. L. 2011. Automated QSAR with a Hierarchy of Global and Local Models. *Mol Inform*, 30, 960-72.
- WORLD HEALTH ORGANISATION. 2017. *Global Hepatitis report* [Online]. Available: <https://www.who.int/publications/i/item/global-hepatitis-report-2017> [Accessed July 8<sup>th</sup>, 2021].
- WU, X., CAI, S., LI, Z., ZHENG, C., XUE, X., ZENG, J. & PENG, J. 2016. Potential effects of telbivudine and entecavir on renal function: a systematic review and meta-analysis. *Virol J*, 13, 64.
- YAN, H., PENG, B., LIU, Y., XU, G., HE, W., REN, B., JING, Z., SUI, J. & LI, W. 2014. Viral entry of hepatitis B and D viruses and bile salts transportation share common molecular determinants on sodium taurocholate cotransporting polypeptide. *J Virol*, 88, 3273-84.
- YAN, H., ZHONG, G., XU, G., HE, W., JING, Z., GAO, Z., HUANG, Y., QI, Y., PENG, B., WANG, H., FU, L., SONG, M., CHEN, P., GAO, W., REN, B., SUN, Y., CAI, T., FENG, X., SUI, J. & LI, W. 2012. Sodium taurocholate cotransporting polypeptide is a functional receptor for human hepatitis B and D virus. *eLife*, 1.
- YANG, L., LIU, F., TONG, X., HOFFMANN, D., ZUO, J. & LU, M. 2019. Treatment of Chronic Hepatitis B Virus Infection Using Small Molecule Modulators of Nucleocapsid Assembly: Recent Advances and Perspectives. *ACS Infect Dis*, 5, 713-724.

- YAO, D., LI, H., GOU, Y., ZHANG, H., VLESSIDIS, A. G., ZHOU, H., EVMIRIDIS, N. P. & LIU, Z. 2009. Betulinic acid-mediated inhibitory effect on hepatitis B virus by suppression of manganese superoxide dismutase expression. *FEBS J.*, 276, 2599-614.
- ZHAN, X. K., LI, J. L., ZHANG, S., XING, P. Y. & XIA, M. F. 2018. Betulinic acid exerts potent antitumor effects on paclitaxel-resistant human lung carcinoma cells (H460) via G2/M phase cell cycle arrest and induction of mitochondrial apoptosis. *Oncol. Lett.*, 16, 3628-3634.
- ZHANG, D. M., XU, H. G., WANG, L., LI, Y. J., SUN, P. H., WU, X. M., WANG, G. J., CHEN, W. M. & YE, W. C. 2015. Betulinic Acid and its Derivatives as Potential Antitumor Agents. *Med. Res. Rev.*, 35, 1127-55.
- ZHANG, T. Y., YUAN, Q., ZHAO, J. H., ZHANG, Y. L., YUAN, L. Z., LAN, Y., LO, Y. C., SUN, C. P., WU, C. R., ZHANG, J. F., ZHANG, Y., CAO, J. L., GUO, X. R., LIU, X., MO, X. B., LUO, W. X., CHENG, T., CHEN, Y. X., TAO, M. H., SHIH, J. W., ZHAO, Q. J., ZHANG, J., CHEN, P. J., YUAN, Y. A. & XIA, N. S. 2016. Prolonged suppression of HBV in mice by a novel antibody that targets a unique epitope on hepatitis B surface antigen. *Gut*, 65, 658-71.
- ZHAO, Q. & GUO, J. T. 2020. Have the Starting Lineup of Five for Hepatitis B Virus Covalently Closed Circular DNA Synthesis Been Identified? *Hepatology*, 72, 1142-1144.
- ZOULIM, F., LEBOSSE, F. & LEVRERO, M. 2016. Current treatments for chronic hepatitis B virus infections. *Curr Opin Virol*, 18, 109-16.
- ZUCO, V., SUPINO, R., RIGHETTI, S. C., CLERIS, L., MARCHESI, E., GAMBACORTI-PASSERINI, C. & FORMELLI, F. 2002. Selective cytotoxicity of betulinic acid on tumor cell lines, but not on normal cells. *Cancer Lett.*, 175, 17-25.

## 8 Danksagungen

An dieser Stelle möchte ich mich bei all denjenigen bedanken, die mich während der Anfertigung dieser Arbeit unterstützt, motiviert und ertragen haben.

Zunächst danke ich Herrn Prof. Dr. Joachim Geyer, der meine Doktorarbeit betreut und begutachtet hat, für die hilfreichen Anregungen und die konstruktive Kritik bei der Erstellung dieser Arbeit. Mit Stolz blicke ich auf unsere gemeinsamen Erfolge während meiner Zeit am Institut zurück.

Dank gilt auch Frau Prof. Dr. Melanie Hamann für ihre immer freundliche und hilfsbereite Art und die gemeinsame Durchführung von Lehraufgaben, die mir mit ihr und meinen Kolleginnen und Kollegen viel Freude bereitet haben.

Ich bedanke mich bei dem Koordinator des LOEWE-Zentrums „DRUID“, Herrn Prof. Dr. Stephan Becker, und bei der ehemaligen Koordinatorin, Frau Prof. Dr. Katja Becker, für die finanzielle Unterstützung meiner Forschung.

Ich danke Dr. Gary Grosser dafür, dass er mich zu meinen Anfangszeiten unter seine Fittiche genommen hat und in den Künsten der Arbeit mit Radioisotopen unterwiesen hat.

Ich danke meinem Postdoc Dr. Simon Müller für seine meist konstruktive Kritik und alle lehrreichen Anekdoten, die er zum Besten gegeben hat. Besonders danke ich für sein stets offenes Ohr sowohl für fachliche als auch persönliche Angelegenheiten.

Ebenfalls möchte ich mich bei all meinen Kolleginnen und Kollegen bedanken, die mir mit viel Geduld, Interesse und Hilfsbereitschaft zur Seite standen. Bedanken möchte ich mich für die zahlreichen interessanten Debatten und Ideen, die maßgeblich dazu beigetragen haben, dass diese Doktorarbeit in dieser Form vorliegt:

Danke Massimo Palatini, für die gemeinsame Studien- und Doktorandenzeit. Mit deinem Humor war jeder Arbeitstag eine Freude, egal, welche Versuche auch schiefgingen und welche Frustration auch aufkam.

Danke (Sir) Matthias Gorecki, für die gemeinsame Zeit im Büro und Labor. Neben fachlicher Kompetenz hast du auch stets mit Humor und Freundschaft gegläntzt.

Vielen Dank an Edda Wacker, das Organisationstalent in unserem Institut und die Person, zu der man immer gehen kann, wenn man irgendetwas bürokratisches wissen möchte! Uns verbindet nicht nur dasselbe Geburtsdatum, sondern auch Freundschaft, die hoffentlich weiterhin so bestehen bleibt. Ich wünsche dir und Moritz mit eurer Familie alles Gute und

bedanke mich an dieser Stelle herzlich bei Ingrid Feike, die dich vertritt (nicht ersetzt!), während du dich neben den beiden Jungs Thore und Pavo um eure kleine Evi kümmerst.

Danke an alle aktuellen Kolleginnen und Kollegen, die ich überdies auch gerne als meine Freunde bezeichne: Lisa Wagner, Marie Wannowius, Dr. Emre Karakus, Dr. Dariusz Zakrzewicz, Mies Abdallah, Daniela Nürnberger und Orhan Çakan.

Danke auch an alle ehemaligen Kolleginnen und Kollegen, von denen ich viel lernen durfte und mit denen ich viel gelacht habe: Matthias und Saskia Holtemeyer, Josefine Bennien, Maria Wüst, Dajana Gräfe und Kira Lowjaga.

Vielen Dank auch an all unsere technischen Assistentinnen, Silke Leiting, Bärbel Fühler, Anita Neubauer und Regina Leidolf, die immer mit Rat und Tat an der Seite von uns Doktoranden stehen und uns auf unserem Weg zur Promotion maßgeblich unterstützen.

Außerdem gilt mein Dank Birgit Kaus und Marion Wagner, die immer dafür gesorgt haben, dass sich jeder am Institut seiner Arbeit mit voller Kraft widmen kann, ohne sich Gedanken um leere Pipettenspitzenboxen, Epiboxen oder jedweder anderer Art von Boxen machen zu müssen.

Vielen Dank auch an Christoph Zimmermann, der mit seinem technischen Knowhow bisher jedem am Institut weiterhelfen konnte.

Abschließend möchte ich mich ganz besonders bei meiner gesamten Familie bedanken!

Meinen Eltern Annemie und Werner danke ich dafür, dass sie immer an mich glauben und mir den langen Weg durch mein Studium und die Promotion ermöglicht haben.

Meinen Geschwistern Stephanie und Jennifer danke ich für unseren Zusammenhalt, der nicht selbstverständlich ist und der mir immer den Rücken gestärkt hat.

Ich danke meiner wundervollen Frau Christina, dass sie mich jeden Tag erneut mit ihrem Engagement in ihrem Beruf als praktizierende Tierärztin dazu inspiriert, mein Bestes zu geben. Ohne deinen Rückhalt, den ich schon während unserer gemeinsamen Studienzzeit genießen durfte, hätte ich es niemals so weit geschafft.



Michael Kirstgen

Gießen, 10.12.2021

## **9 Anhang**

Es folgen Publikationen I, II, III und IV als Anhang.





# OPEN Selective hepatitis B and D virus entry inhibitors from the group of pentacyclic lupane-type betulin-derived triterpenoids

Michael Kirstgen<sup>1</sup>, Kira Alessandra Alicia Theresa Lowjaga<sup>1</sup>, Simon Franz Müller<sup>1</sup>, Nora Goldmann<sup>2</sup>, Felix Lehmann<sup>2</sup>, Sami Alakurtti<sup>3,4</sup>, Jari Yli-Kauhaluoma<sup>3</sup>, Dieter Glebe<sup>2</sup> & Joachim Geyer<sup>1,5</sup>✉

Current treatment options against hepatitis B and D virus (HBV/HDV) infections have only limited curative effects. Identification of Na<sup>+</sup>/taurocholate co-transporting polypeptide (NTCP) as the high-affinity hepatic receptor for both viruses in 2012 enables target-based development of HBV/HDV cell-entry inhibitors. Many studies already identified appropriate NTCP inhibitors. However, most of them interfere with NTCP's physiological function as a hepatic bile acid transporter. To overcome this drawback, the present study aimed to find compounds that specifically block HBV/HDV binding to NTCP without affecting its transporter function. A novel assay was conceptualized to screen for both in parallel; virus binding to NTCP (measured via binding of a preS1-derived peptide of the large HBV/HDV envelope protein) and bile acid transport via NTCP. Hits were subsequently validated by in vitro HDV infection studies using NTCP-HepG2 cells. Derivatives of the birch-derived pentacyclic lupane-type triterpenoid betulin revealed clear NTCP inhibitory potency and selectivity for the virus receptor function of NTCP. Best performing compounds in both aspects were 2, 6, 19, and 25. In conclusion, betulin derivatives show clear structure–activity relationships for potent and selective inhibition of the HBV/HDV virus receptor function of NTCP without tackling its physiological bile acid transport function and therefore are promising drug candidates.

Infections with the Hepatitis B (HBV) and D (HDV) viruses are the main cause of hepatocellular carcinoma (HCC) and liver cirrhosis as consequences of chronic hepatitis. Although vaccination is possible, more than 250 million people worldwide suffer from chronic hepatitis based on HBV/HDV infections, and 887,000 deaths can be traced back to this every year<sup>1</sup>. The genome of the enveloped DNA virus HBV consists of 3.2 kb which encode for three envelope proteins, referred to as small (SHBs), middle (MHBs), and large (LHBs)<sup>2</sup>. The 2–48 N-terminal amino acids of the myristoylated preS1 domain (myr-preS1<sub>2-48</sub> lipopeptide) of the LHBs are essential for virus binding to hepatocytes<sup>3,4</sup>. As HDV is a satellite virus of HBV and bears identical envelope proteins, it also shares this myr-preS1<sub>2-48</sub> lipopeptide<sup>5</sup>. About 5% of all chronic HBV carriers are additionally infected with HDV<sup>1</sup>. This co-infection causes more rapid disease progression, increased mortality rates, and increased incidence of HCC and liver cirrhosis<sup>6</sup>. To date, there are only few treatment options for HBV and HDV infections available. Chronic hepatitis can usually be controlled by antiviral therapy with nucleoside reverse transcriptase inhibitors and interferon. This is, however, rarely curative. Furthermore, interferon therapy is highly prone to adverse drug reactions and nucleoside reverse transcriptase inhibitors have to be given life-long<sup>7,8</sup>.

A promising novel drug target to block HBV/HDV virus entry into hepatocytes is represented by the Na<sup>+</sup>/taurocholate co-transporting polypeptide NTCP (gene symbol *SLC10A1*), which has been identified as the bona fide hepatic receptor for HBV/HDV<sup>9,10</sup>. It is generally accepted that HBV/HDV entry into hepatocytes essentially involves attachment of the virus particles to heparan sulfate proteoglycans<sup>11</sup>, followed by high-affinity binding of

<sup>1</sup>Biomedical Research Center Seltersberg (BFS), Institute of Pharmacology and Toxicology, Faculty of Veterinary Medicine, Justus Liebig University Giessen, Schubertstr. 81, 35392 Giessen, Germany. <sup>2</sup>National Reference Center for Hepatitis B Viruses and D Viruses, Institute of Medical Virology, Justus Liebig University Giessen, 35392 Giessen, Germany. <sup>3</sup>Drug Research Program, Division of Pharmaceutical Chemistry and Technology, Faculty of Pharmacy, University of Helsinki, Viikinkaari 5 E, P.O. Box 56, 00014 Helsinki, Finland. <sup>4</sup>VTT Technical Research Centre of Finland, Biologinkuja 7, P.O. Box 1000, 02044 Espoo, Finland. <sup>5</sup>email: Joachim.M.Geyer@vetmed.uni-giessen.de

the myr-preS1 domain of the large envelope protein to certain domains of NTCP that finally triggers subsequent steps such as endocytosis of the virus-receptor complex<sup>12</sup>.

It is known for long that an artificial myr-preS1<sub>2-48</sub> lipopeptide itself can block *in vitro* HBV/HDV infection in a dose-dependent manner with inhibitory constants (IC<sub>50</sub>) in the low nanomolar range<sup>8</sup>. Based on this, a synthetic analogue of the myr-preS1<sub>2-48</sub> lipopeptide, called bulevirtide (generic name, formerly known as Myrcludex B), was developed as a therapeutic agent against HBV and HDV infections. Several clinical studies have been successfully completed and very recently, bulevirtide was approved as a new drug to treat hepatitis D in Europe and Russia and will be marketed under the brand name Hepcludex<sup>13</sup>. Furthermore, it was demonstrated that viral DNA (HBV) and RNA (HDV) levels can be reduced significantly in chronically infected patients with a combination of bulevirtide and pegylated interferon alpha (PEG-IFNα)<sup>14</sup>. These data clearly indicate that NTCP is an appropriate drug target to control hepatic HBV/HDV levels. In addition, an HBV/HDV entry inhibitor addressing NTCP might be beneficial to prevent new infections of hepatocytes during chronic infection with HBV/HDV<sup>12</sup>.

Physiologically, NTCP is expressed dominantly at the basolateral membrane of hepatocytes and acts as a sodium-dependent uptake carrier of bile salts to enable their enterohepatic recirculation<sup>15-17</sup>. Thus, NTCP has a dual function as bile salt transporter and virus receptor. It is already known that both functions interfere with each other. The myr-preS1<sub>2-48</sub> lipopeptide can block the bile salt transport in primary human hepatocytes and NTCP-overexpressing HepG2 hepatoma cells in a concentration-dependent manner. Vice versa, bile salts can prevent myr-preS1<sub>2-48</sub> lipopeptide binding to NTCP as well as *in vitro* HBV infection<sup>10,18</sup>. Based on this, it was expected that in clinical trials using bulevirtide as a therapeutic agent, the total plasma bile salt levels would increase significantly. In a current study on healthy volunteers who received 10 mg bulevirtide, which is above the therapeutic dose, total plasma bile salt levels indeed increased 19.2-fold, and single bile salts even higher (e.g. 124-fold in the case of taurocholic acid, further referred to as TC)<sup>19</sup>. This data can be interpreted as dysregulation of the bile acid homeostasis under bulevirtide treatment.

On the basis of the therapeutically used effects of bulevirtide, a promising second strategy for the development of HBV/HDV entry inhibitors targeting NTCP would be to (I) investigate small molecules with oral bioavailability which (II) block virus binding to NTCP, but (III) without tackling its physiologically important bile salt transporter activity at relevant therapeutic drug concentrations. Currently, several studies identified novel chemical entry inhibitors for HBV and HDV by screening for bile salt transport inhibitors<sup>20</sup> or by screening for inhibitors of myr-preS1<sub>2-48</sub> lipopeptide attachment and/or *in vitro* HBV/HDV infection<sup>21</sup> in appropriate cell culture models overexpressing NTCP. However, none of these studies addressed and fulfilled all of the criteria outlined above. In contrast, the present study aimed to find small molecular HBV/HDV entry inhibitors that specifically block myr-preS1<sub>2-48</sub> lipopeptide binding to NTCP without affecting its bile salt transport function. We analyzed a set of derivatives of the pentacyclic lupane-type triterpenoid betulin, and indeed found individual compounds that were quite potent and selective for myr-preS1<sub>2-48</sub> lipopeptide binding inhibition and significantly blocked *in vitro* HDV infection of NTCP-expressing HepG2 cells. These compounds now can be further optimized for increased potency and then can be forwarded for *in vivo* infection experiments.

## Results

**Screening assay for bile acid transport and myr-preS1<sub>2-48</sub> lipopeptide binding.** The major goal of the present study was to analyze in parallel the effect of inhibitors on both, bile acid transport via NTCP and myr-preS1<sub>2-48</sub> lipopeptide binding to NTCP in a cell culture system. This was achieved by plating NTCP-HEK293 cells onto 96-well plates and by using tritium-labelled analytes, being [<sup>3</sup>H]taurocholic acid ([<sup>3</sup>H]TC) and [<sup>3</sup>H]myr-preS1<sub>2-48</sub> lipopeptide ([<sup>3</sup>H]preS1), which were analyzed in a microplate scintillation counter. For validation of this assay, transport of 1 μM [<sup>3</sup>H]TC first was inhibited by increasing concentrations of TC (concentrations ranging from 0.1 to 1,000 μM) itself and by myr-preS1<sub>2-48</sub> lipopeptide (concentrations ranging from 0.001 to 10 μM). In addition, binding of 5 nM [<sup>3</sup>H]preS1 was inhibited by myr-preS1<sub>2-48</sub> lipopeptide itself (concentrations ranging from 0.001 to 10 μM) and by TC (concentrations ranging from 0.1 to 1,000 μM). As shown in Fig. 1a, TC showed nearly equipotent inhibition of the [<sup>3</sup>H]TC transport with IC<sub>50</sub> of 30 μM and of the [<sup>3</sup>H]preS1 binding with IC<sub>50</sub> of 42 μM. The same was true for myr-preS1<sub>2-48</sub> lipopeptide as the inhibitor that revealed IC<sub>50</sub> of 0.35 μM for [<sup>3</sup>H]TC transport inhibition and IC<sub>50</sub> of 0.55 μM for [<sup>3</sup>H]preS1 binding inhibition (Fig. 1b). These data clearly confirm the previously shown interference of the transport and receptor function of NTCP<sup>10,18</sup> and demonstrate the functionality of this screening assay. Furthermore, these data indicate that the myr-preS1<sub>2-48</sub> lipopeptide has an about 100-fold higher inhibitory potency (IC<sub>50</sub> = 0.35 μM / 0.55 μM) in both assays compared to the physiological transport substrate TC (IC<sub>50</sub> = 30 μM / 42 μM). Four reference compounds were analyzed (concentrations ranging from 0.1 to 1,000 μM) which had shown inhibition of the transporter and receptor function of NTCP before, namely ciglitazone<sup>22</sup>, troglitazone<sup>22</sup>, cyclosporine A<sup>23-25</sup>, and rapamycin<sup>26</sup>. Interestingly, all compounds showed comparable inhibition of [<sup>3</sup>H]TC uptake and [<sup>3</sup>H]preS1 binding with IC<sub>50</sub> values of 1 μM and 1.3 μM for ciglitazone (Fig. 1c), 1.9 μM and 2.5 μM for troglitazone (Fig. 1d), 14 μM and 26 μM for cyclosporine A (Fig. 1e), as well as 34 μM and 21 μM for rapamycin (Fig. 1f), respectively. These compounds therefore can be classified as inhibitors, non-selective for one of the two measured functions of NTCP. Among them, ciglitazone and troglitazone had a tenfold higher inhibitory potency compared to cyclosporine A and rapamycin, demonstrating that diverse compounds differ in their potency as NTCP inhibitors. Cyclosporine A, rapamycin and TC showed comparable inhibitory pattern and potency in both assays, as shown by similar IC<sub>50</sub> values.

**Screening of betulin derivatives for bile acid transport and [<sup>3</sup>H]preS1 binding inhibition.** Next, 30 derivatives of betulin were tested in both assays and IC<sub>50</sub> values were determined for [<sup>3</sup>H]TC transport inhibition and [<sup>3</sup>H]preS1 binding inhibition. Chemical structures of all compounds are depicted in Table 1. All derive

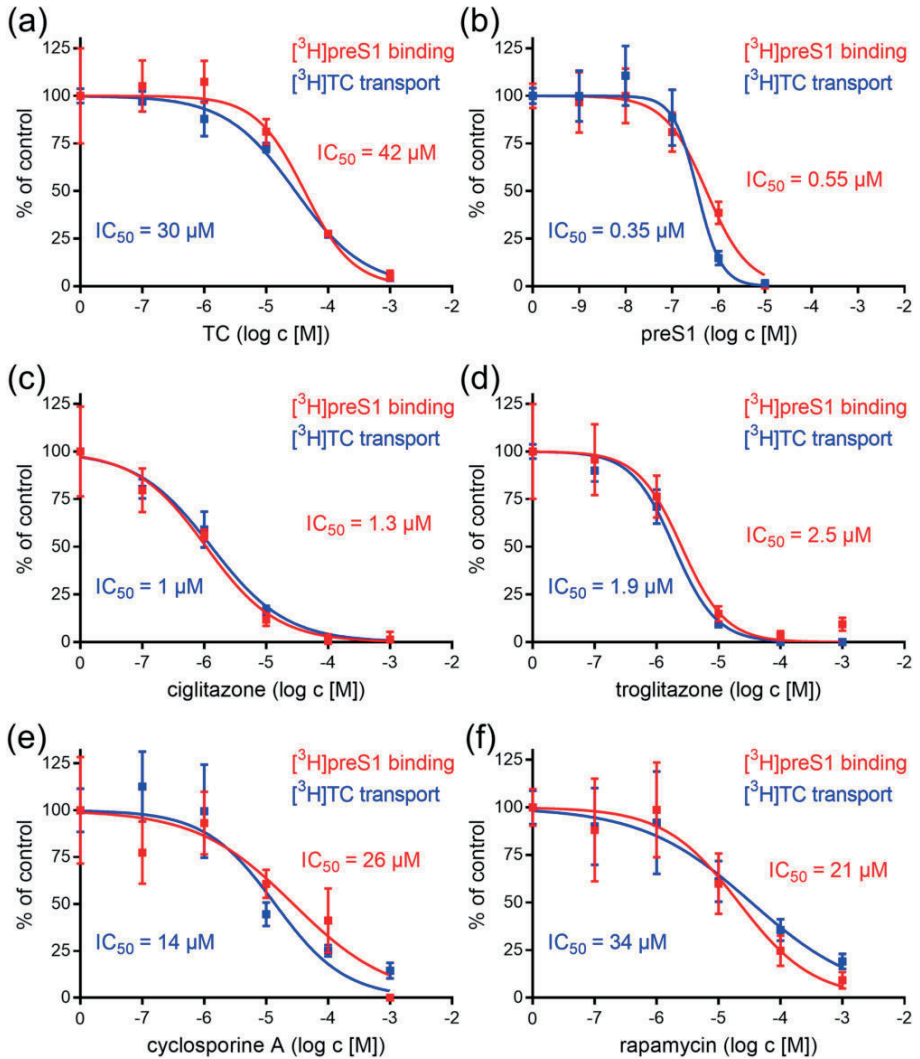
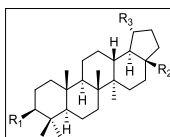
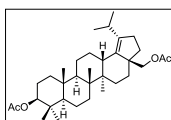


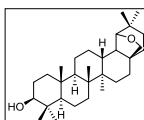
**Figure 1.**  $[^3\text{H}]$ TC transport and  $[^3\text{H}]$ preS1 binding screening assay. NTCP-HEK293 cells were seeded onto 96-well plates and were incubated with tetracycline in order to induce expression of the human NTCP protein. Cells without tetracycline treatment were used as 0% controls of  $[^3\text{H}]$ TC uptake and  $[^3\text{H}]$ preS1 binding, respectively. Cells were subjected to bile acid transport experiments with  $1 \mu\text{M}$   $[^3\text{H}]$ TC and myr-preS1<sub>2-48</sub> lipopeptide binding experiments with  $5 \text{ nM}$   $[^3\text{H}]$ preS1, each over 10 min at  $37^\circ\text{C}$ . Experiments were performed with solvent alone (set to 100%) and with increasing concentrations of the indicated inhibitors. The mean of the 0% control was subtracted to calculate net  $[^3\text{H}]$ TC transport rates (shown in blue) as well as net  $[^3\text{H}]$ preS1 binding rates (shown in red), which are depicted in the diagrams (expressed as % of control at the y-axis). Half maximal inhibitory concentrations ( $\text{IC}_{50}$ ) were calculated by nonlinear regression analysis using the equation  $\log(\text{inhibitor})$  versus response (GraphPad Prism). In order to validate the assay, (a) TC and (b) myr-preS1<sub>2-48</sub> lipopeptide were used as inhibitors. Furthermore, the already established NTCP inhibitors (c) ciglitazone, (d) troglitazone, (e) cyclosporine A, and (f) rapamycin were analyzed for  $[^3\text{H}]$ TC transport inhibition and  $[^3\text{H}]$ preS1 binding inhibition. Data represent means  $\pm$  SD of quadruplicate determinations of representative experiments.



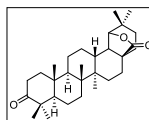
No	Compound	R <sub>1</sub>	R <sub>2</sub>	R <sub>3</sub>
1	Betulin	OH	CH <sub>2</sub> OH	CH <sub>3</sub> -C=CH <sub>2</sub>
2	20,29-Dihydrobetulin	OH	CH <sub>2</sub> OH	CH <sub>3</sub> -CH-CH <sub>3</sub>
3	Lupeol	OH	Me	CH <sub>3</sub> -C=CH <sub>2</sub>
4	Betulinic acid	OH	CO <sub>2</sub> H	CH <sub>3</sub> -C=CH <sub>2</sub>
5	Methyl betulinate	OH	CO <sub>2</sub> Me	CH <sub>3</sub> -C=CH <sub>2</sub>
6	Betunaldehyde oxime	OH	CH=NOH	CH <sub>3</sub> -C=CH <sub>2</sub>
7	28- <i>O</i> -(Bromoacetyl)betulin	OH	CH <sub>2</sub> O <sub>2</sub> C(CH <sub>2</sub> ) <sub>2</sub> Br	CH <sub>3</sub> -C=CH <sub>2</sub>
8	28- <i>O</i> -Succinoylbetulin	OH	CH <sub>2</sub> O <sub>2</sub> C(CH <sub>2</sub> ) <sub>2</sub> CO <sub>2</sub> H	CH <sub>3</sub> -C=CH <sub>2</sub>
9	3,28-Di- <i>O</i> -succinoylbetulin	O <sub>2</sub> C(CH <sub>2</sub> ) <sub>2</sub> CO <sub>2</sub> H	CH <sub>2</sub> O <sub>2</sub> C(CH <sub>2</sub> ) <sub>2</sub> CO <sub>2</sub> H	CH <sub>3</sub> -C=CH <sub>2</sub>
10	28- <i>O</i> -(3,3-Dimethylglutaroyl)betulin	OH	CH <sub>2</sub> O <sub>2</sub> C(CH <sub>2</sub> )CM <sub>2</sub> (CH <sub>2</sub> )CO <sub>2</sub> H	CH <sub>3</sub> -C=CH <sub>2</sub>
11	3- <i>O</i> -(3,3-Dimethylglutaroyl)betulinic acid	O <sub>2</sub> C(CH <sub>2</sub> )CM <sub>2</sub> (CH <sub>2</sub> )CO <sub>2</sub> H	CO <sub>2</sub> H	CH <sub>3</sub> -C=CH <sub>2</sub>
12	3,28-Di- <i>O</i> -(3,3-dimethylglutaroyl)betulin	O <sub>2</sub> C(CH <sub>2</sub> )CM <sub>2</sub> (CH <sub>2</sub> )CO <sub>2</sub> H	CH <sub>2</sub> O <sub>2</sub> C(CH <sub>2</sub> )CM <sub>2</sub> (CH <sub>2</sub> )CO <sub>2</sub> H	CH <sub>3</sub> -C=CH <sub>2</sub>
13	28-(Tetrahydro-2 <i>H</i> -pyran-2-yl)betulin	OH	CH <sub>2</sub> O(THP)	CH <sub>3</sub> -C=CH <sub>2</sub>
14	28- <i>O</i> -Nicotinoylbetulin	OH	CH <sub>2</sub> O <sub>2</sub> C(3- <i>Py</i> )	CH <sub>3</sub> -C=CH <sub>2</sub>
15	28- <i>O</i> -Cinnamoylbetulin	OH	CH <sub>2</sub> O <sub>2</sub> C(CH=CH)Ph(- <i>E</i> )	CH <sub>3</sub> -C=CH <sub>2</sub>
16	3,28-Di- <i>O</i> -(dihydrocinnamoyl)betulin	O <sub>2</sub> C(CH <sub>2</sub> ) <sub>2</sub> Ph	CH <sub>2</sub> O <sub>2</sub> C(CH <sub>2</sub> ) <sub>2</sub> Ph	CH <sub>3</sub> -C=CH <sub>2</sub>
17	Lupenone	O=	Me	CH <sub>3</sub> -C=CH <sub>2</sub>
18	Betunaldehyde	O=	CHO	CH <sub>3</sub> -C=CH <sub>2</sub>
19	Betulonoyl dimethyl-L-aspartate	O=	CO[Asp(OMe)-OMe]	CH <sub>3</sub> -C=CH <sub>2</sub>
20	20,29-Dihydrobetulonic acid	O=	CO <sub>2</sub> H	CH <sub>3</sub> -CH-CH <sub>3</sub>
21	3- <i>O</i> -Acetylbetulinic acid	OAc	CO <sub>2</sub> H	CH <sub>3</sub> -C=CH <sub>2</sub>
22	3- <i>O</i> -Acetylbetulin	OAc	CH <sub>2</sub> OH	CH <sub>3</sub> -C=CH <sub>2</sub>
23	3- <i>O</i> -Acetyl-28-(tetrahydro-2 <i>H</i> -pyran-2-yl)betulin	OAc	CH <sub>2</sub> O(THP)	CH <sub>3</sub> -C=CH <sub>2</sub>
24	3,28-Di- <i>O</i> -acetylbetulin	OAc	CH <sub>2</sub> OAc	CH <sub>3</sub> -C=CH <sub>2</sub>
25	3,28-Di- <i>O</i> -acetyl-29-hydroxybetulin	OAc	CH <sub>2</sub> OAc	HOCH <sub>2</sub> -C=CH <sub>2</sub>
26	3,28-Di- <i>O</i> -acetyl-20,30-epoxybetulin	OAc	CH <sub>2</sub> OAc	
27	3- <i>O</i> -Caffeoylbetulin	O <sub>2</sub> C(CH=CH)(3,4-di-OH-C <sub>6</sub> H <sub>3</sub> )-( <i>E</i> )	CH <sub>2</sub> OH	CH <sub>3</sub> -C=CH <sub>2</sub>



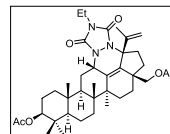
28 3,28-Di-*O*-acetyl-18,19-dehydro-20,29-dihydrobetulin



29 Allobetulin



30 3-Oxoallobetulin



31 4'-Ethyl-1,2',4'-triazoline-3',5'-dione-fused 3,28-di-*O*-acetylbetulin

**Table 1.** Structures of the betulin derivatives that were used for [<sup>3</sup>H]TC transport inhibition and [<sup>3</sup>H]preS1 binding inhibition experiments. These compounds derived from a TargoSet (Adipogen AG) or were synthesized as outlined elsewhere<sup>53–54</sup>. Ac, acetyl; Asp, aspartate; Et, ethyl; Me, methyl; Ph, phenyl; Pyr, pyridinyl; THP, 2*H*-tetrahydropyranyl.

Compound	IC <sub>50</sub> ([ <sup>3</sup> H]TC uptake) [μM] <sup>a</sup>	IC <sub>50</sub> ([ <sup>3</sup> H]preS1 binding) [μM] <sup>b</sup>	Selectivity index <sup>c</sup>
Betulinic acid (4)	0.65–1.08	1.57–2.93	1
20,29-Dihydrobetulonic acid (20)	2.74–5.46	2.95–7.66	1
3,28-Di-O-succinoylbetulini (9)	3.11–5.02	2.94–10.15	1
28-O-(3,3-Dimethylglutaroyl)betulini (10)	3.00–5.91	2.48–7.02	1
3-O-(3,3-Dimethylglutaroyl)betulinic acid (11)	3.08–4.53	3.00–5.21	1
3,28-Di-O-(3,3-dimethylglutaroyl)betulini (12)	4.17–10.71	4.97–10.14	1
3-O-Acetylbetulini (22)	36.47–151.80	20.64–87.35	2
Methyl betulinate (5)	47.05–99.97	12.66–83.46	2
28-O-Succinoylbetulini (8)	5.35–10.60	1.61–4.11	3
Betunaldehyde (18)	88.53–175.00	25.98–52.00	3
28-O-Nicotinoylbetulini (14)	185.40–531.50	36.48–109.10	5
3-O-Acetylbetulinic acid (21)	7.19–30.33	1.81–5.31	5
3,28-Di-O-acetylbetulini (24)	> 1,000	52.55–756.00	> 5
3,28-Di-O-(dihydrocinnamoyl)betulini (16)	176.20–1232.00	24.79–229.20	6
4'-Ethyl-1',2',4'-triazoline-3',5'-dione-fused 3,28-di-O-acetylbetulini (31)	614.20–1286.00	89.71–224.60	6
Betulin (1)	568.80–983.40	48.29–247.10	7
28-O-Cinnamoylbetulini (15)	72.39–235.50	10.89–31.75	7
3-O-Acetyl-28-(tetrahydro-2H-pyran-2-yl)betulini (23)	119.00–947.20	10.95–113.70	10
Lupenone (17)	145.70–396.70	13.10–35.45	11
28-O-(Bromoacetyl)betulini (7)	63.53–126.00	5.28–11.14	11
3,28-Di-O-acetyl-20,30-epoxybetulini (26)	331.80–891.20	26.46–72.96	12
3,28-Di-O-acetyl-18,19-dehydro-20,29-dihydrobetulini (28)	> 1,000	29.95–132.80	> 16
Lupeol (3)	> 1,000	26.93–97.94	> 19
28-(Tetrahydro-2H-pyran-2-yl)betulini (13)	115.80–628.00	9.34–19.54	19
3-O-Caffeoylbetulini (27)	84.98–195.00	3.35–10.00	22
Allobetulin (29)	212.30–674.80	9.67–20.80	27
Betulonoyl dimethyl-L-aspartate (19)	297.60–1430.00	21.84–202.60	28
3-Oxoallobetulin (30)	> 1,000	17.87–54.43	> 32
Betunaldehyde oxime (6)	359.80–759.00	6.61–18.29	48
20,29-Dihydrobetulini (2)	157.80–428.90	1.74–7.14	65
3,28-Di-O-acetyl-29-hydroxybetulini (25)	> 1,000	5.29–13.04	> 125

**Table 2.** The indicated 31 betulin derivatives were analyzed for [<sup>3</sup>H]TC transport inhibition and [<sup>3</sup>H]preS1 binding inhibition in NTPC-HEK293 cells. IC<sub>50</sub> values were calculated from a range of five inhibitor concentrations (0.1–1,000 μM) and are listed with their 95% confidence intervals. Selectivity indices for [<sup>3</sup>H]TC transport inhibition/[<sup>3</sup>H]preS1 binding were calculated from the IC<sub>50</sub> means. The higher this index, the more selective the respective inhibitor. <sup>a</sup> Inhibition of 1 μM [<sup>3</sup>H]TC uptake; <sup>b</sup> inhibition of 5 nM [<sup>3</sup>H]preS1 binding; <sup>c</sup> calculated from mean IC<sub>50</sub> TC:preS1.

from the betulin core structure by chemical modifications. These include methyl, succinyl, acetyl, bromoacetyl, dimethylglutaryl, caffeoyl, oxime, tetrahydropyranyl, cinnamoyl, nicotinoyl, L-aspartyl- or 1,2,4-triazoline-3,5-dione conjugations mostly at positions 3' and/or 28', as well as oxidations of the hydroxyl groups at positions 3' and/or 28'. Compound **29** represents allobetulin and compound **30** 3-oxoallobetulin. All IC<sub>50</sub> values for [<sup>3</sup>H]TC transport and [<sup>3</sup>H]preS1 binding are listed in Table 2 with their 95% confidence intervals, and selected diagrams are shown in Fig. 2. In the case of [<sup>3</sup>H]TC uptake inhibition, the IC<sub>50</sub> values ranged from 1 μM (**4**) up to values > 1,000 μM with very low, if any transport inhibition (**3**, **24**, **25**, **28** and **30**). This clearly indicates structure–activity relationships over three orders of magnitude. Most of the betulin derivatives showed quite potent inhibition of [<sup>3</sup>H]preS1 binding with IC<sub>50</sub> values ranging from 2–3 μM (**4**, **8**, **21**) up to 199 μM (**24**), also demonstrating clear structure–activity relationships over a broad inhibitor concentration range.

In addition, ratios between the IC<sub>50</sub> values for [<sup>3</sup>H]TC transport inhibition and the IC<sub>50</sub> values for [<sup>3</sup>H]preS1 binding inhibition were calculated and are further referred to as selectivity index. The higher this index, the more selective the respective compound for myr-preS1<sub>2–48</sub> lipopeptide inhibition. Therefore, the data listed in Table 2 are not only helpful to identify potent myr-preS1<sub>2–48</sub> lipopeptide binding inhibitors but also to assess their selectivity. These values ranged from an index of 1, including more potent (e.g. **4**) and less potent (e.g. **12**) non-selective inhibitors, up to an index of > 60, including the highly selective and potent inhibitors **2** and **25**. Figure 2 depicts selected diagrams which show the inhibitory curves for the [<sup>3</sup>H]TC transport inhibition (in blue) and [<sup>3</sup>H]preS1 binding inhibition (in red). This panel shows compounds with different characteristics. Within the group of potent [<sup>3</sup>H]preS1 binding inhibitors (IC<sub>50</sub> < 10 μM), there were (I) non-selective inhibitors

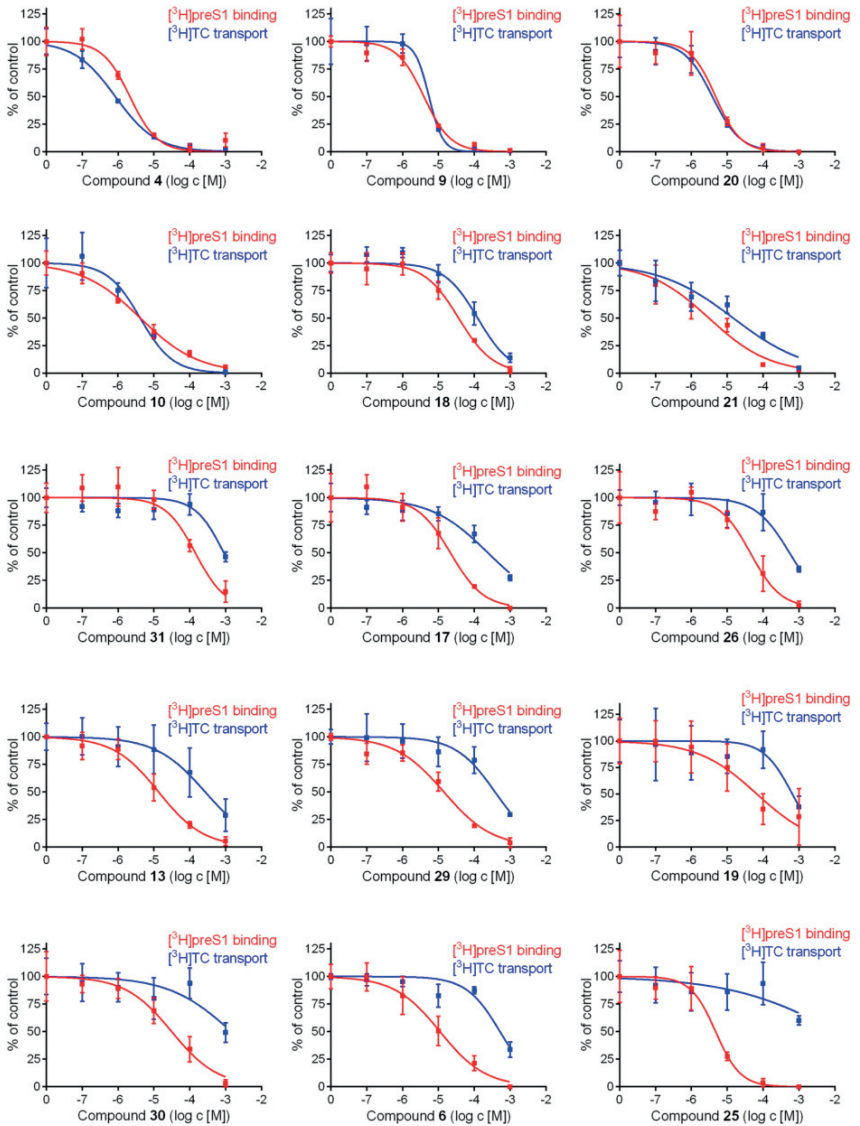


**Figure 2.** Inhibition of  $[^3\text{H}]$ preS1 peptide binding and  $[^3\text{H}]$ TTC transport by betulin derivatives. NTCP-HEK293 cells were incubated with tetracycline in order to induce NTCP expression and were used for bile acid transport experiments with  $1\ \mu\text{M}$   $[^3\text{H}]$ TTC and for myr-preS1<sub>2-48</sub> lipopeptide binding experiments with  $5\ \text{nM}$   $[^3\text{H}]$ preS1, each over 10 min at  $37\ ^\circ\text{C}$ . Cells without tetracycline treatment were used as 0% controls of  $[^3\text{H}]$ TTC uptake and  $[^3\text{H}]$ preS1 binding, respectively. Experiments were performed with solvent alone (set to 100%) and with increasing concentrations of the indicated inhibitor. The mean of the 0% control was subtracted to calculate net  $[^3\text{H}]$ TTC transport rates (shown in blue) as well as net  $[^3\text{H}]$ preS1 binding rates (shown in red), both expressed as % of control at the y-axis. Half maximal inhibitory concentrations ( $\text{IC}_{50}$ ) were calculated by nonlinear regression analysis using the equation  $\log(\text{inhibitor})$  vs. response (GraphPad Prism). The figure shows selected diagrams. Chemical structures of the compounds are depicted in Table 1, the respective  $\text{IC}_{50}$  values are listed in Table 2. Data represent means  $\pm$  SD of quadruplicate determinations ( $n = 4$ ).

(4, 9, 10, and 20), (II) poorly selective inhibitors (e.g. 21), and highly selective inhibitors, being 2 and 25. Also, from the group of less potent [ $^3\text{H}$ ]preS1 binding inhibitors ( $\text{IC}_{50}$  = 11–50  $\mu\text{M}$ ), some were poorly selective (e.g. 18) and others were highly selective (e.g. 13, 17, 19 and 30). Taken together, these data clearly indicate structure–activity relationships of the betulin derivatives for both, bile acid transport inhibition and myr-preS1<sub>2-48</sub> lipopeptide binding inhibition.

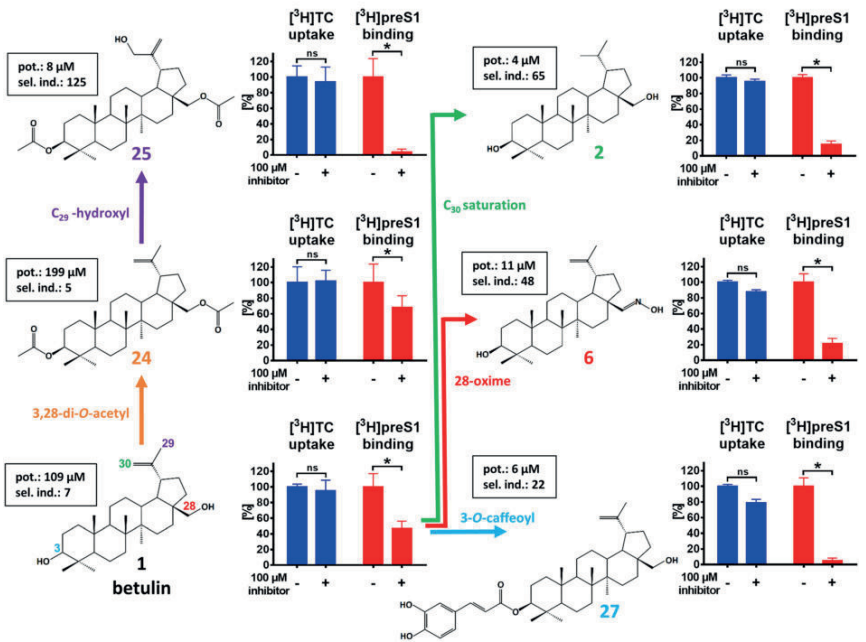
**Most relevant modifications for structure–activity relationships.** Closer analysis of the structure–activity relationships of the betulin derivatives revealed several interesting patterns that can be used to further optimize the potency and selectivity index of these compounds in order to end up with an even more suitable HBV/HDV entry inhibitor from the class of betulin derivatives. Of note, betulin (1) itself showed relatively low inhibitory potency for bile acid transport inhibition ( $\text{IC}_{50}$  = 748  $\mu\text{M}$ ) and [ $^3\text{H}$ ]preS1 binding inhibition ( $\text{IC}_{50}$  = 109  $\mu\text{M}$ ) resulting in a selectivity index of 7. However, relatively moderate modifications at the betulin core structure revealed significantly improved potency and selectivity index of the individual compounds. Some of these modifications are depicted in more detail in Fig. 3a/3b and involve modifications at positions 3', 28', 29', and 30'. While the diacetylated betulin derivative 3,28-di-O-acetylbetulin (24) itself has a relatively low potency for [ $^3\text{H}$ ]preS1 binding inhibition ( $\text{IC}_{50}$  = 199  $\mu\text{M}$ ) and poor selectivity (selectivity index: 5) (Fig. 3, shown in orange), additional C<sub>29</sub> hydroxylation (25) improved the potency for [ $^3\text{H}$ ]preS1 binding inhibition to  $\text{IC}_{50}$  = 8  $\mu\text{M}$  and increased the selectivity index to 125 (Fig. 3, shown in purple). 3-O-caffeoyl (27) conjugation of betulin (1) also reduced the  $\text{IC}_{50}$  value for [ $^3\text{H}$ ]preS1 binding inhibition to 6  $\mu\text{M}$  and increased the selectivity index to 22 (Fig. 3, shown in light blue). Replacement of the 28-hydroxyl group of betulin by an oxime group (6) increased the inhibitory potency for [ $^3\text{H}$ ]preS1 binding by one order of magnitude (109  $\mu\text{M}$  vs. 11  $\mu\text{M}$ ) and also improved the selectivity index (7 vs. 48) (Fig. 3, shown in red). The most successful modification, however, was the saturation of the double bond between C<sub>20</sub> and C<sub>30</sub>, which increased the potency for [ $^3\text{H}$ ]preS1 binding inhibition to  $\text{IC}_{50}$  of 4  $\mu\text{M}$ , while maintaining the low degree of interference with the bile acid transport with  $\text{IC}_{50}$  of 260  $\mu\text{M}$  (selectivity index: 65) (Fig. 3, shown in green).

**Acidic betulin derivatives are potent, but non-selective inhibitors of NTCP.** All potent ( $\text{IC}_{50}$  preS1 binding < 10  $\mu\text{M}$ ) and non-selective (selectivity index < 10) NTCP inhibitors from the group of betulin derivatives bear at least one acidic group. This applies to compounds 4, 8–12, 20, and 21 (Tab. 1). Based on their pKa values, these compounds are predominantly deprotonated and negatively charged at pH 7.4, similar to bile acids. In order to investigate the role of the pH-dependent negative charge of these compounds, the acidic derivatives 4 (pKa = 4.8) and 8 (pKa = 4.1) were tested for [ $^3\text{H}$ ]TC uptake inhibition and [ $^3\text{H}$ ]preS1 binding inhibition at pH 7.4 and pH 5.5. Betulin (1) was included as a non-acidic compound for control. In the case of compound 4 a shift of the  $\text{IC}_{50}$  value for [ $^3\text{H}$ ]TC uptake inhibition from 0.8 to 103  $\mu\text{M}$  was observed (Fig. 4, upper panel). Compound 8 also showed an  $\text{IC}_{50}$  shift from 8 to 200  $\mu\text{M}$  by lowering the pH from 7.4 to 5.5. Interestingly, the  $\text{IC}_{50}$  values for [ $^3\text{H}$ ]preS1 binding inhibition did not change at lower pH (Fig. 4, lower panel). Apart from this effect on the inhibition pattern, acidification of the incubation medium also affected the absolute [ $^3\text{H}$ ]TC uptake and [ $^3\text{H}$ ]preS1 binding rates (Fig. 4, bar graphs). Both functions of NTCP were significantly lower at pH of 5.5, most likely due to pH sensitive amino acid residues at the sites of substrate/preS1 binding.

**Betulin derivatives inhibit HDV infection.** Selected betulin derivatives were investigated for their inhibitory potency of in vitro HDV infection of NTCP-expressing HepG2 hepatoma cells. These experiments were of particular interest as in the [ $^3\text{H}$ ]preS1 assays, [ $^3\text{H}$ ]preS1 peptide binding is just used as a surrogate parameter for virus binding to NTCP. Of note, these infection experiments were performed in a different cell line as the screening assays and the betulin inhibitors had to be incubated much longer for the in vitro infection experiments (6 h) compared to the [ $^3\text{H}$ ]preS1 binding assay (15 min). While NTCP-HepG2 cells without inhibitor were used as control (set to 100% infection rate), co-incubation with 0.5  $\mu\text{M}$  of the myr-preS1<sub>2-48</sub> lipopeptide completely abolished infection of the cells (set to 0% infection rate). As inhibitors for in vitro HDV infection, betulinic acid (4) was used as a potent but non-selective inhibitor, 20,29-dihydrobetulin (2) as a potent and highly selective inhibitor, as well as lupenone (17) and betulonoyl dimethyl-L-aspartate (19) as less potent but still selective inhibitors. All four compounds significantly blocked in vitro HDV infection of the NTCP-HepG2 cells in a concentration-dependent manner (Fig. 5), clearly indicating that betulin derivatives represent an interesting novel compound class of HBV/HDV entry inhibitors. Of note, none of the compounds induced toxicity in the cells even after long term incubation at high (300  $\mu\text{M}$ /600  $\mu\text{M}$ ) inhibitor concentrations (Fig. 5h).

**Inhibition of HDV infection cannot be attributed to drug-induced internalization of NTCP.** Compounds 4 and 17 underwent further investigations to clarify, whether their inhibitory effects on in vitro HDV infection may have been attributed to drug-induced internalization of NTCP. Therefore, NTCP-expressing HepG2 hepatoma cells were pretreated with 600  $\mu\text{M}$  of the respective compound for 15 min or 6 h, respectively (Fig. 5e,f). Subsequently, cells were washed three times with tempered PBS, before [ $^3\text{H}$ ]TC (1  $\mu\text{M}$ ) uptake and [ $^3\text{H}$ ]preS1 (5 nM) binding were analyzed for 10 min at 37 °C. Cells pretreated with solvent (DMEM) alone served as 100% controls. Data from HepG2 cells without NTCP expression were set to 0%. Even after three intense washing steps, [ $^3\text{H}$ ]TC uptake was significantly reduced after short (15 min) and long (6 h) term preincubation with compound 4. In contrast, [ $^3\text{H}$ ]preS1 binding did not change, clearly confirming plasma membrane localization of NTCP even after long term preincubation with high inhibitor concentrations of 600  $\mu\text{M}$ . In the case of compound 17, no differences were observed after short term (15 min) preincubation, while [ $^3\text{H}$ ]TC uptake and [ $^3\text{H}$ ]preS1 binding slightly changed in opposite directions after long term (6 h) preincuba-

(a)



(b)

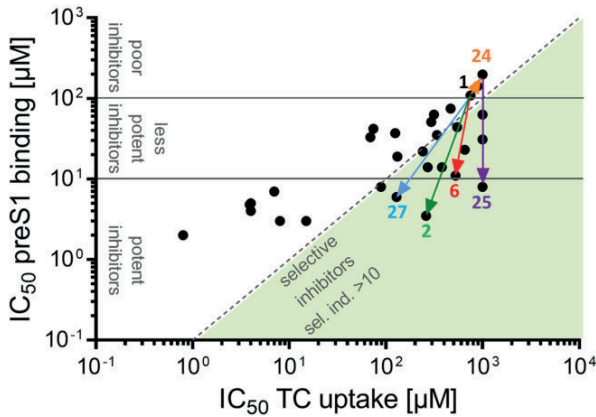




**Figure 3.** Structure–activity relationships of betulin derivatives for [ $^3\text{H}$ ]TC transport inhibition and [ $^3\text{H}$ ]preS1 binding inhibition. Chemical modifications at the lupane skeleton of betulin revealed clear structure–activity relationships for the potency (pot.,  $\text{IC}_{50}$  of [ $^3\text{H}$ ]preS1 binding inhibition) and virus selectivity index (sel. ind., ratio  $\text{IC}_{50}$  [ $^3\text{H}$ ]TC transport inhibition /  $\text{IC}_{50}$  [ $^3\text{H}$ ]preS1 binding inhibition). (a) 3,28-di-*O*-acetylation (shown in orange), additional  $\text{C}_{29}$ -hydroxylation (shown in purple), 3-*O*-modification with caffeeoyl (shown in light-blue), 28-oxime generation (shown in red), and  $\text{C}_{30}$  saturation (shown in green) of the betulin core structure improve the potency and/or selectivity index of the respective compounds. The respective inhibition pattern are illustrated by bar graphs for [ $^3\text{H}$ ]TC uptake (shown in dark-blue) and [ $^3\text{H}$ ]preS1 peptide binding (shown in red), respectively, in the presence or absence of a fix concentration (100  $\mu\text{M}$ ) of the respective betulin derivative. Graphs show means  $\pm$  SD of quadruplicate determinations. \*Significantly different with  $p < 0.01$  (two-way ANOVA with Sidak's multiple comparison test); ns, not significant. (b) The diagram shows all  $\text{IC}_{50}$  values for [ $^3\text{H}$ ]TC uptake inhibition and [ $^3\text{H}$ ]preS1 binding inhibition of the respective compounds. Effects ( $\text{IC}_{50}$  shifts) of the structural modifications are illustrated by arrows, starting from the core structure betulin (compound 1). Compounds can be divided into three groups regarding their potency to inhibit [ $^3\text{H}$ ]preS1 binding: potent inhibitors ( $\text{IC}_{50} \leq 10 \mu\text{M}$ ), less potent inhibitors ( $10 \mu\text{M} < \text{IC}_{50} < 100 \mu\text{M}$ ) and poor inhibitors ( $\text{IC}_{50} \geq 100 \mu\text{M}$ ). Compounds with a selectivity index of  $> 10$  are classified as selective inhibitors.

tion. These data confirm that also after preincubation with compound 17, NTCP remained at the plasma membrane.

## Discussion

The identification of the hepatic bile acid transporter NTCP as the high-affinity receptor for HBV and HDV is the basis for the development of a novel class of anti-HBV/anti-HDV drugs, being cell-entry inhibitors targeting NTCP<sup>9</sup>. Since then, many studies have identified compounds that are capable to inhibit the virus receptor function of NTCP: Hepludex<sup>13</sup>, cyclosporine A and other cyclosporine derivatives<sup>23–25</sup>, ezetimibe<sup>10</sup>, irbesartan<sup>27</sup>, ritonavir<sup>28</sup>, (-)-epigallocatechin-3-gallate<sup>29</sup>, vanitaracin A<sup>30</sup>, Ro41-5253<sup>31</sup>, proanthocyanidin<sup>32</sup>, zafirlukast<sup>33</sup>, sulfasalazine<sup>29</sup>, and Chicago Sky Blue 6B (an azo dye)<sup>33</sup>. Among them, Hepludex is a peptide-based drug and cannot be administered orally<sup>13</sup>. Furthermore, it has correspondingly complex manufacturing, storage, and distribution requirements. Therefore, it is still desirable to develop a small molecular drug with HBV/HDV cell-entry inhibitor activity that can be orally applied and would be easier to handle.

Many of the other mentioned compounds, e.g. cyclosporine A, were previously known to inhibit the bile acid transport function of NTCP<sup>17</sup>. Others were identified as novel HBV/HDV inhibitors and later revealed their interference with the physiological bile acid transport function of NTCP. Overall, this interference indicates that NTCP domains relevant for substrate binding and transport overlap with the domains mediating myr-preS1<sub>2–48</sub> lipopeptide / virus binding to NTCP. However, there are also some hints that both functions can be separated. In a previous study, we identified amino acid G158 of the human NTCP as absolutely essential for myr-preS1<sub>2–48</sub> lipopeptide binding and in vitro HBV and HDV infection. This amino acid is located at a domain (amino acids 157–165) that previously was shown to be involved in myr-preS1<sub>2–48</sub> binding to human NTCP<sup>9,18</sup>. Accordingly, G158R NTCP mutants were completely unsusceptible for in vitro HBV/HDV infection, but still supported transport of bile acids. It was discussed that the larger amino acid side chain of arginine compared to glycine might sterically preclude myr-preS1 peptide binding, while bile acids can still bind to their respective binding pocket<sup>34</sup>. Furthermore, Shimura et al.<sup>25</sup> showed for the cyclosporine derivative SCY995 higher potency against in vitro HBV infection ( $\text{IC}_{50} < 8 \mu\text{M}$ ) than for bile acid transport inhibition ( $\text{IC}_{50} > 25 \mu\text{M}$ ).

Based on this, the present study was designed to enable the identification of a selective HBV/HDV cell-entry inhibitor from the group of small molecules. Therefore, all test compounds were a priori tested for both, inhibition of [ $^3\text{H}$ ]preS1 binding to NTCP as a surrogate parameter for HBV/HDV infection and inhibition of [ $^3\text{H}$ ]TC transport via NTCP. In the present study, a novel chemical class of promising HBV/HDV cell-entry inhibitors was identified, represented by derivatives of the natural pentacyclic lupane-type triterpenoid betulin. Betulin can be isolated from various plant species, belonging to a variety of families such as Betulaceae, Platanaceae, Dilleniaceae, Rhamnaceae, Rosaceae, and Fagaceae<sup>35,36</sup>. Characteristics of the lupane skeleton of betulin are the five-membered E ring and the isopropylidene group<sup>37</sup>. Interestingly, nearly all betulin derivatives tested in the present study significantly inhibited [ $^3\text{H}$ ]TC transport and [ $^3\text{H}$ ]preS1 binding. However, the ratios between the  $\text{IC}_{50}$  values for transport inhibition and for [ $^3\text{H}$ ]preS1 binding inhibition were quite different and the resulting selectivity indices ranged from 1 up to 65. The latter was the case for compound 2 with an  $\text{IC}_{50}$  of 4  $\mu\text{M}$  for [ $^3\text{H}$ ]preS1 binding inhibition and an  $\text{IC}_{50}$  of 260  $\mu\text{M}$  for bile acid transport inhibition. Some other compounds showed no transport inhibition at all, being 24, 25, 28, and 30, but at least in the case of 25, potent inhibition of [ $^3\text{H}$ ]preS1 peptide binding with  $\text{IC}_{50}$  of 8  $\mu\text{M}$ . This data clearly indicate structure–activity relationships for both NTCP functions. Of note, only small changes in the molecular structure of the betulin derivatives significantly changed their potency and selectivity index. Moreover, hydroxylation of compound 24 to compound 25, as an example, improved both factors in parallel: potency for [ $^3\text{H}$ ]preS1 binding inhibition and the selectivity index. Also other modifications of the betulin molecule (1) such as 3-*O*-cafeeoyl conjugation (compound 27) or  $\text{C}_{20}$ - $\text{C}_{30}$  saturation (compound 2) significantly improved both factors simultaneously.

Inhibition studies at pH 5.5 revealed additional structure–activity relationships regarding the charge of the tested compounds. All potent but non-selective inhibitors (Fig. 3b) bear at least one acidic group at R1 and/or R2 (see Tab. 1) and show pKa values between 4–5. Therefore, compounds from this group are predominantly deprotonated and negatively charged at physiological pH of 7.4, representing the standard condition in the inhibition assays. For comparison, also conjugated bile acids (pKa = 1–4) are predominantly deprotonated and negatively charged at physiological pH<sup>38–40</sup>. Based on this it can be speculated that acidic betulin derivatives may not only be

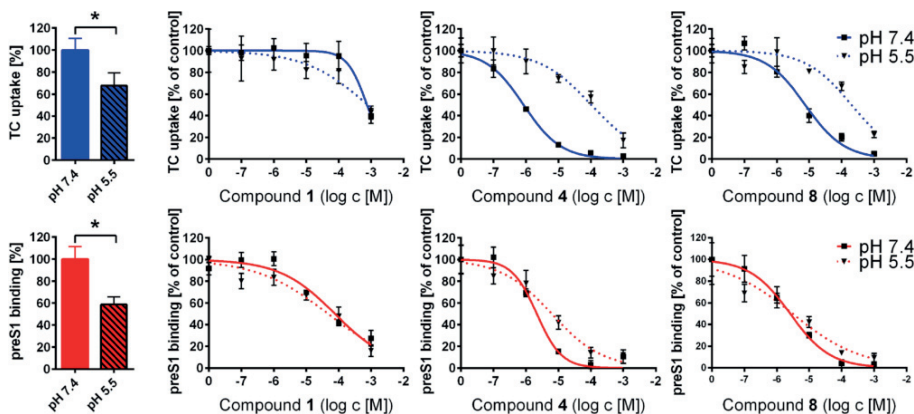


**Figure 4.** Influence of pH on the inhibition pattern of acidic betulin derivatives. NTCPC-HEK293 cells were incubated with tetracycline in order to induce NTCPC expression and were used for bile acid transport experiments with  $1 \mu\text{M}$   $^3\text{H}$ TTC and for myr-preS1<sub>1-48</sub> lipopeptide binding experiments with  $5 \text{ nM}$   $^3\text{H}$ preS1, each over 10 min at  $37^\circ\text{C}$ . Cells without tetracycline treatment served as control (set to 0%). Experiments were performed with solvent alone (set to 100%) and with increasing concentrations of the indicated inhibitors in the range of 0.1 to  $1,000 \mu\text{M}$  at pH 7.4 and pH 5.5, respectively. Diagrams show inhibition curves at pH 7.4 (solid lines) and pH 5.5 (dashed lines). The mean of the 0% control was subtracted to calculate net  $^3\text{H}$ TTC transport rates (shown in blue) as well as net  $^3\text{H}$ preS1 binding rates (shown in red), both expressed as % of control at the y-axis. Bar graphs show the relative  $^3\text{H}$ TTC uptake rates (blue bars) and  $^3\text{H}$ preS1 binding rates (red bars) at pH 7.4 (filled bars) and pH 5.5 (striped bars), respectively, expressed as pmol/10 min/well. Half maximal inhibitory concentrations ( $\text{IC}_{50}$ ) were calculated by nonlinear regression analysis using the equation  $\log(\text{inhibitor})$  vs. response (GraphPad Prism). Data represent means  $\pm$  SD of quadruplicate determinations ( $n=4$ ). \*Significantly different with  $p < 0.01$  (unpaired t-test with Welch's correction).

inhibitors but also transporter substrates of NTCPC. This would explain, why these compounds (representatively shown for compounds 4 and 8) largely lost their  $^3\text{H}$ TTC uptake inhibitory potency when the pH was reduced to 5.5 and, thereby reducing the relative charge of the molecules. In contrast, the  $^3\text{H}$ preS1 binding inhibitory potency was insensitive to this pH shift and only showed little differences between pH 7.4 and pH 5.5 conditions. This again indicates that the transporter and the receptor function of NTCPC can be separated under certain experimental conditions and that blocking of the preS1 peptide binding site of NTCPC does not require negative charge of the inhibitor. In contrast to compounds 4 and 8, betulin itself (compound 1) does not bear any acidic group. Consequently, betulin could be less active at the bile acid binding site, what would explain the relatively low potency for TC uptake inhibition ( $\text{IC}_{50} = 748 \mu\text{M}$ ) at neutral and acidic pH values. However, no uniform legality could be established for the other chemical modifications of betulin, which would precisely predict the potency and selectivity pattern of the respective betulin derivative. Nevertheless, based on the structure-activity relationships described in the present study it is most likely that even more potent betulin derivatives can be identified, while sparing the cross-reactivity on the bile acid transport function of NTCPC.

Among the betulin derivatives, betulinic acid (4) particularly underwent intensive toxicological assessments<sup>35,41–43</sup>. In vitro and in vivo model systems consistently categorized betulinic acid (4) as a safe compound with low toxicity. More recently, no toxic effects were observed in rats that obtained single i.p. application of  $400 \text{ mg/kg}$  or in mice receiving  $100 \text{ mg/kg}$  i.p. every 3–4 days for a total of six treatments, or  $500 \text{ mg/kg}$  i.p. once<sup>35,42,43</sup>. Unfortunately, betulinic acid (4), although potent in  $^3\text{H}$ preS1 binding inhibition ( $\text{IC}_{50} = 2 \mu\text{M}$ ), is not selective and showed equipotent inhibition of the bile acid transport function of NTCPC at least at physiological pH. Therefore, betulinic acid (4) is not regarded as the optimal HBV/HDV entry inhibitor candidate from the betulin class of compounds. Apart from betulinic acid (4), betulin (1) also has a good safety profile. Betulin (1) is approved for medical use in humans and is currently available as a betulin containing gel (Oleogel-S10, Episalvan). It was authorized in 2016 by the European Medicines Agency (EMA) for treatment of partial thickness wounds in adults. This gel contains an extract from birch bark of *Betula pendula* Roth, *Betula pubescens* Ehrh., and hybrids of both species, obtained with *n*-heptane as the extraction solvent. The resulting betulin (1) concentrations are in the range of 72–88 mg betulin (1) per 100 mg extract. The gel itself is composed of 10% birch bark extract in 90% sunflower oil. Moreover, Episalvan is currently undergoing a phase III efficacy and safety study in patients with inherited epidermolysis bullosa (EB) that started in 2017 with an estimated enrollment of 250 participants (NCT03068780). Based on this good safety profile and the established use in human medicine, betulin (1) is an attractive early lead candidate for selective HBV/HDV cell-entry inhibition. However, despite its superior selectivity in comparison to betulinic acid (4), the potency for  $^3\text{H}$ preS1 binding inhibition is relatively

low ( $IC_{50} = 109 \mu\text{M}$ ). Nevertheless, the present study clearly demonstrates that even small modifications of the lupane skeleton of betulin can improve the potency and selectivity of the respective compounds significantly. Therefore, it seems likely that advanced rational drug design can further improve this compound class to end up with a potent and selective HBV/HDV cell-entry inhibitor.

Apart from the above-mentioned clinical application, several previous studies showed that betulin (1) and betulin derivatives have a broad spectrum of pharmacological effects, including anti-cancer, anti-viral, anti-microbial, anti-inflammatory, and anti-fibrotic effects<sup>44–48</sup>. Interestingly, betulinic acid (4) was also used in HBV infection studies before, which showed inhibition of HBV replication by suppression of manganese superoxide dismutase (SOD2) expression with subsequent mitochondrial reactive oxygen species (ROS) over-generation<sup>49</sup>. Based on this and the results from the present study, betulinic acid (4) might have additive HBV/HDV antiviral properties by addressing different cellular targets involved in cell-entry (NTCP) and replication (SOD2). Therefore, further studies with betulin derivatives should take selective NTCP inhibition and potential suppression of SOD2 into account, which was beyond the scope of the present study.

Our [<sup>3</sup>H]preS1 binding assay successfully predicted the inhibitory effect of the betulin derivatives on in vitro HDV infection. A minor but expected limitation is that absolute  $IC_{50}$  values varied between both experimental setups. While the qualitative activity pattern of the betulin derivatives remained the same between the two assays, the absolute  $IC_{50}$  values for in vitro HDV infection inhibition were about one to two orders of magnitude higher than predicted from the [<sup>3</sup>H]preS1 binding experiments. Most likely, several factors contribute to this effect. One factor could be the different incubation times for [<sup>3</sup>H]preS1 binding (minutes) and in vitro HDV infection experiments (hours). Another factor might be the use of different cell lines and incubation media. Whereas, the [<sup>3</sup>H]preS1 binding assays were performed in NTCP-HEK293 cells in pure DMEM, the infection experiments needed to be performed with NTCP-HepG2 cells in HGM containing significant amounts of bovine serum albumin (BSA) as well as polyethylene glycol (PEG). The latter medium conditions potentially alter free drug concentrations due to protein binding. Lowering of the inhibitory potency of betulinic acid (4) due to protein binding has already been identified in a previous study, where this compound was used as inhibitor for the organic anion transporting polypeptide OATP1B3<sup>30</sup>. A further factor could be the different stoichiometry of the single preS1 peptide molecule and the multitude of preS1 domains of the large envelope proteins of HBV/HDV virions. The latter one could need a higher degree of blocked NTCP receptors for successful virus binding and cell-entry inhibition. On this background, it could be beneficial if an NTCP inhibitor would not only be selective, but would also irreversibly block the preS1/virus binding sites at NTCP. However, this was not achieved with the betulin derivatives analyzed in the present study. The data obtained on compounds 4 and 17 more suggest a reversible mode of inhibition for myr-preS1<sub>2–48</sub> peptide binding to NTCP. Their inhibitory effect on [<sup>3</sup>H]preS1 binding was completely abrogated by washing the cell surface with inhibitor-free medium (see Fig. 5e,f). But, these observations clearly indicate that the inhibitory effects of compounds 4 and 17 on HDV infection cannot be attributed to drug-induced internalization of NTCP.

Of interest are also the long-term effects of compounds 4 and 17 on the transporter and receptor function of NTCP. In the case of compound 4 preincubation with 600  $\mu\text{M}$  significantly and selectively reduced the transporter function of NTCP, while NTCP still was completely preS1 peptide binding competent. As compound 4 (betulinic acid) belongs to the group of acidic betulin derivatives one can speculate that betulinic acid is transported by NTCP, accumulates inside the cell during preincubation and so by *trans*-inhibition blocks substrate binding but not preS1 peptide binding to the outer surface of the NTCP protein. This again would support the idea that bile acid and preS1 peptide binding to NTCP occur at separate, but overlapping domains. In contrast, compound 17 showed a paradoxical effect after long term preincubation and increased the capacity for [<sup>3</sup>H]preS1 peptide binding to approximately 130%, while the [<sup>3</sup>H]TC uptake rate was slightly reduced. This could be explained by longer lasting allosteric effects of this compound that differently affects the transport and receptor function of NTCP. The mechanism behind these effects could not be clarified in the present study and needs further investigation, including LC–MS/MS supported direct transport experiments with key betulin derivatives.

In conclusion, betulin derivatives show clear structure–activity relationships for potent and selective inhibition of the HBV/HDV virus receptor function of NTCP without tackling its physiological bile acid transport function. Therefore, betulin derivatives are promising candidates for further development of HBV/HDV cell-entry inhibitors. Further studies with this compound class should additionally focus on the mode of inhibition (reversible vs. irreversible) and should be extended to all relevant HBV genotypes.

## Methods

**NTCP-expressing cell lines.** Human embryonic kidney (HEK293) cells were stably transfected with human NTCP, C-terminally tagged with the FLAG epitope (further referred to as NTCP-HEK293 cells) as reported before<sup>31</sup>. Cells were maintained at 37 °C, 5% CO<sub>2</sub> and 95% humidity in DMEM/F-12 medium (Thermo Fisher Scientific, Waltham, MA, USA) supplemented with 10% fetal calf serum (Sigma-Aldrich, St. Louis, MO, USA), 4 mM L-glutamine (PAA, Cölbe, Germany) and penicillin/streptomycin (PAA). HepG2 cells stably transfected with NTCP-FLAG (further referred to as NTCP-HepG2<sup>10</sup>) were cultured under the same conditions in DMEM with all supplements listed above, except for L-glutamine. For induction of the transgene, the medium was supplemented with 1  $\mu\text{g}/\text{ml}$  tetracycline (Roth, Karlsruhe, Germany) in the case of the NTCP-HEK293 cells or with 2  $\mu\text{g}/\text{ml}$  doxycycline (Sigma-Aldrich) in the case of the NTCP-HepG2 cells.

**Inhibitory concentrations ( $IC_{50}$ ) for [<sup>3</sup>H]preS1 binding and [<sup>3</sup>H]TC transport.** Bile acid transport measurements were performed in the NTCP-HEK293 cells with [<sup>3</sup>H]TC (20 Ci/mmol, 0.09 mCi/ml, Perkin Elmer, Waltham, USA) as reported before<sup>31</sup>. In parallel, [<sup>3</sup>H]preS1 peptide binding experiments were performed with a tritium-labelled myr-preS1<sub>2–48</sub> lipopeptide -HBV subgenotype D3- that was purchased from Pharmaron

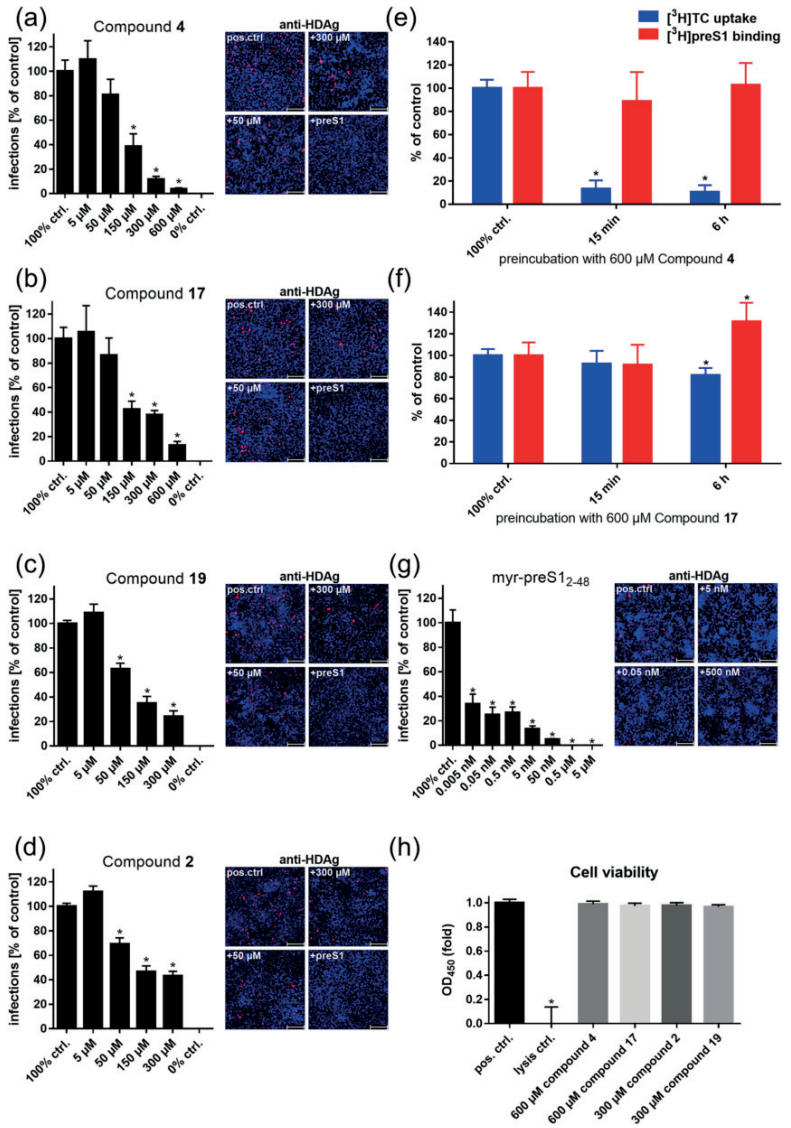


**Figure 5.** Selected betulin derivatives were used for HDV infection inhibition of NTCP-HepG2 cells. NTCP-HepG2 cells were preincubated for 5 min with the indicated concentrations of (a) betulonic acid (compound 4), (b) lupenone (compound 17), (c) betulonoyl dimethyl-L-aspartate (compound 19), (d) 20,29-dihydrobetulin (compound 2), and (g) the myr-preS1<sub>2-48</sub> peptide in DMEM at 37 °C. Then, cells were additionally inoculated with 700 genome equivalents/cell of HDV particles at 37 °C. After 6 h, cells were washed and further incubated with inhibitor- and virus-free medium, and medium was changed every 3–4 days. At day 9 post infection, cells were fixed and an immunostaining against the HDAG was performed, as a marker of HDV infection. The number of infected cells per well was determined by fluorescence microscopy. NTCP-HepG2 cells incubated without inhibitor were used as control (set to 100% infection rate). Infection experiments in the presence of 0.5 μM myr-preS1<sub>2-48</sub> peptide served as control for the 0% infection rate. Scale bars: 100 μm. Data represent means ± SEM of three independent experiments each with triplicate determinations (n = 9). (e, f) Cells were preincubated with 600 μM of compound 4 and compound 17, respectively, for intervals of 15 min and 6 h at 37 °C. Cells treated with solvent (DMEM) alone served as control (set to 100%) and data from cells without induction of NTCP expression were set to 0%. Subsequently, cells were washed three times with tempered PBS and [<sup>3</sup>H]TC (1 μM) uptake as well as [<sup>3</sup>H]preS1 (5 nM) binding were analyzed, respectively. Means of the 0% controls were subtracted and net [<sup>3</sup>H]TC transport rates and net [<sup>3</sup>H]preS1 binding rates are expressed as % of control at the y-axis. Data were combined from two independent experiments, each with quadruplicate determinations (n = 8). (h) Cell viability was determined with an LDH cytotoxicity assay. HepG2 cells treated with HGM w/o test compound were used as positive control and lysed cells as negative control. Data show means ± SD of three independent experiments each with triplicate determinations (n = 9). \*Significantly different from control with *p* < 0.01 (two-way ANOVA with Dunnett's multiple comparison test).

(120 Ci/mmol, 1 mCi/ml, Cardiff, UK). Briefly, cells were seeded onto polylysine-coated 96-well plates, induced with 1 μg tetracycline per ml, and grown to confluence over 72 h at 37 °C. Then, cells were washed once with tempered phosphate buffered saline (PBS, 137 mM NaCl, 2.7 mM KCl, 1.5 mM KH<sub>2</sub>PO<sub>4</sub>, 7.3 mM Na<sub>2</sub>HPO<sub>4</sub>, pH 7.4) at 37 °C and preincubated with 80 μl DMEM for 5 min at 37 °C. The medium was replaced by 80 μl DMEM containing the respective betulin derivative (concentrations ranging from 0.1 to 1,000 μM) or solvent alone (100% uptake/binding control), and cells were further incubated for 5 min at 37 °C. After this preincubation, bile acid transport experiments were started by adding 20 μl DMEM containing 5 μM [<sup>3</sup>H]TC (final concentration: 1 μM). Binding of [<sup>3</sup>H]preS1 was initiated by adding 20 μl DMEM containing 25 nM [<sup>3</sup>H]preS1 (final concentration: 5 nM). Experiments were stopped after 10 min by two-times washing with ice-cold PBS. For 0% uptake/binding control, the NTCP-HEK293 cells were not induced with tetracycline (-tet). Cell-associated radioactivity of [<sup>3</sup>H]TC or [<sup>3</sup>H]preS1 was quantified by liquid scintillation counting in a Packard Microplate Scintillation Counter TopCount NXT (Packard Instrument Company, Meriden, USA). Transport rates and [<sup>3</sup>H]preS1 binding were determined in counts per minute (cpm). The mean of the 0% control was subtracted and the net [<sup>3</sup>H]TC transport rates and net [<sup>3</sup>H]preS1 binding rates, respectively, were expressed as % of control. Experiments at pH 5.5 were performed the same way, using DMEM acidified with hydrochloric acid (32%, Roth). A set of betulin derivatives was purchased from Adipogen AG (Liestal, Switzerland), including the compounds betulin (1), betulonic acid (4), lupeol (3), betulonaldehyde (18), lupenone (17), 3-*O*-caffeoylbetulin (27), 3,28-di-*O*-acetylbetulin (24), 28-*O*-(3,3-dimethylglutaryl)betulin (10), 3,28-di-*O*-(3,3-dimethylglutaryl)betulin (12), 28-*O*-succinoylbetulin (8), 3,28-di-*O*-succinoylbetulin (9), 3-*O*-(3,3-dimethylglutaryl)betulonic acid (11), and 3-*O*-acetylbetulonic acid (21) (TargoSet). All other betulin derivatives were synthesized as outlined elsewhere<sup>53–54</sup>. IC<sub>50</sub> values were calculated from quadruplicate determinations by GraphPad Prism 6 (GraphPad, San Diego, CA, USA).

**HDV infection experiments.** For infection experiments NTCP-HepG2 cells were cultured in 96-well plates in Hepatocyte Growth Medium (HGM) consisting of William's E Medium (Thermo Fisher Scientific) containing 2% bovine serum albumin (BSA, Roth), 2 mM L-Glutamin (Thermo Fisher Scientific), 100 μg/ml gentamicin (Thermo Fisher Scientific), 10 nM dexamethasone (Sigma-Aldrich), 1 mM sodium pyruvate (Thermo Fisher Scientific), 1 × Insulin-Transferrin-Selen (Thermo Fisher Scientific), 2% DMSO (Merck, Darmstadt, Germany), 4% polyethylene glycol (Sigma-Aldrich) and 2 μg/ml doxycycline (Sigma-Aldrich) as reported<sup>10</sup>. Subsequently, cells were washed with DMEM and cultured in HGM supplemented with 2% DMSO, 2% BSA and 2 μg/ml doxycycline. NTCP-HepG2 cells were preincubated for 5 min with inhibitors solved in 80 μl HGM per well in concentrations ranging from 5 μM to 300 μM (compounds 2 and 19) or from 5 μM to 600 μM (compounds 4 and 17). HDV stock solved in 20 μl HGM per well was added for infection and cells were incubated for 6 h with final concentration of 700 genome equivalents/cell of HDV particles. HDV production was done in vitro as described before<sup>55,56</sup>. RT-qPCR was performed to determine genome equivalents. Every three days medium was changed until cells were fixed at 9 days post infection with 3% paraformaldehyde (Sigma-Aldrich) in PBS, for 30 min at room temperature (RT). Cells were permeabilized with 0.2% Triton X 100 (Roth) in PBS for 30 min at RT, and blocked by incubation with 5% bovine serum albumin (Roth) in PBS, for 30 min at RT. Then, cells were immunostained with purified human anti-HDV-positive serum at 37 °C for 1 h (1:400 dilution). Goat anti-human IgG secondary antibody coupled to Alexa Fluor fluorophore (1:400 dilution, Thermo Fisher Scientific) was added for 1 h at 37 °C for detection of Hepatitis Delta antigen (HDAG) as described before<sup>54</sup>. Nuclei were stained with Hoechst 33342 (1 μg/ml, Thermo Fisher Scientific).

**Preincubation studies in NTCP-HepG2 cells.** NTCP-expressing HepG2 hepatoma cells were seeded onto rat tail collagen coated 24-well plates, induced with 2 μg doxycycline per ml, and grown to confluence over 72 h at 37 °C. For experiments, cells were preincubated with a fix concentration (600 μM) of compound 4 and

compound **17**, respectively, solved in 300  $\mu$ l DMEM for intervals of 15 min or 6 h at 37 °C. Cells treated with solvent alone (DMEM) were used as 100% controls. Cells without induction of NTCPC expression by doxycycline were used as 0% controls. Subsequently, cells were washed three times with tempered PBS. Then, [ $^3$ H]TC uptake and [ $^3$ H]preS1 binding experiments were started by adding 300  $\mu$ l of 1  $\mu$ M [ $^3$ H]TC or 5 nM [ $^3$ H]preS1, respectively. After 10 min, experiments were stopped by washing the cells 5 times with ice-cold PBS. Cell-associated radioactivity was quantified by liquid scintillation counting as described above. [ $^3$ H]TC uptake and [ $^3$ H]preS1 binding rates were determined in pmol/mg protein/10 min. Means of the 0% controls were subtracted and the net [ $^3$ H]TC uptake and net [ $^3$ H]preS1 binding rates, respectively, were expressed as % of control. Data were calculated from two independent experiments, each with quadruplicate determinations by GraphPad Prism 6 (GraphPad, San Diego, CA, USA).

**Cytotoxicity assay.** Pierce lactate dehydrogenase (LDH) cytotoxicity assay (Thermo Fisher Scientific) was performed according to the manufacturer's protocol. Briefly, NTCPC-HepG2 cells were incubated with 300  $\mu$ M or 600  $\mu$ M of the respective betulin derivatives over 6 h at 37 °C. 45 min before the end of incubation, lysis buffer was added to the maximal LDH control. After 6 h, 50  $\mu$ l of each sample and control medium were transferred to a new well plate, 50  $\mu$ l of the reaction mixture were added and incubation was performed over 30 min at room temperature. Finally, the reaction was stopped by adding 50  $\mu$ l of stop solution and samples were measured by ELISA reader (GloMax-Multi Detection System, Promega, Madison, WI, USA).

**Structure modeling and pKa determination.** 2D compound structures were generated using the MAESTRO 12.2 Molecular Modeling Interface of SCHRÖDINGER, Inc. (New York City, NY, USA). The Jaguar pKa prediction module of the SCHRÖDINGER software was used to calculate pKa values of compounds **4** and **8**.

**Statistics.** Determination of IC<sub>50</sub> values was done by nonlinear regression analysis using the equation log(inhibitor) vs. response settings of the GraphPad Prism 6.0 software (GraphPad). Data of bile acid transport and [ $^3$ H]preS1 binding are expressed as means  $\pm$  SD from quadruplicate determinations. IC<sub>50</sub> values are listed with their 95% confidence intervals in Table 2. In addition, mean IC<sub>50</sub> values were calculated for each experiment. Infection studies show data from three independent experiments, each with triplicate determinations represented as means  $\pm$  SEM. Statistical analyses of the HDV infection experiments and NTCPC-HepG2 preincubation studies were performed by two-way ANOVA, followed by Dunnett's multiple comparison test by GraphPad Prism 6.0, considering  $p < 0.01$  as statistically significant.

#### Data availability

Obtained and analyzed data of this study are available from the corresponding author on request.

Received: 15 July 2020; Accepted: 27 November 2020

Published online: 10 December 2020

#### References

- World Health Organization. Global hepatitis report 2017. Geneva 2017. Licence:CC BY-NC-SA 3.0 IGO. (2017).
- Glebe, D. & Bremer, C. M. The molecular virology of hepatitis B virus. *Semin. Liver. Dis.* **33**, 103–112. <https://doi.org/10.1055/s-0033-1345717> (2013).
- Glebe, D. *et al.* Mapping of the hepatitis B virus attachment site by use of infection-inhibiting preS1 lipopeptides and tupaia hepatocytes. *Gastroenterology* **129**, 234–245. <https://doi.org/10.1053/j.gastro.2005.03.090> (2005).
- Gripone, P., Cammie, I. & Urban, S. Efficient inhibition of hepatitis B virus infection by acylated peptides derived from the large viral surface protein. *J. Virol.* **79**, 1613–1622. <https://doi.org/10.1128/JVI.79.3.1613-1622.2005> (2005).
- Hughes, S. A., Wedemeyer, H. & Harrison, P. M. Hepatitis delta virus. *Lancet* **378**, 73–85. [https://doi.org/10.1016/S0140-6736\(10\)61931-9](https://doi.org/10.1016/S0140-6736(10)61931-9) (2011).
- Sureau, C. & Negro, F. The hepatitis delta virus: Replication and pathogenesis. *J. Hepatol.* **64**, S102–S116. <https://doi.org/10.1016/j.jhep.2016.02.013> (2016).
- Martinez, M. G., Villeret, F., Testoni, B. & Zoulim, F. Can we cure hepatitis B virus with novel direct-acting antivirals?. *Liver Int.* **40**(Suppl 1), 27–34. <https://doi.org/10.1111/liv.14364> (2020).
- World Health Organization. Guidelines for the prevention, care and treatment of persons with chronic hepatitis b infection. (2015).
- Yan, H. *et al.* Sodium taurocholate cotransporting polypeptide is a functional receptor for human hepatitis B and D virus. *eLife* <https://doi.org/10.7554/eLife.00049>.
- König, A. *et al.* Kinetics of the bile acid transporter and hepatitis B virus receptor Na<sup>+</sup>/taurocholate cotransporting polypeptide (NTCP) in hepatocytes. *J. Hepatol.* **61**, 867–875. <https://doi.org/10.1016/j.jhep.2014.05.018> (2014).
- Lamas Longarela, O. *et al.* Proteoglycans act as cellular hepatitis delta virus attachment receptors. *PLoS ONE* **8**, e58340. <https://doi.org/10.1371/journal.pone.0058340> (2013).
- Fukano, K., Tsukuda, S., Watahi, K. & Wakita, T. Concept of Viral Inhibitors via NTCP. *Semin. Liver Dis.* **39**, 78–85. <https://doi.org/10.1055/s-0038-1676804> (2019).
- MYR Pharmaceuticals. <http://myr-pharma.com/>. (2020).
- Bogomolov, P. *et al.* Treatment of chronic hepatitis D with the entry inhibitor myrcludex B: first results of a phase II/IIIa study. *J. Hepatol.* **65**, 490–498. <https://doi.org/10.1016/j.jhep.2016.04.016> (2016).
- Geyer, J., Wilke, T. & Petzinger, E. The solute carrier family SLC10: more than a family of bile acid transporters regarding function and phylogenetic relationships. *Arch. Pharmacol.* **372**, 413–431. <https://doi.org/10.1007/s00210-006-0043-8> (2006).
- Stieger, B. The role of the sodium-taurocholate cotransporting polypeptide (NTCP) and of the bile salt export pump (BSEP) in physiology and pathophysiology of bile formation. *Handb. Exp. Pharmacol.* [https://doi.org/10.1007/978-3-642-14541-4\\_5](https://doi.org/10.1007/978-3-642-14541-4_5) (2011).
- Döring, B., Lütkeke, T., Geyer, J. & Petzinger, E. The SLC10 carrier family: transport functions and molecular structure. *Curr. Top. Membr.* **70**, 105–168. <https://doi.org/10.1016/B978-0-12-394316-3.00004-1> (2012).
- Ni, Y. *et al.* Hepatitis B and D viruses exploit sodium taurocholate co-transporting polypeptide for species-specific entry into hepatocytes. *Gastroenterology* **146**, 1070–1083. <https://doi.org/10.1053/j.gastro.2013.12.024> (2014).

19. Blank, A. et al. The NTCP-inhibitor Myrcludex B: effects on Bile Acid Disposition and Tenofovir Pharmacokinetics. *Clin. Pharmacol. Ther.* **103**, 341–348. <https://doi.org/10.1002/cpt.744> (2018).
20. Goh, B. et al. Development of a mass spectrometric screening assay for hepatitis B virus entry inhibitors. *J. Pharm. Biomed. Anal.* **178**, 112959. <https://doi.org/10.1016/j.jpba.2019.112959> (2020).
21. Iwamoto, M. et al. Evaluation and identification of hepatitis B virus entry inhibitors using HepG2 cells overexpressing a membrane transporter NTCP. *Biochem. Biophys. Res. Commun.* **443**, 808–813. <https://doi.org/10.1016/j.bbrc.2013.12.052> (2014).
22. Fukano, K. et al. Troglitazone impedes the oligomerization of sodium taurocholate cotransporting polypeptide and entry of hepatitis B virus into hepatocytes. *Front. Microbiol.* **9**, 3257. <https://doi.org/10.3389/fmicb.2018.03257> (2018).
23. Watashi, K. et al. Cyclosporin A and its analogs inhibit hepatitis B virus entry into cultured hepatocytes through targeting a membrane transporter, sodium taurocholate cotransporting polypeptide (NTCP). *Hepatology* **59**, 1726–1737. <https://doi.org/10.1002/hep.26982> (2014).
24. Nkongolo, S. et al. Cyclosporin A inhibits hepatitis B and hepatitis D virus entry by cyclophilin-independent interference with the NTCP receptor. *J. Hepatol.* **60**, 723–731. <https://doi.org/10.1016/j.jhep.2013.11.022> (2014).
25. Shimura, S. et al. Cyclosporin derivatives inhibit hepatitis B virus entry without interfering with NTCP transporter activity. *J. Hepatol.* **66**, 685–692. <https://doi.org/10.1016/j.jhep.2016.11.009> (2017).
26. Saso, W. et al. A new strategy to identify hepatitis B virus entry inhibitors by AlphaScreen technology targeting the envelope-receptor interaction. *Biochem. Biophys. Res. Commun.* <https://doi.org/10.1016/j.bbrc.2018.04.187> (2018).
27. Wang, X. J. et al. Irbesartan, an FDA approved drug for hypertension and diabetic nephropathy, is a potent inhibitor for hepatitis B virus entry by disrupting Na(+)-dependent taurocholate cotransporting polypeptide activity. *Antiviral Res.* **120**, 140–146. <https://doi.org/10.1016/j.antiviral.2015.06.007> (2015).
28. Blanchet, M., Sureau, C. & Labonte, P. Use of FDA approved therapeutics with hNTCP metabolic inhibitory properties to impair the HDV lifecycle. *Antiviral Res.* **106**, 111–115. <https://doi.org/10.1016/j.antiviral.2014.03.017> (2014).
29. Huang, H. C. et al. (-)-Epigallocatechin-3-gallate inhibits entry of hepatitis B virus into hepatocytes. *Antiviral Res.* **111**, 100–111. <https://doi.org/10.1016/j.antiviral.2014.09.009> (2014).
30. Kaneko, M. et al. A novel tricyclic polyketide, vanitaracin A, specifically inhibits the entry of hepatitis B and D viruses by targeting sodium taurocholate cotransporting polypeptide. *J. Virol.* **89**, 11945–11953. <https://doi.org/10.1128/JVI.01855-15> (2015).
31. Tsukuda, S. et al. Dysregulation of retinoic acid receptor diminishes hepatocyte permissiveness to hepatitis B virus infection through modulation of sodium taurocholate cotransporting polypeptide (NTCP) expression. *J. Biol. Chem.* **290**, 5673–5684. <https://doi.org/10.1074/jbc.M114.602540> (2015).
32. Tsukuda, S. et al. A new class of hepatitis B and D virus entry inhibitors, proanthocyanidin and its analogs, that directly act on the viral large surface proteins. *Hepatology* **65**, 1104–1116. <https://doi.org/10.1002/hep.28952> (2017).
33. Donkers, J. M. et al. Reduced hepatitis B and D viral entry using clinically applied drugs as novel inhibitors of the bile acid transporter NTCP. *Sci. Rep.* **7**, 15307. <https://doi.org/10.1038/s41598-017-15338-0> (2017).
34. Müller, S. F., König, A., Döring, B., Glebe, D. & Geyer, J. Characterisation of the hepatitis B virus cross-species transmission pattern via Na+/taurocholate co-transporting polypeptides from 11 New World and Old World primate species. *PLoS ONE* **13**, e0199200. <https://doi.org/10.1371/journal.pone.0199200> (2018).
35. Cichewicz, R. H. & Kouzi, S. A. Chemistry, biological activity, and chemotherapeutic potential of betulinic acid for the prevention and treatment of cancer and HIV infection. *Med. Res. Rev.* **24**, 90–114. <https://doi.org/10.1002/med.10053> (2004).
36. Moghaddam, M. G., Ahmad, F. B., Samzadeh-Kermani, A. Biological Activity of Betulinic Acid: A Review. *Pharmacol. Pharm.* **03**, 119–123. <https://doi.org/10.4236/pp.2012.32018> (2012)
37. Zhang, D. M. et al. Betulinic acid and its derivatives as potential antitumor agents. *Med. Res. Rev.* **35**, 1127–1155. <https://doi.org/10.1002/med.21353> (2015).
38. Greupink, R. et al. In silico identification of potential cholestasis-inducing agents via modeling of Na(+)-dependent taurocholate cotransporting polypeptide substrate specificity. *Toxicol. Sci.* **129**, 35–48. <https://doi.org/10.1093/toxsci/ks188> (2012).
39. Kim, R. B. et al. Modulation by drugs of human hepatic sodium-dependent bile acid transporter (sodium taurocholate cotransporting polypeptide) activity. *J. Pharmacol. Exp. Ther.* **291**, 1204–1209 (1999).
40. Kouzuki, H., Suzuki, H., Stieger, B., Meier, P. J. & Sugiyama, Y. Characterization of the transport properties of organic anion transporting polypeptide 1 (oatp1) and Na(+)/taurocholate cotransporting polypeptide (Ntcp): comparative studies on the inhibitory effect of their possible substrates in hepatocytes and cDNA-transfected COS-7 cells. *J. Pharmacol. Exp. Ther.* **292**, 505–511 (2000).
41. Kessler, J. H., Mullauer, F. B., de Roo, G. M. & Medema, J. P. Broad in vitro efficacy of plant-derived betulinic acid against cell lines derived from the most prevalent human cancer types. *Cancer Lett.* **251**, 132–145. <https://doi.org/10.1016/j.canlet.2006.11.003> (2007).
42. Zucco, V. et al. Selective cytotoxicity of betulinic acid on tumor cell lines, but not on normal cells. *Cancer Lett.* **175**, 17–25. [https://doi.org/10.1016/s0304-3835\(01\)00718-2](https://doi.org/10.1016/s0304-3835(01)00718-2) (2002).
43. Pisha, E. et al. Discovery of betulinic acid as a selective inhibitor of human melanoma that functions by induction of apoptosis. *Nat. Med.* **1**, 1046–1051. <https://doi.org/10.1038/nm1095-1046> (1995).
44. Zhan, X. K., Li, J. L., Zhang, S., Xing, P. Y. & Xia, M. F. Betulinic acid exerts potent antitumor effects on paclitaxel-resistant human lung carcinoma cells (H460) via G2/M phase cell cycle arrest and induction of mitochondrial apoptosis. *Oncol. Lett.* **16**, 3628–3634. <https://doi.org/10.3892/ol.2018.9097> (2018).
45. Chen, Y. et al. The design, synthesis and structure-activity relationships associated with C28 amine-based betulinic acid derivatives as inhibitors of HIV-1 maturation. *Bioorg. Med. Chem. Lett.* **28**, 1550–1557. <https://doi.org/10.1016/j.bmcl.2018.03.067> (2018).
46. Adeleke, G. E. & Adaramoye, O. A. Betulinic acid protects against N-nitrosodimethylamine-induced redox imbalance in testes of rats. *Redox Rep.* **22**, 556–562. <https://doi.org/10.1080/13510002.2017.1322750> (2017).
47. Laavola, M. et al. Betulin derivatives effectively suppress inflammation in vitro and in vivo. *J. Nat. Prod.* **79**, 274–280. <https://doi.org/10.1021/acs.jnatprod.5b00709> (2016).
48. Wan, Y. et al. The anti-fibrotic effect of betulinic acid is mediated through the inhibition of NF-kappaB nuclear protein translocation. *Chem. Biol. Interact.* **195**, 215–223. <https://doi.org/10.1016/j.cb.2012.01.002> (2012).
49. Yao, D. et al. Betulinic acid-mediated inhibitory effect on hepatitis B virus by suppression of manganese superoxide dismutase expression. *FEBS J.* **276**, 2599–2614. <https://doi.org/10.1111/j.1742-4658.2009.06988.x> (2009).
50. Oh, Y. et al. Inhibition of organic anion transporting polypeptide 1B1 and 1B3 by betulinic acid: effects of preincubation and albumin in the media. *J. Pharm. Sci.* **107**, 1713–1723. <https://doi.org/10.1016/j.xpts.2018.02.010> (2018).
51. Geyer, J. et al. Cloning and functional characterization of human sodium-dependent organic anion transporter (SLC10A6). *J. Biol. Chem.* **282**, 19728–19741. <https://doi.org/10.1074/jbc.M702663200> (2007).
52. Alakurtti, S. et al. Synthesis and anti-leishmanial activity of heterocyclic betulin derivatives. *Bioorg. Med. Chem.* **18**, 1573–1582. <https://doi.org/10.1016/j.bmcl.2010.01.003> (2010).
53. Pohjala, L., Alakurtti, S., Ahola, T., Yli-Kauhaluoma, J. & Tammela, P. Betulin-derived compounds as inhibitors of alphavirus replication. *J. Nat. Prod.* **72**, 1917–1926. <https://doi.org/10.1021/mp9003245> (2009).
54. Salin, O. et al. Inhibitory effect of the natural product betulin and its derivatives against the intracellular bacterium Chlamydia pneumoniae. *Biochem. Pharmacol.* **80**, 1141–1151. <https://doi.org/10.1016/j.bcp.2010.06.051> (2010).
55. Rasche, A. et al. Highly diversified shrew hepatitis B viruses corroborate ancient origins and divergent infection patterns of mammalian hepadnaviruses. *Proc. Natl. Acad. Sci. U. S. A.* **116**, 17007–17012. <https://doi.org/10.1073/pnas.1908072116> (2019).

56. de Carvalho Dominguez Souza, B. F. *et al.* A novel hepatitis B virus species discovered in capuchin monkeys sheds new light on the evolution of primate hepadnaviruses. *J. Hepatol.* **68**, 1114–1122, <https://doi.org/10.1016/j.jhep.2018.01.029> (2018).

### Acknowledgements

The authors want to acknowledge Edda Wacker for critical reading of the manuscript and Anita Neubauer for her competent support in carrying out the experiments. We also thank Dr. Gary Grosser for his excellent scientific support regarding the setup of inhibition studies. This study was supported by Flex Funds from the LOEWE-Center DRUID (Novel Drug Targets against Poverty-related and Neglected Tropical Infectious Diseases) and in part by the Deutsche Forschungsgemeinschaft (DFG, German Research Foundation) – Projektnummer 197785619 – SFB 1021 and the Foundation for Research of Natural Resources in Finland, Marjatta ja Eino Kollin Säätiö, and the COST Action CM-0801 (New drugs for neglected diseases).

### Author contributions

M.K., S.F.M., K.A.A.T.L. and J.G. conceived the experiments, M.K., S.F.M. and K.A.A.T.L. performed the experiments, M.K., S.F.M., K.A.A.T.L. and J.G. analyzed and interpreted the results, N.G., F.L. and D.G. provided materials and laboratories for infection studies, S.A. and J.Y.K. provided derivatives of betulin, M.K., S.F.M., K.A.A.T.L. and J.G. wrote the manuscript. All authors reviewed the manuscript.

### Funding

Open Access funding enabled and organized by Projekt DEAL.

### Competing interests

The authors declare no competing interests.

### Additional information

**Correspondence** and requests for materials should be addressed to J.G.

**Reprints and permissions information** is available at [www.nature.com/reprints](http://www.nature.com/reprints).

**Publisher's note** Springer Nature remains neutral with regard to jurisdictional claims in published maps and institutional affiliations.



**Open Access** This article is licensed under a Creative Commons Attribution 4.0 International License, which permits use, sharing, adaptation, distribution and reproduction in any medium or format, as long as you give appropriate credit to the original author(s) and the source, provide a link to the Creative Commons licence, and indicate if changes were made. The images or other third party material in this article are included in the article's Creative Commons licence, unless indicated otherwise in a credit line to the material. If material is not included in the article's Creative Commons licence and your intended use is not permitted by statutory regulation or exceeds the permitted use, you will need to obtain permission directly from the copyright holder. To view a copy of this licence, visit <http://creativecommons.org/licenses/by/4.0/>.

© The Author(s) 2020





## Article

# Hepatitis D Virus Entry Inhibitors Based on Repurposing Intestinal Bile Acid Reabsorption Inhibitors

Michael Kirstgen <sup>1</sup>, Kira Alessandra Alicia Theresa Lowjaga <sup>1</sup>, Simon Franz Müller <sup>1</sup> , Nora Goldmann <sup>2</sup>, Felix Lehmann <sup>2</sup> , Dieter Glebe <sup>2,3</sup>, Karl-Heinz Baringhaus <sup>4</sup> and Joachim Geyer <sup>1,\*</sup>

<sup>1</sup> Institute of Pharmacology and Toxicology, Biomedical Research Center Sellertersberg (BFS), Faculty of Veterinary Medicine, Justus Liebig University Giessen, Schubertstr. 81, 35392 Giessen, Germany; michael.kirstgen@vetmed.uni-giessen.de (M.K.); Kira.A.Lowjaga@vetmed.uni-giessen.de (K.A.A.T.L.); Simon.Mueller@vetmed.uni-giessen.de (S.F.M.)

<sup>2</sup> Institute of Medical Virology, National Reference Center for Hepatitis B Viruses and Hepatitis D Viruses, Justus Liebig University Giessen, 35392 Giessen, Germany; Nora.Goldmann@viro.med.uni-giessen.de (N.G.); Felix.Lehmann@viro.med.uni-giessen.de (F.L.); Dieter.Glebe@viro.med.uni-giessen.de (D.G.)

<sup>3</sup> German Center for Infection Research (DZIF), Giessen-Marburg-Langen Partner Site, 35392 Giessen, Germany

<sup>4</sup> Sanofi-Aventis Deutschland GmbH, 65926 Frankfurt, Germany; Karl-Heinz.Baringhaus@sanofi.com

\* Correspondence: Joachim.M.Geyer@vetmed.uni-giessen.de; Tel.: +49-641-99-38404; Fax: +49-641-99-38409

**Abstract:** Identification of Na<sup>+</sup>/taurocholate co-transporting polypeptide (NTCP) as high-affinity hepatic entry receptor for the Hepatitis B and D viruses (HBV/HDV) opened the field for target-based development of cell-entry inhibitors. However, most of the HBV/HDV entry inhibitors identified so far also interfere with the physiological bile acid transporter function of NTCP. The present study aimed to identify more virus-selective inhibitors of NTCP by screening of 87 propanolamine derivatives from the former development of intestinal bile acid reabsorption inhibitors (BARIs), which interact with the NTCP-homologous intestinal apical sodium-dependent bile acid transporter (ASBT). In NTCP-HEK293 cells, the ability of these compounds to block the HBV/HDV-derived preS1-peptide binding to NTCP (virus receptor function) as well as the taurocholic acid transport via NTCP (bile acid transporter function) were analyzed in parallel. Hits were subsequently validated by performing in vitro HDV infection experiments in NTCP-HepG2 cells. The most potent compounds S985852, A000295231, and S973509 showed in vitro anti-HDV activities with IC<sub>50</sub> values of 15, 40, and 70 μM, respectively, while the taurocholic acid uptake inhibition occurred at much higher IC<sub>50</sub> values of 24, 780, and 490 μM, respectively. In conclusion, repurposing of compounds from the BARI class as novel HBV/HDV entry inhibitors seems possible and even enables certain virus selectivity based on structure-activity relationships.

**Keywords:** HBV; HDV; NTCP; ASBT; bile acid transport; entry inhibitor; structure-activity relationship



**Citation:** Kirstgen, M.; Lowjaga, K.A.A.T.; Müller, S.F.; Goldmann, N.; Lehmann, F.; Glebe, D.; Baringhaus, K.-H.; Geyer, J. Hepatitis D Virus Entry Inhibitors Based on Repurposing Intestinal Bile Acid Reabsorption Inhibitors. *Viruses* **2021**, *13*, 666. <https://doi.org/10.3390/v13040666>

Academic Editor: Delphine M. Muriaux

Received: 4 March 2021

Accepted: 9 April 2021

Published: 12 April 2021

**Publisher's Note:** MDPI stays neutral with regard to jurisdictional claims in published maps and institutional affiliations.



**Copyright:** © 2021 by the authors. Licensee MDPI, Basel, Switzerland. This article is an open access article distributed under the terms and conditions of the Creative Commons Attribution (CC BY) license (<https://creativecommons.org/licenses/by/4.0/>).

## 1. Introduction

Hepatitis B (HBV) and D (HDV) virus infections are the main cause of hepatocellular carcinoma (HCC) and liver cirrhosis as consequences of chronic hepatitis. Available vaccination cannot change that more than 250 million people worldwide currently suffer from HBV/HDV chronic infections, which are associated with more than 800,000 deaths annually [1]. The 3.2 kb comprising genome of the enveloped DNA virus HBV encodes for three envelope proteins, referred to as small (SHBs), middle (MHBs), and large (LHBs) [2]. The myristoylated preS1 domain (myr-preS1<sub>2-48</sub> lipopeptide), constituting the 2-48 N-terminal amino acids of the LHBs, is essential for virus binding to its hepatic receptor [3,4]. As an HBV satellite virus, HDV is coated with the identical HBV envelope proteins. Therefore, HBV and HDV virus binding to hepatocytes shares the identical mechanism [5]. Approximately 5% of all chronic HBV carriers are superinfected with HDV [1]. This results in more rapid disease progression, increased mortality rates, and increased incidence of HCC and

liver cirrhosis [6]. Nucleoside reverse transcriptase inhibitors and interferon are used as a common therapy to keep HBV/HDV associated chronic hepatitis under control. Unfortunately, this therapy rarely leads to cure. Furthermore, interferon therapy is highly prone to adverse drug reactions and nucleoside reverse transcriptase inhibitors have to be given life-long [7,8].

An appropriate drug target to prevent HBV/HDV virus entry into hepatocytes is represented by the Na<sup>+</sup>/taurocholate co-transporting polypeptide NTCP (gene symbol *SLC10A1*). In 2012, NTCP was identified as the bona fide hepatic receptor for HBV/HDV [9,10]. After attachment of the HBV/HDV virus particles to heparan sulfate proteoglycans, the high-affinity binding to NTCP via the virus myr-preS<sub>12-48</sub> lipopeptide is essential for virus entry [11,12]. This myr-preS<sub>12-48</sub> lipopeptide itself has the ability to block HBV/HDV binding to NTCP and infection with inhibitory constants (IC<sub>50</sub>) in the low nanomolar range [4]. Based on this mechanism, the synthetic myr-preS<sub>12-48</sub> lipopeptide analog Hepcludex® (MYR GmbH, Bad Homburg, Germany) was developed and approved as the first-in-class HDV entry inhibitor [13]. This opened the door for the development of further HBV/HDV entry inhibitors, preferably based on small molecules with oral bioavailability and low impact on the physiological bile acid transporter function of NTCP [14]. In a previous study, we could demonstrate that small molecules from the group of pentacyclic triterpenoids show anti-HDV activity *in vitro*. An additional desired effect was a certain selectivity for blocking of the virus receptor function of NTCP, while interference with the physiological bile acid transport function only occurred at very high inhibitor concentrations [15].

In search of further appropriate HBV/HDV entry inhibitor drug candidates, the present study focused on inhibitors of the apical sodium-dependent bile acid transporter (ASBT, gene symbol *SLC10A2*). As an additional member of the solute carrier family SLC10, ASBT represents the intestinal counterpart to NTCP for the maintenance of the enterohepatic circulation of bile acids [14]. ASBT is localized at the apical brush border membrane of ileal enterocytes and here is essential for the reabsorption of bile acids from the intestinal lumen [16]. Several inhibitors of ASBT have been developed and approved as bile acid reabsorption inhibitors (BARIs), including elobixibat, odeixibat, linerixibat, volixibat, and maralixibat. These drugs prevent bile acid reabsorption from the gut, reduce bile acid reflux to the liver and increase the hepatic de novo bile acid synthesis from cholesterol. In the end, this has an LDL cholesterol-lowering effect [17]. The present study aimed to repurpose BARIs as novel HBV/HDV entry inhibitors based on the close phylogenetic relationship and functional homology of ASBT and NTCP [18]. Therefore, 87 compounds from the BARI chemical class of propanolamines were screened for blocking of the virus receptor and bile acid transporter functions of NTCP. We could show structure-activity relationships (SAR) for some of the compounds regarding efficient blocking of myr-preS<sub>12-48</sub> lipopeptide binding to NTCP. Some compounds even showed certain virus-selectivity and blocked the physiological bile acid transport function only at very high inhibitor concentrations. Based on the results of the present study, repurposing of compounds from the BARI class as novel HBV/HDV entry inhibitors seems possible and even enables certain virus selectivity based on SAR.

## 2. Materials and Methods

### 2.1. NTCP-Expressing Cell Lines

Human embryonic kidney (HEK293) cells were stably transfected with human NTCP, C-terminally tagged with the FLAG epitope (further referred to as NTCP-HEK293 cells) as reported before [19]. Cells were maintained at 37 °C, 5% CO<sub>2</sub>, and 95% humidity in DMEM/F-12 medium (Thermo Fisher Scientific, Waltham, MA, USA) supplemented with 10% fetal calf serum (Sigma-Aldrich, St. Louis, MO, USA), 4 mM L-glutamine (PAA, Cölbe, Germany) and penicillin/streptomycin (PAA). HepG2 cells stably transfected with NTCP-FLAG (further referred to as NTCP-HepG2 [10]) were cultured under the same conditions in DMEM with all supplements listed above, except for L-glutamine. For induction of the transgene, the medium was supplemented with 1 µg/mL tetracycline (Roth, Karlsruhe,

Germany) in the case of the NTCP-HEK293 cells or with 2 µg/mL doxycycline (Sigma-Aldrich) in the case of the NTCP-HepG2 cells.

### 2.2. Inhibitory Concentrations (IC<sub>50</sub>) for [<sup>3</sup>H]preS1 Binding and [<sup>3</sup>H]Taurocholic Acid Transport

Bile acid transport measurements were performed in NTCP-HEK293 cells as described [15]. Briefly, [<sup>3</sup>H]taurocholic acid, further referred to as [<sup>3</sup>H]TC, (20 Ci/mmol, 0.09 mCi/mL, Perkin Elmer, Waltham, MA, USA) was used as substrate. In parallel, [<sup>3</sup>H]preS1 peptide binding experiments were performed with a tritium-labelled myr-preS1<sub>2-48</sub> lipopeptide-HBV subgenotype D3- that was purchased from Pharmaron (120 Ci/mmol, 1 mCi/mL, Cardiff, UK). Cells were seeded onto polylysine-coated 96-well plates, induced with 1 µg tetracycline per ml, and grown to confluence over 72 h at 37 °C. Then, cells were washed once with tempered phosphate buffered saline (PBS, 137 mM NaCl, 2.7 mM KCl, 1.5 mM KH<sub>2</sub>PO<sub>4</sub>, 7.3 mM Na<sub>2</sub>HPO<sub>4</sub>, pH 7.4) at 37 °C, and pre-incubated with 80 µL DMEM for 5 min at 37 °C. The medium was replaced by 80 µL DMEM containing the respective inhibitor (concentrations ranging from 0.1 to 1000 µM) or solvent alone (100% uptake/binding control), and cells were further incubated for 5 min at 37 °C. After pre-incubation, bile acid transport experiments were started by adding 20 µL DMEM containing 5 µM [<sup>3</sup>H] TC (final concentration: 1 µM). Binding of [<sup>3</sup>H]preS1 was initiated by adding 20 µL DMEM containing 25 nM [<sup>3</sup>H]preS1 (final concentration: 5 nM). Experiments were stopped after 10 min by two-times washing with ice-cold PBS. For 0% uptake/binding control, the NTCP-HEK293 cells were not induced with tetracycline (-tet). Cell-associated radioactivity of [<sup>3</sup>H]TC or [<sup>3</sup>H]preS1 was quantified by liquid scintillation counting in a Packard Microplate Scintillation Counter TopCount NXT (Packard Instrument Company, Meriden, CT, USA). Transport rates and [<sup>3</sup>H]preS1 binding were determined in counts per minute (cpm). The mean of the 0% control was subtracted and the net [<sup>3</sup>H]TC transport rates and net [<sup>3</sup>H]preS1 binding rates, respectively, were expressed as percentage of control. A set of 87 test compounds was provided by Sanofi-Aventis Deutschland GmbH (Frankfurt, Germany). IC<sub>50</sub> values were calculated from quadruplicate determinations by GraphPad Prism 6 (GraphPad, San Diego, CA, USA).

### 2.3. HDV Infection Experiments

HDV production was done in vitro as described before [20,21]. RT-qPCR was performed to determine genome equivalents. NTCP-HepG2 cells were pre-incubated for 5 min with inhibitors solved in 80 µL HGM per well in concentrations ranging from 5 µM to 300 µM. Infection experiments were performed in NTCP-HepG2 cells as described [15]. Briefly, during infection, cells were cultured in 96-well plates in Hepatocyte Growth Medium (HGM) consisting of William's E Medium (Thermo Fisher Scientific) containing 2% bovine serum albumin (BSA, Roth), 2 mM L-glutamine (Thermo Fisher Scientific), 100 µg/mL gentamicin (Thermo Fisher Scientific), 10 nM dexamethasone (Sigma-Aldrich), 1 mM sodium pyruvate (Thermo Fisher Scientific), 1 × Insulin-Transferrin-Selen (Thermo Fisher Scientific), 2% DMSO (Merck, Darmstadt, Germany), 4% polyethylene glycol (Sigma-Aldrich), and 2 µg/mL doxycycline (Sigma-Aldrich). HDV stock solved in 20 µL HGM per well was added for infection and cells were incubated for 6 h with a final concentration of 120 genome equivalents/cell of HDV particles. Subsequently, cells were washed with DMEM and cultured in HGM supplemented with 2% DMSO, 2% BSA and 2 µg/mL doxycycline. Every three days, medium was changed until cells were fixed at 9 days post infection with 3% paraformaldehyde (Sigma-Aldrich) in PBS, for 30 min at room temperature (RT). Cells were permeabilized with 0.2% Triton X 100 (Roth) in PBS for 30 min at RT, and blocked by incubation with 5% bovine serum albumin (Roth) in PBS for 30 min at RT. Then, cells were immunostained with purified human anti-HDV-positive serum at 37 °C for 1 h (1:400 dilution). Goat anti-human IgG secondary antibody coupled to Alexa Fluor fluorophore (1:400 dilution, Thermo Fisher Scientific) was added for 1 h at 37 °C for detection of Hepatitis Delta antigen (HDAG) as described before [22]. Nuclei were stained with Hoechst 33342 (1 µg/mL, Thermo Fisher Scientific).

#### 2.4. Cytotoxicity Assay

In Vitro Toxicology Assay Kit (Sigma-Aldrich) was used to perform a 3-[4,5-dimethylthiazole-2-yl]-2,5-diphenyltetrazolium bromide (MTT) assay to measure the cytotoxicity of the indicated compounds according to the manufacturer's protocol. Briefly, NTCP-HepG2 cells were incubated with 100  $\mu$ L of the indicated concentrations of the respective compound solved in HGM over 6 h at 37 °C. After 6 h, medium was replaced by inhibitor-free HGM and cells were cultured for additional 24 h. Then, medium was removed and 100  $\mu$ L DMEM containing 0.5 mg/mL MTT were added and cells were incubated for 1 h at 37 °C. Finally, the medium was replaced by 100  $\mu$ L isopropyl alcohol (Sigma-Aldrich) and samples were measured by ELISA reader (GloMax-Multi Detection System, Promega, Madison, WI, USA).

#### 2.5. Structure Modeling

The 2D compound structures were generated from an SDfile, associated to the tested compounds and provided by Sanofi-Aventis Deutschland GmbH, using the MAESTRO 12.2 Molecular Modeling Interface of SCHRÖDINGER, Inc. (New York City, NY, USA).

#### 2.6. Statistics

Determination of IC<sub>50</sub> values was done by nonlinear regression analysis using the equation log(inhibitor) vs. response settings of the GraphPad Prism 6.0 software (GraphPad). Data of bile acid transport and myr-preS1<sub>2-48</sub> lipopeptide binding are expressed as means  $\pm$  SD from quadruplicate determinations. IC<sub>50</sub> values are listed with their 95% confidence intervals in Table 1. In addition, mean IC<sub>50</sub> values were calculated for each experiment. Cytotoxicity studies represent data from two independent experiments, each with quadruplicate determinations. Statistical analysis was done by one-way ANOVA, followed by Dunnett's multiple comparison test by GraphPad Prism 6.0, considering  $p < 0.01$  as statistically significant. Infection studies show data from three independent experiments, each with triplicate determinations represented as means  $\pm$  SEM. Statistical analyses of the HDV infection experiments were performed by two-way ANOVA, followed by Dunnett's multiple comparison test by GraphPad Prism 6.0, considering  $p < 0.01$  as statistically significant.

**Table 1.** The indicated compounds were analyzed for [<sup>3</sup>H]TC transport inhibition and [<sup>3</sup>H]preS1 binding inhibition in NTCP-HEK293 cells. IC<sub>50</sub> values were calculated from a range of five inhibitor concentrations (0.1–1000  $\mu$ M) and they are listed with their 95% confidence intervals. Selectivity indices for [<sup>3</sup>H]TC transport inhibition/[<sup>3</sup>H]preS1 binding inhibition were calculated from the IC<sub>50</sub> means. The higher this index, the more selective the respective inhibitor. Selected compounds were additionally tested for in vitro HDV infection in NTCP-HepG2 cells.

Compound	IC <sub>50</sub> ([ <sup>3</sup> H]TC Uptake) [ $\mu$ M] <sup>a</sup>	IC <sub>50</sub> ([ <sup>3</sup> H]preS1 Binding) [ $\mu$ M] <sup>b</sup>	Selectivity Index <sup>c</sup>	In Vitro HDV Infection <sup>d</sup>
S985852	13 to 34	8 to 24	2	IC <sub>50</sub> ~ 15 $\mu$ M
A000028897	16 to 62	3 to 24	3	toxic
A000295480	145 to 1323	32 to 297	4	ND
S973515	413 to 1238	39 to 148	9	ND
A000289041	>1000	35 to 224	18	ND
S973509	202 to 775	3 to 10	53	IC <sub>50</sub> ~ 70 $\mu$ M
A000295231	341 to 1221	4 to 29	65	IC <sub>50</sub> ~ 40 $\mu$ M
A000295013	>1000	73 to 194	313	ND

<sup>a</sup> Inhibition of 1  $\mu$ M [<sup>3</sup>H]TC uptake; <sup>b</sup> inhibition of 5 nM [<sup>3</sup>H]preS1 binding; <sup>c</sup> calculated from mean IC<sub>50</sub> TC:preS1; <sup>d</sup> see also Figures 4 and 5; ND, not determined.

### 3. Results

For inhibition of myr-preS1<sub>2-48</sub> lipopeptide binding to NTCP, 87 propanolamine derivatives were used as potential inhibitors. These derived from a previous development of ASBT-inhibiting BARIs at Sanofi-Aventis Deutschland GmbH. In a first step, all compounds

were used at 100  $\mu\text{M}$  inhibitory concentration in transport / binding assays with 1  $\mu\text{M}$  [ $^3\text{H}$ ]TC / 5 nM [ $^3\text{H}$ ]preS1 (Figure 1). The best performing compounds from this pre-screen were defined as those with <50% remaining [ $^3\text{H}$ ]preS1 binding in the presence of inhibitor compared to untreated control. In total, eight compounds fulfilled this condition (red dots in Figure 1). All of them are structurally presented in Figure 2.

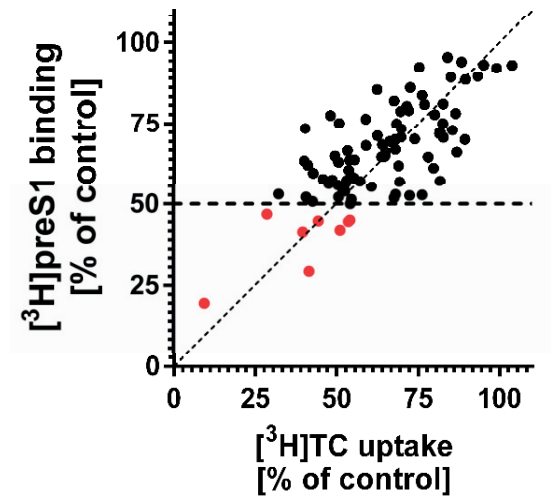


**Figure 1.** Inhibitory potency of 87 propanolamine derivatives on [ $^3\text{H}$ ]TC uptake via NTCP and [ $^3\text{H}$ ]preS1 lipopeptide binding to NTCP. NTCP-HEK293 cells were seeded onto 96-well plates and were incubated with tetracycline to induce expression of NTCP. Experiments were performed in the presence of 100  $\mu\text{M}$  inhibitor to block uptake of 1  $\mu\text{M}$  [ $^3\text{H}$ ]TC (shown at the x-axis) and binding of 5 nM [ $^3\text{H}$ ]preS1 (shown at the y-axis) over 10 min at 37  $^{\circ}\text{C}$ . Control experiments were performed with solvent alone (set to 100%). Red dots represent the compounds S985852, A000028897, A000295480, S973515, A000289041, S973509, A000295231, and A000295013, which showed <50% remaining [ $^3\text{H}$ ]preS1 binding compared to untreated control. Bisector is illustrated as dashed line. Compounds below the bisector line represent superior inhibitors of [ $^3\text{H}$ ]preS1 lipopeptide binding compared to [ $^3\text{H}$ ]TC uptake inhibition.

For these eight compounds, detailed inhibitory assays were performed with inhibitor concentrations ranging from 0.1  $\mu\text{M}$  to 1000  $\mu\text{M}$ , in order to determine  $\text{IC}_{50}$  values for inhibition of 1  $\mu\text{M}$  [ $^3\text{H}$ ]TC transport via NTCP and 5 nM [ $^3\text{H}$ ]preS1 binding to NTCP (Figure 3). Resulting  $\text{IC}_{50}$  values are listed as 95% confidence intervals in Table 1. As an additional variable for interpretation of the inhibitory pattern of the compounds, a selectivity index was implemented. This index is the non-dimensional quotient from the  $\text{IC}_{50}$  values for [ $^3\text{H}$ ]TC uptake and [ $^3\text{H}$ ]preS1 binding inhibition and describes the degree of virus/preS1 selectivity. In this case, the myr-preS1<sub>2-48</sub> lipopeptide binding represents a surrogate for HBV/HDV binding to NTCP. The higher the selectivity index, the higher the inhibitory impact on myr-preS1<sub>2-48</sub> lipopeptide binding of the tested compound compared to the inhibitory impact on taurocholic acid uptake.

The  $\text{IC}_{50}$  values for [ $^3\text{H}$ ]TC transport inhibition ranged from 21 up to >1000  $\mu\text{M}$  and the  $\text{IC}_{50}$  values for [ $^3\text{H}$ ]preS1 peptide inhibition ranged from 14 up to 119  $\mu\text{M}$ , but without any significant correlation, indicating that both functions of NTCP are differently addressed by these propanolamine inhibitors. Interestingly, the compounds significantly

differed in their virus/preS1 selectivity. While three compounds (S985852, A000295480, and A000028897) were more or less non-selective, others were more selective for preS1-peptide inhibition, being S973509, A000295231, and A000295013, with selectivity indices of 53, 65, 313, respectively (Figure 3, Table 1). However, the selectivity index of 313 for compound A000295013 must not be overestimated. This high index is the result of an undeterminable  $IC_{50}$  value for  $[^3H]TC$  uptake inhibition ( $IC_{50} > 1000 \mu M$ ) in combination with a quite low activity against  $[^3H]preS1$ -peptide binding with  $IC_{50}$  of approximately  $130 \mu M$ . Consequently, this compound represents a potentially selective but not potent inhibitor of myr-preS1<sub>2-48</sub> lipopeptide binding. Furthermore, the observed  $IC_{50}$  values of the compounds A000295480, S973515, and A000289041 for  $[^3H]preS1$  binding inhibition were relatively high, what made these compounds less attractive for further investigation.

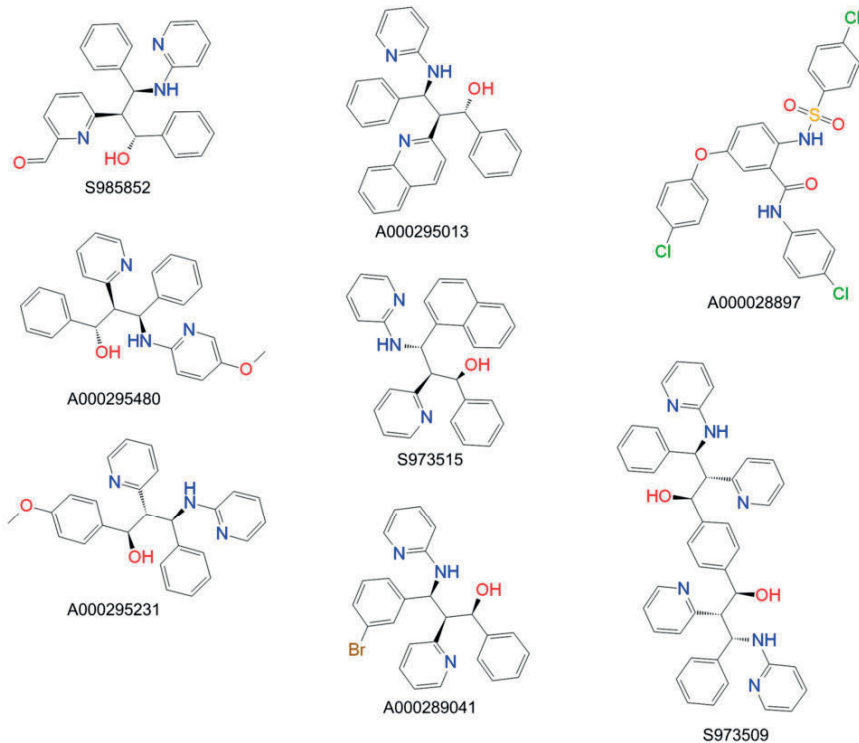


**Figure 2.** Structures of the eight most potent propanolamine  $[^3H]preS1$  lipopeptide binding inhibitors (see Figure 1).

Based on this, for subsequent *in vitro* infection studies, we selected compounds S985852 and A000028897 as potent but non-selective inhibitors as well as compounds S973509 and A000295231 as potent and selective inhibitors of viral preS1-binding to NTCP. Next, cytotoxicity of these compounds on NTCP-overexpressing HepG2 cells, being the model cell line for *in vitro* HDV infection experiments, was analyzed at low ( $5 \mu M$ ), middle ( $50 \mu M$ ), and high ( $300 \mu M$ ) inhibitor concentrations. Corresponding to the time-schedule for *in vitro* HDV infection, these cytotoxicity assays were performed for a 6 h time span of compound incubation (Figure 4).

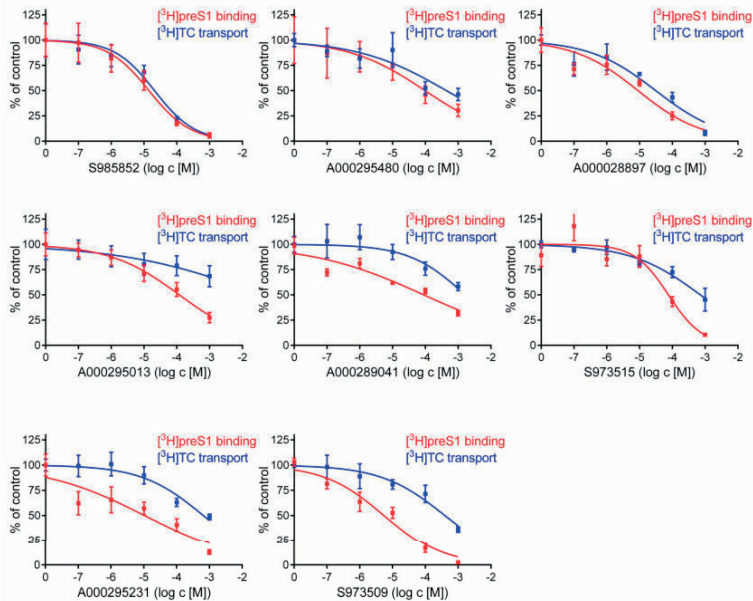


**Figure 3.** Inhibition of  $[^3\text{H}]$ preS1 peptide binding to NTCP and  $[^3\text{H}]$ JTC transport via NTCP at increasing concentrations of propanolamine derivatives. NTCP-HEK293 cells were seeded onto 96-well plates and were incubated with tetracycline to induce expression of NTCP. Cells without tetracycline treatment were used as 0% controls for both assays. Bile acid transport experiments were performed with  $1\ \mu\text{M}$   $[^3\text{H}]$ JTC and binding experiments were performed with  $5\ \text{nM}$   $[^3\text{H}]$ preS1. Both assays were performed over 10 min at  $37\ ^\circ\text{C}$  with increasing concentrations of the indicated inhibitors. Control experiments were performed with solvent alone (set to 100%). The mean of the 0% control was subtracted to calculate net  $[^3\text{H}]$ JTC transport rates (shown in blue) as well as net  $[^3\text{H}]$ preS1 binding rates (shown in red), which are expressed as % of control at the y-axis. Half-maximal inhibitory concentrations ( $\text{IC}_{50}$ ) were calculated by nonlinear regression analysis using the equation  $\log(\text{inhibitor})$  vs. response (GraphPad Prism). Data represent means  $\pm$  SD of quadruplicate determinations of representative experiments.

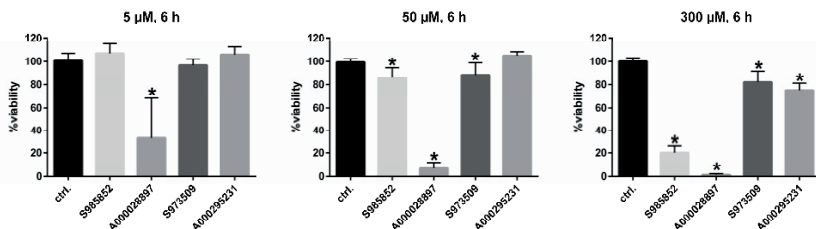


**Figure 4.** Cytotoxicity studies in NTCP-HepG2 cells. An MTT cytotoxicity assay was performed with the indicated propanolamine derivatives at  $5\ \mu\text{M}$ ,  $50\ \mu\text{M}$ , and  $300\ \mu\text{M}$  inhibitor concentrations, incubated over a time span of 6 h at  $37\ ^\circ\text{C}$ . Solvent control was set to 100%. Data represent means  $\pm$  SD of two independent experiments, each with quadruplicate determinations ( $n = 8$ ). \* Significantly different to control with  $p < 0.01$ .

As indicated in Figure 4, compound A000028897 was excluded at this point due to obvious cytotoxicity even at low (5  $\mu$ M) concentrations. All other compounds did not show strong cytotoxic effects at concentrations of 5 and 50  $\mu$ M. However, compound S985852 showed critical cytotoxicity at 300  $\mu$ M, which is way above the determined  $IC_{50}$  value for [ $^3$ H]preS1 binding inhibition (being 8–24  $\mu$ M), so this compound was not excluded for infection experiments.

The remaining three compounds were tested for their potency to block in vitro HDV infection of NTCP-overexpressing HepG2 cells. Compounds S985852, S973509, and A000295231 showed a significant concentration-dependent inhibition of in vitro HDV infection (Figure 5), thereby confirming the pre-screen with the myr-preS1<sub>2-48</sub> lipopeptide (Figure 3). Of note, the  $IC_{50}$  values for [ $^3$ H]preS1 peptide inhibition and in vitro HDV infection inhibition were within the same range. In particular, compound S985852 yielded identical  $IC_{50}$  values of approximately 15  $\mu$ M for both, the [ $^3$ H]preS1 binding assay and the HDV infection experiments. The respective  $IC_{50}$  values of compound S973509 differed by a factor of ten. The pre-screen delivered an  $IC_{50}$  of 7  $\mu$ M, whereas infection studies yielded an  $IC_{50}$  of 70  $\mu$ M. For compound A000295231,  $IC_{50}$  values were 17  $\mu$ M for the [ $^3$ H]preS1 pre-screen and 40  $\mu$ M for the infection studies.

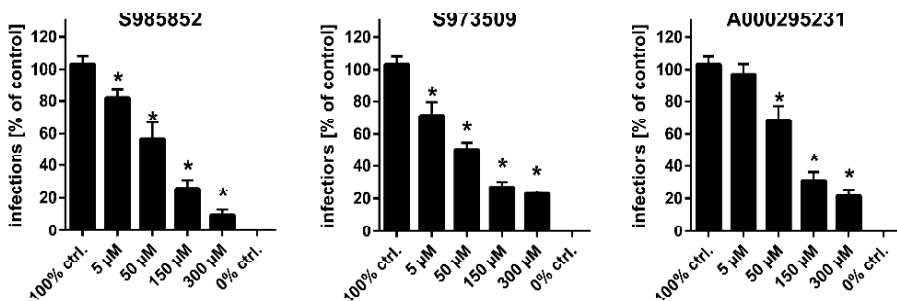


**Figure 5.** HDV infection studies. NTCP-HepG2 cells were pre-incubated for 5 min with the indicated concentrations of the indicated inhibitors in DMEM at 37 °C. Then, cells were additionally inoculated with 120 genome equivalents/cell of HDV particles at 37 °C. After 6 h, cells were washed and further incubated with inhibitor- and virus-free medium, and medium was changed every 3–4 days. At day 9 post infection, cells were fixed and an immunostaining against the HDAG was performed, as a marker of HDV infection. The number of infected cells per well was determined by fluorescence microscopy. NTCP-HepG2 cells incubated without inhibitor were used as control (set to 100% infection rate). Infection experiments in the presence of 0.5  $\mu$ M myr-preS1<sub>2-48</sub> lipopeptide served as 0% control (representing 0% infection rate). Data represent means  $\pm$  SEM of three independent experiments, each with triplicate determinations ( $n = 9$ ). \* Significantly different to 100% control with  $p < 0.01$ .

Finally, we closely analyzed structure-activity relationships (SAR) of selected propanolamine derivatives that can be used for further activity and selectivity optimization (Figure 6). Starting from the inactive propanolamine compound A000295238, isomerization and substitution of C<sub>3</sub> by nitrogen (compound S957291) significantly increased the inhibitory potency for [ $^3$ H]ITC uptake and [ $^3$ H]preS1 binding inhibition. Additional OCH<sub>3</sub> coupling at C<sub>27</sub> (compound A000295231) even further improved the inhibitory potency. This compound showed an  $IC_{50}$  of ~40  $\mu$ M for in vitro HDV infection inhibition and selectivity index of 65. Therefore, A000295231 represents the most promising compound of the present study. In contrast, addition of an amino group at the same C<sub>27</sub> position (compound A000295724) made this compound inactive. The same was true for N-substitution of compound S957291 at position C<sub>28</sub>, resulting in compound S958009. However, coupling of an OH-group or OCH<sub>3</sub>-group at C<sub>28</sub> (compounds A000296584 and S963601, respectively) resulted in significant, but less active inhibitors of



[<sup>3</sup>H]preS1 lipopeptide binding. These compounds were not analyzed more in detail in the present study.

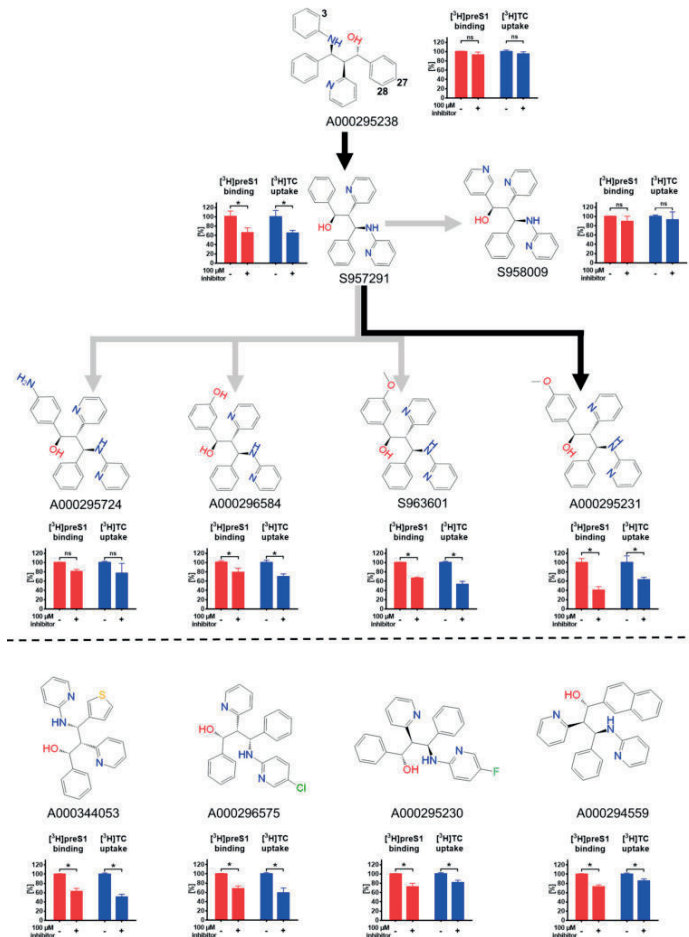


**Figure 6.** Structure-activity relationships of propanolamine derivatives for [<sup>3</sup>H]JTC transport inhibition and [<sup>3</sup>H]preS1 binding inhibition. The respective inhibition pattern are illustrated by bar graphs for [<sup>3</sup>H]JTC uptake (shown in blue) and [<sup>3</sup>H]preS1 peptide binding (shown in red) in the presence (+) or absence (−) of a 100 μM inhibitor concentration of the respective propanolamine derivative. Graphs show means ± SD of triplicate determinations. \* Significantly different with *p* < 0.01 (two-way ANOVA with Sidak's multiple comparison test); ns, not significant. Chemical modifications and isomerization of the propanolamine derivatives revealed clear structure-activity relationships for more potent [<sup>3</sup>H]preS1 lipopeptide binding inhibition (A000295231 > S957291 > A000295238). Several propanolamine derivatives showed significant but less potent [<sup>3</sup>H]preS1 lipopeptide binding inhibition. Four representative compounds (A000344053, A000296575, A000295230, A000294559) are shown.

Figure 6 shows the structures of four additional propranolamine inhibitors of the [<sup>3</sup>H]preS1 lipopeptide binding to NTCP. These compounds are characterized by substitutions of a benzyl group by thiophenyl (compound A000344053) or naphthyl groups (compound A000294559) and by Cl (compound A000296575) or F addition (compound A000295230). However, as none of these compounds showed >50% inhibition of [<sup>3</sup>H]preS1 peptide binding, they were not analyzed more in detail in the present study. Taken together, these SAR data clearly indicate that propranolamine derivatives can be modified towards more selective bile acid transport inhibition and towards more potent myr-preS1<sub>2-48</sub> lipopeptide binding inhibition.

#### 4. Discussion

The numbers from the global hepatitis report and the fact that to date only one single approved HDV entry inhibitor (bulevirtide, Hepcludex<sup>®</sup>) is available underline the need of more therapeutics against this serious disease [1,4]. Many recent studies focused on NTCP inhibition in order to prevent virus entry into hepatocytes, using cyclosporine A and other cyclosporine derivatives [23–26], ezetimibe [10], irbesartan [27], ritonavir [28], (-)-epigallocatechin-3-gallate [29], vanitaracin A [30], Ro41-5253 [31], proanthocyanidin [32], zafirlukast [33], sulfasalazine [33], and Chicago Sky Blue 6B (an azo dye) [33]. Most of these inhibitors represent non-selective inhibitors of NTCP that are prone to increase serum bile acids and to interfere with the bile acid homeostasis [34]. However, there are some hints that both functions of NTCP, the virus receptor function and the bile acid transporter function, can separately be addressed with inhibitors that are more selective [15,25].

In a previous study, we demonstrated that amino acid G158 of the human NTCP is essential for myr-preS1<sub>2-48</sub> lipopeptide binding to NTCP and in vitro HBV and HDV infection. This amino acid is located at a domain (amino acids 157–165) that was shown before to be important for myr-preS1<sub>2-48</sub> lipopeptide binding to human NTCP [9,35]. Consequently, G158R NTCP mutants were insusceptible for in vitro HBV/HDV infection, but still transported bile acids. It was hypothesized that the larger amino acid side chain of arginine compared to glycine might sterically preclude myr-preS1<sub>2-48</sub> lipopeptide binding, while bile acids can still bind to their binding pocket [22].

In addition, we recently identified small molecules from the group of pentacyclic triterpenoids to be potent HDV entry inhibitors with less effect on the bile acid transport function of NTCP [15]. Likewise, Shimura et al. [25] showed for the cyclosporine derivative SCY995 higher potency against in vitro HBV infection than for bile acid transport inhibition. These findings illustrate the possibility to develop entry inhibitors with oral bioavailability that do not strongly interfere with the physiological bile acid transport function of NTCP.

A common approach for identification of novel active compounds against a given therapeutic target is high-throughput screening (HTS). This technique can rapidly generate data of large subsets of molecules using automated experimental assays [36]. However, hit rates of HTS are quite low (0.01%–0.1%), generating immense drug discovery costs [37,38]. The approach of the presented study was therefore more targeted. We considered that inhibitors of other bile acid transporters, especially the intestinal bile acid transporter ASBT, might also be good inhibitors of NTCP and, thereby potential HDV entry inhibitors. In fact, we identified 3 out of 87 propranolamine derivatives (S985852, S973509, A000295231) to be active against in vitro HDV infection. These propranolamine compounds were previously used to optimize the activity of this compound class against ASBT. Of note, two of the compounds (S973509, A000295231) showed even some selectivity towards the virus receptor function of NTCP and interfered with the physiological bile acid transport function of NTCP only at very high inhibitor concentrations. Overall, this represents a hit rate of approximately 3% at this small sample size, which can be described as excellent enrichment compared to classical HTS.

In addition, it can be emphasized that our screening approach, using [<sup>3</sup>H]preS1 binding inhibition as a surrogate for HDV binding inhibition, represents an advantageous tool for identification of new entry inhibitors. Especially, compound S985852 showed

identical IC<sub>50</sub> values for both assays. This clearly demonstrates the predictivity of the [<sup>3</sup>H]preS1 lipopeptide binding assay, but nevertheless, data from the [<sup>3</sup>H]preS1 binding experiments have to be verified by direct infection experiments. Although HBV and HDV share the identical surface proteins and the same mechanism of interaction with NTCP via the myr-preS1<sub>2-48</sub> lipopeptide [5], future studies should confirm that also HBV entry is inhibited upon treatment with the inhibitors presented in this study. In addition, it would be interesting to study the efficacy of virus entry inhibition in an HBV/HDV coinfection setting.

The use of compounds known to interact with ASBT could provide further advantages for the development of NTCP inhibitors. If an NTCP inhibitor would be transported from the intestinal lumen via ASBT as a substrate, this would increase intestinal absorption and would result in high inhibitor concentrations in the portal blood. Consequently, inhibitor concentrations at the site of NTCP expression at the basolateral membrane of hepatocytes would be relatively high. In theory, when an inhibitor would be a substrate of both carriers, NTCP and ASBT, this would even enable enterohepatic circulation similar to the physiological cycling of bile acids between liver and gut. Based on this, it would be worth analyzing if the identified NTCP inhibitors from the propanolamine class are also substrates of ASBT and/or NTCP. However, it must be considered that inhibition of ASBT also interferes with the reabsorption of bile acids from the intestinal lumen. This could lead to typical side effects of BARIs, being diarrhea, steatorrhea, and abdominal pain [17].

The structure-activity relationships demonstrated in the present study for propanolamine derivatives make clear that even slight chemical modifications of these molecules were decisive for their inhibitory potential and selectivity to interact with the virus receptor function of NTCP. Interestingly, only few structural differences occur between active and inactive compounds as well as between selective and non-selective inhibitors (see Figure 6). Even more interesting, the study demonstrates that molecules, originally designed as ASBT inhibitors, show cross-reactivity with the closely related NTCP carrier and this cross-reactivity can be used in a positive way to discover potential drug candidates for HBV/HDV entry inhibition. Further studies should now investigate the mode of action of selected candidates (competitive vs. non-competitive inhibition; reversible vs. irreversible inhibition; substrate vs. non-substrate inhibitor) and should be extended to all relevant HDV and HBV genotypes. In addition, the effect of these compounds on other liver-associated transport proteins, such as members of the organic anion transporting polypeptide (OATP) family should be considered. Upon successful completion of these studies, an appropriate *in vivo* model could be used to investigate the *in vivo* efficacy of the propanolamine NTCP inhibitors.

In conclusion, repurposing of compounds from the BARIs class as novel HDV entry inhibitors seems possible and even enables certain virus selectivity based on structure-activity relationships.

**Author Contributions:** M.K., S.F.M., K.A.A.T.L. and J.G. conceived the experiments, M.K., S.F.M. and K.A.A.T.L. performed the experiments, M.K., S.F.M., K.A.A.T.L. and J.G. analyzed and interpreted the results, N.G., F.L. and D.G. provided materials and laboratories for infection studies, K.-H.B. provided the test compounds, M.K. and J.G. wrote the manuscript. All authors have read and agreed to the published version of the manuscript.

**Funding:** This study was supported by Flex Funds from the LOEWE-Center DRUID (Novel Drug Targets against Poverty-related and Neglected Tropical Infectious Diseases) and in part by the Deutsche Forschungsgemeinschaft (DFG, German Research Foundation)—Projektnummer 197785619—SFB 1021.

**Institutional Review Board Statement:** Not applicable.

**Informed Consent Statement:** Not applicable.

**Data Availability Statement:** Obtained and analyzed data of this study are available from the corresponding author on request. Compounds are accessible on the basis of a material transfer agreement (MTA) and upon availability in the compound collection.

**Conflicts of Interest:** The authors declare no conflict of interest.





## References

1. World Health Organization. *Global Hepatitis Report 2017*; Licence: CC BY-NC-SA 3.0 IGO; World Health Organization: Geneva, Switzerland, 2017.
2. Glebe, D.; Bremer, C.M. The molecular virology of hepatitis B virus. *Semin. Liver. Dis.* **2013**, *33*, 103–112. [[CrossRef](#)]
3. Glebe, D.; Urban, S.; Knoop, E.V.; Cag, N.; Krass, P.; Grün, S.; Bulavaite, A.; Sasnauskas, K.; Gerlich, W.H. Mapping of the hepatitis B virus attachment site by use of infection-inhibiting preS1 lipopeptides and tupaia hepatocytes. *Gastroenterology* **2005**, *129*, 234–245. [[CrossRef](#)] [[PubMed](#)]
4. Gripon, P.; Cannie, I.; Urban, S. Efficient inhibition of hepatitis B virus infection by acylated peptides derived from the large viral surface protein. *J. Virol.* **2005**, *79*, 1613–1622. [[CrossRef](#)] [[PubMed](#)]
5. Hughes, S.A.; Wedemeyer, H.; Harrison, P.M. Hepatitis delta virus. *Lancet* **2011**, *378*, 73–85. [[CrossRef](#)]
6. Sureau, C.; Negro, F. The hepatitis delta virus: Replication and pathogenesis. *J. Hepatol.* **2016**, *64*, S102–S116. [[CrossRef](#)]
7. Martinez, M.G.; Villeret, F.; Testoni, B.; Zoulim, F. Can we cure hepatitis B virus with novel direct-acting antivirals? *Liver Int.* **2020**, *40* (Suppl. 1), 27–34. [[CrossRef](#)]
8. World Health Organization. *Guidelines for the Prevention, Care and Treatment of Persons with Chronic Hepatitis B Infection*; World Health Organization: Geneva, Switzerland, 2015.
9. Yan, H.; Zhong, G.; Xu, G.; He, W.; Jing, Z.; Gao, Z.; Huang, Y.; Qi, Y.; Peng, B.; Wang, H.; et al. Sodium taurocholate cotransporting polypeptide is a functional receptor for human hepatitis B and D virus. *eLife* **2012**, *1*. [[CrossRef](#)] [[PubMed](#)]
10. König, A.; Döring, B.; Mohr, C.; Geipel, A.; Geyer, J.; Glebe, D. Kinetics of the bile acid transporter and hepatitis B virus receptor Na<sup>+</sup>/taurocholate cotransporting polypeptide (NTCP) in hepatocytes. *J. Hepatol.* **2014**, *61*, 867–875. [[CrossRef](#)] [[PubMed](#)]
11. Lamas Longarela, O.; Schmidt, T.T.; Schöneweis, K.; Romeo, R.; Wedemeyer, H.; Urban, S.; Schulze, A. Proteoglycans act as cellular hepatitis delta virus attachment receptors. *PLoS ONE* **2013**, *8*, e58340. [[CrossRef](#)]
12. Fukano, K.; Tsukuda, S.; Watashi, K.; Wakita, T. Concept of Viral Inhibitors via NTCP. *Semin. Liver Dis.* **2019**, *39*, 78–85. [[CrossRef](#)]
13. MYR Pharmaceuticals. 2020. Available online: <http://myr-pharma.com/> (accessed on 24 February 2021).
14. Geyer, J.; Wilke, T.; Petzinger, E. The solute carrier family SLC10: More than a family of bile acid transporters regarding function and phylogenetic relationships. *Arch. Pharmacol.* **2006**, *372*, 413–431. [[CrossRef](#)] [[PubMed](#)]
15. Kirstgen, M.; Lowjaga, K.A.A.T.; Müller, S.F.; Goldmann, N.; Lehmann, F.; Alakurtti, S.; Yli-Kauhaluoma, J.; Glebe, D.; Geyer, J. Selective hepatitis B and D virus entry inhibitors from the group of pentacyclic lupane-type betulin-derived triterpenoids. *Sci. Rep.* **2020**, *10*, 21772. [[CrossRef](#)] [[PubMed](#)]
16. Xiao, L.; Pan, G. An important intestinal transporter that regulates the enterohepatic circulation of bile acids and cholesterol homeostasis: The apical sodium-dependent bile acid transporter (SLC10A2/ASBT). *Clin. Res. Hepatol. Gastroenterol.* **2017**, *41*, 509–515. [[CrossRef](#)] [[PubMed](#)]
17. Kramer, W.; Glombik, H. Bile acid reabsorption inhibitors (BARI): Novel hypolipidemic drugs. *Curr. Med. Chem.* **2006**, *13*, 997–1016. [[CrossRef](#)] [[PubMed](#)]
18. Dawson, P.A.; Oelkers, P. Bile acid transporters. *Curr. Opin. Lipidol.* **1995**, *6*, 109–114. [[CrossRef](#)] [[PubMed](#)]
19. Geyer, J.; Döring, B.; Meerkamp, K.; Ugele, B.; Bakhiya, N.; Fernandes, C.F.; Godoy, J.R.; Glatt, H.; Petzinger, E. Cloning and functional characterization of human sodium-dependent organic anion transporter (SLC10A6). *J. Biol. Chem.* **2007**, *282*, 19728–19741. [[CrossRef](#)] [[PubMed](#)]
20. Rasche, A.; Lehmann, F.; König, A.; Goldmann, N.; Corman, V.M.; Moreira-Soto, A.; Geipel, A.; van Riel, D.; Vakulenko, Y.A.; Sander, A.-L.; et al. Highly diversified shrew hepatitis B viruses corroborate ancient origins and divergent infection patterns of mammalian hepadnaviruses. *Proc. Natl. Acad. Sci. USA* **2019**, *116*, 17007–17012. [[CrossRef](#)]
21. de Carvalho Dominguez Souza, B.F.; König, A.; Rasche, A.; de Oliveira Carneiro, I.; Stephan, N.; Corman, V.M.; Roppert, P.L.; Goldmann, N.; Kepper, R.; Müller, S.F.; et al. A novel hepatitis B virus species discovered in capuchin monkeys sheds new light on the evolution of primate hepadnaviruses. *J. Hepatol.* **2018**, *68*, 1114–1122. [[CrossRef](#)]
22. Müller, S.F.; König, A.; Döring, B.; Glebe, D.; Geyer, J. Characterisation of the hepatitis B virus cross-species transmission pattern via Na<sup>+</sup>/taurocholate co-transporting polypeptides from 11 New World and Old World primate species. *PLoS ONE* **2018**, *13*, e0199200. [[CrossRef](#)]
23. Watashi, K.; Sluder, A.; Daito, T.; Matsunaga, S.; Ryo, A.; Nagamori, S.; Iwamoto, M.; Nakajima, S.; Tsukuda, S.; Borroto-Esoda, K.; et al. Cyclosporin A and its analogs inhibit hepatitis B virus entry into cultured hepatocytes through targeting a membrane transporter, sodium taurocholate cotransporting polypeptide (NTCP). *Hepatology* **2014**, *59*, 1726–1737. [[CrossRef](#)]
24. Nkongolo, S.; Ni, Y.; Lempp, F.A.; Kaufman, C.; Linder, T.; Esser-Nobis, K.; Lohmann, V.; Mier, W.; Mehrle, S.; Urban, S. Cyclosporin A inhibits hepatitis B and hepatitis D virus entry by cyclophilin-independent interference with the NTCP receptor. *J. Hepatol.* **2014**, *60*, 723–731. [[CrossRef](#)] [[PubMed](#)]
25. Shimura, S.; Watashi, K.; Fukano, K.; Peel, M.; Sluder, A.; Kawai, F.; Iwamoto, M.; Tsukuda, S.; Takeuchi, J.S.; Miyake, T. Cyclosporin derivatives inhibit hepatitis B virus entry without interfering with NTCP transporter activity. *J. Hepatol.* **2017**, *66*, 685–692. [[CrossRef](#)] [[PubMed](#)]

26. Liu, Y.; Ruan, H.; Li, Y.; Sun, G.; Liu, X.; He, W.; Mao, F.; He, M.; Yan, L.; Zhong, G.; et al. Potent and Specific Inhibition of NTCP-Mediated HBV/HDV Infection and Substrate Transporting by a Novel, Oral-Available Cyclosporine A Analogue. *J. Med. Chem.* **2020**. [[CrossRef](#)]
27. Wang, X.J.; Hu, W.; Zhang, T.-Y.; Mao, Y.-Y.; Liu, N.-N.; Wang, S.-Q. Irbesartan, an FDA approved drug for hypertension and diabetic nephropathy, is a potent inhibitor for hepatitis B virus entry by disturbing Na(+)-dependent taurocholate cotransporting polypeptide activity. *Antiviral Res.* **2015**, *120*, 140–146. [[CrossRef](#)]
28. Blanchet, M.; Sureau, C.; Labonté, P. Use of FDA approved therapeutics with hNTCP metabolic inhibitory properties to impair the HDV lifecycle. *Antiviral Res.* **2014**, *106*, 111–115. [[CrossRef](#)]
29. Huang, H.C.; Tao, M.-H.; Hung, T.-M.; Chen, J.-C.; Lin, Z.-J.; Huang, C. (-)-Epigallocatechin-3-gallate inhibits entry of hepatitis B virus into hepatocytes. *Antiviral Res.* **2014**, *111*, 100–111. [[CrossRef](#)]
30. Kaneko, M.; Watashi, K.; Kamisuki, S.; Matsunaga, H.; Iwamoto, M.; Kawai, F.; Ohashi, H.; Tsukuda, S.; Shimura, S.; Suzuki, R.; et al. A Novel Tricyclic Polyketide, Vanitaracin A, Specifically Inhibits the Entry of Hepatitis B and D Viruses by Targeting Sodium Taurocholate Cotransporting Polypeptide. *J. Virol.* **2015**, *89*, 11945–11953. [[CrossRef](#)] [[PubMed](#)]
31. Tsukuda, S.; Watashi, K.; Iwamoto, M.; Suzuki, R.; Aizaki, H.; Okada, M.; Sugiyama, M.; Kojima, S.; Tanaka, Y.; Mizokami, M.; et al. Dysregulation of retinoic acid receptor diminishes hepatocyte permissiveness to hepatitis B virus infection through modulation of sodium taurocholate cotransporting polypeptide (NTCP) expression. *J. Biol. Chem.* **2015**, *290*, 5673–5684. [[CrossRef](#)]
32. Tsukuda, S.; Watashi, K.; Hojima, T.; Isogawa, M.; Iwamoto, M.; Omagari, K.; Suzuki, R.; Aizaki, H.; Kojima, S.; Sugiyama, M.; et al. A new class of hepatitis B and D virus entry inhibitors, proanthocyanidin and its analogs, that directly act on the viral large surface proteins. *Hepatology* **2017**, *65*, 1104–1116. [[CrossRef](#)]
33. Donkers, J.M.; Zehnder, B.; van Westen, G.J.P.; Kwakkenbos, M.J.; Jzerman, A.P.I.; Oude Elferink, R.P.J.; Beuers, U.; Urban, S.; van de Graaf, S.F. Reduced hepatitis B and D viral entry using clinically applied drugs as novel inhibitors of the bile acid transporter NTCP. *Sci. Rep.* **2017**, *7*, 15307. [[CrossRef](#)] [[PubMed](#)]
34. Blank, A.; Eidam, A.; Haag, M.; Hohmann, N.; Burhenne, J.; Schwab, M.; van de Graaf, S.F.; Meyer, M.R.; Maurer, H.H.; Meier, K.; et al. The NTCP-inhibitor Myrcludex B: Effects on Bile Acid Disposition and Tenofovir Pharmacokinetics. *Clin. Pharmacol. Ther.* **2018**, *103*, 341–348. [[CrossRef](#)]
35. Ni, Y.; Lempp, F.A.; Mehrle, S.; Nkongolo, S.; Kaufman, C.; Fälth, M.; Stindt, J.; Königer, C.; Nassal, M.; Kubitz, R.; et al. Hepatitis B and D viruses exploit sodium taurocholate co-transporting polypeptide for species-specific entry into hepatocytes. *Gastroenterology* **2014**, *146*, 1070–1083. [[CrossRef](#)] [[PubMed](#)]
36. Mueller, R.; Dawson, E.S.; Meiler, J.; Rodriguez, A.L.; Chauder, B.A.; Bates, B.S.; Felts, A.S.; Lamb, J.P.; Menon, U.N.; Jadhav, S.B.; et al. Discovery of 2-(2-benzoxazolyl amino)-4-aryl-5-cyanopyrimidine as negative allosteric modulators (NAMs) of metabotropic glutamate receptor 5 (mGlu(5)): From an artificial neural network virtual screen to an in vivo tool compound. *ChemMedChem* **2012**, *7*, 406–414. [[CrossRef](#)] [[PubMed](#)]
37. Thorne, N.; Auld, D.S.; Inglese, J. Apparent activity in high-throughput screening: Origins of compound-dependent assay interference. *Curr. Opin. Chem. Biol.* **2010**, *14*, 315–324. [[CrossRef](#)]
38. Butkiewicz, M.; Lowe Jr., E.W.; Mueller, R.; Mendenhall, J.L.; Teixeira, P.L.; Weaver, C.D.; Meiler, J. Benchmarking ligand-based virtual High-Throughput Screening with the PubChem database. *Molecules* **2013**, *18*, 735–756. [[CrossRef](#)] [[PubMed](#)]

Article

# Identification of Novel HBV/HDV Entry Inhibitors by Pharmacophore- and QSAR-Guided Virtual Screening

Michael Kirstgen <sup>1</sup>, Simon Franz Müller <sup>1</sup> , Kira Alessandra Alicia Theresa Lowjaga <sup>1</sup>, Nora Goldmann <sup>2</sup>, Felix Lehmann <sup>2</sup> , Sami Alakurtti <sup>3,4</sup>, Jari Yli-Kauhaluoma <sup>3</sup> , Karl-Heinz Baringhaus <sup>5</sup>, Reimar Krieg <sup>6</sup>, Dieter Glebe <sup>2,7</sup> and Joachim Geyer <sup>1,\*</sup> 

- <sup>1</sup> Institute of Pharmacology and Toxicology, Faculty of Veterinary Medicine, Justus Liebig University Giessen, 35392 Giessen, Germany; michael.kirstgen@vetmed.uni-giessen.de (M.K.); Simon.Mueller@vetmed.uni-giessen.de (S.F.M.); Kira.A.Lowjaga@vetmed.uni-giessen.de (K.A.A.T.L.)
- <sup>2</sup> Institute of Medical Virology, National Reference Center for Hepatitis B Viruses and Hepatitis D Viruses, Justus Liebig University Giessen, 35392 Giessen, Germany; Nora.Goldmann@viro.med.uni-giessen.de (N.G.); Felix.Lehmann@viro.med.uni-giessen.de (F.L.); Dieter.Glebe@viro.med.uni-giessen.de (D.G.)
- <sup>3</sup> Drug Research Program, Division of Pharmaceutical Chemistry and Technology, Faculty of Pharmacy, University of Helsinki, Viikinkaari 5 E, FI-00014 Helsinki, Finland; sami.alakurtti@neste.com (S.A.); jari.yli-kauhaluoma@helsinki.fi (J.Y.-K.)
- <sup>4</sup> VTT Technical Research Centre of Finland, Biologinkuja 7, FI-02044 Espoo, Finland
- <sup>5</sup> Sanofi-Aventis Deutschland GmbH, 65926 Frankfurt, Germany; Karl-Heinz.Baringhaus@sanofi.com
- <sup>6</sup> Institute of Anatomy II, University Hospital Jena, Teichgraben 7, 07743 Jena, Germany; REIMAR.KRIEG@med.uni-jena.de
- <sup>7</sup> German Center for Infection Research (DZIF), Partner Site Giessen-Marburg-Langen, 35392 Giessen, Germany
- \* Correspondence: Joachim.M.Geyer@vetmed.uni-giessen.de; Tel.: +49-641-99-38404; Fax: +49-641-99-38409



**Citation:** Kirstgen, M.; Müller, S.F.; Lowjaga, K.A.A.T.; Goldmann, N.; Lehmann, F.; Alakurtti, S.; Yli-Kauhaluoma, J.; Baringhaus, K.-H.; Krieg, R.; Glebe, D.; et al. Identification of Novel HBV/HDV Entry Inhibitors by Pharmacophore- and QSAR-Guided Virtual Screening. *Viruses* **2021**, *13*, 1489. <https://doi.org/10.3390/v13081489>

Academic Editors: Bruno Coutard and Franck Touret

Received: 24 June 2021  
Accepted: 24 July 2021  
Published: 29 July 2021

**Publisher's Note:** MDPI stays neutral with regard to jurisdictional claims in published maps and institutional affiliations.



**Copyright:** © 2021 by the authors. Licensee MDPI, Basel, Switzerland. This article is an open access article distributed under the terms and conditions of the Creative Commons Attribution (CC BY) license (<https://creativecommons.org/licenses/by/4.0/>).

**Abstract:** The hepatic bile acid transporter Na<sup>+</sup>/taurocholate co-transporting polypeptide (NTCP) was identified in 2012 as the high-affinity hepatic receptor for the hepatitis B and D viruses (HBV/HDV). Since then, this carrier has emerged as promising drug target for HBV/HDV virus entry inhibitors, but the synthetic peptide Hepcludex<sup>®</sup> of high molecular weight is the only approved HDV entry inhibitor so far. The present study aimed to identify small molecules as novel NTCP inhibitors with anti-viral activity. A ligand-based bioinformatic approach was used to generate and validate appropriate pharmacophore and QSAR (quantitative structure–activity relationship) models. Half-maximal inhibitory concentrations (IC<sub>50</sub>) for binding inhibition of the HBV/HDV-derived preS1 peptide (as surrogate parameter for virus binding to NTCP) were determined in NTCP-expressing HEK293 cells for 150 compounds of different chemical classes. IC<sub>50</sub> values ranged from 2 μM up to >1000 μM. The generated pharmacophore and QSAR models were used for virtual screening of drug-like chemicals from the ZINC<sup>15</sup> database (~11 million compounds). The 20 best-performing compounds were then experimentally tested for preS1-peptide binding inhibition in NTCP-HEK293 cells. Among them, four compounds were active and revealed experimental IC<sub>50</sub> values for preS1-peptide binding inhibition of 9, 19, 20, and 35 μM, which were comparable to the QSAR-based predictions. All these compounds also significantly inhibited *in vitro* HDV infection of NTCP-HepG2 cells, without showing any cytotoxicity. The best-performing compound in all assays was ZINC000253533654. In conclusion, the present study demonstrates that virtual compound screening based on NTCP-specific pharmacophore and QSAR models can predict novel active hit compounds for the development of HBV/HDV entry inhibitors.

**Keywords:** HBV; HDV; NTCP; entry inhibitor; QSAR; pharmacophore; virtual screen

## 1. Introduction

Chronic hepatitis following hepatitis B (HBV) and D (HDV) virus infections is the main cause of hepatocellular carcinoma (HCC) and liver cirrhosis. Even the availability of vaccination does not prevent the more than 800,000 deaths annually from the long-term

effects of chronic liver inflammation associated with HBV/HDV infections [1]. Both viruses are coated with identical envelope proteins that are coded by the 3.2 kb DNA genome of HBV [2]. The RNA genome of HDV does not code for any envelope protein. Therefore, HDV acts as a so-called satellite virus and makes use of the envelope proteins derived from the HBV genome [3,4]. This is the reason why HDV can only spread in the presence of an HBV infection. In addition, the interaction of both viruses with their cellular entry receptor NTCP is based on the common envelope proteins (HBs) [5]. NTCP (Na<sup>+</sup>/taurocholate co-transporting polypeptide, gene symbol *SLC10A1*) represents a physiologically important hepatic bile acid transporter and was also identified as the hepatic entry receptor for HBV and HDV. High affinity binding of both viruses to NTCP is mediated by the myristoylated preS1 domain (myr-preS1<sub>2-48</sub> lipopeptide), consisting of the 2–48 N-terminal amino acids of the large surface protein (LHBs). As a common but mostly non-curative therapy for virus-related chronic hepatitis, nucleos(t)ide-analogue (NUC) reverse transcriptase inhibitors (for HBV) and interferon (for both HBV/HDV) are used. Unfortunately, interferon therapy is highly prone to adverse drug reactions and NUCs have to be given life-long [6,7].

Identification of NTCP as an hepatic receptor for HBV/HDV in 2012 enabled the development of NTCP inhibitors as HBV/HDV entry inhibitors [8,9]. The mentioned myr-preS1<sub>2-48</sub> lipopeptide itself has the ability to block in vitro HBV/HDV infection with inhibitory constants (IC<sub>50</sub>) in the low nanomolar range [4]. Based on that, a synthetic analogue of this lipopeptide (Hepcludex<sup>®</sup>) has been developed and was recently approved as first HDV entry inhibitor interacting with NTCP [10]. Furthermore, numerous studies identified novel chemical entry inhibitors for HBV and HDV by screening for bile salt transport inhibitors [11] or by screening for inhibitors of myr-preS1<sub>2-48</sub> lipopeptide attachment and/or in vitro HBV/HDV infection [12] in appropriate hepatoma cell culture models overexpressing NTCP. However, to date, none of these small molecules have been able to enter the clinical development phase so far.

In previous studies, we identified individual compounds from two different classes (betulin and propanolamine derivatives) that were quite potent for myr-preS1<sub>2-48</sub> lipopeptide binding inhibition and significantly blocked in vitro HDV infection of NTCP-expressing HepG2 cells [13,14]. In the present study, we aimed to expand the group of small molecule NTCP inhibitors by pharmacophore-based virtual screening (VS) of compound libraries.

A well-established method of identifying novel inhibitor candidates for cellular drug targets is high-throughput screening (HTS) of chemical libraries. This technique can rapidly generate data of large subsets of molecules using automated experimental assays [15]. However, hit rates of HTS are only between 0.01% and 0.1% [16], which leads to immense drug discovery costs [17]. An alternative is given by so-called quantitative structure–activity relationship (QSAR) analysis as a ligand-based method for drug design [18]. In principle, this represents a bioinformatic method for building mathematical models that describe the correlation between physicochemical properties of ligands and continuous (IC<sub>50</sub>, EC<sub>50</sub>, K<sub>i</sub>, etc.) or categorical (active, inactive, toxic, nontoxic, etc.) properties, by using statistical regression techniques [19]. Nowadays, these models are used for VS approaches to predicting activities for compounds of large chemical databases (e.g., ZINC<sup>15</sup> [20]). Only substances with the best predicted activities are then selected for experimental validation [21]. Hit rates of this method range from 1% to 40% depending on the predictability of the generated model [22]. Compared to experimental HTS, QSAR-based VS of chemical libraries often results in higher hit rates of biologically active compounds at lower costs [22]. In the present study, we demonstrate that by QSAR-based VS novel small molecule inhibitors of NTCP can be identified that indeed showed proof-of-concept inhibition of HDV infection.

## 2. Materials and Methods

### 2.1. NTCP-Expressing Cell Lines

Human embryonic kidney (HEK293) cells were stably transfected with human NTCP and C-terminally tagged with the FLAG epitope (further referred to as NTCP-HEK293 cells) as reported before [23,24]. Cells were maintained at 37 °C, 5% CO<sub>2</sub>, and 95% humidity in

DMEM/F-12 medium (Thermo Fisher Scientific, Waltham, MA, USA) supplemented with 10% fetal calf serum (Sigma-Aldrich, St. Louis, MO, USA), 4 mM L-glutamine (PAA, Cölbe, Germany), and penicillin/streptomycin (PAA). HepG2 cells stably transfected with NTCP-FLAG (further referred to as NTCP-HepG2 [9]) were cultured under the same conditions in DMEM with all supplements listed above, except for L-glutamine. For induction of the transgene, the medium was supplemented with 1 µg/mL tetracycline (Roth, Karlsruhe, Germany) in the case of the NTCP-HEK293 cells or with 2 µg/mL doxycycline (Sigma-Aldrich) in the case of the NTCP-HepG2 cells.

## 2.2. Inhibitory Concentrations ( $IC_{50}$ ) for [ $^3H$ ]preS1 Binding and [ $^3H$ ]TC Transport

Bile acid transport measurements were performed in NTCP-HEK293 cells with tritium-labelled taurocholic acid (further referred to as [ $^3H$ ]TC) (20 Ci/mmol, 0.09 mCi/mL, Perkin Elmer, Waltham, MA, USA). In parallel, peptide-binding experiments were performed with a tritium-labelled myr-preS1<sub>2-48</sub> lipopeptide -HBV subgenotype D3- (further referred to as [ $^3H$ ]preS1) that was purchased from Pharmaron (120 Ci/mmol, 1 mCi/mL, Cardiff, UK) as reported [13]. Briefly, cells were seeded onto polylysine-coated 96-well plates, induced with 1 µg tetracycline per ml, and grown to confluence over 72 h at 37 °C. Then, cells were washed once with tempered phosphate buffered saline (PBS, 137 mM NaCl, 2.7 mM KCl, 1.5 mM KH<sub>2</sub>PO<sub>4</sub>, 7.3 mM Na<sub>2</sub>HPO<sub>4</sub>, pH 7.4) at 37 °C and preincubated with 80 µL DMEM for 5 min at 37 °C. The medium was replaced by 80 µL DMEM containing the respective inhibitor (concentrations ranging from 0.1 to 1000 µM) or solvent alone (100% uptake/binding control), and cells were further incubated for 5 min at 37 °C. After this pre-incubation, bile acid transport experiments were started by adding 20 µL DMEM containing 5 µM [ $^3H$ ]TC (final concentration: 1 µM). Binding of [ $^3H$ ]preS1 was initiated by adding 20 µL DMEM containing 25 nM [ $^3H$ ]preS1 (final concentration: 5 nM). Experiments were stopped after 10 min by washing twice with ice-cold PBS. For 0% uptake/binding control, the NTCP-HEK293 cells were not induced with tetracycline (-tet). Cell-associated radioactivity of [ $^3H$ ]TC or [ $^3H$ ]preS1 was quantified by liquid scintillation counting in a Packard Microplate Scintillation Counter TopCount NXT (Packard Instrument Company, Meriden, USA). Transport rates and [ $^3H$ ]preS1 binding were determined in counts per minute (cpm). The mean of the 0% control was subtracted and the net [ $^3H$ ]TC transport rates and net [ $^3H$ ]preS1 binding rates, respectively, were expressed as % of control.  $IC_{50}$  values were calculated from quadruplicate determinations by GraphPad Prism 6 (GraphPad, San Diego, CA, USA).

## 2.3. HDV Infection Experiments

HDV production was done in vitro as described before [25,26]. RT-qPCR was performed to determine HDV RNA genome equivalents. NTCP-HepG2 cells were preincubated for 5 min with inhibitors solved in 80 µL hepatocyte growth medium (HGM) per well in concentrations ranging from 5 µM to 300 µM. Infection experiments were performed in NTCP-HepG2 cells as described [13]. Briefly, during infection, cells were cultured in 96-well plates in HGM consisting of William's E Medium (Thermo Fisher Scientific) containing 2% bovine serum albumin (BSA, Roth), 2 mM L-glutamine (Thermo Fisher Scientific), 100 µg/mL gentamicin (Thermo Fisher Scientific), 10 nM dexamethasone (Sigma-Aldrich), 1 mM sodium pyruvate (Thermo Fisher Scientific), 1× insulin-transferrin-selen (Thermo Fisher Scientific), 2% DMSO (Merck, Darmstadt, Germany), 4% polyethylene glycol (Sigma-Aldrich), and 2 µg/mL doxycycline (Sigma-Aldrich). HDV stock solved in 20 µL HGM per well was added for infection and cells were incubated for 6 h with final concentration of 120 genome equivalents/cell of HDV particles. Subsequently, cells were washed with DMEM and cultured in HGM supplemented with 2% DMSO, 2% BSA, and 2 µg/mL doxycycline. Every three days medium was changed until cells were fixed at day 9 post infection with 3% paraformaldehyde (Sigma-Aldrich) in PBS, for 30 min at room temperature (RT). Cells were permeabilized with 0.2% Triton X 100 (Roth) in PBS for 30 min at RT, and blocked by incubation with 5% bovine serum albumin (Roth) in PBS, for 30 min



at RT. Then, cells were immunostained with purified human anti-HDV-positive serum at 37 °C for 1 h (1:400 dilution). Goat anti-human IgG secondary antibody coupled to Alexa Fluor fluorophore (1:400 dilution, Thermo Fisher Scientific) was added for 1 h at 37 °C for detection of hepatitis delta antigen (HDAG) as described before [27]. Nuclei were stained with Hoechst 33,342 (1 µg/mL, Thermo Fisher Scientific).

#### 2.4. Cytotoxicity Assay

The In Vitro Toxicology Assay Kit (Sigma-Aldrich) was used to perform a 3-[4,5-dimethylthiazole-2-yl]-2,5-diphenyltetrazolium bromide (MTT) assay to measure the cytotoxicity of the indicated compounds according to the manufacturer's protocol. Briefly, NTCP-HepG2 cells were incubated with 100 µL of the indicated concentrations of the respective compound solved in HGM over 6 h at 37 °C. After 6 h, the medium was replaced by inhibitor-free HGM and cells were cultured for additional 24 h. Then medium was removed and 100 µL DMEM containing 0.5 mg/mL MTT were added and cells were incubated for 1 h at 37 °C. Finally, the medium was replaced by 100 µL isopropyl alcohol (Sigma-Aldrich) and samples were measured by ELISA reader (GloMax-Multi Detection System, Promega, Madison, WI, USA).

#### 2.5. Tested Compounds

A set of betulin derivatives (TargoSet) was purchased from Adipogen AG (Liestal, Switzerland). All other betulin derivatives were synthesized as outlined elsewhere [28–30]. In total, data from 31 betulin derivatives were taken into account. A set of 87 test compounds was provided by Sanofi-Aventis Deutschland GmbH (Frankfurt, Germany) [14]. A set of 18 arylmethylamino steroids was provided by Krieg et al. [31]. A set of 20 compounds, which can be found in the ZINC<sup>15</sup> database [20] (<https://zinc.docking.org/>, 7 May 2021), was purchased from MolPort (Riga, Latvia). All other tested compounds were purchased from Sigma-Aldrich.

#### 2.6. Data Preparation

The software MAESTRO Molecular Modeling Interface (Version 12.2) of SCHRÖDINGER, Inc. (<https://www.schrodinger.com/>, 15 June 2020, New York City, NY, USA) was used. All 2D structures were imported as *sdf* files into the MAESTRO Molecular Modeling Interface and were cured and standardized using LigPrep [32] with the following settings: force field OPLS\_2005 (default setting); ionization state at target pH 7.4 (Epik; custom setting); desalt (default setting); generate tautomers (default setting); retain specified chiralities (default setting).

#### 2.7. Pharmacophore Generation

Generation of pharmacophore model was performed using PHASE [33] with the following settings: active = IC<sub>50</sub> < 10 µM (binding affinity > 5; custom setting); inactive = IC<sub>50</sub> > 20 µM (binding affinity < 4.7; custom setting); hypothesis should match at least 50% of actives (default setting); 4 to 5 features in the hypothesis (default setting); difference criterion 0.5 (default setting); create excluded volume shell from actives and inactives (default setting); minimum number of inactives that must experience a clash = 1 (default setting); minimum distance between active surface and excluded volumes 1 Å (default setting); excluded volume sphere radii 1 Å (default setting).

#### 2.8. Atom-Based QSAR-Model Generation

Atom-based QSAR models were built using PHASE [33] with the following settings: random training set 70% (custom setting) (59 compounds training set, 26 compounds test set); grid spacing = 1 Å (default setting); maximum PLS factors = 7 (custom setting). Determined IC<sub>50</sub> values were used as property input, expressed as "binding affinity" =  $-\log(\text{IC}_{50} [\text{M}])$ .

### 2.9. Virtual Screening

The downloaded database was prepared for pharmacophore-screening using PHASE [33] with the following settings: skip duplicate ligands (default setting); generate 10 ligand conformers and minimize output (custom setting); generate possible states at pH 7.4 (epik; custom setting); retain specified chiralities (default setting); retain at most 4 low-energy stereoisomers per ligand (default setting); generate up to 1 low-energy 5- and 6-membered ring conformations (default setting); remove high-energy ionization/tautomer states (default setting); prefilter by Lipinski's Rule (custom setting).

### 2.10. Statistics

Determination of  $IC_{50}$  values was done by nonlinear regression analysis using the equation  $\log(\text{inhibitor})$  vs. response settings of the GraphPad Prism 6.0 software (GraphPad). Data of bile acid transport and [ $^3H$ ]preS1 binding were expressed as means  $\pm$  SD from quadruplicate determinations. Infection studies show data from three independent experiments, each with triplicate determinations represented as means  $\pm$  SD. Statistical analysis of the HDV infection experiments were performed by two-way ANOVA, followed by Dunnett's multiple comparison test by GraphPad Prism 6.0, considering  $p < 0.01$  as statistically significant. Statistical data of presented bioinformatic models originated from the MAESTRO Molecular Modeling Interface.

## 3. Results

The most important factor for the predictability of pharmacophore and QSAR models is the quality of data input [34]. To ensure input of data from congeneric experiments, we performed all experiments with the identical cell line and protocol, as described before [13,14]. Namely, we used all test compounds as inhibitors for [ $^3H$ ]preS1-peptide binding inhibition to NTCP and [ $^3H$ ]TC transport inhibition via NTCP, both in NTCP-expressing HEK293 cells. These experiments were performed with four different groups of test compounds, including 31 betulin-derived triterpenoids [13], and 87 propranolamine derivatives [14]. Both groups of compounds were analyzed before as novel NTCP inhibitors in our laboratory. In addition, a set of 18 arylmethylamino steroids that previously showed antiparasitic activity against *Plasmodium falciparum* and *Schistosoma mansoni* [31] was used for NTCP inhibition for the first time in the present study (Supplementary Figures S1 and S2). And finally, a group of 55 structurally unrelated compounds that were reported as NTCP inhibitors in the literature [35–46] were included in the [ $^3H$ ]preS1-peptide binding inhibition experiments. Figure 1 gives an overview about the workflow of the present study.

In a first step, all compounds were used at 100  $\mu M$  inhibitory concentration in binding experiments with 5 nM [ $^3H$ ]preS1-peptide and transport experiments with 1  $\mu M$  [ $^3H$ ]TC in NTCP-overexpressing HEK293 cells (Supplementary Figure S3). For all compounds that showed more than 50% inhibition of [ $^3H$ ]preS1-peptide binding inhibition, detailed half-maximal inhibitory concentrations ( $IC_{50}$ ) were determined. However, for some of the compounds a sigmoidal concentration-dependent dose-response relationship could not be determined experimentally. Therefore, these compounds were removed from the dataset. This was important to avoid distortion of subsequent models due to non-valid  $IC_{50}$  data. In total, a data set consisting of 85 compounds with valid  $IC_{50}$  data could be compiled.  $IC_{50}$  values for the betulin [13] and propranolamine [14] derivatives were taken from previous studies of our laboratory. The inhibition pattern of the arylmethylamino steroids is presented in detail in Supplementary Figure S1. The  $IC_{50}$  values for [ $^3H$ ]preS1-peptide binding inhibition of this compound class ranged from 8–251  $\mu M$ . The most potent compound was steroid 12c with an  $IC_{50}$  for [ $^3H$ ]preS1-peptide binding inhibition of 8  $\mu M$ . Structures of the three most potent [ $^3H$ ]preS1-peptide binding inhibitors of this compound class are depicted in Supplementary Figure S2.

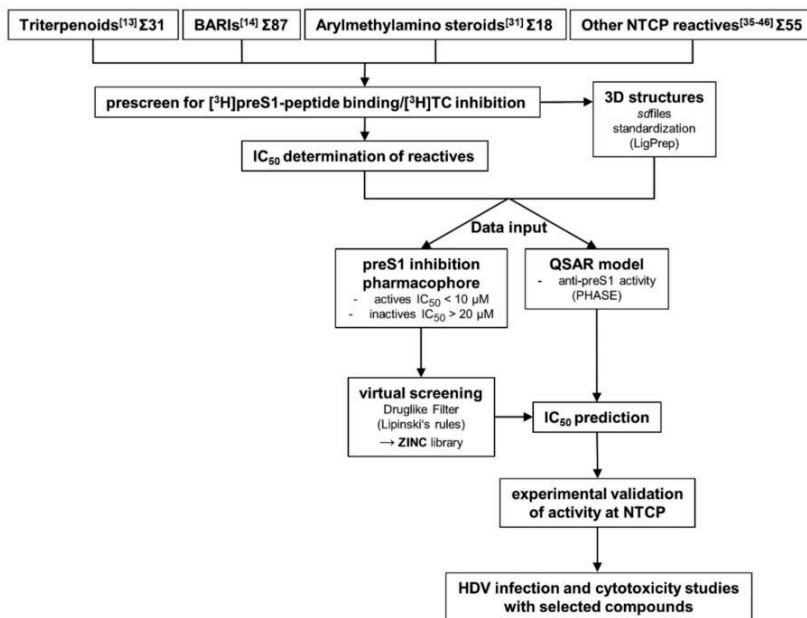


**Figure 1.** Workflow of the study. The study started with four different compound groups. Three of them were identified as NTCP inhibitors before (see references [13,14,35–46]). Arylmethylamino steroids were shown to have antiparasitic activity (see reference [31]) and were established as novel NTCP inhibitors for the first time in the present study. BARIs = bile acid reabsorption inhibitors; QSAR = quantitative structure-activity relationship.

For QSAR modeling, all  $IC_{50}$  values were transformed by  $-\log(IC_{50} [M])$  conversion into binding affinity values as indicated in Table 1. In addition, data of the chemical structures were collected and were saved as 2D *sdf* files. For curation and standardization of the chemical structures, LigPrep [32] was used (encoded in the software of the Schrödinger Suite which can be executed through the Maestro graphical user interface). In total, the  $IC_{50}$  values for [ $^3H$ ]preS1-peptide binding inhibition from the 85 data set compounds revealed binding affinities between 1 ( $IC_{50} > 1000 \mu M$ ) and 5.699 ( $IC_{50} = 2 \mu M$ ). The compounds then were divided into a training set to generate the QSAR model (59 compounds, Table 1) and a test set to validate the QSAR model (26 compounds, Table 4) as described in the Material and Methods Section 2.8.

**Table 1.** Training set to generate an atom-based QSAR model for anti-preS1 activity. Listed are experimentally determined binding affinities ( $-\log(IC_{50} [M])$ ) of ligands and predicted binding affinities by the resulting QSAR model. Error describes the difference from the experimentally determined to the predicted binding affinity. Previous descriptions of the compounds as NTCP inhibitors are referenced. As an exception, the arylmethylamino “steroid” compounds are introduced here as novel NTCP inhibitors for the first time.

Ligand Name	Binding Affinity	Prediction	Error
Rosiglitazone [35]	5.699	5.836	0.137
28-O-Succinoylbetulin [13]	5.523	5.278	−0.245
3-O-Acetylbetulinic acid [13]	5.523	5.214	−0.309

Table 1. Cont.

Ligand Name	Binding Affinity	Prediction	Error
Ginkgolic acid 17:1 [39]	5.523	5.821	0.298
Troglitazone [35]	5.523	5.448	−0.075
Ginkgolic acid 15:1 [39]	5.523	5.461	−0.062
28-O-(3,3-dimethylglutaroyl)betulin [13]	5.398	5.365	−0.033
Ritonavir [36]	5.398	5.243	−0.155
20,29-Dihydrobetulonic acid [13]	5.319	4.993	−0.326
3,28-Di-O-succinoylbetulin [13]	5.301	5.200	−0.101
3-O-Caffeoylbetulin [13]	5.222	5.310	0.088
3,28-Di-O-(3,3-dimethylglutaroyl)betulin [13]	5.155	5.163	0.008
Steroid 12c [31]	5.097	5.043	−0.054
28-O-(Bromoacetyl)betulin [13]	5.097	4.878	−0.219
S973509 [14]	5.046	5.027	−0.019
A00028897 [14]	5.046	5.090	0.044
A000295231 [14]	5.000	5.004	0.004
Erythrosin B [39]	5.000	5.087	0.087
Betulinaldehyde oxime [13]	4.959	4.848	−0.111
28-(2 <i>H</i> -Tetrahydropyran-2-yl)betulin [13]	4.854	4.746	−0.108
Allobetulin [13]	4.854	4.843	−0.011
Efavirenz [36]	4.796	4.646	−0.149
Rifampicin [47]	4.745	4.849	0.105
Steroid 9c [31]	4.745	4.718	−0.026
28-O-Cinnamoylbetulin [13]	4.721	4.715	−0.006
Rapamycin [41]	4.678	4.683	0.005
Simvastatin [37]	4.638	4.554	−0.084
Cyclosporine A [38,43–46]	4.585	4.472	−0.113
Losartan [37]	4.538	4.620	0.082
Methyl betulinate [13]	4.481	4.692	0.211
Steroid 8c [31]	4.469	4.538	0.070
3-O-Acetyl-28-(2 <i>H</i> -tetrahydropyran-2-yl)betulin [13]	4.456	4.593	0.137
Nimodipine [37]	4.444	4.429	−0.015
Betulonic aldehyde [13]	4.432	4.426	−0.006
Bromosulphthalein [42]	4.420	4.506	0.085
3-O-Acetylbetulin [13]	4.377	4.389	0.012
Steroid 13c [31]	4.367	4.182	−0.184
3,28-Di-O-acetyl-20,30-epoxybetulin [13]	4.357	4.321	−0.035
Steroid 1g [31]	4.310	4.148	−0.162
Steroid 1o [31]	4.260	4.255	−0.005
28-O-Nicotinoylbetulin [13]	4.201	4.258	0.057
3,28-Di-O-acetyl-18,19-dehydro-20,29-dihydrobetulin [13]	4.201	4.235	0.034
Bendroflumethiazide [37]	4.201	4.263	0.062
Tioconazole [37]	4.125	4.308	0.183
S973515 [14]	4.119	3.989	−0.130
Steroid 7c [31]	4.066	4.142	0.076
Steroid 5c [31]	4.056	4.066	0.011
A000295480 [14]	4.009	4.098	0.089
Steroid 3c [31]	3.996	3.994	−0.002
Betulin [13]	3.963	4.454	0.492
Steroid 4c [31]	3.959	4.005	0.046
A000295013 [14]	3.924	3.865	−0.059
Steroid 1e [31]	3.910	3.988	0.078
4'-Ethyl-1',2',4'-triazoline-3',5'-dione-fused 3,28-di-O-acetylbetulin [13]	3.848	3.741	−0.107
3,28-Di-O-acetylbetulin [13]	3.701	3.939	0.238
Steroid 1c [31]	3.652	3.642	−0.010
Olmesartan [37]	3.129	3.057	−0.072
Irbesartan [37]	3.032	3.076	0.045
Rosuvastatin [37]	1.000	0.918	−0.082

The atom-based QSAR model, illustrated in Figure 2, was built using PHASE [33]. This model describes three-dimensionally all necessary features to block [ $^3\text{H}$ ]preS1-peptide binding to NTCP. Seven scenarios with different numbers of partial least squares (PLS) factors of the chosen regression model were generated and statistically analyzed (Table 2). A number of four PLS factors revealed the highest value of Pearson-r for the predicted activities of the test set of 0.4614. Therefore, this model composition was chosen for all further investigations. The standard deviation (SD) of the regression for the chosen model was at 0.153 with a coefficient of determination ( $R^2$ ) of 0.9519. The stability index of  $-0.242$  of this model illustrates that the texture of the model is strongly dependent on the training set composition. The variance ratio (F) of 357.3 indicates statistically significant regression and the significance level (P) of  $-41$  indicates a great degree of confidence for the variance ratio (Table 2).

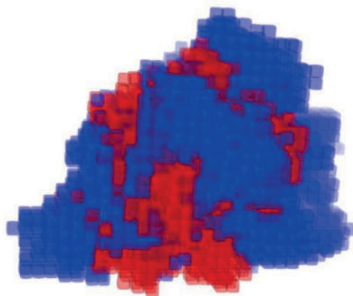


**Figure 2.** Atom-based QSAR model of anti-preS1 activity. The three dimensional view of the QSAR model illustrates the spatial distribution of contributions to the model. The cubes of the model are colored by the sign of the coefficient: blue for positive coefficients and red for negative coefficients. Positive coefficients indicate an increase in activity, negative coefficients a decrease. Edge length of cubes = 1 Å.

**Table 2.** Statistics of the generated atom-based QSAR model for anti-preS1 activity. Listed are data of a total of seven scenarios with different numbers of partial least squares factors of the regression model (# PLS Factors). SD = standard deviation of the regression;  $R^2$  = coefficient of determination for the regression of the scatter plot of the training set (see Table 1 and Figure 3A); stability = stability of the model predictions to changes in the training set composition with a maximum value of 1 (meaning stable); F = variance ratio (large values of F indicate a more statistically significant regression); P = significance level of variance ratio (smaller values indicate a greater degree of confidence); Pearson-r = value of Pearson-R for the predicted activities of the test set (see Table 4 and Figure 3B). A number of four PLS factors revealed the highest Pearson-r for the prediction of activities of the training set ligands (0.4614) and therefore was chosen as the model for the first VS.

# PLS Factors	SD	$R^2$	Stability	F	P	Pearson-r
1	0.4671	0.5998	0.245	95.9	-14	0.2709
2	0.3093	0.8273	0.055	150.9	-25	0.3074
3	0.2314	0.9048	-0.216	196.5	-31	0.358
4	0.153	0.9591	-0.242	357.3	-41	0.4614
5	0.1038	0.9815	-0.298	635.2	-50	0.408
6	0.079	0.9894	-0.335	922	-56	0.4073
7	0.053	0.9953	-0.345	1766.9	-65	0.4124

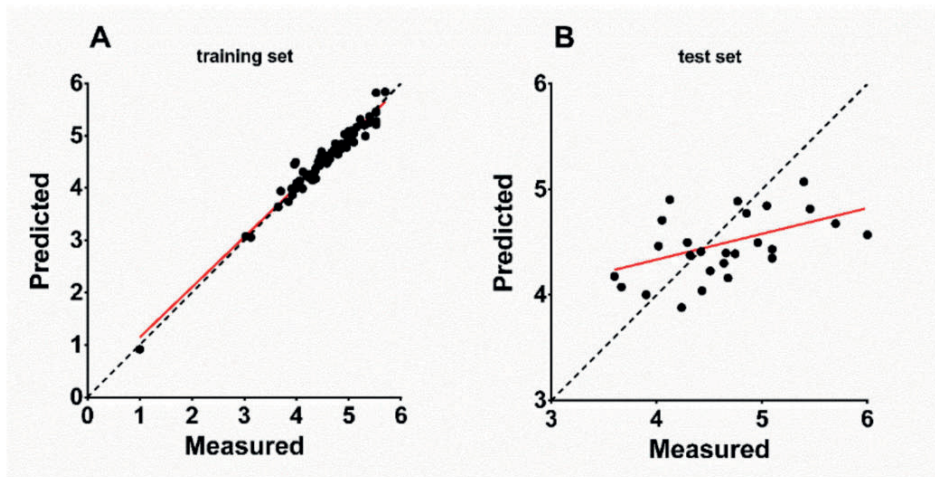


**Figure 3.** Predicted vs. measured binding affinities ( $-\log(\text{IC}_{50} \text{ M})$ ) of (A) training set and (B) test set NTCP inhibitor compounds based on the generated atom-based QSAR model. Red lines indicate linear regression of the scatterplots. (A) Training set (59 compounds, Table 1):  $R^2 = 0.9591$ , slope = 0.959. (B) Test set (26 compounds, Table 4):  $R^2 = 0.2163$ , slope = 0.2439. Bisector (dashed line) illustrates optimal prediction.

Distribution of the atom types of the QSAR model is shown in Table 3 for all seven scenarios of PLS factors. Listed are the percentages of H-bond donor, hydrophobic/non-polar, negative/positive ionic, electron withdrawing, and other regions in the model. The proportions of these attributes point to the relative importance of each attribute for the NTCP inhibitory potency of the respective compound. Interestingly, the attribute proportions did not strongly differ between the respective numbers of PLS factors and were calculated to ~5% H-bond donor, ~60% hydrophobic/non-polar, <1% negative or positive ionic, and ~30% electron withdrawing (Table 3). This means that the amount and distribution of hydrophobic or nonpolar regions is the most important factor for the potency of the inhibitor, while positive or negative ionic residues are of low importance. As expected, there was a strong correlation between the experimentally measured and the QSAR-based predicted binding affinity of the 59 training set compounds with  $R^2$  of 0.9591 and slope of 0.959 (Figure 3A). Based on this, the binding affinities of the 26 test-set compounds were predicted via the atom-based QSAR model and these ranged from 0.918 ( $\text{IC}_{50} > 1000 \mu\text{M}$ ) to 5.836 ( $\text{IC}_{50} = 1.5 \mu\text{M}$ ) with a mean error of prediction of  $-0.005$  (Table 4). Figure 3B shows the correlation between the experimentally measured and the QSAR-based predicted binding affinities of the 26 test-set compounds that revealed  $R^2$  of 0.2163 and slope of 0.2439. For five out of the 26 compounds the prediction was quite exact, representing ~20% high-level predictability. These compounds are steroid 7s (error  $-0.01$ ), raloxifene (error 0.057), compound S985852 (error  $-0.08$ ), steroid 2c (error 0.102), and pioglitazone (error 0.119) (Table 4).

**Table 3.** Distribution of atom types of the generated QSAR model. Listed are numbers of partial least squares factors of the regression model (# PLS factors), the relative proportions to the model of H-bond donor, hydrophobic (= non-polar), negative ionic, positive ionic, electron-withdrawing, and other atom types. The data for four PLS factors are highlighted since this model was used for VS.

# PLS Factors	H-Bond Donor	Hydrophobic/ non-Polar	Negative Ionic	Positive Ionic	Electron- Withdrawing	Other
1	0.045	0.635	0	0	0.285	0.035
2	0.048	0.618	0	0	0.297	0.037
3	0.049	0.613	0	0	0.300	0.038
4	0.053	0.606	0	0	0.301	0.040
5	0.055	0.601	0	0	0.301	0.041
6	0.056	0.600	0.001	0.001	0.302	0.041
7	0.056	0.601	0	0	0.302	0.040

**Table 4.** Test set to validate the atom-based QSAR model for anti-preS1 activity. Listed are experimentally determined binding affinities ( $-\log(\text{IC}_{50} \text{ M})$ ) of ligands and predicted binding affinity by the resulting QSAR model. Error describes the difference between the experimentally determined and the predicted binding affinity. Previous descriptions of the compounds as NTCP inhibitors are referenced. As an exception, the arylmethylamino “steroid” compounds are introduced here as novel NTCP inhibitors for the first time.

Ligand Name	Binding Affinity	Prediction	Error
Ciglitazone [35]	6.000	4.570	−1.430
Betulinic acid [13]	5.699	4.677	−1.022
20,29-Dihydrobetulin [13]	5.456	4.815	−0.641
3-O-(3,3-Dimethylglutaroyl)betulinic acid [13]	5.398	5.073	−0.325
3,28-Di-O-acetyl-29-hydroxybetulin [13]	5.097	4.433	−0.664
Saquinavir [36]	5.097	4.349	−0.748
Emodin [39]	5.046	4.845	−0.201
Ginkgolic acid 13:0 [39]	4.959	4.496	−0.462
S985852 [14]	4.854	4.774	−0.080
Pioglitazone [35]	4.770	4.888	0.119
Nitrendipine [37]	4.745	4.390	−0.354
Glyburide [37]	4.678	4.161	−0.517
Lupenone [13]	4.658	4.398	−0.259
Betulonoyl dimethyl-L-aspartate [13]	4.638	4.300	−0.338
3-Oxoallobetulin [13]	4.509	4.228	−0.281
Steroid 6c [31]	4.432	4.040	−0.392
Steroid 7s [31]	4.420	4.410	−0.010
Raloxifene [37]	4.319	4.376	0.057
Lupeol [37]	4.292	4.497	0.204
Steroid 1s [31]	4.237	3.881	−0.356
3,28-Di-O-(dihydrocinnamoyl)betulin [13]	4.125	4.902	0.777
A000289041 [14]	4.051	4.708	0.657
Nifedipine [37]	4.018	4.463	0.445
Steroid 2c [31]	3.900	4.002	0.102
Steroid 2s [31]	3.666	4.075	0.410
Steroid 2o [31]	3.600	4.176	0.576

To limit the computing power for the VS with the generated QSAR model, the compounds of the ZINC<sup>15</sup> library were preselected by screening with an anti-preS1 activity pharmacophore model (Figure 4). All settings for the pharmacophore hypothesis generation are described in the Material and Methods Section 2.7. Active compounds with  $\text{IC}_{50} < 10 \mu\text{M}$  for inhibition of [<sup>3</sup>H]preS1-peptide binding to NTCP were used to determine features of the pharmacophore and inactive inhibitors with  $\text{IC}_{50} > 20 \mu\text{M}$  were used to define excluding volumes. As shown in Figure 4, the hypothesis of an anti-preS1 activity pharmacophore model revealed three hydrophobic spheres and one H-bond acceptor sphere together with clustered excluding volumes. Subsequently, ~11 million compounds

of the ZINC<sup>15</sup> library were screened with the illustrated pharmacophore hypothesis. In addition, drug likeness filtering was applied by PHASE [33] for this virtual screen. More than 177,000 hit compounds were identified that matched with all pharmacophore features, representing a hit rate of approximately 1.6%. These compounds then were further screened with the atom-based QSAR model resulting in a compound list with predicted anti-preS1 activities. The top 20 hits that were commercially available are listed in Table 5 and their chemical structures are illustrated in Figure 5. The predicted IC<sub>50</sub> values for [<sup>3</sup>H]preS1-peptide binding inhibition at NTCP ranged from 7 to 16 μM (Table 5).

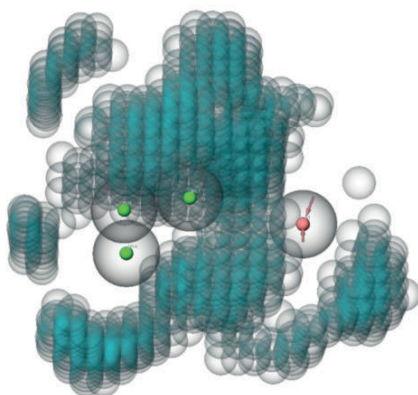


**Figure 4.** Anti-preS1 activity pharmacophore model for virtual pre-screen of the ZINC<sup>15</sup> library. The model consists of three hydrophobic spheres (shown with green center) and one H-bond acceptor sphere (shown with red center). Excluding volumes are illustrated as blue bubbles. Binding affinities and structures of ligands from Tables 1 and 4 served as data input. Excluded volume sphere radii are 1 Å.

**Table 5.** Top 20 commercially available hits from VS of the ZINC<sup>15</sup> compound library [20] (total amount of compounds: 10,844,830; downloaded on 15 May 2020; reactivity: standard; purchasability: in-stock; pH: ref mid (7.4); charge: −2, −1, 0, +1, +2; subset: drug-like). All downloaded data were processed as described in the Material and Methods section. Compounds showing anti-HDV activity are highlighted in red.

Compound ID	Predicted Anti-PreS1 Activity (IC <sub>50</sub> μM)	Compound ID	Predicted Anti-PreS1 Activity (IC <sub>50</sub> μM)
ZINC000021526502	7	ZINC000014961126	9
ZINC000253533654	7	ZINC000009431397	9
ZINC000067883878	8	ZINC000096409439	9
ZINC000009562125	8	ZINC000245343836	9
ZINC000253533159	8	ZINC000095964703	10
ZINC000183743244	8	ZINC000022590653	10
ZINC000011937386	8	ZINC000074798117	10
ZINC000067805841	9	ZINC000011909435	11
ZINC000067490628	9	ZINC000252677946	13
ZINC000078122008	9	ZINC000012520032	16



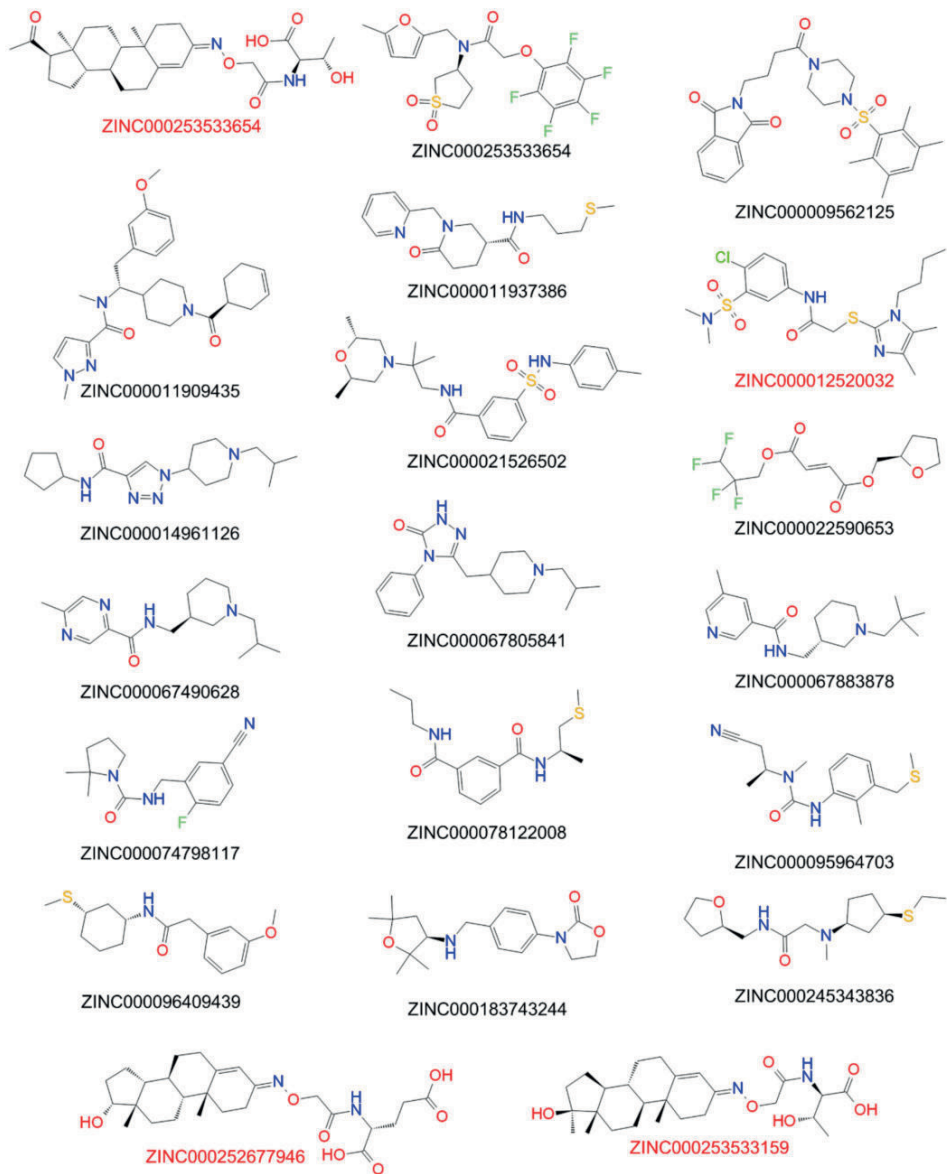


**Figure 5.** Structures of the top-20-hit compounds from virtual QSAR screening. Red-marked compounds proved anti-HDV activity (see Figure 8).

These 20 compounds were purchased and tested at 100  $\mu\text{M}$  inhibitory concentrations in binding experiments with 5 nM [ $^3\text{H}$ ]preS1-peptide and transport experiments with 1  $\mu\text{M}$  [ $^3\text{H}$ ]TC, both in NTCP-overexpressing HEK293 cells. Among this compound set only the compounds ZINC000012520032, ZINC000253533654, ZINC000253533159, and ZINC000252677946 revealed more than 50% [ $^3\text{H}$ ]preS1-peptide binding inhibition (Figure 6). Therefore, only these four compounds were further analyzed for  $\text{IC}_{50}$  inhibitory concentrations (Figure 7) and proof-of-concept HDV infection inhibition (Figure 8). As shown in Figure 7, all four compounds revealed concentration-dependent inhibition of [ $^3\text{H}$ ]TC transport via NTCP and [ $^3\text{H}$ ]preS1-peptide binding to NTCP with  $\text{IC}_{50}$  ranging from 11 to 51  $\mu\text{M}$  and 9 to 35  $\mu\text{M}$ , respectively (Table 6). All compounds were nearly equipotent in both inhibitory assays and, therefore, can be classified as novel non-selective NTCP inhibitors. Of note, the experimentally determined  $\text{IC}_{50}$  values for [ $^3\text{H}$ ]preS1-peptide binding inhibition fulfilled quite well the QSAR prediction with a deviation factor of  $<2.5$  for all four compounds. In particular, compound ZINC000253533654 showed almost exactly the predicted activity. Summarizing that from a data set of almost 11 million chemical compounds from the ZINC<sup>15</sup> library, a subset of 20 compounds could be filtered out, of which four compounds indeed showed concentration-dependent inhibition of myr-preS1<sub>2-48</sub> lipopeptide binding. So we obtained a predictability value of approximately 20% for our two-step VS approach.

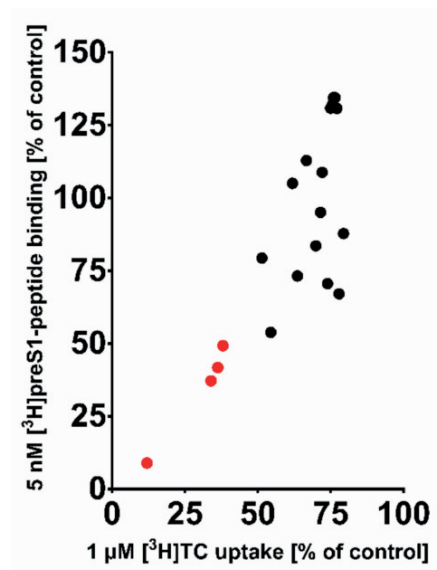


**Figure 6.** Residual [ $^3\text{H}$ ]TC transport activity via NTCP vs. residual [ $^3\text{H}$ ]preS1-peptide binding to NTCP in the presence of the top-20-hit compounds from the virtual QSAR screen. All compounds were used at 100  $\mu\text{M}$  inhibitor concentrations in transport assays with 1  $\mu\text{M}$  [ $^3\text{H}$ ]TC and binding assays with 5 nM [ $^3\text{H}$ ]preS1-peptide, both in NTCP-HEK293 cells for 10 min at 37  $^{\circ}\text{C}$ . Compounds resulting in less than 50% residual [ $^3\text{H}$ ]preS1-peptide binding compared to solvent control are highlighted in red. For these compounds  $\text{IC}_{50}$  values were determined as indicated in Figure 7.

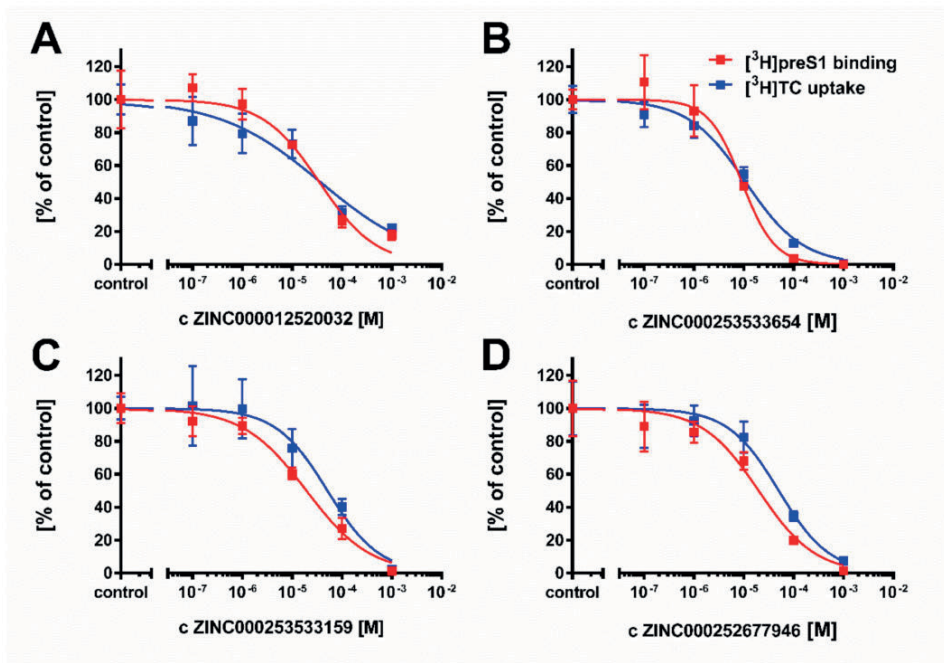


**Figure 7.** Determination of  $IC_{50}$  values of selected compounds for inhibition of  $[^3H]$ preS1 peptide binding to NTCP and  $[^3H]$ TC transport via NTCP at increasing inhibitor concentrations. (A) Substance ZINC000012520032, (B) Substance ZINC000253533654, (C) Substance ZINC000253533159; (D) Substance ZINC000252677946. NTCP-HEK293 cells were seeded onto 96-well plates and were incubated with tetracycline to induce expression of NTCP. Cells without tetracycline treatment were used as 0% controls for both assays. Bile acid transport experiments were performed with  $1 \mu M$   $[^3H]$ TC and binding experiments were performed with  $5 \text{ nM}$   $[^3H]$ preS1-peptide. Both assays were performed over 10 min at  $37^\circ C$  with increasing concentrations of the indicated inhibitors. Control experiments were performed with solvent alone (set to 100%). The mean of the 0% control was subtracted to calculate net  $[^3H]$ TC transport rates (shown in blue) as well as net  $[^3H]$ preS1 binding rates (shown in red), which are expressed as % of control at the y-axis.  $IC_{50}$  values were calculated by nonlinear regression analysis using the equation  $\log(\text{inhibitor})$  vs. response (GraphPad Prism). Data represent means  $\pm$  SD of quadruplicate determinations of representative experiments.

Following the workflow, the four hit compounds were experimentally validated for their inhibitory potency on in vitro HDV infection in NTCP-expressing HepG2 hepatoma cells (Figure 8). All four compounds showed significant concentration-dependent inhibition of HDV infection with a potency rank order of ZINC000253533654 > ZINC000012520032 > ZINC000253533159 > ZINC000252677946. Cytotoxicity studies revealed no toxic effects even at highest inhibitor concentration of  $300 \mu M$  over 6 h of incubation, representing the experimental conditions of the HDV infection experiments (Figure 9).

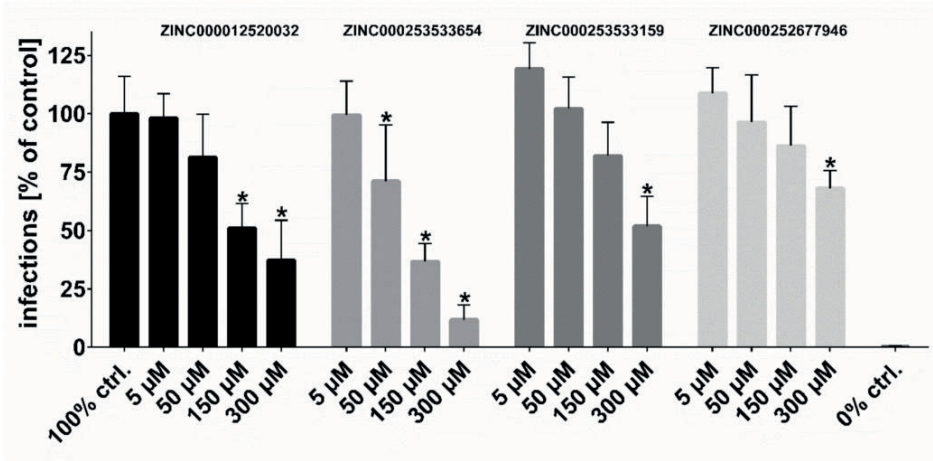


**Figure 8.** HDV infection studies. NTCP-HepG2 cells were pre-incubated for 5 min with the indicated concentrations of the respective inhibitors in DMEM at 37 °C. Then, cells were additionally inoculated with 120 genome equivalents/cell of HDV particles at 37 °C. After 6 h, cells were washed and further incubated with inhibitor- and virus-free medium, and medium was changed every 3–4 days. At day 9 post infection, cells were fixed and an immunostaining against the HDAg was performed, as a marker of HDV infection. The number of infected cells per well was determined by fluorescence microscopy. NTCP-HepG2 cells incubated without inhibitor were used as control (set to 100% infection rate). Infection experiments in the presence of 0.5 µM myr-preS1<sub>2-48</sub> lipopeptide served as 0% control (representing 0% infection rate). Data represent means ± SD of three independent experiments, each with triplicate determinations (n = 9). \* Significantly lower than 100% control with  $p < 0.01$ .

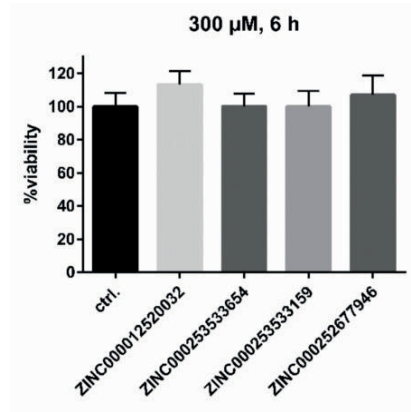


**Figure 9.** Cytotoxicity studies in NTCP-HepG2 cells. An MTT cytotoxicity assay was performed with the indicated compounds at 5 µM, 50 µM, 150 µM, and 300 µM inhibitor concentrations, incubated over a time span of 6 h at 37 °C. Solvent control was set to 100%. Data represent means ± SD of two independent experiments, each with triplicate determinations (n = 6). Even at the highest concentrations, no cytotoxic effects could be observed.

**Table 6.** Predictivity validation of the atom-based QSAR model.

Compound ID	Predicted Anti-PreS1 Activity (IC <sub>50</sub> μM)	Experimentally Determined Anti-PreS1 Activity (IC <sub>50</sub> μM)	Experimentally Determined Anti-TC Activity (IC <sub>50</sub> μM)
ZINC000012520032	16	35	37
ZINC000253533654	7	9	11
ZINC000253533159	8	19	51
ZINC000252677946	13	20	51

#### 4. Discussion

The aim of the present study was to identify novel inhibitors of NTCP with drug-like characteristics as potential therapeutics against HBV and HDV infections. HTS was not an option due to financial limitations. In addition, structure-based drug design was not possible, because no valid structural model is currently available for human NTCP. So, we decided to apply ligand-based bioinformatic methods for pharmacophore- and QSAR-guided VS of compound libraries. Our ligand-based approach is not necessarily a disadvantage, because inhibitor design solely based on crystallographic structures of the target protein can be critical due to inadequate resolution [48] or crystallization-related artifacts of the ligand–protein complex [49]. Furthermore, crystallographic studies may ignore discrete conformational states and anisotropic motion of the protein [50,51].

For ligand-based drug design, however, some aspects have to be taken into account to achieve appropriate and valid results. Data from congeneric experiments are necessary, all using the identical target, cell line, and experimental assay [33]. Therefore, we performed inhibition studies for all compounds used for pharmacophore and QSAR modeling with the identical experimental setup. But as NTCP seems to have different substrate and inhibitor binding sites [24], we cannot be sure that all analyzed compounds bind to the identical binding site at NTCP. This is a limitation of the approach used and a possible reason for inaccurate predictions. Also, we cannot exclude that some compounds inhibit NTCP in a competitive manner, while others may induce allosteric effects. These limitations underline the importance of the proof-of-concept in vitro HDV infection experiments that we performed with the four best-performing compounds of the present study.

The design of our inhibition and infection studies allowed us to categorize the identified inhibitors as HDV entry inhibitors acting at NTCP, as (I) their binding to NTCP was demonstrated by inhibition of [<sup>3</sup>H]TC uptake and [<sup>3</sup>H]preS1-peptide binding and (II) they were only present in the infection assay for the first 6 h of HDV exposure of the NTCP-HepG2 cells, representing the early entry phase. However, since we cannot rule out the possibility that some inhibitors might also be transported via NTCP into the HepG2 cells, additional post-entry anti-HDV effects might also be possible.

Starting from ~11 million compounds of the ZINC<sup>15</sup> library, we identified, in our two-step pharmacophore and QSAR VS, four out of 20 compounds that fulfilled potent [<sup>3</sup>H]preS1-peptide binding inhibition as predicted by the QSAR model and additional proof-of-concept concentration-dependent antiviral activity in the in vitro HDV infection experiments. We thus achieved a predictability of approximately 20% for our VS system, which lays in the acceptable range of 1% to 40% for such approaches [22]. These results indicate that the percentage of compounds that do not optimally fulfil the basic requirements for ligand-based VS is low enough in our data set to obtain a reliable prediction.

When considering the correlation of measured versus predicted activities of the test set of the generated QSAR model, a R<sup>2</sup> value of 0.2163 seems to be very weak. However, it is recommended not to define the accuracy of a generated QSAR model by its R<sup>2</sup>, due to its sensitivity to the variance in the dependent variable [52]. Furthermore, as the test set was considerably smaller than the training set, fluctuations in the R<sup>2</sup> value of the test set could easily occur due to fluctuations in the test set variance [52]. The fact that the QSAR model predicted the activity of five test-set compounds out of 26 nearly exactly should be taken into consideration rather than the calculated R<sup>2</sup>. In our VS system, we were able to reproduce this predictability of approximately 20%. In addition, hit compounds not

only showed inhibitory potency to block [ $^3\text{H}$ ]preS1-peptide binding to NTCP but also significantly reduced HDV infection in a concentration-dependent manner. This clearly supports the applicability of our screening system for the discovery of novel HBV/HDV inhibitors acting at NTCP. Of note, none of the hit compounds showed any cytotoxic effects on the HepG2 cell line used for infection studies, even at the highest concentrations of 300  $\mu\text{M}$ . This makes these compounds attractive for further development.

Subsequent studies can be versatile. Obtained data can be used as additional input for recalculations of the generated pharmacophore and QSAR models. In addition, further hits from the top-100 list of predicted [ $^3\text{H}$ ]preS1-peptide binding inhibitors can be experimentally validated and used for model optimization. Furthermore, the results of the present study can be assessed on the basis of the outcome of our previous studies with the betulin and propranolamine derivatives [13,14]. For both compound groups we could clearly show that only small molecular changes had significant impact on the anti-preS1 activity of the individual compounds. Furthermore, by chemical modifications we achieved a certain virus selectivity of the compounds, which is advantageous to maintaining the physiological bile acid transport function of NTCP during preS1/virus binding inhibition. As an example, the propranolamine compound A000295231 revealed a selectivity index (calculated from the mean  $\text{IC}_{50}$  for transport inhibition/preS1 binding inhibition) of 65. In the case of the betulin derivatives, 3,28-di-O-acetyl-29-hydroxybetulin revealed quite potent inhibition of the [ $^3\text{H}$ ]preS1-peptide binding to NTCP, but did not inhibit the [ $^3\text{H}$ ]TC transport via NTCP at all. Based on this, it would be worth generating and test sets of structural derivatives for their anti-preS1 activity. Of note, the compounds ZINC000253533654, ZINC000252677946, and ZINC000253533159 are structural homologs all based on a steroid core structure, the same as for the groups of betulin and arylmethylamino steroids. Based on this, a steroid core structure might be favorable for NTCP inhibitors.

Apart from the goal to find potent and virus-selective NTCP inhibitors for HBV/HDV entry inhibition, potent bile acid transport inhibitors acting on NTCP might also have clinical implications. As examples, patients with cholestatic liver diseases, obesity, dyslipidemia, nonalcoholic steatohepatitis, or primary biliary cholangitis could profit from hepatic bile acid uptake inhibition [10,53]. Based on this, the data of the present study can also be used for pharmacophore and QSAR modelling with a focus on potent bile acid inhibition irrespective of anti-preS1 activity [24,53].

In conclusion, the present study demonstrates, for the first time, pharmacophore and QSAR models for preS1-peptide binding inhibition at NTCP. With a two-step VS approach, novel NTCP inhibitors were identified with high prediction rate and accuracy and even demonstrated anti-HDV activity. These compounds can be used for further development of small molecular HBV/HDV entry inhibitors.

**Supplementary Materials:** The following are available online at <https://www.mdpi.com/article/10.3390/v13081489/s1>, Figure S1: Determination of  $\text{IC}_{50}$  values of 18 arylmethylamino steroids; Figure S2: Structures of selected arylmethylamino steroids with potent [ $^3\text{H}$ ]preS1 peptide binding inhibition; Figure S3: Residual [ $^3\text{H}$ ]TC transport activity via NTCP vs. residual [ $^3\text{H}$ ]preS1-peptide binding to NTCP.

**Author Contributions:** M.K., S.F.M., K.A.A.T.L. and J.G. conceived the experiments; M.K., S.F.M. and K.A.A.T.L. performed the experiments; M.K., S.F.M., K.A.A.T.L. and J.G. analyzed and interpreted the results; N.G., F.L. and D.G. provided materials and laboratories for infection studies; S.A., J.Y.-K., K.-H.B. and R.K. provided test compounds; and M.K. and J.G. wrote the manuscript. All authors have read and agreed to the published version of the manuscript.

**Funding:** This study was supported by FlexFunds from the LOEWE-Center DRUID (Novel Drug Targets against Poverty-Related and Neglected Tropical Infectious Diseases) and in part by the Deutsche Forschungsgemeinschaft (DFG, German Research Foundation)—Projektnummer 197785619—SFB 1021 as well as by the Foundation for Research of Natural Resources in Finland, Marjatta ja Eino Kollin Säätiö, and the COST Action CM-0801 (New drugs for neglected diseases).

**Institutional Review Board Statement:** Not applicable.

**Informed Consent Statement:** Not applicable.

**Data Availability Statement:** Obtained and analyzed data of this study are available from the corresponding author on request.

**Acknowledgments:** We thank Gary Grosser for his excellent scientific support regarding the setup of inhibition studies.

**Conflicts of Interest:** The authors declare no conflict of interest.

## References

1. World Health Organization. *Global Hepatitis Report 2017*; Geneva 2017. Licence:CC BY-NC-SA 3.0 IGO; WHO: Geneva, Switzerland, 2017.
2. Glebe, D.; Bremer, C.M. The molecular virology of hepatitis B virus. *Semin. Liver. Dis.* **2013**, *33*, 103–112. [\[CrossRef\]](#)
3. Glebe, D.; Urban, S.; Knoop, E.V.; Cag, N.; Krass, P.; Grun, S.; Bulavaite, A.; Sasnauskas, K.; Gerlich, W.H. Mapping of the hepatitis B virus attachment site by use of infection-inhibiting preS1 lipopeptides and tupaia hepatocytes. *Gastroenterology* **2005**, *129*, 234–245. [\[CrossRef\]](#)
4. Gripon, P.; Cannie, I.; Urban, S. Efficient inhibition of hepatitis B virus infection by acylated peptides derived from the large viral surface protein. *J. Virol.* **2005**, *79*, 1613–1622. [\[CrossRef\]](#)
5. Hughes, S.A.; Wedemeyer, H.; Harrison, P.M. Hepatitis delta virus. *Lancet* **2011**, *378*, 73–85. [\[CrossRef\]](#)
6. Martinez, M.G.; Villeret, F.; Testoni, B.; Zoulim, F. Can we cure hepatitis B virus with novel direct-acting antivirals? *Liver Int.* **2020**, *40* (Suppl. S1), 27–34. [\[CrossRef\]](#) [\[PubMed\]](#)
7. World Health Organization. *Guidelines for the Prevention, Care and Treatment of Persons with Chronic Hepatitis b Infection*; WHO: Geneva, Switzerland, 2015.
8. Yan, H.; Zhong, G.; Xu, G.; He, W.; Jing, Z.; Gao, Z.; Huang, Y.; Qi, Y.; Peng, B.; Wang, H.; et al. Sodium taurocholate cotransporting polypeptide is a functional receptor for human hepatitis B and D virus. *eLife* **2012**, *1*. [\[CrossRef\]](#) [\[PubMed\]](#)
9. König, A.; Döring, B.; Mohr, C.; Geipel, A.; Geyer, J.; Glebe, D. Kinetics of the bile acid transporter and hepatitis B virus receptor Na<sup>+</sup>/taurocholate cotransporting polypeptide (NTCP) in hepatocytes. *J. Hepatol.* **2014**, *61*, 867–875. [\[CrossRef\]](#) [\[PubMed\]](#)
10. MYR Pharmaceuticals. Available online: <http://myr-pharma.com/> (accessed on 15 May 2021).
11. Goh, B.; Choi, J.; Kang, J.A.; Park, S.G.; Seo, J.; Kim, T.Y. Development of a mass spectrometric screening assay for hepatitis B virus entry inhibitors. *J. Pharm. Biomed. Anal.* **2020**, *178*, 112959. [\[CrossRef\]](#) [\[PubMed\]](#)
12. Iwamoto, M.; Watashi, K.; Tsukuda, S.; Aly, H.H.; Fukasawa, M.; Fujimoto, A.; Suzuki, R.; Aizaki, H.; Ito, T.; Koikwai, O.; et al. Evaluation and identification of hepatitis B virus entry inhibitors using HepG2 cells overexpressing a membrane transporter NTCP. *Biochem. Biophys. Res. Commun.* **2014**, *443*, 808–813. [\[CrossRef\]](#)
13. Kirstgen, M.; Lowjaga, K.; Müller, S.F.; Goldmann, N.; Lehmann, F.; Alakurtti, S.; Yli-Kauhaluoma, J.; Glebe, D.; Geyer, J. Selective hepatitis B and D virus entry inhibitors from the group of pentacyclic lupane-type betulin-derived triterpenoids. *Sci. Rep.* **2020**, *10*, 21772. [\[CrossRef\]](#)
14. Kirstgen, M.; Lowjaga, K.A.A.T.; Müller, S.F.; Goldmann, N.; Lehmann, F.; Glebe, D.; Baringhaus, K.-H.; Geyer, J. Hepatitis D Virus Entry Inhibitors Based on Repurposing Intestinal Bile Acid Reabsorption Inhibitors. *Viruses* **2021**, *13*, 666. [\[CrossRef\]](#) [\[PubMed\]](#)
15. Mueller, R.; Dawson, E.S.; Meiler, J.; Rodriguez, A.L.; Chauder, B.A.; Bates, B.S.; Felts, A.S.; Lamb, J.P.; Menon, U.N.; Jadhav, S.B.; et al. Discovery of 2-(2-benzoxazolyl amino)-4-aryl-5-cyanopyrimidine as negative allosteric modulators (NAMs) of metabotropic glutamate receptor 5 (mGlu(5)): From an artificial neural network virtual screen to an in vivo tool compound. *ChemMedChem* **2012**, *7*, 406–414. [\[CrossRef\]](#)
16. Thorne, N.; Auld, D.S.; Ingles, J. Apparent activity in high-throughput screening: Origins of compound-dependent assay interference. *Curr. Opin. Chem. Biol.* **2010**, *14*, 315–324. [\[CrossRef\]](#)
17. Butkiewicz, M.; Lowe, E.W., Jr.; Mueller, R.; Mendenhall, J.L.; Teixeira, P.L.; Weaver, C.D.; Meiler, J. Benchmarking ligand-based virtual High-Throughput Screening with the PubChem database. *Molecules* **2013**, *18*, 735–756. [\[CrossRef\]](#)
18. Hansch, C.; Fujita, T.  $\rho$ - $\sigma$ - $\pi$  Analysis. A Method for the Correlation of Biological Activity and Chemical Structure. *J. Am. Chem. Soc.* **1964**, *86*, 1616–1626. [\[CrossRef\]](#)
19. Cherkasov, A.; Muratov, E.N.; Fourches, D.; Varnek, A.; Baskin, I.I.; Cronin, M.; Dearden, J.; Gramatica, P.; Martin, Y.C.; Todeschini, R.; et al. QSAR modeling: Where have you been? Where are you going to? *J. Med. Chem.* **2014**, *57*, 4977–5010. [\[CrossRef\]](#)
20. Sterling, T.; Irwin, J.J. ZINC 15-Ligand Discovery for Everyone. *J. Chem. Inf. Model.* **2015**, *55*, 2324–2337. [\[CrossRef\]](#)
21. Kar, S.; Roy, K. How far can virtual screening take us in drug discovery? *Expert Opin. Drug Discov.* **2013**, *8*, 245–261. [\[CrossRef\]](#)
22. Neves, B.J.; Braga, R.C.; Melo-Filho, C.C.; Moreira-Filho, J.T.; Muratov, E.N.; Andrade, C.H. QSAR-Based Virtual Screening: Advances and Applications in Drug Discovery. *Front Pharmacol.* **2018**, *9*, 1275. [\[CrossRef\]](#)
23. Geyer, J.; Döring, B.; Meerkamp, K.; Ugele, B.; Bakhiya, N.; Fernandes, C.F.; Godoy, J.R.; Glatt, H.; Petzinger, E. Cloning and functional characterization of human sodium-dependent organic anion transporter (SLC10A6). *J. Biol. Chem.* **2007**, *282*, 19728–19741. [\[CrossRef\]](#) [\[PubMed\]](#)

24. Grosser, G.; Müller, S.F.; Kirstgen, M.; Döring, B.; Geyer, J. Substrate Specificities and Inhibition Pattern of the Solute Carrier Family 10 Members NTCP, ASBT and SOAT. *Front. Mol. Biosci.* **2021**, *8*. [\[CrossRef\]](#)
25. Rasche, A.; Lehmann, F.; König, A.; Goldmann, N.; Corman, V.M.; Moreira-Soto, A.; Geipel, A.; van Riel, D.; Vakulenko, Y.A.; Sander, A.L.; et al. Highly diversified shrew hepatitis B viruses corroborate ancient origins and divergent infection patterns of mammalian hepadnaviruses. *Proc. Natl. Acad. Sci. USA* **2019**, *116*, 17007–17012. [\[CrossRef\]](#) [\[PubMed\]](#)
26. De Carvalho Dominguez Souza, B.F.; König, A.; Rasche, A.; de Oliveira Carneiro, I.; Stephan, N.; Corman, V.M.; Roppert, P.L.; Goldmann, N.; Kepper, R.; Müller, S.F.; et al. A novel hepatitis B virus species discovered in capuchin monkeys sheds new light on the evolution of primate hepadnaviruses. *J. Hepatol.* **2018**, *68*, 1114–1122. [\[CrossRef\]](#)
27. Müller, S.F.; König, A.; Döring, B.; Glebe, D.; Geyer, J. Characterisation of the hepatitis B virus cross-species transmission pattern via Na<sup>+</sup>/taurocholate co-transporting polypeptides from 11 New World and Old World primate species. *PLoS ONE* **2018**, *13*, e0199200. [\[CrossRef\]](#) [\[PubMed\]](#)
28. Alakurtti, S.; Heiska, T.; Kiriazis, A.; Sacerdoti-Sierra, N.; Jaffe, C.L.; Yli-Kauhaluoma, J. Synthesis and anti-leishmanial activity of heterocyclic betulin derivatives. *Bioorg. Med. Chem.* **2010**, *18*, 1573–1582. [\[CrossRef\]](#) [\[PubMed\]](#)
29. Pohjala, L.; Alakurtti, S.; Ahola, T.; Yli-Kauhaluoma, J.; Tammela, P. Betulin-derived compounds as inhibitors of alphavirus replication. *J. Nat. Prod.* **2009**, *72*, 1917–1926. [\[CrossRef\]](#) [\[PubMed\]](#)
30. Salin, O.; Alakurtti, S.; Pohjala, L.; Siiskonen, A.; Maass, V.; Maass, M.; Yli-Kauhaluoma, J.; Vuorela, P. Inhibitory effect of the natural product betulin and its derivatives against the intracellular bacterium *Chlamydia pneumoniae*. *Biochem. Pharmacol.* **2010**, *80*, 1141–1151. [\[CrossRef\]](#)
31. Krieg, R.; Jortzik, E.; Goetz, A.A.; Blandin, S.; Wittlin, S.; Elhabiri, M.; Rahbari, M.; Nuryyeva, S.; Voigt, K.; Dahse, H.M.; et al. Arylmethylamino steroids as antiparasitic agents. *Nat. Commun.* **2017**, *8*, 14478. [\[CrossRef\]](#)
32. Chen, I.J.; Foloppe, N. Drug-like bioactive structures and conformational coverage with the LigPrep/ConfGen suite: Comparison to programs MOE and catalyst. *J. Chem. Inf. Model.* **2010**, *50*, 822–839. [\[CrossRef\]](#) [\[PubMed\]](#)
33. Dixon, S.L.; Smondyrev, A.M.; Knoll, E.H.; Rao, S.N.; Shaw, D.E.; Friesner, R.A. PHASE: A new engine for pharmacophore perception, 3D QSAR model development, and 3D database screening: 1. Methodology and preliminary results. *J. Comput. Aided Mol. Des.* **2006**, *20*, 647–671. [\[CrossRef\]](#)
34. Williams, A.J.; Ekins, S. A quality alert and call for improved curation of public chemistry databases. *Drug Discov. Today* **2011**, *16*, 747–750. [\[CrossRef\]](#)
35. Fukano, K.; Tsukuda, S.; Oshima, M.; Suzuki, R.; Aizaki, H.; Ohki, M.; Park, S.Y.; Muramatsu, M.; Wakita, T.; Sureau, C.; et al. Troglitazone Impedes the Oligomerization of Sodium Taurocholate Cotransporting Polypeptide and Entry of Hepatitis B Virus Into Hepatocytes. *Front. Microbiol.* **2018**, *9*, 3257. [\[CrossRef\]](#) [\[PubMed\]](#)
36. McRae, M.P.; Lowe, C.M.; Tian, X.; Bourdet, D.L.; Ho, R.H.; Leake, B.F.; Kim, R.B.; Brouwer, K.L.; Kashuba, A.D. Ritonavir, saquinavir, and efavirenz, but not nevirapine, inhibit bile acid transport in human and rat hepatocytes. *J. Pharmacol. Exp. Ther.* **2006**, *318*, 1068–1075. [\[CrossRef\]](#) [\[PubMed\]](#)
37. Dong, Z.; Ekins, S.; Polli, J.E. Structure-activity relationship for FDA approved drugs as inhibitors of the human sodium taurocholate cotransporting polypeptide (NTCP). *Mol. Pharm.* **2013**, *10*, 1008–1019. [\[CrossRef\]](#)
38. Liu, Y.; Ruan, H.; Li, Y.; Sun, G.; Liu, X.; He, W.; Mao, F.; He, M.; Yan, L.; Zhong, G.; et al. Potent and Specific Inhibition of NTCP-Mediated HBV/HDV Infection and Substrate Transporting by a Novel, Oral-Available Cyclosporine A Analogue. *J. Med. Chem.* **2020**. [\[CrossRef\]](#)
39. Shen, Z.-W.; Luo, M.-Y.; Hu, H.-H.; Zhou, H.; Jiang, H.-D.; Yu, L.-S.; Zeng, S. Screening and verifying potential NTCP inhibitors from herbal medicinal ingredients using the LLC-PK1 cell model stably expressing human NTCP. *Chin. J. Nat. Med.* **2016**, *14*, 549–560. [\[CrossRef\]](#)
40. Dong, Z.; Ekins, S.; Polli, J.E. A substrate pharmacophore for the human sodium taurocholate co-transporting polypeptide. *Int. J. Pharm.* **2015**, *478*, 88–95. [\[CrossRef\]](#)
41. Saso, W.; Tsukuda, S.; Ohashi, H.; Fukano, K.; Morishita, R.; Matsunaga, S.; Ohki, M.; Ryo, A.; Park, S.Y.; Suzuki, R.; et al. A new strategy to identify hepatitis B virus entry inhibitors by AlphaScreen technology targeting the envelope-receptor interaction. *Biochem. Biophys. Res. Commun.* **2018**. [\[CrossRef\]](#)
42. Hata, S.; Wang, P.; Eftychiou, N.; Ananthanarayanan, M.; Batta, A.; Salen, G.; Pang, K.S.; Wolkoff, A.W. Substrate specificities of rat oatp1 and ntcp: Implications for hepatic organic anion uptake. *Am. J. Physiol. Gastrointest. Liver Physiol.* **2003**, *285*, 829–839. [\[CrossRef\]](#) [\[PubMed\]](#)
43. Mita, S.; Suzuki, H.; Akita, H.; Hayashi, H.; Onuki, R.; Hofmann, A.F.; Sugiyama, Y. Inhibition of bile acid transport across Na<sup>+</sup>/taurocholate cotransporting polypeptide (SLC10A1) and bile salt export pump (ABCB11)-coexpressing LLC-PK1 cells by cholestasis-inducing drugs. *Drug Metab. Dispos.* **2006**, *34*, 1575–1581. [\[CrossRef\]](#)
44. Nkongolo, S.; Ni, Y.; Lempp, F.A.; Kaufman, C.; Lindner, T.; Esser-Nobis, K.; Lohmann, V.; Mier, W.; Mehrle, S.; Urban, S. Cyclosporin A inhibits hepatitis B and hepatitis D virus entry by cyclophilin-independent interference with the NTCP receptor. *J. Hepatol.* **2014**, *60*, 723–731. [\[CrossRef\]](#) [\[PubMed\]](#)
45. Shimura, S.; Watashi, K.; Fukano, K.; Peel, M.; Sluder, A.; Kawai, F.; Iwamoto, M.; Tsukuda, S.; Takeuchi, J.S.; Miyake, T.; et al. Cyclosporin derivatives inhibit hepatitis B virus entry without interfering with NTCP transporter activity. *J. Hepatol.* **2017**, *66*, 685–692. [\[CrossRef\]](#) [\[PubMed\]](#)



46. Watashi, K.; Sluder, A.; Daito, T.; Matsunaga, S.; Ryo, A.; Nagamori, S.; Iwamoto, M.; Nakajima, S.; Tsukuda, S.; Borroto-Esoda, K.; et al. Cyclosporin A and its analogs inhibit hepatitis B virus entry into cultured hepatocytes through targeting a membrane transporter, sodium taurocholate cotransporting polypeptide (NTCP). *Hepatology* **2014**, *59*, 1726–1737. [[CrossRef](#)]
47. Dong, Z.; Ekins, S.; Polli, J.E. Quantitative NTCP pharmacophore and lack of association between DILI and NTCP Inhibition. *Eur. J. Pharm. Sci.* **2015**, *66*, 1–9. [[CrossRef](#)] [[PubMed](#)]
48. Beeley, N.R.A.; Sage, C. GPCRs: An update on structural approaches to drug discovery. *Targets* **2003**, *2*, 19–25. [[CrossRef](#)]
49. Klebe, G. Virtual ligand screening: Strategies, perspectives and limitations. *Drug Discov. Today* **2006**, *11*, 580–594. [[CrossRef](#)]
50. DePristo, M.A.; de Bakker, P.L.; Blundell, T.L. Heterogeneity and inaccuracy in protein structures solved by X-ray crystallography. *Structure* **2004**, *12*, 831–838. [[CrossRef](#)]
51. Srivastava, A.; Nagai, T.; Srivastava, A.; Miyashita, O.; Tama, F. Role of Computational Methods in Going beyond X-ray Crystallography to Explore Protein Structure and Dynamics. *Int. J. Mol. Sci.* **2018**, *19*, 3401. [[CrossRef](#)]
52. Dixon, S.L.; Duan, J.; Smith, E.; Von Bargen, C.D.; Sherman, W.; Repasky, M.P. AutoQSAR: An automated machine learning tool for best-practice QSAR modeling. *Future Med. Chem.* **2016**, *8*, 1825–1839. [[CrossRef](#)]
53. Appelman, M.D.; Wettengel, J.M.; Protzer, U.; Oude Elferink, R.P.J.; van de Graaf, S.F.J. Molecular regulation of the hepatic bile acid uptake transporter and HBV entry receptor NTCP. *Biochim. Biophys. Acta Mol. Cell Biol. Lipids* **2021**, *1866*, 158960. [[CrossRef](#)]



# Substrate Specificities and Inhibition Pattern of the Solute Carrier Family 10 Members NTCP, ASBT and SOAT

Gary Grosser<sup>†</sup>, Simon Franz Müller<sup>†</sup>, Michael Kirstgen, Barbara Döring and Joachim Geyer<sup>\*</sup>

Institute of Pharmacology and Toxicology, Faculty of Veterinary Medicine, Justus Liebig University Giessen, Biomedical Research Center Seltersberg (BFS), Giessen, Germany

## OPEN ACCESS

### Edited by:

Cesare Indiveri,  
University of Calabria, Italy

### Reviewed by:

Giuliano Clarimboli,  
University of Münster, Germany  
Miriam Zacchia,  
University of Campania Luigi Vanvitelli,  
Italy

### \*Correspondence:

Joachim Geyer  
Joachim.M.Geyer@vetmed.uni-  
giessen.de

<sup>†</sup>These authors have contributed  
equally to this work and share first  
authorship.

### Specialty section:

This article was submitted to  
Cellular Biochemistry,  
a section of the journal  
Frontiers in Molecular Biosciences

Received: 01 April 2021

Accepted: 04 May 2021

Published: 17 May 2021

### Citation:

Grosser G, Müller SF, Kirstgen M,  
Döring B and Geyer J (2021) Substrate  
Specificities and Inhibition Pattern of  
the Solute Carrier Family 10 Members  
NTCP, ASBT and SOAT.  
*Front. Mol. Biosci.* 8:689757.  
doi: 10.3389/fmolb.2021.689757

Three carriers of the solute carrier family SLC10 have been functionally characterized so far. Na<sup>+</sup>/taurocholate cotransporting polypeptide NTCP is a hepatic bile acid transporter and the cellular entry receptor for the hepatitis B and D viruses. Its intestinal counterpart, apical sodium-dependent bile acid transporter ASBT, is responsible for the reabsorption of bile acids from the intestinal lumen. In addition, sodium-dependent organic anion transporter SOAT specifically transports sulfated steroid hormones, but not bile acids. All three carriers show high sequence homology, but significant differences in substrate recognition that makes a systematic structure-activity comparison attractive in order to define the protein domains involved in substrate binding and transport. By using stably transfected NTCP-, ASBT-, and SOAT-HEK293 cells, systematic comparative transport and inhibition experiments were performed with more than 20 bile acid and steroid substrates as well as different inhibitors. Taurolithocholic acid (TLC) was identified as the first common substrate of NTCP, ASBT and SOAT with  $K_m$  values of 18.4, 5.9, and 19.3  $\mu$ M, respectively. In contrast, lithocholic acid was the only bile acid that was not transported by any of these carriers. Troglitazone, BSP and erythrosine B were identified as pan-SLC10 inhibitors, whereas cyclosporine A, irbesartan, ginkgolic acid 17:1, and betulinic acid only inhibited NTCP and SOAT, but not ASBT. The HBV/HDV-derived myr-preS1 peptide showed equipotent inhibition of the NTCP-mediated substrate transport of taurocholic acid (TC), dehydroepiandrosterone sulfate (DHEAS), and TLC with  $IC_{50}$  values of 182 nM, 167 nM, and 316 nM, respectively. In contrast, TLC was more potent to inhibit myr-preS1 peptide binding to NTCP with  $IC_{50}$  of 4.3  $\mu$ M compared to TC ( $IC_{50}$  = 70.4  $\mu$ M) and DHEAS ( $IC_{50}$  = 52.0  $\mu$ M). Based on the data of the present study, we propose several overlapping, but differently active binding sites for substrates and inhibitors in the carriers NTCP, ASBT, SOAT.

**Keywords:** SLC10A1, SLC10A2, substrate specificity, drug target, NTCP, transport inhibitor, cross-reactivity, SLC10A6

## INTRODUCTION

The solute carrier family SLC10, also known as the “sodium bile acid cotransporter family” currently consists of seven members (SLC10A1-SLC10A7) (Geyer et al., 2006; Claro da Silva et al., 2013). Three of them (SLC10A1, SLC10A2, and SLC10A6) have been functionally characterized, while the members SLC10A3, SLC10A4, SLC10A5, and SLC10A7 are still orphan carriers (Fernandes

et al., 2007; Geyer et al., 2007; Godoy et al., 2007; Karakus et al., 2020). The founding members of the SLC10 carrier family were cloned in the early 1990s and were termed Na<sup>+</sup>/taurocholate cotransporting polypeptide (NTCP, gene symbol *SLC10A1*) (Hagenbuch and Meier, 1994) and apical sodium-dependent bile acid transporter (ASBT, gene symbol *SLC10A2*) (Wong et al., 1996), both sharing 39% amino acid sequence identity. NTCP is exclusively expressed at the basolateral (sinusoidal) membrane of hepatocytes (Ananthanarayanan et al., 1994; Stieger et al., 1994) and here mediates sodium-coupled uptake of taurocholic acid (TC) and other bile acids (BA) with a Na<sup>+</sup>:BA stoichiometry of 2:1 (Hagenbuch and Meier, 1996; Weinman, 1997). ASBT is typically expressed in the apical brush border membrane of enterocytes of the terminal ileum (Shneider et al., 1995), where it transports conjugated BAs with high affinity in a sodium-dependent manner (Craddock et al., 1998). Both carriers are essentially involved in the maintenance of the enterohepatic circulation of BAs (Döring et al., 2012). In 2007, we cloned an additional SLC10 carrier, named sodium-dependent organic anion transporter (SOAT, gene symbol *SLC10A6*) (Geyer et al., 2007). Although SOAT shows the highest sequence identity of 48% to ASBT, it does not represent a BA transporter (Geyer et al., 2007). In contrast, SOAT specifically transports 3' sulfated steroid hormones such as estrone-3-sulfate (E<sub>1</sub>S), estradiol-3-sulfate, dehydroepiandrosterone sulfate (DHEAS), androstenediol-3-sulfate, androsterone-3-sulfate, and pregnenolone sulfate (PREGS) (Fietz et al., 2013) and, thereby, has a role for steroid supply to different organs (Geyer et al., 2017). In addition, SOAT transports 17' sulfated steroids such as testosterone-17β-sulfates, but not steroid disulfates such as 17β-estradiol-3,17-disulfate (Grosser et al., 2018).

Apart from their roles as physiological uptake carriers for BAs and sulfated steroid hormones, all three carriers were also established as drug targets. In 2012, NTCP was identified as the high-affinity hepatic entry receptor for the hepatitis B (HBV) and hepatitis D (HDV) viruses (Yan et al., 2012; Drexler et al., 2013). More precisely, both viruses bind to NTCP with their 2–48 N-terminal amino acids of the myristoylated preS1 domain (so-called myr-preS1 peptide) of the large envelope protein and this triggers the cellular entry of the virus/NTCP complex (Iwamoto et al., 2019). Interestingly, BA binding and myr-preS1 peptide binding to NTCP directly interfere with each other. BAs can block myr-preS1 peptide binding to NTCP and *in vitro* HBV/HDV infection, while myr-preS1 peptide binding to NTCP inhibits BA transport (König et al., 2014; Ni et al., 2014). Apart from the myr-preS1 peptide, several small molecules were detected that also block virus binding to NTCP *in vitro*, such as cyclosporine A, ezetimibe, irbesartan, ritonavir, troglitazone or betulinic acid (Fukano et al., 2019; Kirstgen et al., 2020; Li et al., 2020; Wettengel and Burwitz, 2020), but none of them is clinically approved for HBV/HDV entry inhibition yet. In contrast, pharmacological inhibitors of ASBT, such as odevixibat and maralixibat, are already in clinical use. These so-called bile acid reabsorption inhibitors (BARIs) are used to treat BA-related diseases such as intrahepatic cholestasis, primary biliary cholangitis, Alagille syndrome, or non-alcoholic

steatohepatitis (Karpen et al., 2020). In addition, BARIs are used to treat chronic constipation by increasing the intestinal BA content and to lower plasma LDL-cholesterol levels by increasing the *de novo* hepatic synthesis of BAs from the precursor cholesterol (Kramer and Glombik, 2006; Al-Dury and Marshall, 2018). SOAT is expressed in breast cancer and here mediates the uptake of pro-proliferative sulfated estrogen precursors. Inhibition of SOAT had anti-proliferative effects in breast cancer cells *in vitro*, and so was proposed as potential novel anti-cancer drug target (Karakus et al., 2018).

Since the cloning of SOAT it is still an open question why the close phylogenetic relationship of ASBT and SOAT is not reflected at the functional level, while the more distant carriers NTCP and ASBT are close functional homologs. Therefore, in the present study we aimed to compare systematically the substrate specificities of NTCP, ASBT and SOAT and their inhibition pattern. Based on the data of the present study, we propose several overlapping substrate and inhibitor binding sites at the three carriers that have to be considered as potential off-target sites when one of these carriers is addressed with pharmacological inhibitors. Furthermore, we identified taurolicholic acid (TLC) as the first common substrate of all three carriers.

## MATERIALS AND METHODS

### Radiochemicals and Chemicals

[<sup>3</sup>H]Dehydroepiandrosterone sulfate ([<sup>3</sup>H]DHEAS), [<sup>3</sup>H]estrone-3-sulfate ([<sup>3</sup>H]E<sub>1</sub>S), [<sup>3</sup>H]cortisone, [<sup>3</sup>H]pregnenolone sulfate ([<sup>3</sup>H]PREGS), [<sup>3</sup>H]chenodeoxycholic acid, [<sup>3</sup>H]lithocholic acid and [<sup>3</sup>H]taurocholic acid ([<sup>3</sup>H]TC) were imported via BIOTREND Chemikalien GmbH (Cologne, Germany) from the manufacturer American Radiolabeled Chemicals, Inc. (St. Louis, United States). [<sup>3</sup>H]Cortisol was obtained from Perkin Elmer, Inc. (Boston, United States). [<sup>3</sup>H]Estrone-3β-D-glucuronide and [<sup>3</sup>H]estradiol-17β-D-glucuronide were generously provided by Dr. Bernhard Ugele (Munich, Germany). [<sup>3</sup>H]Cholic acid, [<sup>3</sup>H]deoxycholic acid, [<sup>3</sup>H]ursodeoxycholic acid, [<sup>3</sup>H]sarcosine cholic acid, [<sup>3</sup>H]glycodeoxycholic acid, [<sup>3</sup>H]glycochenodeoxycholic acid, [<sup>3</sup>H]glycoursoxycholic acid, [<sup>3</sup>H]taurodeoxycholic acid, [<sup>3</sup>H]tauroursodeoxycholic acid and [<sup>3</sup>H]taurochenodeoxycholic acid were generously provided by Prof. Dr. Alan Hofmann, University of California (San Diego, United States). [<sup>3</sup>H]Taurolicholic acid ([<sup>3</sup>H]TLC) was synthesized as described before (Lowjaga et al., 2021).

Estrone-3-sulfate (E<sub>1</sub>S), pregnenolone sulfate (PREGS), dehydroepiandrosterone sulfate (DHEAS), and taurocholic acid (TC) were obtained from Sigma-Aldrich (St. Louis, United States). Zeocin and hygromycin were purchased from Invitrogen (Groningen, Netherlands). A set of betulin derivatives (betulin, betulinic acid, lupenone, 3-O-caffeoyl betulin) was purchased from Adipogen AG (Liestal, Switzerland). Ezetimibe, bromosulphthalein (BSP), irbesartan, losartan, erythrosine B, and ginkgolic acid C17:1, and all other chemicals if not stated otherwise were purchased from Sigma-Aldrich (St. Louis, United States). Cyclosporine A was purchased

from Tokyo Chemical Industry (Tokyo, Japan). Troglitazone was purchased from Cayman Chemical (Michigan, United States).

### NTCP-HEK293, ASBT-HEK293, and SOAT-HEK293 Cells

The full-length open reading frames of NTCP, ASBT, and SOAT were cloned based on the cDNA sequences with GenBank accession numbers NM\_003049 (NTCP), NM\_000452 (ASBT) and NM\_197965 (SOAT), respectively, as reported before (Geyer et al., 2007; Grosser et al., 2015). Sequence verified clones were used for stable transfection of Flp-In T-REX HEK293 cells (HEK293-FlpIn) according to the manufacturer's instructions (Invitrogen) as reported (Geyer et al., 2007). From the generated NTCP-HEK293, ASBT-HEK293, and SOAT-HEK293 cells transgene expression can be induced by tetracycline treatment. Cells were maintained under D-MEM/F12 medium supplemented with 10% fetal calf serum (Sigma-Aldrich), L-glutamine (4 mM), penicillin (100 U/ml) and streptomycin (100 µg/ml) (further referred to as standard medium) at 37°C, 5% CO<sub>2</sub>, and 95% humidity. All cell culture materials and substances were purchased from Thermo Fisher Scientific (Waltham, United States) if not stated otherwise.

### Cultivation and Induction of Stably Transfected HEK293 Cells for Uptake, Inhibition or Binding Studies

Stably SLC10 transporter transfected NTCP-HEK293, ASBT-HEK293, SOAT-HEK293 cells and the HEK293-FlpIn maternal cell line were seeded on 24-well plates (if not stated otherwise for individual assays). Well plates were coated with poly-D-lysine prior to seeding of 125,000 cells per well. Cells were grown with 1 ml of standard medium per well with or without tetracycline (1 mg/ml) for 72 h to induce carrier expression before respective assays were started. HEK293-FlpIn cells were cultivated with standard medium and served as control.

### Substrate Screening in NTCP-HEK293, ASBT-HEK293, SOAT-HEK293, and HEK293-FlpIn Cells

Cells were washed three times with phosphate buffered saline (PBS) (137 mM NaCl, 2.7 mM KCl, 1.5 mM KH<sub>2</sub>PO<sub>4</sub>, 7.3 mM Na<sub>2</sub>HPO<sub>4</sub>, pH 7.4, 37°C). Afterward, cells were preincubated at 37°C with sodium transport buffer (containing 142.9 mM NaCl, 4.7 mM KCl, 1.2 mM MgSO<sub>4</sub>, 1.2 mM KH<sub>2</sub>PO<sub>4</sub>, 1.8 mM CaCl<sub>2</sub>, and 20 mM HEPES (all chemicals from Sigma-Aldrich), adjusted to pH 7.4), or with choline transport buffer (equimolar substitution of sodium chloride with choline chloride). Uptake experiments were initiated by replacing the preincubation buffer by 500 µL transport buffer containing the radiolabeled test compound and were performed at 37°C. Transport was terminated by removing the transport buffer and washing five-times with ice-cold PBS. Cell monolayers were lysed in 1 N NaOH with 0.1% SDS and the cell-associated radioactivity was determined by liquid scintillation counting. Protein content of

individual wells was determined by Lowry assay as reported before (Geyer et al., 2007).

### Transport Inhibition in NTCP-HEK293, ASBT-HEK293, SOAT-HEK293, and HEK293-FlpIn Cells

Cells were washed three times with PBS and were preincubated with the respective inhibitor in sodium transport buffer for 5 min at 37°C. Uptake was initiated by adding the respective radiolabeled substrate to the well and incubating for a fixed time as indicated in the figures at 37°C. Transport was terminated by removing the transport buffer and washing five-times with ice-cold PBS. Cell monolayers were lysed in 1 N NaOH with 0.1% SDS and the cell-associated radioactivity and protein content was determined as described above. For uptake inhibition with the myr-preS1 peptide the sodium transport buffer contained additionally MEM-amino acid solution (ThermoFisher) at 1:50 dilution.

### Binding Assays With the Myr-preS1 Peptide

NTCP-HEK293 cells were seeded into 24-well-dishes as described above. For every set of induced wells an equal number of not-induced wells were used as respective background controls. Cells were washed three times with PBS and then preincubated with sodium transport buffer supplemented with MEM-amino acid solution (ThermoFisher) at 1:50 dilution at 37°C for 5 min. The fluorescent myr-preS1-Al633 peptide was added with a final concentration of 10 nM and binding experiments were performed over 10 min at 37°C. Then, cells were washed twice with buffer at 37°C and transferred to the fluorescence reader Typhoon (GE Healthcare, Chicago, United States) to quantitatively determine bound fluorescence signals as established in our lab before (Müller et al., 2018). For calculation of the NTCP-specific binding signal, the mean background signal from the not-induced cells was subtracted. Net binding rates in the absence of any inhibitor were set to 100%.

### Phylogenetic Analysis

Phylogenetic analysis of the SLC10 carriers was performed using the proteins with the following GenBank accession numbers. NP\_003040.1 for NTCP/SLC10A1, NP\_000443.2 for ASBT/SLC10A2, NP\_689892.1 for SLC10A3, NP\_689892.1 for SLC10A4, NP\_001010893.1 for SLC10A5, NP\_932069.1 for SOAT/SLC10A6, AAI50309.1 for SLC10A7, and O15245.2 for OCT1 as outroot. In addition, the bacterial proteins Asbt<sub>Nm</sub> (PDB: 3ZUY.A) and Abst<sub>Yf</sub> (PDB: 4N7X.A) were included. The phylogenetic tree was generated based on sequence alignment ClustalW (Lasergene DNASTAR) and was visualized with the FigTree tool (tree.bio.ed.ac.uk). Scale bar represents 0.1 changes per site on horizontal distance.

### Quantitative Real Time PCR of Transporter Expression

The mRNA expression pattern of NTCP, ASBT and SOAT in the NTCP-HEK293, ASBT-HEK293, SOAT-HEK293, and HEK293-FlpIn

cells was analyzed by quantitative real-time PCR with cDNA from the indicated tetracycline induced stably transfected cell lines. RNA was isolated from the respective stably transfected cells or control cells grown in 6 well plates following 72 h of growth. The medium and any detached cells were removed from the well. Total RNA isolation was performed by using peqGOLD RNAPure reagent (PeqLab, Erlangen, Germany) according to the manufacturer's protocol. The RNA concentration was determined by measuring absorbance at 260 nm with a Beckmann spectrophotometer DU-640 (Beckmann, Munich, Germany). Complementary cDNA was synthesized from the RNA samples using SuperScript III First-Strand Synthesis System for RT-PCR according to the manufacturer's protocol (Invitrogen, Karlsruhe). Relative carrier expression was calculated by the  $2^{-\Delta\Delta CT}$  method and represents carrier expression x-times higher compared with the calibrator (NTCP expression in SOAT-HEK293 cells). ACTB served as endogenous control. Values represent means of duplicate determinations. Relative gene expression analysis was performed by real-time PCR amplification on an ABI PRISM 7300 thermal cycler (Applied Biosystems, Darmstadt, Germany) using the TaqMan Gene Expression Assays Hs01399354\_m1 for SOAT, Hs00166561\_m1 for ASBT, Hs00161820\_m1 for NTCP, and Hs99999903\_m1 for ACTB (Applied Biosystems, Darmstadt, Germany). Real-time amplification was performed in 96-well optical plates using 5  $\mu$ L cDNA, 1.25  $\mu$ L TaqMan Gene Expression Assay, 12.5  $\mu$ L TaqMan universal PCR Master Mix and 6.25  $\mu$ L water in each 25  $\mu$ L reaction. The plates were heated for 10 min at 95°C, and 45 cycles of 15 s at 95°C and 60 s at 60°C were applied.

## Data Analysis and Statistics

All transport or inhibition graphs were generated with GraphPad Prism 6.0 (GraphPad). Determination of IC<sub>50</sub> values was done by nonlinear regression analysis using the equation log (inhibitor) vs. response settings. If not stated otherwise in the legends all data represent means  $\pm$  SD of at least triplicate determinations of representative experiments.

## In silico Docking

The crystal structures of two bacterial SLC10-homologous carriers have been published, namely Asbt from *Neisseria meningitidis* (Asbt<sub>Nm</sub>) and Asbt from *Yersinia frederiksenii* (Asbt<sub>Yf</sub>) (Hu et al., 2011; Zhou et al., 2014). Based on a more recent publication that verified the crystal structure of Asbt<sub>Yf</sub> (4n7x.1.a) as an outward facing model for BA transporters (Wang et al., 2021) we generated outward facing homology models of NTCP, ASBT and SOAT based on this structure via the SWISS-MODEL server (<https://swissmodel.expasy.org>). These models were used as input structures in SwissDock (<http://www.swissdock.ch/docking>) and were *in silico* docked with TLC with standard parameters. The obtained docked clusters and models were visualized with the UCSF CHIMERA software (<https://www.cgl.ucsf.edu/chimera/>). For visualization, docked clusters were reduced to TLC molecules in reasonable proximity to the putative outward facing binding pocket.

**TABLE 1** | Substrate specificities and transport activity grading for NTCP, ASBT and SOAT. The primary transport data are indicated in **Figure 1**. The following grading was used. "—" represents no significant uptake compared to sodium-free control. Mean uptake "+" for values below 10, "++" for values between 10 and 100, and "+++" for values above 100 pmol/mg protein/10 min for sulfated steroid hormones. Mean uptake of bile acids "+" for values below 500, "++" for values between 500 and 1000, and "+++" for values above 1000 pmol/mg protein/30 min.

	NTCP	ASBT	SOAT
Cholic acid	++	+	—
Chenodeoxycholic acid	+	+	—
Deoxycholic acid	+	+	—
Ursodeoxycholic acid	+	—	—
Lithocholic acid	—	—	—
Sarcosine cholic acid	+	+	—
Glycocholic acid	+++	++	—
Glycochenodeoxycholic acid	+++	++	—
Glycodeoxycholic acid	+++	++	—
Glyoursodeoxycholic acid	+++	++	—
Taurocholic acid	+++	++	—
Taurochenodeoxycholic acid	+++	++	—
Taurodeoxycholic acid	+++	++	—
Tauroursodeoxycholic acid	+++	++	—
Taurolithocholic acid	+++	+++	++
DHEAS	+	—	++
E <sub>1</sub> S	++	—	+
PREGS	+++	—	+++
Estrone- $\beta$ -D-glucuronide	+	—	—
Estradiol-17 $\beta$ -D-glucuronide	—	—	—
Cortisone	—	—	—
Cortisol	—	—	—

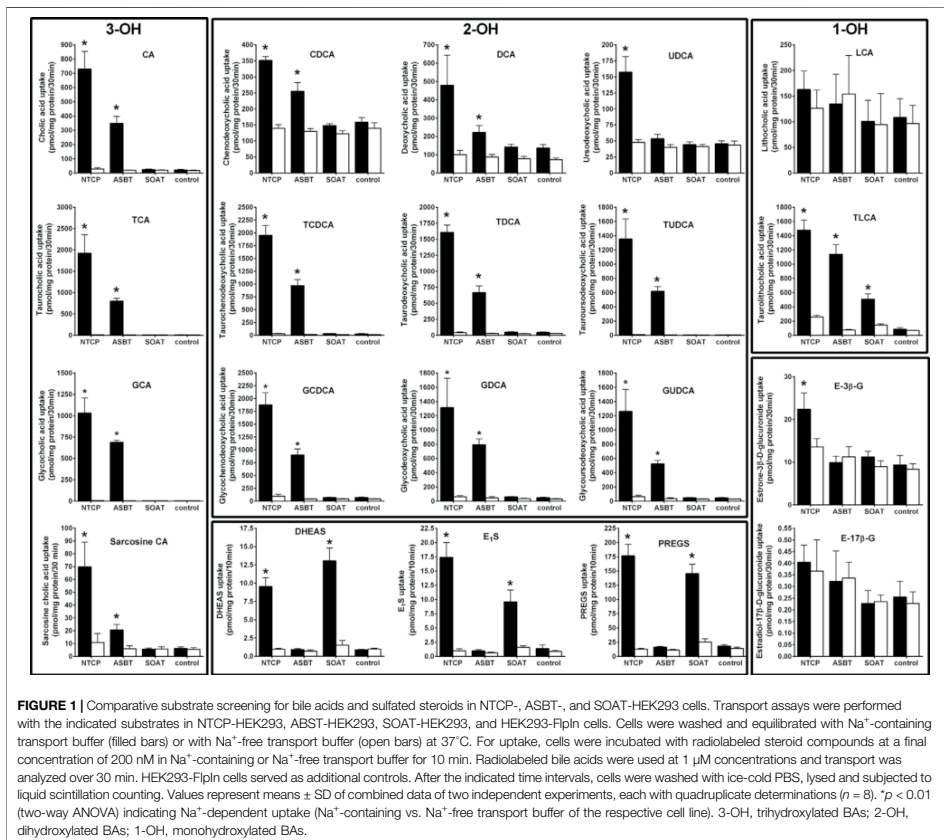
## Pharmacophore Calculation

Generation of pharmacophore models was performed using PHASE (Dixon et al., 2006), integrated into the MAESTRO Molecular Modeling Interface (Version 12.2) of SCHRODINGER, Inc. ([www.schrodinger.com](http://www.schrodinger.com), New York City, NY, United States). The following settings were used. Active/inactive (see **Table 1**), hypothesis should match at least 50% of actives, 4–5 features in the hypothesis, difference criterion 0.5, create excluded volume shell from actives and inactives, minimum number of inactives that must experience a clash = 1, minimum distance between active surface and excluded volumes 1 Å, excluded volume sphere radii 1 Å.

## RESULTS

### Comparative Substrate Screening for NTCP, ASBT, and SOAT

This study focused explicitly on comparative transport studies with NTCP, ASBT and SOAT. Therefore, stably transfected HEK293 cells were generated based on the identical HEK293-FlpIn cell line and following the identical protocol. The generated cell lines NTCP-HEK293, ASBT-HEK293, and SOAT-HEK293 showed significant overexpression of the respective carrier as shown by comparative quantitative expression analysis (see **Supplementary Figure S1**).



In a first approach, these cell lines were used to analyze the sodium-dependent uptake of different BAs and steroid derivatives (Figure 1). Therefore, all transport studies were performed in sodium-containing transport buffer (filled bars) as well as in sodium-free transport buffer (open bars). The non-transfected HEK293-F1pIn cell line served as additional control. In detail, this panel of test compounds included different unconjugated BAs as well as glycine-conjugated and taurine-conjugated BAs. All BAs derived from cholic acid can be classified as 3 $\alpha$ ,7 $\alpha$ ,12 $\alpha$ -trihydroxylated (3-OH) BAs. Together with the 3 $\alpha$ ,7 $\alpha$ -dihydroxylated (2-OH) chenodeoxycholic acid-derived BAs, these are primary BAs synthesized in the liver. Two other groups of dihydroxylated BAs, namely deoxycholic acid and ursodeoxycholic acid result from bacterial de-conjugation and isomerization, respectively. These are classified as secondary BAs. In

addition, the 3 $\alpha$ -monohydroxylated (1-OH) BA lithocholic acid results from bacterial de-conjugation in the gut. Secondary BAs are mostly reabsorbed in their unconjugated forms and then can be re-conjugated in the liver with glycine or taurine. As an additional BA derivative, sarcosine cholic acid was included. From the group of steroid conjugates, three sulfo-conjugated steroids, namely E $\beta$ S, DHEAS, and PREGS were analyzed, as well as the steroid glucuronides estrone-3 $\beta$ -D-glucuronide and estradiol-17 $\beta$ -D-glucuronide. Finally, the glucocorticoids cortisone and cortisol were used for transport experiments.

All primary transport data are presented in Figure 1. Additionally, the primary transport data were arranged in a graded manner in Table 1 for better overview and comparability. As expected, NTCP and ASBT showed significant and sodium-dependent transport activity for nearly

all BAs analyzed. The transport rates of taurine- and glycine-conjugated BAs by ASBT and NTCP are obviously higher compared to the unconjugated forms. Among the group of unconjugated BAs, ursodeoxycholic acid was only transported by NTCP, but not by ASBT, and lithocholic acid was the only BA that was transported neither by NTCP nor by ASBT. Of note, also the BA derivative sarcosine cholic acid was significantly transported by NTCP and ASBT in a sodium-dependent manner. Apart from the group of BAs, NTCP showed also significant transport activity for the steroid conjugates DHEAS, E<sub>1</sub>S, PREGS, and estrone-3 $\beta$ -D-glucuronide, but not for estradiol-17 $\beta$ -D-glucuronide. The steroid sulfate carrier SOAT showed significant transport activity for DHEAS, E<sub>1</sub>S, and PREGS as expected, but was transport negative for the steroid glucuronides and for nearly all BAs. Surprisingly, SOAT showed significant sodium-dependent uptake of TLC and, therefore, TLC is the only common substrate of all three carriers NTCP, ASBT and SOAT, identified so far.

### Comparative Transport Kinetics for NTCP, ASBT, and SOAT

To closer analyze the TLC transport via NTCP, ASBT, and SOAT, transport kinetics were comparatively analyzed for all three carriers. In addition, the transport kinetics for TC, DHEAS, E<sub>1</sub>S, and PREGS were determined. The primary transport data are presented in **Figure 2** and the Michaelis-Menten parameters  $K_m$  and  $V_{max}$  are listed in **Table 2**. The apparent  $K_m$  values for TLC were within the same range for all three carriers, being 18.4, 5.9, and 19.3  $\mu$ M for NTCP, ASBT, and SOAT, respectively. The  $V_{max}$  values ranged in the order NTCP > ASBT > SOAT. The transport kinetics for TC were well comparable between NTCP and ASBT with  $K_m$  of 13.1 and 14.7  $\mu$ M as well as  $V_{max}$  of 2395 and 1821 pmol/mg protein/min, respectively. Also, the transport kinetics for the sulfated steroid hormones were comparable between NTCP and SOAT with  $K_m$  of 56.1 and 28.7  $\mu$ M for DHEAS, as well as 8.8 and 11.3  $\mu$ M for PREGS, respectively. However, SOAT showed a much lower  $K_m$  of 12.0  $\mu$ M and  $V_{max}$  of 585 pmol/mg protein/min compared to NTCP ( $K_m$  = 57.6  $\mu$ M and  $V_{max}$  = 2367 pmol/mg protein/min) for the substrate E<sub>1</sub>S. Of note, the transport data of E<sub>1</sub>S, DHEAS, and PREGS for SOAT were taken from a previous study, that used however exactly the same SOAT-HEK293 cell lines and measuring methodology (Geyer et al., 2007).

### TLC, TC, and DHEAS as Inhibitors of NTCP, ASBT, and SOAT

As shown in **Figure 3**, TLC, TC, and DHEAS were used at increasing inhibitor concentrations to block the transport of the respective radiolabeled transport substrates [<sup>3</sup>H]TLC, [<sup>3</sup>H]TC, and [<sup>3</sup>H]DHEAS at all three carriers NTCP, ASBT, and SOAT. As expected, TLC inhibited the transport of [<sup>3</sup>H]TLC via NTCP, ASBT, and SOAT with comparable IC<sub>50</sub> values of 1.4  $\mu$ M, 4.0  $\mu$ M, and 2.6  $\mu$ M, respectively (**Table 3**). Very similar was also the inhibition of the [<sup>3</sup>H]TC transport by increasing concentrations

of TC with IC<sub>50</sub> values of 5.4  $\mu$ M and 5.7  $\mu$ M for NTCP and ASBT, respectively. A large difference occurred, however, when DHEAS was used as inhibitor of the [<sup>3</sup>H]DHEAS transport via NTCP and SOAT. While an IC<sub>50</sub> value of 3.4  $\mu$ M was measured for NTCP, this value was much higher (at 51.7  $\mu$ M) for SOAT. This is most likely a result of the stimulatory effect of DHEAS on its own transport. This was observed at low micromolar concentrations several times before (data not shown). So, DHEAS can be classified as a mixed stimulator/inhibitor. When TLC was used as inhibitor of the [<sup>3</sup>H]TC or [<sup>3</sup>H]DHEAS transport via the respective carrier, the IC<sub>50</sub> values were all within the same range between 1.7 and 3.9  $\mu$ M, indicating that TLC is an equipotent inhibitor of NTCP, ASBT, and SOAT, irrespective of the substrate used for transport measurements. In contrast, DHEAS showed a very different pattern, when it was used as transport inhibitor. With the transport substrate [<sup>3</sup>H]TLC, DHEAS was a potent inhibitor with an IC<sub>50</sub> of 15  $\mu$ M for SOAT, but only a weak inhibitor (IC<sub>50</sub> = 431.7  $\mu$ M) for NTCP, while ASBT was only inhibited by DHEAS at very high inhibitory concentrations above 1000  $\mu$ M. In the same line, the IC<sub>50</sub> for DHEAS inhibition of the [<sup>3</sup>H]TC transport was much lower for NTCP (IC<sub>50</sub> = 21.5  $\mu$ M) than for ASBT (IC<sub>50</sub> = 453.1  $\mu$ M). This indicates that ASBT is not only transport negative for DHEAS, but seems to bind DHEAS as an inhibitor only at very high concentrations. In contrast, TC although not transported by SOAT, was a moderate inhibitor of SOAT when the transport of [<sup>3</sup>H]TLC (IC<sub>50</sub> = 143  $\mu$ M) or [<sup>3</sup>H]DHEAS (IC<sub>50</sub> = 99.7  $\mu$ M) was analyzed. Overall, this indicates that TLC, TC, and DHEAS are only good inhibitors at these carriers, which are also transport positive for the respective compound. Accordingly, TC is a weak inhibitor of SOAT, and DHEAS is a very weak inhibitor at ASBT. Another interesting observation was that the transport of [<sup>3</sup>H]TLC can only weakly be inhibited by TC and DHEAS, even if these compounds are transported by the respective carriers. This finding may point to the presence of separate or multiple binding sites for TLC and TC/DHEAS at the respective carriers.

### Betulin-Based Inhibitors of NTCP, ASBT, and SOAT

As the next group of inhibitors, several betulin derivatives (structures see **Figure 8**) were analyzed at increasing concentrations as inhibitors of the [<sup>3</sup>H]TLC, [<sup>3</sup>H]TC, and [<sup>3</sup>H]DHEAS transport via the respective SLC10 carriers (**Table 4**). As shown in **Figure 4**, there is no common inhibition pattern and the half-maximal inhibitory concentrations showed a correlation neither for the individual carrier, nor for the betulin derivative used as inhibitor, nor for the substrate used for the transport measurements. While some of the betulin derivatives were quite potent inhibitors for NTCP and SOAT, this was not the case for ASBT. For this carrier, the only relevant inhibition was observed for 3-O-caffeoyl betulin when [<sup>3</sup>H]TLC was used as substrate with an IC<sub>50</sub> of 99.7  $\mu$ M. In contrast, betulinic acid potently inhibited NTCP and SOAT, in particular when [<sup>3</sup>H]DHEAS was used as substrate (IC<sub>50</sub> = 0.3 and 1.2  $\mu$ M, respectively). In a similar manner, lupenone and betulin

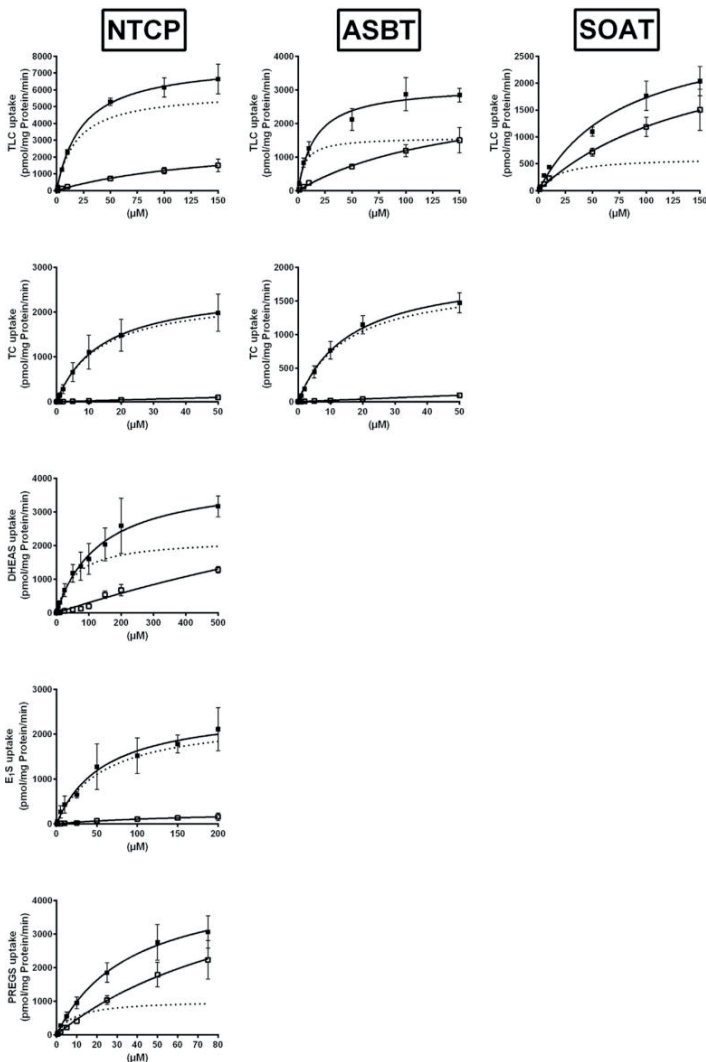


**FIGURE 2 |** NTCP, ASBT, and SOAT transport kinetics. Concentration-dependent uptake was analyzed in NTCP-HEK293, ASBT-HEK293, and SOAT-HEK293 cells for the indicated substrates at increasing substrate concentrations. Stably transfected HEK293 cells were pretreated with 1  $\mu\text{g}/\text{ml}$  tetracycline to induce carrier expression. HEK293-Fln cells were used as control. Uptake was analyzed for 1 min at 37°C. Afterward, the medium was removed and each cell monolayer was washed and processed to determine the protein content and cell-associated radioactivity. Specific uptake was calculated by subtracting non-specific uptake of the HEK293-Fln control cells (open squares) from uptake into carrier-overexpressing HEK293 cells (filled squares) and is shown by broken lines. The values represent means  $\pm$  SD of duplicate experiments, each with triplicate determinations ( $n = 6$ ). Transport kinetic parameters are summarized in **Table 2**.



**TABLE 2** | Transport kinetic parameters for TLC, TC, DHEAS, E<sub>1</sub>S, and PREGS uptake via NTCP, ASBT, and SOAT. Michaelis-Menten kinetic parameters ( $K_m$  and  $V_{max}$ ) were calculated by nonlinear regression analysis from the primary transport data shown in **Figure 2**. Values represent means  $\pm$  SD of combined data of two independent experiments, each with triplicate determinations ( $n = 6$ ).

	Substrate	Apparent $K_m$ ( $\mu$ M)	$V_{max}$ (pmol/mg protein/min)
NTCP	TLC	18.4 $\pm$ 2.3	5915 $\pm$ 189
	TC	13.1 $\pm$ 0.8	2395 $\pm$ 59
	DHEAS	56.1 $\pm$ 8.0	2198 $\pm$ 101.7
	E <sub>1</sub> S	57.6 $\pm$ 11.3	2367 $\pm$ 170.8
ASBT	PREGS	8.8 $\pm$ 2.1	1036 $\pm$ 69.1
	TLC	5.9 $\pm$ 1.8	1585 $\pm$ 99.7
SOAT	TC	14.7 $\pm$ 1.5	1821 $\pm$ 75.1
	TLC	19.3 $\pm$ 6.8	617 $\pm$ 57
	DHEAS <sup>a</sup>	28.7 $\pm$ 3.9	1899 $\pm$ 81
	E <sub>1</sub> S <sup>a</sup>	12.0 $\pm$ 2.3	585 $\pm$ 34
	PREGS <sup>a</sup>	11.3 $\pm$ 3.0	2168 $\pm$ 134

<sup>a</sup>Values in *italic* taken from Geyer et al. (2007).

are strong inhibitors at NTCP, when [<sup>3</sup>H]TLC was used as the substrate, while they lost their inhibitory potency, when [<sup>3</sup>H]DHEAS was used as substrate. This clearly indicates that the inhibitory potency of the individual betulins not only depends on the respective carrier, but also on the substrate that is used for the transport measurements. The fact that lupenone, 3-O-caffeoyl betulin and betulin had a generally higher inhibitory potency when [<sup>3</sup>H]TLC was used as the substrate additionally points to separated substrate binding sites for the substrates TLC and TC/DHEAS as already emphasized above. The only exception from this rule is betulinic acid that was much more potent as inhibitor at NTCP and SOAT when [<sup>3</sup>H]DHEAS was used as a substrate compared to [<sup>3</sup>H]TLC. However, it has to be noted that it cannot be completely excluded that betulinic acid is a transported substrate of these carrier as hypothesized before (Kirstgen et al., 2020). This could explain the differing inhibition pattern of this acidic derivative compared to the other non-acidic betulin derivatives.

## Non-Steroidal Inhibitors of NTCP, ASBT, and SOAT

The inhibitor screening was also extended to compounds that previously were identified as non-steroidal inhibitors of NTCP or SOAT, including cyclosporine A, ezetimibe, bromosulphthalein (BSP), irbesartan, losartan, troglitazone, erythrosine B, and ginkgolic acid 17:1 (Table 5, selected structures see Figure 8). All these compounds not only inhibited the transport function of NTCP, but also its role as HBV/HDV entry receptor in previous studies (Fukano et al., 2019). Therefore, these experiments also aimed to analyze the cross-reactivity of these antiviral drug candidates at the most NTCP-related proteins ASBT and SOAT. For these measurements, again all three potential transport substrates, [<sup>3</sup>H]TLC, [<sup>3</sup>H]TC, and [<sup>3</sup>H]DHEAS, were analyzed in the absence (positive control) and the presence of a fixed 100  $\mu$ M inhibitor concentration. All inhibitors then were graded as strong, medium or weak inhibitor based on the residual transport activity of 0–19% (+++), 20–49% (++) and 50–79% (+), respectively, in the presence of

inhibitor. Generally, these NTCP inhibitors showed significant cross-reactivity with SOAT and/or ASBT, at least with one of the investigated transport substrates. Therefore, compounds that were previously classified as specific NTCP inhibitors should rather be considered pan-SLC10 inhibitors. One exception was ezetimibe that only showed weak inhibitory potential at NTCP exclusively for TC as substrate. As previously shown for the betulin derivatives, the choice of the investigated SLC10 carrier substrate can affect the classification as inhibitor. As an example, losartan and ginkgolic acid 17:1 showed identical inhibitory classification for TLC and TC at NTCP, as well as for TLC and DHEAS at SOAT. However, their inhibitory potential for DHEAS as the transported substrate at NTCP revealed huge difference in classification. In contrast, irbesartan and cyclosporine A showed similar inhibition pattern at NTCP and SOAT, irrespective of the substrate used for transport measurements. However, irbesartan and cyclosporine A did not inhibit ASBT at all. This indicates that the transport of a particular substrate ([<sup>3</sup>H]TLC, [<sup>3</sup>H]TC, [<sup>3</sup>H]DHEAS) can be differentially addressed with a particular inhibitor, what would support the idea of different substrate binding sites in the SLC10 carriers.

## Cross-Inhibition of the HBV/HDV-Derived Myr-preS1 Peptide with TLC, TC, and DHEAS

We used two different assays to analyze the myr-preS1 peptide binding behavior in dependence of the substrate used. First, [<sup>3</sup>H]TC, [<sup>3</sup>H]TLC, and [<sup>3</sup>H]DHEAS transport was analyzed at increasing concentrations of myr-preS1 serving as inhibitor of transport (Figure 5A). Interestingly, myr-preS1 was quasi equipotent for the inhibition of the [<sup>3</sup>H]TC and [<sup>3</sup>H]DHEAS transport with IC<sub>50</sub> values of 182 nM and 167 nM, respectively. In contrast, higher concentrations were needed for half-maximal inhibition of the [<sup>3</sup>H]TLC transport (IC<sub>50</sub> = 316 nM). In a second assay, the binding of the myr-preS1 peptide to NTCP was analyzed in the presence of increasing concentrations of TLC, TC, and DHEAS serving as peptide binding inhibitors (Figure 5B). Again, TC and DHEAS were quasi equipotent in this assay with IC<sub>50</sub> values of 70.4  $\mu$ M and 52.0  $\mu$ M, respectively, whereas an order of magnitude lower concentrations of TLC were needed to replace the myr-preS1 peptide from its binding sites at NTCP (IC<sub>50</sub> = 4.3  $\mu$ M). This again underlines the different behavior of TLC in its binding to NTCP compared with TC and DHEAS.

## Comparative Analysis of NTCP, ASBT, and SOAT Homology Models

In order to visualize the 3-dimensional structures of NTCP, ASBT and SOAT, homology models were generated as shown in Figure 6. The backbone structures (Figure 6A) of the three carriers are very similar and are composed of nine transmembrane domains (TMDs). Structurally, the proteins can be subdivided into a core domain, composed of TMDs 2–4 and 7–9, and a panel domain, composed of TMDs 1, 5 and 6, according to the structures of the bacterial proteins Asbt<sub>tm</sub> (PDB: 3ZUYA) and Abst<sub>tf</sub> (PDB: 4N7XA) (Hu et al., 2011; Zhou et al., 2014). For homology modeling, the outward-

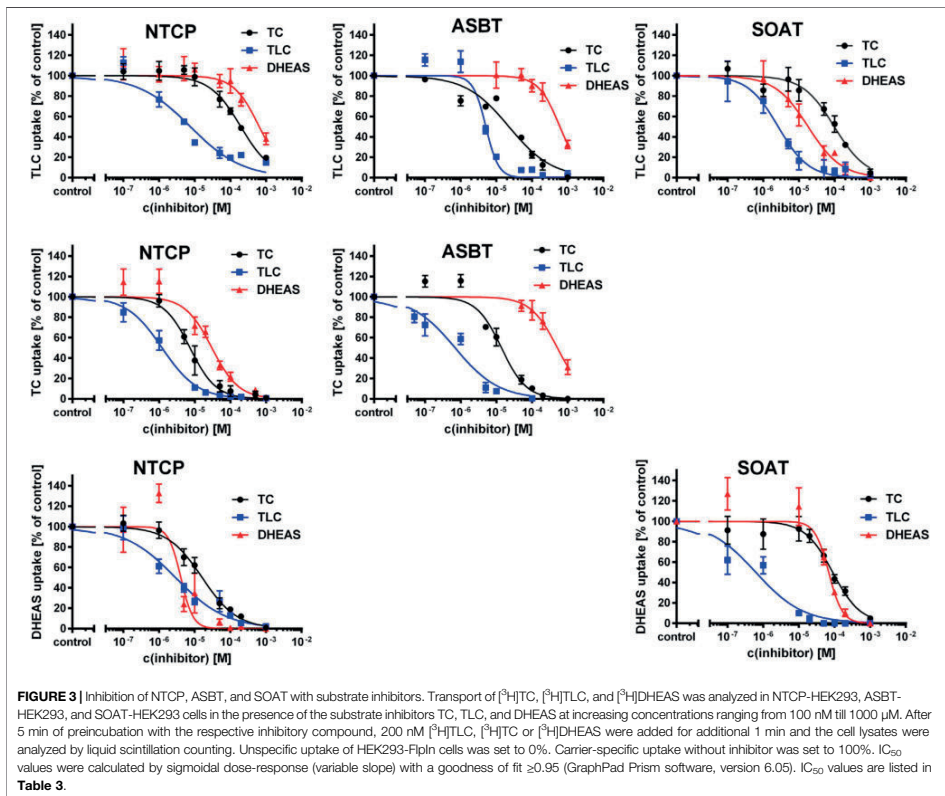


**TABLE 3** | Half-maximal inhibitory concentrations (IC<sub>50</sub>) for substrate inhibitors at NTCP, ASBT, and SOAT. [<sup>3</sup>H]TLC, [<sup>3</sup>H]TC, and [<sup>3</sup>H]DHEAS substrate uptake was analyzed in NTCP-HEK293, ASBT-HEK293, and SOAT-HEK293 cells in the presence of the indicated substrate inhibitors TC, TLC, and DHEAS at increasing concentrations. The primary transport data are presented in **Figure 3**.

Substrate	Inhibitor	NTCP (IC <sub>50</sub> in μM)	ASBT (IC <sub>50</sub> in μM)	SOAT (IC <sub>50</sub> in μM)
<sup>3</sup> H]TLC	TC	140.8	45.9	<b>143.0</b>
	TLC	1.4	4.0	2.6
	DHEAS	431.7	>1000	15.0
<sup>3</sup> H]TC	TC	5.4	5.7	—
	TLC	1.7	1.9	—
	DHEAS	21.5	<b>453.1</b>	—
<sup>3</sup> H]DHEAS	TC	14.0	—	<b>99.7</b>
	TLC	1.8	—	3.9
	DHEAS	3.4	—	51.7

*Bold face:* inhibitor = not transported as substrate. *Underlined:* Inhibitor = transported substrate.

open Asbt<sub>YF</sub> model (PDB: 4N7X.1.A) was used that shows an outward-exposed substrate binding cavity between the panel and core domains as recently verified (Wang et al., 2021). The

molecular surface of the NTCP, ASBT and SOAT homology models was colored according to Coulomb potential (**Figure 6B**) or by amino acid residue hydrophobicity (**Figure 6C**) and revealed

**TABLE 4** | Half-maximal inhibitory concentrations ( $IC_{50}$ ) for non-substrate triterpenoid inhibitors at NTCP, ASBT, and SOAT. [ $^3$ H]TLC, [ $^3$ H]TC, and [ $^3$ H]DHEAS substrate uptake was analyzed in NTCP-HEK293, ASBT-HEK293, and SOAT-HEK293 cells in the presence of the indicated non-substrate inhibitors at increasing concentrations. The primary transport data are presented in **Figure 4**.

Substrate	Inhibitor	NTCP ( $IC_{50}$ in $\mu$ M)	ASBT ( $IC_{50}$ in $\mu$ M)	SOAT ( $IC_{50}$ in $\mu$ M)
[ $^3$ H]TLC	Betulinic acid	5.7	193.3	9.5
	Lupenone	11.8	>1000	122.4
	3-O-Caffeoyl betulin	2.1	99.7	37.8
	Betulin	45.8	191.5	50.1
[ $^3$ H]TC	Betulinic acid	0.8	>1000	—
	Lupenone	240.4	>1000	—
	3-O-Caffeoyl betulin	128.7	498.6	—
	Betulin	747.9	>1000	—
[ $^3$ H]DHEAS	Betulinic acid	0.3	—	1.2
	Lupenone	>1000	—	664.5
	3-O-Caffeoyl betulin	49.1	—	301.1
	Betulin	>1000	—	912.2

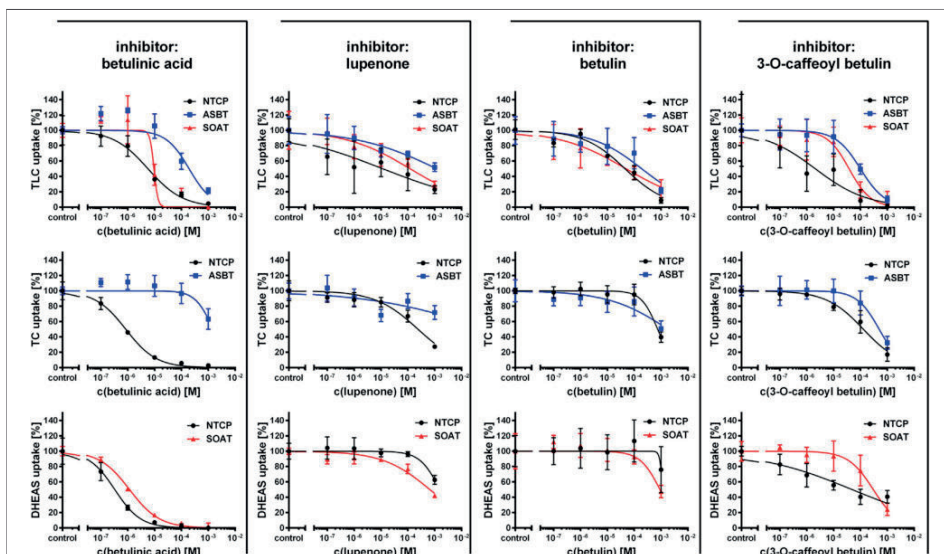


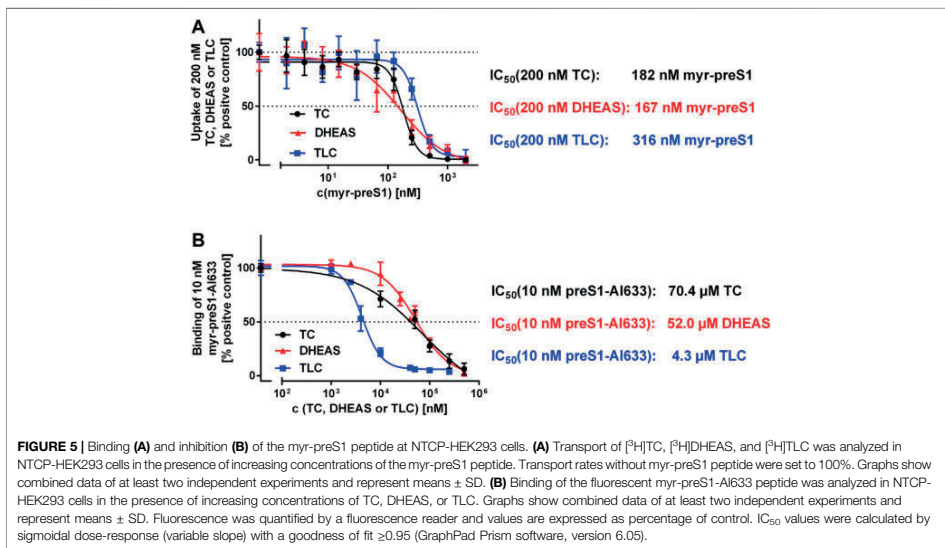
**FIGURE 4** | Inhibition of NTCP, ASBT, and SOAT with non-substrate betulin-based inhibitors. Transport of [ $^3$ H]TC, [ $^3$ H]TLC, and [ $^3$ H]DHEAS was analyzed in NTCP-HEK293, ASBT-HEK293, and SOAT-HEK293 cells in the presence of different proposed non-substrate triterpenoid inhibitors as indicated at increasing concentrations ranging from 100 nM till 1000  $\mu$ M. After 5 min of preincubation with the respective inhibitory compound, 1  $\mu$ M [ $^3$ H]TLC, [ $^3$ H]TC or [ $^3$ H]DHEAS were added for additional 10 min at 37°C and the cell lysates were analyzed by liquid scintillation counting. Experiments performed without inhibitor were set to 100%. Means of negative controls were subtracted to calculate net transport rates (expressed as percentage of control). Data represent means  $\pm$  SD of quadruplicate determinations of representative experiments.  $IC_{50}$  values were calculated by sigmoidal dose-response (variable slope) with a goodness of fit  $\geq 0.95$  (GraphPad Prism software, version 6.05).  $IC_{50}$  values are listed in **Table 4**.

significant differences for both physical parameters. Therefore, no common pattern can be recognized in the substrate binding cavities of NTCP, ASBT, and SOAT. In addition, the models were used for *in silico* docking with TLC as the ligand, using the docking module of

SWISS-Dock. As shown in **Figure 6D**, TLC showed several potential docking/binding sites at the proposed substrate binding cavities and in this case showed partly overlapping orientation for the three carriers NTCP, ASBT, and SOAT (**Figure 6D**).

**TABLE 5** | Inhibitor screening for NTCP, ASBT and SOAT. [ $^3$ H]TLC, [ $^3$ H]TC, and [ $^3$ H]DHEAS substrate uptake was analyzed in NTCP-HEK293, ASBT-HEK293, and SOAT-HEK293 cells in the presence of the indicated inhibitors at 100  $\mu$ M inhibitory concentrations. Grading of the net uptake compared to the non-inhibited control was: "-" for 80–100% residual uptake of the respective substrate compared to positive control (w/o inhibitor), "+" for 50–79% residual uptake (weak inhibition), "++" for 20–49% residual uptake (medium inhibition) and "+++" for 0–19% residual uptake (strong inhibition). Experiments were performed in duplicate each with triplicate determinations ( $n = 6$ ).

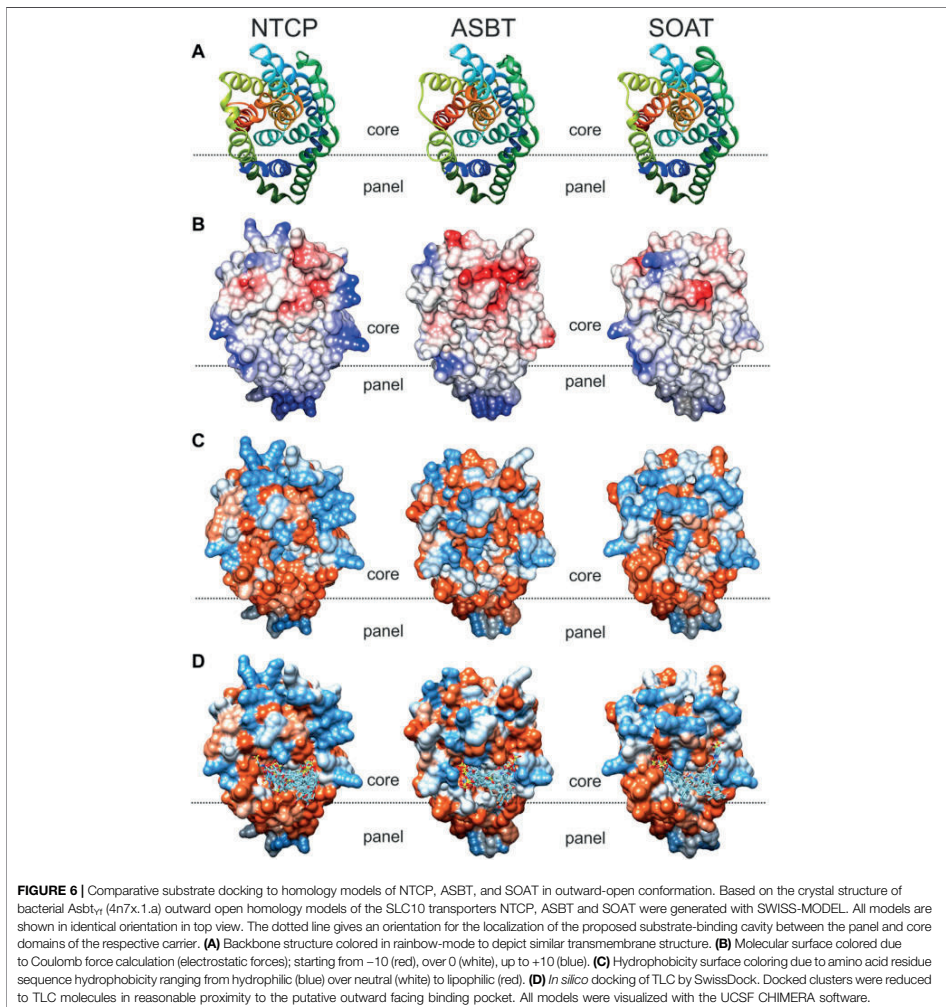
Inhibitor	NTCP substrate			ASBT substrate		SOAT substrate	
	TLC	TC	DHEAS	TLC	TC	TLC	DHEAS
Cyclosporine A	+	++	+++	-	-	+	+
Ezetimibe	-	+	-	-	-	-	-
BSP	+	++	++	+	++	+++	+++
Irbesartan	++	++	+++	-	-	+++	++
Troglitazone	+++	+++	++	+++	+++	+++	+++
Erythrosine B	+	+++	+	+	+	+	++
Ginkgolic acid 17:1	+	+	++	-	-	++	+++
Losartan	+	+	-	-	-	++	+++



## Comparative Analysis of NTCP, ASBT, and SOAT Substrate Pharmacophore Models

Finally, the substrate recognition pattern of NTCP, ASBT, and SOAT was visualized by common substrate pharmacophore modeling based on the data shown in Table 1. The pharmacophores are presented for each transporter in the first line of Figure 7. In addition, the SLC10 substrates TLC, TC and DHEAS are fitted into all pharmacophore models. The NTCP and ASBT pharmacophores are quite similar and are characterized by one hydrogen bond donor, one hydrogen bond acceptor and three hydrophobic features that all are similarly oriented to each other. However, in comparison to NTCP, ASBT revealed much more excluding values. As

consequence, DHEAS does not fit into the ASBT pharmacophore model due to steric overlap of the 3' sulfate group with the excluded space. In contrast, TC and TLC fit quite well in both pharmacophores of NTCP and ASBT. The pharmacophore model of SOAT is significantly different from those of NTCP and ASBT and revealed two hydrogen bond acceptor groups and three hydrophobic features. In addition, the SOAT pharmacophore is significantly restricted by spacious excluding values. As consequence, TC does not fit into this pharmacophore model due to steric overlap of the 7' and 12' hydroxyl groups with the excluded space. In contrast, the flat DHEAS molecule fits perfectly into this pharmacophore. Interestingly, also TLC fits into the SOAT pharmacophore. While the terminal sulfate group of the taurine residue

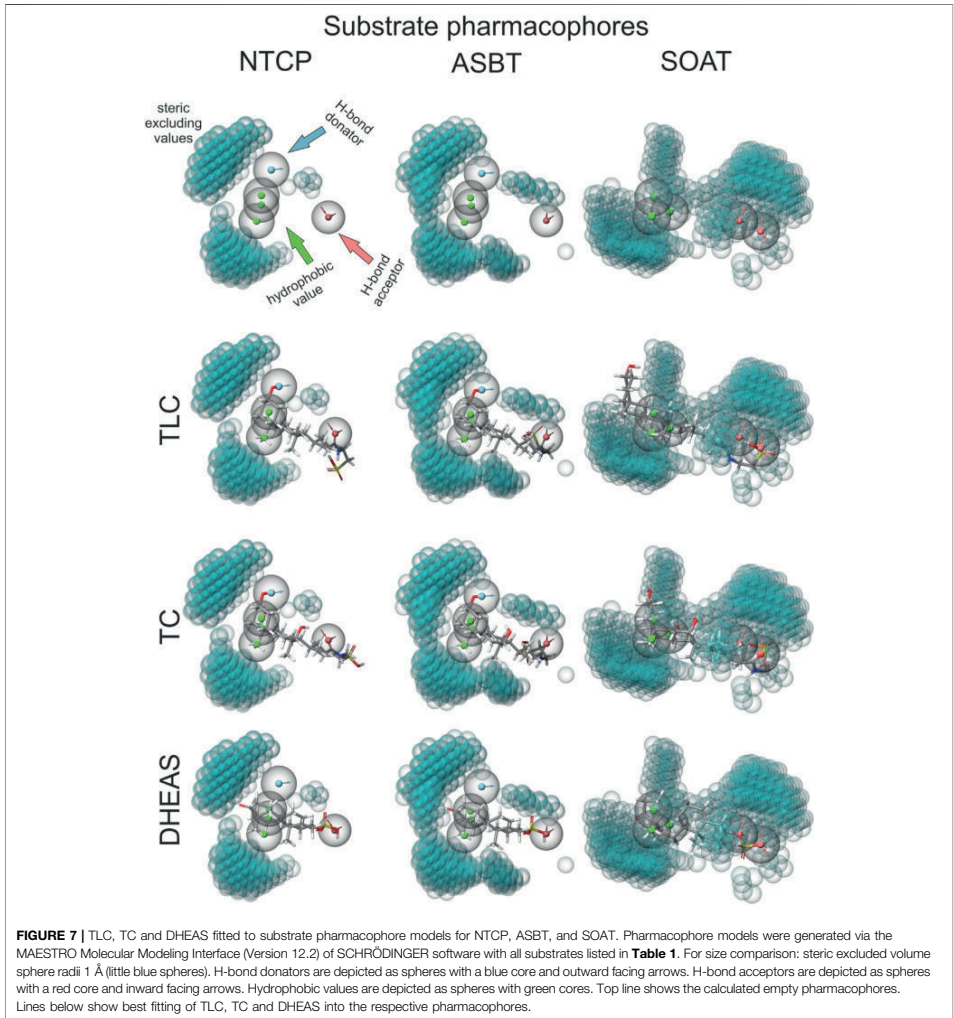


covers one of the hydrogen bond acceptor groups that is occupied by the 3' sulfate group in the case of DHEAS, the bent steroid rings A and B stretch out into the free space of the pharmacophore. This suggests substrate recognition of DHEAS and TLC in an antiparallel manner (see **Figure 8**). However, this is only possible when the BA molecule is not additionally hydroxylated, as it is the case for TC.

## DISCUSSION

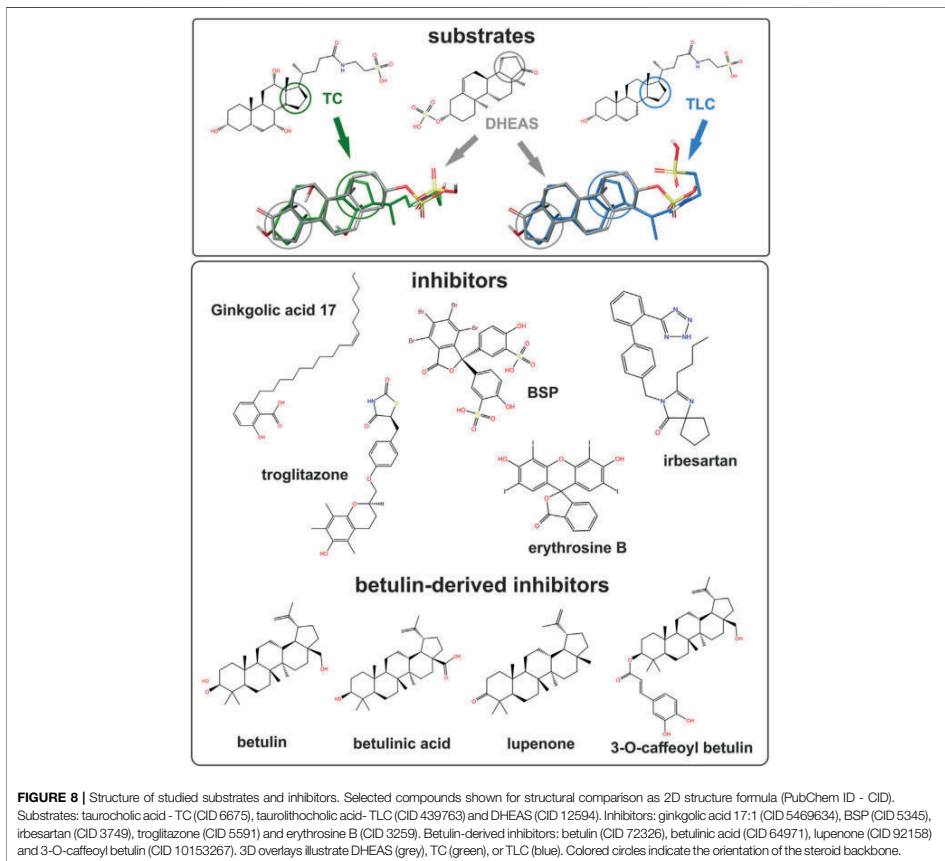
### Physiological Relevance of NTCP, ASBT, and SOAT

The present study suggests overlapping substrate and inhibitor binding sites for the SLC10 carriers NTCP, ASBT, and SOAT. Nevertheless, each carrier has a unique substrate spectrum to fulfill



its tissue-specific role for the cellular uptake of BAs and/or sulfated steroid hormones. Based on the current knowledge, BA transport via NTCP in the liver and via ASBT in the ileum is essential for the maintenance of the enterohepatic circulation of BAs (Geyer et al., 2006) and so the physiological role of both carriers in BA transport is quite clear. In addition, NTCP could be important for the hepatic excretion of sulfated steroid hormones, such as DHEAS (Geyer et al., 2017). In contrast, a transport function for sulfated steroids

would not make sense physiologically for ASBT, because relevant levels of sulfated steroid hormones are not present in the lumen of the ileum. SOAT is more widespread in its expression and was detected in germ cells of the testis, skin, placenta, mammary gland and some other hormone-dependent tissues (Geyer et al., 2007; Fietz et al., 2013; Grosser et al., 2013; Karakus et al., 2018). By SOAT-mediated uptake of sulfated steroid hormones from the blood and subsequent cleavage by the steroid sulfatase (so-called



intracrine steroid synthesis) seems to contribute to the steroid regulation of many hormone-dependent tissues (Geyer et al., 2017). Apart from steroid hormones, BAs gained increasing attention as signaling molecules with broad metabolic effects acting via membrane bound (TGR5) and nuclear (FXR) receptors (Di Ciaula et al., 2017). Against this background, the transport of TLC via SOAT could also be of physiological relevance in the periphery. TLC is formed in the liver by taurine conjugation of lithocholic acid that is absorbed from the gut as secondary BA independent from carrier-/ASBT-mediated uptake. However, TLC excreted into the duodenum via bile can also be reabsorbed via ASBT in the terminal ileum before this compound undergoes bacterial deconjugation in more distal parts of the gut. TLC then can be taken up from the portal blood into hepatocytes by NTCP. In addition to this

intestinal and hepatic transport of TLC, SOAT might play a role for TLC transport in peripheral organs. Of note, TLC is getting increasing attention as signaling and regulatory molecule and SOAT could be involved in its distribution. As an example, TLC recently showed to induce relaxation of human and mouse peripheral airways that were pre-contracted by acetylcholine stimulation (Urso et al., 2020). As SOAT is also expressed in the lung (Fietz et al., 2013), SOAT-mediated uptake of TLC might be of relevance there.

### Phylogenetic Relationship and Substrate Recognition of NTCP, ASBT, and SOAT

Based on Bayesian phylogenetic analysis we previously reported that the genes coding for ASBT (*SLC10A2*) and SOAT (*SLC10A6*)

emerged from a common ancestor by gene duplication (Geyer et al., 2006). This finding is supported by the very close homology of the gene structure of both genes with six coding exons and highly conserved sequences at the exon-intron boundaries. In the same way, the genes for NTCP (*SLC10A1*) and *SLC10A4* emerged from a common ancestor gene, but both genes are less homologous as indicated by the number of five (*SLC10A1*) and three (*SLC10A4*) coding exons. Even earlier, both subclades (*SLC10A2/SLC10A6* and *SLC10A1/SLC10A4*) have a common ancestor (see **Supplementary Figure S1**). Based on this, it is surprising that ASBT and SOAT show a contrary substrate spectrum. While ASBT is specific for BA transport, SOAT is a specific transporter for sulfate steroid hormones. NTCP, in contrast, has a much wider substrate spectrum and can transport both substrate groups and some additional compounds such as estradiol- $\beta$ -D-glucuronide that are not transported by ASBT and SOAT (**Figure 1**). The most likely explanation for this functional divergence is that the common ancestor of NTCP, ASBT and SOAT already incorporated all functions. While these functions for BA and steroid sulfate transport then were split into ASBT and SOAT, respectively, NTCP maintained the full substrate spectrum of the common ancestor. This hypothesis is supported by the fact that SOAT can still bind BAs even if they are not transported and the binding sites for BAs and steroid sulfates even seem to overlap. Accordingly, the transport of [ $^3$ H]DHEAS via SOAT can be potentially inhibited with TC (**Figure 3**) and several other BAs (Geyer et al., 2007). However, this does not fully apply for ASBT, which only can be inhibited with DHEAS at very high inhibitor concentrations. Therefore, ASBT seems to have lost the binding and transport function for sulfated steroids during emergence from the common SOAT/ASBT ancestor. For NTCP, an overlapping substrate-binding site for BAs (TC) and sulfated steroids (DHEAS) can be proposed. Both compounds are transported by NTCP and both are quite potent in inhibiting the transport of the respective other compound. The  $IC_{50}$  for inhibition of the [ $^3$ H]TC transport via NTCP by DHEAS was determined to 21.5  $\mu$ M, while inhibition of the [ $^3$ H]DHEAS transport via NTCP by TC was at 14.0  $\mu$ M and so within the same range. However, it has to be mentioned that the human NTCP\*2 polymorphism, characterized by the amino acid substitution S267F, showed reduced transport activity for TC, but not for E $_1$ S, pointing to structural differences in the substrate recognition of these two substrates (Ruggiero et al., 2021).

### NTCP, ASBT, and SOAT Share Different Overlapping Substrate/Inhibitor Binding Sites

Until now, it was considered that the substrate spectra of ASBT and SOAT have no overlap. Yet in the present study, we demonstrate that TLC can be transported by all three sodium-dependent SLC10 carriers, namely NTCP, ASBT and SOAT. Therefore, the present study established TLC as the first common substrate of these carriers. However, the question if TLC was also a substrate of the common NTCP/

ASBT/SOAT ancestor or if all three carriers later acquired the TLC transport function cannot be finally answered. However, it seems likely that TLC is not only a common, but also an ancient substrate of the SLC10 carriers. Anyhow, the highly conserved transport activity of all three carriers for TLC raises some questions about the exact mode of substrate recognition of this unique substrate.

Substrate recognition of TLC might occur by chance in the substrate-binding site of DHEAS, as TLC shows some structural overlap with DHEAS when oriented in an antiparallel manner, as illustrated in **Figure 8**. In this scenario, the terminal sulfate group of TLC would be recognized instead of the 3' sulfate group of DHEAS, while extensive overlapping hydrophobic interactions are possible via the unmodified steroid core structures of both molecules. Indeed, DHEAS and TLC showed an antiparallel fitting into the SOAT pharmacophore model as shown in **Figure 7**. This is, however, not possible when TLC is additionally hydroxylated at the 7' and/or 12' positions, as it is the case for the BAs TCA, TCDC, or TDCA, which all are not transported by SOAT. According to this hypothesis, TLC would be recognized by the DHEAS substrate-binding site of SOAT, while it binds as a substrate to the BA binding site in NTCP and ASBT.

A second explanation could be a separate substrate-binding site for TLC that is conserved in all three carriers NTCP, ASBT and SOAT. Although this proposed TLC binding site seems to partly overlap with the binding sites for TC and DHEAS, it would allow TLC transport independent from the TC/DHEAS transport activity of the respective carrier. Several findings of the present study support this hypothesis: (I) TLC was found to be an equipotent inhibitor of all three carriers NTCP, ASBT, and SOAT irrespective of the substrate that was used to measure transport activity. This finding can be explained by common binding and transport of TLC for all three carriers and thereby unspecific inhibition of the transport of any other substrate. (II) As the transport of [ $^3$ H]TLC can only weakly be inhibited by TC and DHEAS, even if these compounds are transported by the respective carriers, TLC transport seems to occur independent from TC/DHEAS binding and transport. (III) The non-substrate inhibitors lupenone, 3-O-caffeoyl betulin and betulin had much higher inhibitory potency when [ $^3$ H]TLC was used as the transport substrate compared with [ $^3$ H]TC and [ $^3$ H]DHEAS, indicating that the inhibitor binding site of these betulin derivatives closer overlaps with the TLC binding site compared with the TC/DHEAS binding site.

A broader interpretation of this hypothesis would propose a larger substrate/inhibitor entry zone in the outward oriented space between the core and the panel domain that is characterized by multiple interaction domains for the different substrates (TLC, TC and DHEAS) and inhibitors. This would explain the large cross-inhibition pattern between the different substrate and inhibitor groups. From this entry zone, single or multiple pathways for substrate transport through the transporter protein might exist or only binding of a transport substrate might indeed induce conformational changes that open the substrate-binding zone to the intracellular compartment for substrate release. This scenario



would also explain the existence of pan-SLC10 substrates (TLC) and inhibitors (e.g. erythrosine B, troglitazone, or BSP), while other substrates (TC, DHEAS) and inhibitors (e.g. irbesartan, cyclosporine A, ginkgolic acid 17:1) are specific for a subgroup of SLC10 carriers.

Interestingly, the myr-preS1 lipopeptide showed equipotent inhibition of all substrates (TC, TLC, and DHEAS) of NTCP, suggesting that this peptide completely blocks the access of any substrate to its respective binding site. However, TLC was much more potent in blocking the binding of the myr-preS1 peptide from NTCP compared with TC and DHEAS. This could also be explained by the particular *trans*-inhibitory potential of this compound at NTCP (Lowjaga et al., 2021). TLC, after carrier-mediated uptake or passive diffusion, can bind to an intracellular TLC binding site of NTCP and thereby *trans*-inhibits myr-preS1 peptide and HDV binding from the outside of the cell. Interestingly, this *trans*-inhibitory effect of TLC also inhibited *in vitro* HDV infection of NTCP expressing HepG2 hepatoma cells (Lowjaga et al., 2021). In contrast, such a *trans*-inhibitory effect is not known for the substrates TC and DHEAS, what could explain their lower potential to inhibit myr-preS1 binding to NTCP.

The existence of overlapping multiple substrate binding sites as proposed in the present study for NTCP, ASBT, and SOAT, was described for several other carrier proteins before. As an example, mutagenesis studies of the rat Organic cation transporter 1 (rOct1) revealed overlapping binding sites for different substrates and allosteric effectors (Koeppel, 2019). The multidrug efflux transporter MDR1 P-glycoprotein (syn. ABCB1) is another example of a carrier with multiple substrate binding sites. P-glycoprotein seems to have a large drug-binding pocket with different overlapping sites for binding of individual substrate groups. Thereby, P-glycoprotein can recognize and transport a vast variety of structurally unrelated drugs and toxins (Chufan et al., 2015).

## Cross-Reactivity of Pharmacological Inhibitors of SLC10 Carriers and Clinical Implications

The discovery of NTCP as a high-affinity receptor for HBV and HDV opened the field for the development of HBV/HDV entry inhibitors, preferably based on small molecules with oral bioavailability (Yan et al., 2012; König et al., 2014). In a previous study, we could demonstrate that small molecules from the group of pentacyclic triterpenoids, including betulinic acid and lupenone, show anti-HDV activity *in vitro* making them attractive virus entry inhibitor candidates (Kirstgen et al., 2020). However, as demonstrated in the present study, both compounds show significant cross-reactivity with SOAT, while ASBT transport was not affected by these betulin derivatives. This exemplifies that inhibitors of NTCP, ASBT, and

SOAT should principally tested for cross-reactivity against the other SLC10 carriers. In conclusion, NTCP, ASBT, and SOAT are interesting drug targets and several pharmacological inhibitors have already been established against these carriers. In the present study, overlapping substrate and inhibitor binding sites are proposed that are differently active in NTCP, ASBT, and SOAT. TLC was identified as the first common substrate for all three carriers and it was clearly shown that most of the SLC10 inhibitors are not carrier-specific, but rather cross-react at least with one of the other related SLC10 carriers. This should be considered when pharmacological inhibitors are developed against NTCP, ASBT, or SOAT.

## DATA AVAILABILITY STATEMENT

The original contributions presented in the study are included in the article/**Supplementary Material**, further inquiries can be directed to the corresponding author.

## AUTHOR CONTRIBUTIONS

GG, SM, MK, and JG conceived the experiments; GG, SM, MK, and BD performed the experiments; GG, SM, MK, and JG analyzed and interpreted the results; GG, SM, MK, and JG wrote the manuscript. All authors reviewed the manuscript. All authors contributed to the article and approved the submitted version.

## FUNDING

This study was supported in part by Flex Funds from the LOEWE-Center DRUID (Novel Drug Targets against Poverty-related and Neglected Tropical Infectious Diseases) and in part by the Deutsche Forschungsgemeinschaft (DFG, German Research Foundation)–Projektnummer 197785619 – SFB 1021.

## ACKNOWLEDGMENTS

The authors thank Anita Neubauer, Klaus Schuh and Regina Leidolf for excellent technical assistance. The authors kindly thank Dr. Bernhard Ugele and Prof. Dr. Alan Hofmann for providing radiolabeled substances.

## SUPPLEMENTARY MATERIAL

The Supplementary Material for this article can be found online at: <https://www.frontiersin.org/articles/10.3389/fmolb.2021.689757/full#supplementary-material>

## REFERENCES

- Al-Dury, S., and Marschall, H.-U. (2018). Ileal Bile Acid Transporter Inhibition for the Treatment of Chronic Constipation, Cholestatic Pruritus, and NASH. *Front. Pharmacol.* 9, 931. doi:10.3389/fphar.2018.00931
- Ananthanarayanan, M., Ng, O. C., Boyer, J. L., and Suchy, F. J. (1994). Characterization of Cloned Rat Liver Na(+)-Bile Acid Cotransporter Using Peptide and Fusion Protein Antibodies. *Am. J. Physiol.-Gastrointestinal Liver Physiol.* 267 (4 Pt 1), G637–G643. doi:10.1152/ajpgi.1994.267.4.G637
- Chufan, E. E., Sim, H.-M., and Ambudkar, S. V. (2015). Molecular Basis of the Polyspecificity of P-Glycoprotein (ABCB1). *Adv. Cancer Res.* 125, 71–96. doi:10.1016/bs.acr.2014.10.003
- Claro da Silva, T., Polli, J. E., and Swaan, P. W. (2013). The Solute Carrier Family 10 (SLC10): beyond Bile Acid Transport. *Mol. Aspects Med.* 34 (2, 3), 252–269. doi:10.1016/j.mam.2012.07.004
- Craddock, A. L., Love, M. W., Daniel, R. W., Kirby, L. C., Walters, H. C., Wong, M. H., et al. (1998). Expression and Transport Properties of the Human Ileal and Renal Sodium-dependent Bile Acid Transporter. *Am. J. Physiol.-Gastrointestinal Liver Physiol.* 274 (1), G157–G169. doi:10.1152/ajpgi.1998.274.1.G157
- Di Ciaula, A., Garruti, G., Lunardi Baccetto, R., Molina-Molina, E., Bonfrate, L., Wang, D. Q.-H., et al. (2017). Bile Acid Physiology. *Ann. Hepatol.* 16, S4–S14. doi:10.5604/01.3001.0010.05493
- Dixon, S. L., Smondryev, A. M., Knoll, E. H., Rao, S. N., Shaw, D. E., and Friesner, R. A. (2006). PHASE: a New Engine for Pharmacophore Perception, 3D QSAR Model Development, and 3D Database Screening: 1. Methodology and Preliminary Results. *J. Comput. Aided Mol. Des.* 20 (10–11), 647–671. doi:10.1007/s10822-006-9087-6
- Döring, B., Lütke, T., Geyer, J., and Petzinger, E. (2012). The SLC10 Carrier Family. *Curr. Top. Membr.* 70, 105–168. doi:10.1016/B978-0-12-394316-3.00004-1
- Drexler, J. F., Geipel, A., König, A., Cormann, V. M., van Riel, D., Lejten, L. M., et al. (2013). Bats Carry Pathogenic Hepadnaviruses Antigenically Related to Hepatitis B Virus and Capable of Infecting Human Hepatocytes. *Proc. Natl. Acad. Sci.* 110 (40), 16151–16156. doi:10.1073/pnas.1308049110
- Fernandes, C. F., Godoy, J. R., Döring, B., Cavalcanti, M. C. O., Bergmann, M., Petzinger, E., et al. (2007). The Novel Putative Bile Acid Transporter SLC10A5 Is Highly Expressed in Liver and Kidney. *Biochem. Biophys. Res. Commun.* 361 (1), 26–32. doi:10.1016/j.bbrc.2007.06.160
- Fietz, D., Bakhaus, K., Wapfelhorst, B., Grosser, G., Günther, S., Alber, J., et al. (2013). Membrane Transporters for Sulfated Steroids in the Human Testis - Cellular Localization, Expression Pattern and Functional Analysis. *PLoS One* 8 (5), e62638. doi:10.1371/journal.pone.0062638
- Fukano, K., Tsukuda, S., Watashi, K., and Wakita, T. (2019). Concept of Viral Inhibitors via NTCP. *Semin. Liver Dis.* 39 (1), 078–085. doi:10.1055/s-0038-1676804
- Geyer, J., Bakhaus, K., Bernhardt, R., Blaschka, C., Dezhkam, Y., Fietz, D., et al. (2017). The Role of Sulfated Steroid Hormones in Reproductive Processes. *J. Steroid Biochem. Mol. Biol.* 172, 207–221. doi:10.1016/j.jsbmb.2016.07.002
- Geyer, J., Döring, B., Meerkamp, K., Ugele, B., Bakhiya, N., Fernandes, C. F., et al. (2007). Cloning and Functional Characterization of Human Sodium-dependent Organic Anion Transporter (SLC10A6). *J. Biol. Chem.* 282 (27), 19728–19741. doi:10.1074/jbc.M702663200
- Geyer, J., Wilke, T., and Petzinger, E. (2006). The Solute Carrier Family SLC10: More Than a Family of Bile Acid Transporters Regarding Function and Phylogenetic Relationships. *Naunyn-Schmied Arch. Pharmacol.* 372 (6), 413–431. doi:10.1007/s00210-006-0043-8
- Godoy, J. R., Fernandes, C., Döring, B., Beuerlein, K., Petzinger, E., and Geyer, J. (2007). Molecular and Phylogenetic Characterization of a Novel Putative Membrane Transporter (SLC10A7), Conserved in Vertebrates and Bacteria. *Eur. J. Cell Biol.* 86 (8), 445–460. doi:10.1016/j.ejcb.2007.06.001
- Grosser, G., Bennien, J., Sánchez-Guijo, A., Bakhaus, K., Döring, B., Hartmann, M., et al. (2018). Transport of Steroid 3-sulfates and Steroid 17-sulfates by the Sodium-dependent Organic Anion Transporter SOAT (SLC10A6). *J. Steroid Biochem. Mol. Biol.* 179, 20–25. doi:10.1016/j.jsbmb.2017.09.013
- Grosser, G., Döring, B., Ugele, B., Geyer, J., Kulling, S. E., and Soukup, S. T. (2015). Transport of the Soy Isoflavone Daidzein and its Conjugative Metabolites by the Carriers SOAT, NTCP, OAT4, and OATP2B1. *Arch. Toxicol.* 89 (12), 2253–2263. doi:10.1007/s00204-014-1379-3
- Grosser, G., Fietz, D., Günther, S., Bakhaus, K., Schweigmann, H., Ugele, B., et al. (2013). Cloning and Functional Characterization of the Mouse Sodium-dependent Organic Anion Transporter Soat (Slc10a6). *J. Steroid Biochem. Mol. Biol.* 138, 90–99. doi:10.1016/j.jsbmb.2013.03.009
- Hagenbuch, B., and Meier, P. J. (1994). Molecular Cloning, Chromosomal Localization, and Functional Characterization of a Human Liver Na+/bile Acid Cotransporter. *J. Clin. Invest.* 93 (3), 1326–1331. doi:10.1172/JCI117091
- Hagenbuch, B., and Meier, P. (1996). Sinusoidal (Basolateral) Bile Salt Uptake Systems of Hepatocytes. *Semin. Liver Dis.* 16 (2), 129–136. doi:10.1055/s-2007-1007226
- Hu, N.-J., Iwata, S., Cameron, A. D., and Drew, D. (2011). Crystal Structure of a Bacterial Homologue of the Bile Acid Sodium Symporter ASBT. *Nature* 478 (7369), 408–411. doi:10.1038/nature10450
- Iwamoto, M., Saso, W., Sugiyama, R., Ishii, K., Ohki, M., Nagamori, S., et al. (2019). Epidermal Growth Factor Receptor Is a Host-Entry Cofactor Triggering Hepatitis B Virus Internalization. *Proc. Natl. Acad. Sci. USA* 116, 8487–8492. doi:10.1073/pnas.1811064116
- Karakus, E., Wannowius, M., Müller, S. F., Leitung, S., Leidolf, R., Noppes, S., et al. (2020). The Orphan Solute Carrier SLC10A7 Is a Novel Negative Regulator of Intracellular Calcium Signaling. *Sci. Rep.* 10 (1), 7248. doi:10.1038/s41598-020-64006-3
- Karakus, E., Zahner, D., Grosser, G., Leidolf, R., Gundogdu, C., Sánchez-Guijo, A., et al. (2018). Estrone-3-Sulfate Stimulates the Proliferation of T47D Breast Cancer Cells Stably Transfected with the Sodium-Dependent Organic Anion Transporter SOAT (SLC10A6). *Front. Pharmacol.* 9, 941. doi:10.3389/fphar.2018.00941
- Karpen, S. J., Kelly, D., Mack, C., and Stein, P. (2020). Ileal Bile Acid Transporter Inhibition as an Anticholestatic Therapeutic Target in Biliary Atresia and Other Cholestatic Disorders. *Hepatol. Int.* 14 (5), 677–689. doi:10.1007/s12072-020-10070-w
- Kirstgen, M., Lowjaga, K. A. A. T., Müller, S. F., Goldmann, N., Lehmann, F., Alakurti, S., et al. (2020). Selective Hepatitis B and D Virus Entry Inhibitors from the Group of Pentacyclic Lupane-type Betulin-Derived Triterpenoids. *Sci. Rep.* 10 (1), 21772. doi:10.1038/s41598-020-78618-2
- Koepsell, H. (2019). Multiple Binding Sites in Organic Cation Transporters Require Sophisticated Procedures to Identify Interactions of Novel Drugs. *Biol. Chem.* 400 (2), 195–207. doi:10.1515/hsz-2018-0191
- König, A., Döring, B., Mohr, C., Geipel, A., Geyer, J., and Glebe, D. (2014). Kinetics of the Bile Acid Transporter and Hepatitis B Virus Receptor Na+/taurocholate Cotransporting Polypeptide (NTCP) in Hepatocytes. *J. Hepatol.* 61 (4), 867–875. doi:10.1016/j.jhep.2014.05.018
- Kramer, W., and Glombik, H. (2006). Bile Acid Reabsorption Inhibitors (BARI): Novel Hypolipidemic Drugs. *Curr. Med. Chem.* 13 (9), 997–1016. doi:10.2174/092986706776361003
- Li, X., Liu, H., Cheng, W., Wang, J., Zhang, H., Lu, F., et al. (2020). Juncecellolide B, a Novel Inhibitor of Hepatitis B Virus. *Bioorg. Med. Chem.* 28 (16), 115603. doi:10.1016/j.bmc.2020.115603
- Lowjaga, K. A. A. T., Kirstgen, M., Müller, S. F., Goldmann, N., Lehmann, F., Glebe, D., et al. (2021). Long-term Trans-inhibition of the Hepatitis B and D Virus Receptor NTCP by Taurolithocholic Acid. *Am. J. Physiol.-Gastrointestinal Liver Physiol.* 320 (1), G66–G80. doi:10.1152/ajpgi.00263.2020
- Müller, S. F., König, A., Döring, B., Glebe, D., and Geyer, J. (2018). Characterisation of the Hepatitis B Virus Cross-Species Transmission Pattern via Na+/taurocholate Co-transporting Polypeptides from 11 New World and Old World Primate Species. *PLoS One* 13 (6), e0199200. doi:10.1371/journal.pone.0199200
- Ni, Y., Lempp, F. A., Mehrle, S., Nkongolo, S., Kaufman, C., Fälth, M., et al. (2014). Hepatitis B and D Viruses Exploit Sodium Taurocholate Co-transporting Polypeptide for Species-specific Entry into Hepatocytes. *Gastroenterology* 146 (4), 1070–1083. doi:10.1053/j.gastro.2013.12.024
- Ruggiero, M. J., Malhotra, S., Fenton, A. W., Swint-Kruse, L., Karanicolas, J., and Hagenbuch, B. (2021). A Clinically Relevant Polymorphism in the Na+/taurocholate Cotransporting Polypeptide (NTCP) Occurs at a Rheostat Position. *J. Biol. Chem.* 296, 100047. doi:10.1074/jbc.RA120.014889

- Shneider, B. L., Dawson, P. A., Christie, D. M., Hardikar, W., Wong, M. H., and Suchy, F. J. (1995). Cloning and Molecular Characterization of the Ontogeny of a Rat Ileal Sodium-dependent Bile Acid Transporter. *J. Clin. Invest.* 95 (2), 745–754. doi:10.1172/JCI117722
- Stieger, B., Hagenbuch, B., Landmann, L., Höchli, M., Schroeder, A., and Meier, P. J. (1994). *In situ* Localization of the Hepatocytic Na<sup>+</sup>/taurocholate Cotransporting Polypeptide in Rat Liver. *Gastroenterology* 107 (6), 1781–1787. doi:10.1016/0016-5085(94)90821-4
- Urso, A., D'Ovidio, F., Xu, D., Emala, C. W., Bunnett, N. W., and Perez-Zoghbi, J. F. (2020). Bile Acids Inhibit Cholinergic Constriction in Proximal and Peripheral Airways from Humans and Rodents. *Am. J. Physiol.-Lung Cell Mol. Physiol.* 318 (2), L264–L275. doi:10.1152/ajplung.00242.2019
- Wang, X., Lyu, Y., Ji, Y., Sun, Z., and Zhou, X. (2021). An Engineered Disulfide Bridge Traps and Validates an Outward-Facing Conformation in a Bile Acid Transporter. *Acta Cryst. Sect D Struct. Biol.* 77 (Pt 1), 108–116. doi:10.1107/S205979832001517X
- Weinman, S. A. (1997). Electrogenicity of Na<sup>+</sup>-Coupled Bile Acid Transporters. *Yale J. Biol. Med.* 70 (4), 331–340.
- Wettengel, J. M., and Burwitz, B. J. (2020). Innovative HBV Animal Models Based on the Entry Receptor NTCP. *Viruses* 12 (8), 828. doi:10.3390/v12080828
- Wong, M. H., Rao, P. N., Pettenati, M. J., and Dawson, P. A. (1996). Localization of the Ileal Sodium-Bile Acid Cotransporter Gene (SLC10A2) to Human Chromosome 13q33. *Genomics* 33 (3), 538–540. doi:10.1006/geno.1996.0233
- Yan, H., Zhong, G., Xu, G., He, W., Jing, Z., Gao, Z., et al. (2012). Sodium Taurocholate Cotransporting Polypeptide Is a Functional Receptor for Human Hepatitis B and D Virus. *eLife* 1, 1. doi:10.7554/eLife.00049
- Zhou, X., Levin, E. J., Pan, Y., McCoy, J. G., Sharma, R., Kloss, B., et al. (2014). Structural Basis of the Alternating-Access Mechanism in a Bile Acid Transporter. *Nature* 505 (7484), 569–573. doi:10.1038/nature12811

**Conflict of Interest:** The authors declare that the research was conducted in the absence of any commercial or financial relationships that could be construed as a potential conflict of interest.

Copyright © 2021 Grosser, Müller, Kirstgen, Döring and Geyer. This is an open-access article distributed under the terms of the Creative Commons Attribution License (CC BY). The use, distribution or reproduction in other forums is permitted, provided the original author(s) and the copyright owner(s) are credited and that the original publication in this journal is cited, in accordance with accepted academic practice. No use, distribution or reproduction is permitted which does not comply with these terms.

## GLOSSARY

**CA** Cholic acid

**CDCA** Chenodeoxycholic acid

**DCA** Deoxycholic acid

**UDCA** Ursodeoxycholic acid

**LCA** Lithocholic acid

**Sarcosine CA** Sarcosine cholic acid

**GCA** Glycocholic acid

**GDCA** Glycodeoxycholic acid

**GCDCA** Glychenodeoxycholic acid

**GDCA** Glycoursodeoxycholic acid

**TCA/TC** Taurocholic acid

**TDCA** Taurodeoxycholic acid

**TCDC** Taurochenodeoxycholic acid

**TUDCA** Tauroursodeoxycholic acid

**TLCA/TLC** Tauroolithocholic acid

**DHEAS** Dehydroepiandrosterone sulfate

**PREGS** Pregnenolone sulfate

**E<sub>1</sub>S** Estrone-3-sulfate

**E-3 $\beta$ -D-G** Estrone-3 $\beta$ -D-glucuronide

**E-17 $\beta$ -D-G** Estradiol-17 $\beta$ -D-glucuronide

**HBV** Human Hepatitis B Virus

**HDV** Human Hepatitis D Virus

**NTCP** Na<sup>+</sup>/taurocholate cotransporting polypeptide (SLC10A1)

**ASBT** Apical sodium-dependent bile acid transporter (SLC10A2)

**SOAT** Sodium-dependent organic anion transporter (SLC10A6)



*édition scientifique*  
**VVB LAUFERSWEILER VERLAG**

**VVB LAUFERSWEILER VERLAG**  
**STAUFENBERGRING 15**  
**D-35396 GIESSEN**

Tel: 0641-5599888 Fax: -5599890  
redaktion@doktorverlag.de  
www.doktorverlag.de

**ISBN: 978-3-8359-7033-5**



9 783835 970335